

Ratchet Models of Molecular Motors

Dissertation

zur Erlangung des akademischen Grades
Doktor der Naturwissenschaften (Dr. rer. nat.)
in der Wissenschaftsdisziplin Theoretische Physik

eingereicht an der
Mathematisch-Naturwissenschaftlichen Fakultät der Universität Potsdam

angefertigt am
Max-Planck-Institut für Kolloid- und Grenzflächenforschung in Golm

von

Nicole Jaster

geboren am 24. September 1974 in Haselünne

Potsdam, im Juni 2003

Zusammenfassung

Transportvorgänge in und von Zellen sind von herausragender Bedeutung für das Überleben des Organismus. Muskeln müssen sich kontrahieren können, Chromosomen während der Mitose an entgegengesetzte Enden der Zelle bewegt und Organellen, das sind von Membranen umschlossene Kompartimente, entlang molekularer Schienen transportiert werden.

Molekulare Motoren sind Proteine, deren Hauptaufgabe es ist, andere Moleküle zu bewegen. Dazu wandeln sie die bei der ATP-Hydrolyse freiwerdende chemische Energie in mechanische Arbeit um. Die Motoren des Zellskeletts gehören zu den drei Superfamilien Myosin, Kinesin und Dynein. Ihre Schienen sind Filamente des Zellskeletts, Actin und die Microtubuli.

In dieser Arbeit werden stochastische Modelle untersucht, welche dazu dienen, die Fortbewegung dieser linearen molekularen Motoren zu beschreiben. Die Skala, auf der wir die Bewegung betrachten, reicht von einzelnen Schritten eines Motorproteins bis in den Bereich der gerichteten Bewegung entlang eines Filaments. Ein Einzelschritt überbrückt je nach Protein etwa 10 nm und wird in ungefähr 10 ms zurückgelegt. Unsere Modelle umfassen M Zustände oder Konformationen, die der Motor annehmen kann, während er sich entlang einer eindimensionalen Schiene bewegt. An K Orten dieser Schiene sind Übergänge zwischen den Zuständen möglich. Die Geschwindigkeit des Proteins lässt sich in Abhängigkeit von den vertikalen Übergangsraten zwischen den einzelnen Zuständen analytisch bestimmen. Wir berechnen diese Geschwindigkeit für Systeme mit bis zu vier Zuständen und Orten und können weiterhin eine Reihe von Regeln ableiten, die uns einschätzen helfen, wie sich ein beliebiges vorgegebenes System verhalten wird.

Darüber hinaus betrachten wir entkoppelte Subsysteme, also einen oder mehrere Zustände, die keine Verbindung zum übrigen System haben. Mit einer bestimmten Wahrscheinlichkeit kann ein Motor einen Zyklus von Konformationen durchlaufen, mit einer anderen Wahrscheinlichkeit einen davon unabhängigen anderen.

Aktive Elemente werden in realen Transportvorgängen durch Motorproteine nicht auf die Übergänge zwischen den Zuständen beschränkt sein. In verzerrten Netzwerken oder ausgehend von der diskreten Mastergleichung des Systems können auch horizontale Raten spezifiziert werden und müssen weiterhin nicht mehr die Bedingungen der detaillierten Balance erfüllen. Damit ergeben sich eindeutige, komplette Pfade durch das jeweilige Netzwerk und Regeln für die Abhängigkeit des Gesamtstroms von allen Raten des Systems. Außerdem betrachten wir die zeitliche Entwicklung für vorgegebene Anfangsverteilungen.

Bei Enzymreaktionen gibt es die Idee des Hauptpfades, dem diese bevorzugt folgen. Wir bestimmen optimale Pfade und den maximalen Fluss durch vorgegebene Netzwerke.

Um darüber hinaus die Geschwindigkeit des Motors in Abhängigkeit von seinem Treibstoff ATP angeben zu können, betrachten wir mögliche Reaktionskinetiken, die den Zusammenhang zwischen den unbalancierten Übergangsraten und der ATP-Konzentration bestimmen. Je nach Typ der Reaktionskinetik und Anzahl unbalancierter Raten ergeben sich qualitativ unterschiedliche Verläufe der Geschwindigkeitskurven in Abhängigkeit von der ATP-Konzentration.

Die molekularen Wechselwirkungspotentiale, die der Motor entlang seiner Schiene erfährt, sind unbekannt. Wir vergleichen unterschiedliche einfache Potentiale und die Auswirkungen auf die Transportkoeffizienten, die sich durch die Lokalisation der vertikalen Übergänge im Netzwerkmodell im Vergleich zu anderen Ansätzen ergeben.

Abstract

Transport processes in and of cells are of major importance for the survival of the organism. Muscles have to be able to contract, chromosomes have to be moved to opposing ends of the cell during mitosis, and organelles, which are compartments enclosed by membranes, have to be transported along molecular tracks.

Molecular motors are proteins whose main task is moving other molecules. For that purpose they transform the chemical energy released in the hydrolysis of ATP into mechanical work. The motors of the cytoskeleton belong to the three super families myosin, kinesin and dynein. Their tracks are filaments of the cytoskeleton, namely actin and the microtubuli.

Here, we examine stochastic models which are used for describing the movements of these linear molecular motors. The scale of the movements comprises the regime of single steps of a motor protein up to the directed walk along a filament. A single step bridges around 10 nm , depending on the protein, and takes about 10 ms , if there is enough ATP available. Our models comprise M states or conformations the motor can attain during its movement along a one-dimensional track. At K locations along the track transitions between the states are possible. The velocity of the protein depending on the transition rates between the single states can be determined analytically. We calculate this velocity for systems of up to four states and locations and are able to derive a number of rules which are helpful in estimating the behaviour of an arbitrary given system.

Beyond that we have a look at decoupled subsystems, i.e., one or a couple of states which have no connection to the remaining system. With a certain probability a motor undergoes a cycle of conformational changes, with another probability an independent other cycle.

Active elements in real transport processes by molecular motors will not be limited to the transitions between the states. In distorted networks or starting from the discrete Master equation of the system, it is possible to specify horizontal rates, too, which furthermore no longer have to fulfill the conditions of detailed balance. Doing so, we obtain unique, complete paths through the respective network and rules for the dependence of the total current on all the rates of the system. Besides, we view the time evolutions for given initial distributions.

In enzymatic reactions there is the idea of a main pathway these reactions follow preferably. We determine optimal paths and the maximal flow for given networks.

In order to specify the dependence of the motor's velocity on its fuel ATP, we have a look at possible reaction kinetics determining the connection between unbalanced transitions rates and ATP-concentration. Depending on the type of reaction kinetics and the number of unbalanced rates, we obtain qualitatively different curves connecting the velocity to the ATP-concentration.

The molecular interaction potentials the motor experiences on its way along its track are unknown. We compare different simple potentials and the effects the localization of the vertical rates in the network model has on the transport coefficients in comparison to other models.

Contents

1	Introduction	1
1.1	Introduction to molecular motors	1
1.1.1	Basic biological knowledge on molecular motors	1
1.1.2	Experimental results on the movement of molecular motors	2
1.1.3	Regimes of motor movement and models	3
1.1.4	The mechanochemical cycle of motor proteins	4
1.2	The idea of ratchets	4
1.2.1	History of ratchets	4
1.2.2	Ratchet effect and molecular motors	5
2	Models for molecular motors	7
2.1	Stochastic models	7
2.1.1	Motor cycles	7
2.1.2	Basic ingredients	7
2.1.3	Langevin and Smoluchowski equation	8
2.1.4	Time evolution in the multi-state system	10
2.2	General solution for stationary states	11
2.2.1	Stationary states	11
2.2.2	Boundary conditions and normalization	11
2.2.3	Currents	11
2.2.4	Current-resistance relationships	13
2.2.5	Recursion relation for currents and densities	14
2.2.6	Implementation of periodic boundary conditions	16
2.2.7	Implementation of normalization condition	17
2.2.8	Calculation of the total current	18
3	Results for various (M, K)-models and universal rules	21
3.1	Examples of (M, K) -models	21
3.1.1	The special case of a single internal state	21
3.1.2	Results for two internal levels	22
3.1.3	Model with three states	26
3.1.4	Four internal states	33
3.2	Generic rules for the matrices and polynomials	34
3.2.1	Matrix $\mathbf{A}^{(M,K)}$ and vertical transition rates	34
3.2.2	Polynomials $Pol_i^{(M,K)}$ and vertical transition rates	35
3.3	Enzymatic activity - unbalanced transitions	38
3.3.1	A single unbalanced vertical transition	38
3.3.2	Two unbalanced vertical transitions	40
3.3.3	Four unbalanced vertical transitions	40

4	Decoupled states, horizontal rates and networks	43
4.1	Decoupled states	43
4.1.1	Decoupled states and continuous x -direction	44
4.1.2	Decoupled levels and localized transitions	48
4.1.3	Numerical approach to decoupled levels	50
4.1.4	Coupling parameter and bifurcations	52
4.2	Distorted networks	53
4.2.1	Concepts of distortion and unbalanced transitions in x -direction	54
4.2.2	Application and rules	54
4.3	Master equation and horizontal rates	56
4.3.1	General outline	56
4.3.2	Complete s-cycles and horizontal rates	58
4.3.3	Rules: dependence of the total current on vertical and horizontal rates	62
4.4	Time evolution of initial probability distributions	64
4.4.1	Integration of the Master equation	64
4.4.2	Markov chains in continuous time	75
4.5	Maximum flow and shortest paths	80
4.5.1	The main pathway in unspecified networks	80
4.5.2	Maximum flow and cut-sets	81
4.5.3	Flow carried along motor networks	81
4.5.4	Search for paths	81
4.5.5	Paths with minimal costs	84
5	ATP-concentration and transport properties	85
5.1	Reaction kinetics	85
5.1.1	Michaelis-Menten equation	85
5.1.2	Allosteric effects	86
5.2	Potentials and transport coefficients	90
5.2.1	Fokker-Planck equation and integration	90
5.2.2	Localizing transitions	90
5.2.3	Molecular interaction potentials	92
5.2.4	Free diffusion	94
6	Conclusions And Outlook	97
A	Matrices $\mathbf{A}^{(M,K)}$	I
A.1	Matrix $\mathbf{A}^{(2,3)}$	I
A.2	Matrix $\mathbf{A}^{(2,4)}$	II
A.3	Matrix $\mathbf{A}^{(3,2)}$	VI
A.4	The elements of $\mathbf{A}^{(2,2)}$ derived from a $(3, 2)$ -matrix	VII
A.5	Decoupling of a $(4, 2)$ -network into two $(2, 2)$ -networks	VIII
B	Polynomials and vertices of every state	XI
C	Terminology and basics on graph theory	XIII
D	Stationary probabilities for general $(2, 2)$-networks	XV
E	Algorithms for path problems	XVII
E.1	Maximum-flow problem	XVII
E.2	Shortest-path problem	XVII

Chapter 1

Introduction

The topic of our work are the movements of molecular motors, which we describe by stochastic models based on the idea of ratchets. At the beginning, we provide the reader with an overview explaining the properties of molecular motors, their occurrences in living beings and the idea of ratchets and its foundations.

1.1 Introduction to molecular motors

Molecular motors are ubiquitous in the cells of living beings. The biological outcomes and the experimental results obtained up to now are starting points for choosing models which describe the movements of these motors with respect to the underlying chemistry.

1.1.1 Basic biological knowledge on molecular motors

A eucaryotic cell, which, in contrast to the smaller and simpler procaryotic cells of bacteria, is found in contemporary animals and plants, contains up to one billion of protein molecules. In a single cell of a vertebrate, there are about ten thousand different types of proteins, most of which are spatially oriented. The cytoskeleton, the protein scaffold of eucaryotic cells, creates and maintains a high level of organization, so that the living cell might be compared to a city with services concentrated in different areas and cross-linked in various ways [1]. The cytoskeleton is formed by three different types of protein filaments, namely actin filaments, microtubuli and intermediate filaments, which, among other tasks as stabilizing the cell, serve as tracks for the transport of organelles or of chromosomes to opposite ends of the cell during mitosis. Actin filaments or so-called microfilaments are two-stranded helical polymers of the protein actin and have a diameter between 5 and 9 *nm*. Microtubules are long, hollow cylinders which are made of the protein tubulin. Their outer diameter is 25 *nm*, and they are more rigid than actin filaments. Intermediate filaments have a diameter of around 10 *nm* and consist of intermediate filament proteins. The actin and microtubule tracks are used by molecular motors, which themselves are proteins capable of converting chemical energy into mechanical work without going a roundabout way over heat or electrical energy. This chemical energy, which is used in order to generate cellular motility [2], is released in the hydrolysis of adenosine triphosphate (ATP), see 1.1.4.

Linear molecular motors bind to a cytoskeletal filament, transport cargoes as organelles along it or control the movements of filaments, e.g. by causing them to slide against each other. Repeated cycles of ATP hydrolysis provide the energy necessary for a steady movement.

The contributions of molecular motors to the going well of the human body become obvious if they fail to work properly. There are many diseases or defects in the course of which molecular motors play a role [3]. People with Griscelli syndrome (GS) have a mutation in the molecular motor myosin V, which is involved in organelle transport along actin bundles. Melanosomes are badly transferred from the melanocytic cytoplasm toward their neighbouring keratinocytes. Accordingly,



Figure 1.1: Silvery hair due to mutated myosin V [4].

a typical symptom in patients with GS is their silvery hair, see fig. 1.1. Usher's syndrome, to name a second example, is caused by mutations of myosin VII. The typical symptoms of this syndrome are a loss of hearing, night blindness and a loss of peripheral vision.

There are dozens of different motor proteins in every eucaryotic cell. They differ in the types of filaments they bind to, in the direction of movement along them, and in the cargo they carry. The cytoskeletal motor proteins associate with their filaments through a head region, the motor domain, which binds and hydrolyzes ATP. The proteins undergo a cycle of nucleotide hydrolysis and conformational change with states in which they are bound to their filamental tracks and states in which they are unbound. Through a mechanochemical cycle of filament binding, conformational change, filament release, conformational relaxation, and filament rebinding, the motor protein and its cargo move one step at a time along the filament. The motor head determines the motor's track and the direction of movement along it, while the tail determines the cargo and the corresponding biological function. Altogether, there are three groups of cytoskeletal motor proteins. All known motor proteins which move on actin filaments are members of the myosin superfamily, whereas the motor proteins which move on microtubules are members either of the kinesin superfamily or the dynein family [1]. The only structural element shared among all members of each superfamily is the motor head domain. These heads can be attached to a wide variety of tails, which on the other hand attach to different types of cargo and enable the various family members to perform different functions in the cell.

Fig. 1.2 shows a cartoon of the two types of motor proteins which move along microtubules. In general, kinesins move in the direction of the plus end of the microtubule, dyneins move in the minus direction. However, recently, an experimental group has observed mutants of the motor protein kinesin moving in both directions along their filaments [5], and certain myosins also move in another direction along actin than the majority of the myosin family members [6]. Fig. 1.2 illustrates the many different members of the families of the two motor proteins kinesin and dynein. Presumably, each of these different members carries another cargo, and some dyneins even bind to a microtubule on both ends.

1.1.2 Experimental results on the movement of molecular motors

In vitro motility assays with optical tweezers and glass fibers as well as atomic force microscopes have been used to measure the mechanics of cytoskeletal motors bound to their filaments [2]. Motors which are able to move continuously along their filaments are said to be processive. There

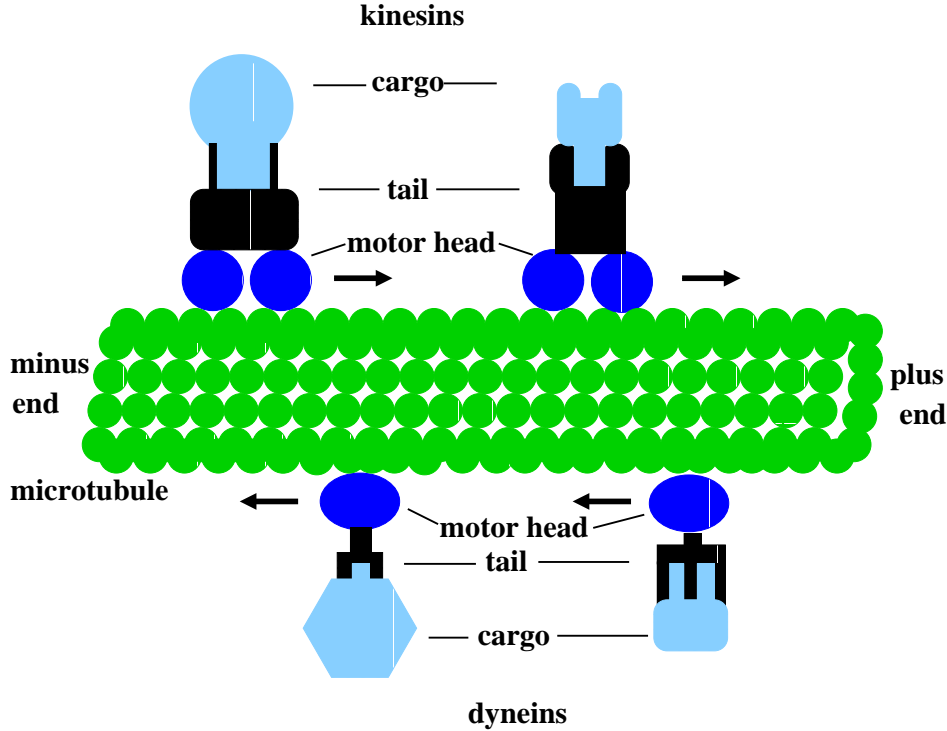


Figure 1.2: The motor proteins of the families kinesin and dynein move along microtubules. This is only a rough cartoon, as naturally-occurring dyneins, e.g., have two or three heads.

have been experiments on two-headed kinesin [7, 8, 9, 10, 11, 12, 13, 14, 15], one-headed kinesin [16], myosin V [17, 18, 19, 20], and dynein [21, 22, 23]. Conventional kinesin, cytoplasmic dynein and myosin V are examples of processive motors.

Several of the experiments on two-headed kinesin have shown that the average motor velocity v increases monotonically with the ATP concentration Γ and exhibits a saturation behaviour for large values of Γ . The hyperbolic form $v(\Gamma) \simeq v_{max}\Gamma/(\Gamma_* + \Gamma)$ has been used to fit the data for zero or small external load forces F [7, 9, 11]. Visscher et al. [15] have assumed force-dependent fit parameters $v_{max}(F)$ and $\Gamma_*(F)$, and have found that the preceding fit is even possible over the whole range of accessible forces, $0 \leq |F| \leq 5.6 pN$, which leads to

$$v(\Gamma, F) \simeq v_{max}(F)\Gamma/[\Gamma_*(F) + \Gamma]. \quad (1.1)$$

Rief et al. as well as Mehta [18, 19] have proposed an analogous relation for the experimental data on myosin V.

1.1.3 Regimes of motor movement and models

Before beginning to model molecular motors, one has to make sure what pieces of information one wants to obtain knowledge on. The starting point for modelling is the differentiation between the three different scales of motor movement as described in the following.

Regime (i) is the regime of the molecular dynamics of a single step. Here, one considers the actual stepping process of the molecular motor in the context of single steps of about $\sim 10 nm$ with corresponding stepping times of $\sim 10 ms$, if there is enough ATP present.

Regime (ii) deals with the directed walk of a motor along a filament. The typical walking distances are in the range of μm and the walking times span seconds.

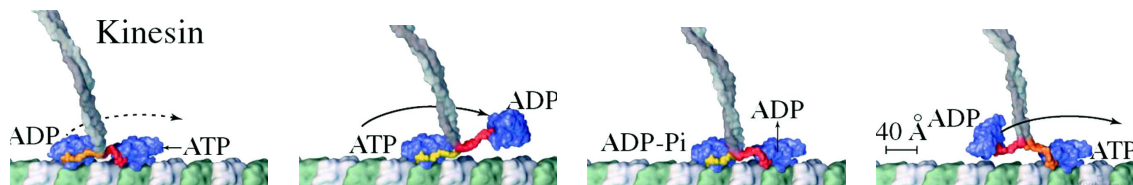


Figure 1.3: Model for the motility cycle of conventional kinesin taken from [28]. The two heads work in a coordinated way to move processively along their filament.

Finally, regime (iii) is concerned with the general topic of intracellular transport. Here, the distances which have to be bridged are many μm or even mm .

Our work deals with the regimes (i) and (ii). We study theoretical models for the motor cycle which governs the short time regime (i) and determine the transport properties for the directed walks of the motor in the intermediate time regime (ii).

Regime (iii) is the topic of [24, 25, 26, 27] and will not be dealt with here.

1.1.4 The mechanochemical cycle of motor proteins

The mechanochemical cycle of the motor proteins is at the root of regime (i). It deals with the question of how the underlying chemistry is coupled to the actual mechanical movement. Water can be added to ATP to form ADP and inorganic phosphate. This hydrolysis of the terminal phosphate of ATP yields between 11 and 13 $kcal/mole$ (around $20 kT/molecule$) of usable energy, depending on the intracellular conditions. Experiments suggest that kinesin spends half of the time of one hydrolysis cycle attached to its filament and the other half detached. At the start of the cycle, one of the two kinesin heads, called the leading head, is bound to the microtubule, while the rear or trailing head is detached. ATP binds to the leading head and causes the rear head to be thrown forward, past the binding site of the attached head, to another binding site further toward the plus end of the microtubule. Release of ADP from the second head and hydrolysis of ATP on the first head, which is now in the rear, brings the dimer back to the original state. Now, the motor protein has moved one step along the filament [1]. The strength of the mechanochemical coupling is a matter of detailed discussions, see 1.2.2.

Fig. 1.3 shows a model for the motility cycle of conventional kinesin, which has been developed by R. D. Vale and R. A. Milligan [28].

1.2 The idea of ratchets

The notion of a ratchet and pawl mechanism was brought up at the beginning of the twentieth century. In a naive approach the second law of thermodynamics seems to be violated with Maxwell's demon having reappeared. Today, there are various modifications of the original ratchet idea, some of which are used in the description of the movements of molecular motors.

1.2.1 History of ratchets

Ever since the discovery of Brownian motion, people have been fascinated by the idea of using thermal fluctuations in order to obtain directed motion, just as on a macroscopic scale the wind drives a windmill in spite of its shifts. It was Smoluchowski, who was the first one to suggest a ratchet and pawl mechanism based on microscopic fluctuations in a conference talk he gave in Münster in 1912 [29].

The heart of Smoluchowski's idea is an axle with paddles at one end and a ratchet and pawl at the other end. A ratchet can be described as a disc with asymmetric saw-teeth. The arrangement as a whole is imagined to be surrounded by a gas under conditions of thermal equilibrium. The random blows of the gas molecules against the paddles can be assumed to cause a rotational

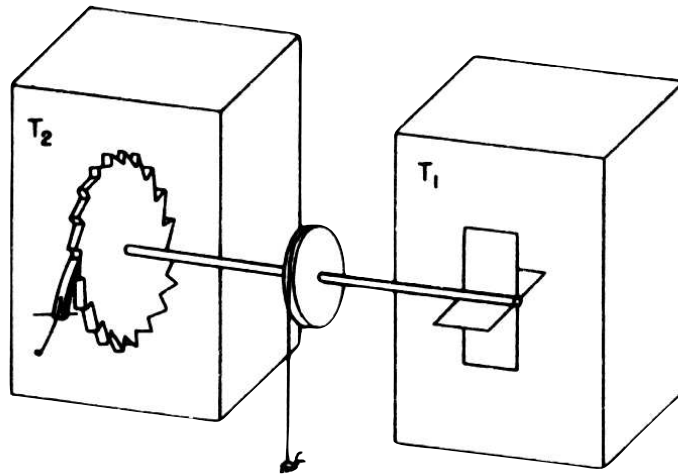


Figure 1.4: Ratchet and pawl system [32]. According to Feynman, the flea can be lifted if the thermal equilibrium is broken with $T_1 > T_2$.

motion. The pawl serves as a rectifier of the random motion, as it prevents the ratchet from backward rotation with a high probability. One might imagine to find a one-way forward rotation on average.

However, this naive idea is wrong. There cannot be a preferred direction of motion, as otherwise one would have constructed a perpetuum mobile of the second kind, which on the other hand would violate the second law of thermodynamics. The mistake is to be found in the mechanism according to which the pawl is assumed to work. The small blows of the gas molecules have to be supposed to be microscopic, therefore the pawl should be extremely small in order to allow for a forward rotation. But under these circumstances, the pawl itself is affected by random thermal fluctuations. The pawl might be lifted, and a backward rotation of the saw-teeth might occur. So on average one will find a balance under conditions of thermal equilibrium which leads to no effective net rotation. Experimental realizations with a triptycene as the ratchet wheel and helicenes as the pawls and springs have shown that there is no net rotation under conditions of thermal equilibrium [30, 31].

In his Lectures on Physics [32], Feynman discusses a situation where the gases surrounding the paddles and the pawl, respectively, do not have the same temperatures. In this extended version of Smoluchowski's idea, see fig. 1.4, he breaks the thermal equilibrium, and concludes that a forward movement is obtained for $T_1 > T_2$, that is, if the temperature of the bath of the paddles is higher than that of the pawl [33]. Then, the flea attached to the string in fig. 1.4 would be lifted, at least as long as the temperatures do not adapt.

1.2.2 Ratchet effect and molecular motors

As explained in 1.2.1, a realization of the concept used in Smoluchowski's gedanken experiment, requires additional ingredients. In general, a ratchet effect is generated when the equilibrium conditions and the spatial inversion symmetry are broken. Fig. 1.5 shows a typical asymmetric ratchet potential. The periodicity of ratchets creates a simple connection to the quite uniform walks of molecular motors along filaments with a regular or even periodic structure on their own. In the case of actin filaments, for example, a pseudorepeat of 37 nm has been identified. So the choice of ratchets in order to describe the potential landscape for the movement of molecular motors is rather obvious.

To explain the directed transport, which molecular motors perform in cells, via a ratchet

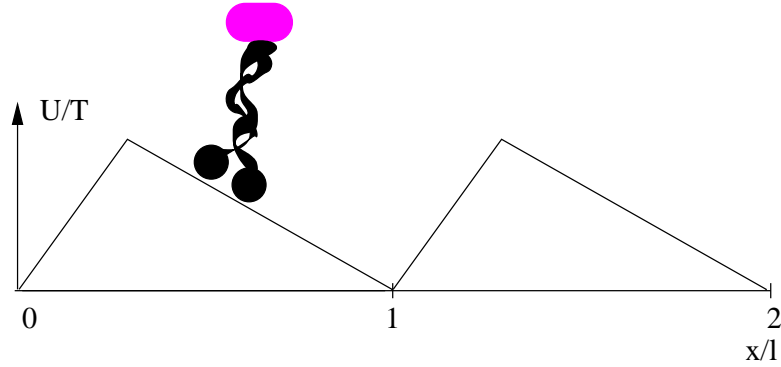


Figure 1.5: The asymmetric potential breaks the spatial inversion symmetry. The cartoon shows a motor carrying a cargo through this potential landscape.

mechanism, one has to focus on the potential landscape they experience and, in addition to that, on the enzymatic activity of the motor, which then breaks the chemical equilibrium. The movements of motors and their enzymatic activities are coupled, and the way this coupling is treated differentiates between different theoretical motor models and has been a matter of debate.

Several models assume a tight coupling including the basic idea that the biochemical cycle is independent of the mechanical movement [34, 35, 36]. The cycle may comprise several conformational states. The movement of the motor is supposed to just follow the cycle.

Models which use uniform ratchets [37, 38, 39] take into account a motor which can attain different internal states and whose degrees of freedom of movement are explicitly considered. Now, the position of the motor is described via a spatial coordinate, while the enzymatic activity is assumed to be independent of the conformation and position.

On the other hand, nonuniform ratchets comprise various internal states as well as the position of the motor, and they consider an enzymatic activity which depends on the spatial position. Their main characteristic are transition rates between the internal states which depend on the spatial coordinate [40, 41].

Besides, there are models with flashing potentials where single potential segments can be switched independently [42]. These models are intermediate between the uniform and nonuniform ratchets.

The approach which is presented in the following uses nonuniform ratchets with M internal states and transitions localized at K locations, see chapter 2 and [43, 44].

Chapter 2

Models for molecular motors

As pointed out in chapter 1, our approach for modelling the directed walks of molecular motors is based on nonuniform stochastic ratchets. These stochastic ratchets are equivalent to diffusion-reaction models or composite Markov processes [45] with space-dependent transition rates. They can be mapped onto stochastic networks of discrete states. Our models can be solved analytically.

2.1 Stochastic models

Our models for molecular motors are based on a Smoluchowski-equation approach. In this section we focus on the basic ingredients of the model and take a look at the time evolution in the multi-state system.

2.1.1 Motor cycles

The cytoskeletal motor proteins associate with their filamental tracks through their head region or motor domain, which binds and hydrolyzes ATP. Coordinated with their cycle of nucleotide hydrolysis and conformational change, the proteins cycle between states in which they are bound strongly to their filament, states in which they are unbound and several intermediate states.

Usually, the mechanochemical cycles of molecular motors are discussed in terms of biochemical reactions and enzyme kinetics, compare the overview in 1.1.4. One then has kinetic pathways which are coupled to the conformational changes of the motor molecule. In our case a pathway denotes a cyclic sequence of molecular conformations which leads to a forward or backward step of the molecular motor along the filament.

2.1.2 Basic ingredients

We use multi-state models with space-dependent transition rates. The basic ingredients are

- (i) a spatial coordinate x which describes the displacement of the centre-of-mass of the motor molecule along the filament,
- (ii) M internal states which represent the various conformations the molecule can attain for a fixed value of x ,
- (iii) K spatial positions per motor cycle at which the motor molecule can undergo transitions between these different internal states [43, 44].

We visualize the meaning of these basic ingredients by taking a second look at fig. 1.3. On the far left, each catalytic core is bound to a tubulin heterodimer along a microtubule. We can say that the motor is in conformation $m = 1$ at location x_1 . It is possible that the motor unbinds or stretches further in both directions along the filament without a change in the centre-of-mass coordinate. In this case the motor would be in the internal state $m = 2$ or $m = 3$ at position x_1 . So, the conformations or states of our models do not necessarily refer to different chemical

conformations in a strict sense, but imply that the motor has somehow changed with respect to its environment.

In the next picture of fig. 1.3, the leading head is still bound, but the second head has moved in the forward direction for 16 nm and is now unbound. The conformation of the motor is again different from the above mentioned, it can be $m = 4$. The centre-of-mass has moved forward to position x_2 . Between this unbound situation and the rebinding in the third picture, the motor head “searches” for the new binding site, so that we can distinguish a couple of subconformations, partly with centre-of-mass coordinates which are different from x_2 or the new one x_3 , 8 nm away from its starting position, in picture three. In the last picture we see that ADP dissociates and ATP binds to the new leading head. If we make a distinction between the two heads, the motor has attained a new conformation once again. After that, the cycle starts again. If there was something different in the second cycle, for example a defect of the filament, we have the choice between not starting at location x_1 again, but introducing further locations, or otherwise starting at x_1 with additional conformations. The second choice is sensible if the lengths of the “substeps” of the cycle are not changed. In general, the distances between the locations x_k where transitions between the states are possible are arbitrary. There are no constraints by a “lattice constant” of any kind.

2.1.3 Langevin and Smoluchowski equation

One of the basic examples of a stochastic process is the Brownian motion of a particle. It is described by the Langevin equation

$$\dot{v} = -\zeta v + f(t). \quad (2.1)$$

In order to explain this equation we imagine a heavy particle whose mass is set to one and which has the velocity v . It moves in a liquid of light particles and receives pushes by the particles of the fluid at random. The pushes cause a slowing-down force $-\zeta v$ with the friction coefficient ζ and the stochastic force $f(t)$.

As a next step, we introduce the probability density

$$P(\xi, t) = \langle \delta(\xi - v(t)) \rangle \quad (2.2)$$

that the Brownian particle has the velocity ξ at time t . The equation of motion for the probability densities is then given by the Fokker-Planck-equation

$$\frac{\partial}{\partial t} P(v, t) = \zeta \frac{\partial}{\partial v} v P(v, t) + \zeta T \frac{\partial^2}{\partial v^2} P(v, t), \quad (2.3)$$

which can also be written as a continuity equation,

$$\frac{\partial}{\partial t} P(v, t) = -\zeta \frac{\partial}{\partial v} \left(-v P(v, t) - T \frac{\partial}{\partial v} P(v, t) \right). \quad (2.4)$$

Here and in the following, we use energy units for the temperature. The current density, which is the part in brackets, contains a drift part and a diffusional part. The equilibrium distribution of the Fokker-Planck equations is the Maxwell distribution with $P(v, t) \propto \exp(-v^2/(2T))$

Now, we have a look at the Brownian motion in an effective external force field $-\partial V(x)/\partial x$. Note that $V(x)$ is proportional to T^{-1} .

The corresponding Langevin equation is

$$\ddot{x} = -\zeta \dot{x} - \frac{\partial V(x)}{\partial x} + f(t). \quad (2.5)$$

The case of a strong damping $\zeta \dot{x} \gg \ddot{x}$ leads to the over-damped Langevin equation

$$\dot{x} = -\frac{D}{T} \frac{\partial V}{\partial x} + r(t) \quad (2.6)$$

with the diffusion coefficient D and the fluctuating force $r(t)$ as given by

$$\begin{aligned} D &\equiv \frac{T}{\zeta}, \\ r(t) &\equiv \frac{1}{\zeta} f(t). \end{aligned} \quad (2.7)$$

In the following we use the probability density

$$P(\xi, t) = \langle \delta(\xi - x(t)) \rangle \quad (2.8)$$

with $P(\xi, t) d\xi$ being the probability of finding the particle at time t at location ξ in the interval $d\xi$. The equation of motion is given by

$$\begin{aligned} \frac{\partial}{\partial t} P(\xi, t) &= -\frac{\partial}{\partial \xi} \langle \delta(\xi - x(t)) \dot{x}(t) \rangle \\ &= -\frac{\partial}{\partial \xi} \left\langle \delta(\xi - x(t)) \left(-\frac{D}{T} \frac{\partial V(\xi)}{\partial \xi} + r(t) \right) \right\rangle \\ &= \frac{\partial}{\partial \xi} \left(\frac{D}{T} P(\xi, t) \frac{\partial V(\xi)}{\partial \xi} \right) - \frac{\partial}{\partial \xi} \langle \delta(\xi - x(t)) r(t) \rangle \end{aligned} \quad (2.9)$$

with

$$\begin{aligned} \langle \delta(\xi - x(t)) r(t) \rangle &= 2D \left\langle \frac{\delta}{\delta r(t)} \delta(\xi - x(t)) \right\rangle \\ &= -2D \frac{\partial}{\partial \xi} \left\langle \delta(\xi - x(t)) \frac{\delta x(t)}{\delta r(t)} \right\rangle \\ &= -D \frac{\partial}{\partial \xi} P(\xi, t). \end{aligned} \quad (2.10)$$

(2.9) and (2.10) yield the Smoluchowski equation

$$\frac{\partial}{\partial t} P(\xi, t) = \frac{\partial}{\partial \xi} \left(\frac{D}{T} P(\xi, t) \frac{\partial V(\xi)}{\partial \xi} \right) + D \frac{\partial^2}{\partial \xi^2} P(\xi, t). \quad (2.11)$$

The Smoluchowski equation on the other hand can be written as a continuity equation,

$$\frac{\partial}{\partial t} P(x, t) = -\frac{\partial}{\partial x} J(x, t) \quad (2.12)$$

with the current

$$J(x, t) = -D \left(\frac{\partial V(x)}{\partial x} + \frac{\partial}{\partial x} \right) P(x, t), \quad (2.13)$$

compare [46, 45, 47].

A stationary solution of the Smoluchowski equation is

$$P(x, t) \propto \exp(-V(x)), \quad (2.14)$$

which leads to a vanishing current. This solution only holds in the case that there are no restrictions of the x -coordinate. In the following, we will use periodic systems where $P(x, t)$ has to fulfill periodic boundary conditions. Nevertheless, the Smoluchowski equation as given by (2.12) can be used to describe the lateral movement for a one-state model of a motor protein, compare chapter 4.1.1, where the periodicity is explicitly imposed.

2.1.4 Time evolution in the multi-state system

In general, we need more than one state to describe the movement of a motor. Actually, it is often necessary to consider more than two states, and accordingly, in contrast to the approaches discussed in [37, 38, 39, 48, 49], we examine multi-state systems. So in our systems, we have a number of M states, and for each of these states we can write down a current equation (2.13), but with level-dependent J_m , D_m , V_m and P_m . Then, we look at the time evolution of the probability densities $P_m(x, t)$ to find the particle or molecular motor at the centre-of-mass coordinate x and in its internal state or level m . The state variable m can attain the M values $m = 1, \dots, M$.

The models include two ingredients by which a change of the probability density $P_m(x)$ may take place, namely

- (i) lateral diffusion within state m , which leads to lateral currents J_m and
- (ii) transitions between the different internal states.

Therefore, the probability densities P_m satisfy the equations

$$\partial P_m(x, t) / \partial t + \partial J_m(x, t) / \partial x = I_m(x, t) \quad (2.15)$$

with the transition current densities I_m and the lateral currents J_m . As we have already pointed out before, the lateral currents J_m have the form (2.13),

$$\begin{aligned} J_m(x, t) &\equiv -D_m \left(\frac{\partial}{\partial x} V_m(x) + \frac{\partial}{\partial x} \right) P_m(x, t) \\ &= -D_m e^{-V_m(x)} \frac{\partial}{\partial x} \left(e^{V_m(x)} P_m(x, t) \right), \end{aligned} \quad (2.16)$$

with the small-scale diffusion coefficient D_m in level m . The friction coefficients are given by T/D_m .

The lateral currents J_m depend on the molecular interaction potentials $U_m(x)$ and on the external force F , which together define the effective force potentials

$$V_m(x) \equiv [U_m(x) - Fx] / T, \quad (2.17)$$

where T is the temperature in energy units. The external force F is an applied tangential force, which might be caused by a cargo. In experimental situations, people use artificial cargoes as beads, which, for example, are held in an optical trap. It is natural to assume periodic and asymmetric molecular interaction potentials $U_m(x)$. The precise shape of the molecular interaction potentials $U_m(x)$ is unknown, though, as these potentials are not accessible to experiments. So, as an example, we might imagine a simple asymmetric ratchet potential as drawn in fig. 1.5. The molecular interaction potentials are assumed to be periodic with the characteristic length scale ℓ representing the potential period, $U_m(x + \ell) = U_m(x)$. In terms of experiments on motor proteins, F is the applied tangential force.

The transition current densities I_m in (2.15) on their parts depend on the transition rate functions Ω_{mn} from state m to state n via

$$I_m(x, t) \equiv \sum_{n, n \neq m} [-P_m(x, t) \Omega_{mn}(x) + P_n(x, t) \Omega_{nm}(x)]. \quad (2.18)$$

The transition rates are localized in space following recent considerations in the context of molecular motors [39, 40, 41], as we assume that the conformational changes of the motor depend on the spatial position, compare 1.2.2, for example given by a localized binding site of the filamental track. In the general case, the transitions can take place between any two states of the system. There is no fixed sequence of transitions.

The transition functions obey $\Omega_{mn}(x) \geq 0$ and are given by

$$\Omega_{mn}(x) \equiv \sum_k \omega_{mn}(x_k) \ell_\Omega \delta(x - x_k), \quad (2.19)$$

so that they are localized at the discrete set of positions $x = x_k$ with $k = 1, \dots, K$ and x_k within the interval $0 \leq x_1 < \dots < x_K < \ell$ [40, 41, 43]. In (2.19), the $\omega_{mn}(x_k) \geq 0$ are transition rates, whereas $\ell_\Omega \ll \ell$ represents a molecular localization length, and $\delta(z)$ is Dirac's delta function.

2.2 General solution for stationary states

Now, the model systems which we have introduced in section 2.1 will be solved for stationary states. Recursion relations for the currents and densities in the system are written down with the use of a transfer matrix formalism. In the end, we obtain a result for the total lateral current, which is proportional to the velocity of the motor particle. A shorter version of this solution procedure is outlined in [43, 44].

2.2.1 Stationary states

Calculating the sum over all M states in (2.18), we find

$$\sum_m I_m(x, t) = 0, \quad (2.20)$$

which is obvious from the structure of (2.18), as each term occurs twice, but the second time with a change in its sign. If the probability densities P_m are stationary with $\partial P_m / \partial t = 0$, we have $\partial P_{tot} / \partial t = 0$ for the total probability $P_{tot} = \sum_m P_m$. Then the total lateral current fulfills $J_{tot} = \sum_m J_m = const$, which is a result of (2.15). We consider such a stationary state, and integrate the expression (2.16) for the lateral currents J_m in the region between x_* and x , which leads to

$$P_m(x) = P_m(x_*) e_m(x_*, x) - \frac{1}{D_m} \int_{x_*}^x dy J_m(y) e_m(x_*, x), \quad (2.21)$$

where we introduce the exponential functions

$$e_m(y, z) \equiv \exp(V_m(y) - V_m(z)) = 1/e_m(z, y), \quad (2.22)$$

which on the other hand depend on the effective force potentials $V_m(x) = [U_m(x) - Fx]/T$ as defined in (2.17). In 2.2.4, equation (2.21) will be evaluated for several choices of the yet unspecified limits x and x_* .

It is clear from their definitions that the exponential functions (2.22) obey the product rule

$$e_m(x_1, x_2) e_m(x_2, x_3) = e_m(x_1, x_3). \quad (2.23)$$

2.2.2 Boundary conditions and normalization

As indicated in fig. 1.5, it stands to reason to choose periodic molecular interaction potentials. The periodicity is an obvious assumption for the rather regular walks of molecular motors with steps and substeps along filaments, which themselves show an inherent periodicity as in the case of the natural pseudorepeat distance of actin. The distances of the sites along the filament where a binding of the motor is most probable are fixed for “normal” filaments and motors. Accordingly, in order to obtain a well-defined stationary state, we restrict ourselves to the finite interval $0 \leq x < \ell$ and use periodic boundary conditions with the box normalization

$$\int_{x_1}^{x_1+\ell} dx P_{tot}(x) = \int_{x_1}^{x_1+\ell} dx \sum_m P_m(x) \equiv 1, \quad (2.24)$$

which implies one particle per box. The size of the box can be identified with the potential period of the periodic potentials $U_m(x)$ or with multiples thereof, so that we have $U_m(x + \ell) = U_m(x)$. The particle velocity v is proportional to the total current with $v = \ell J_{tot}$.

2.2.3 Currents

In (2.19), we have introduced spatially localized transition rates, which are now shown to result in rather simple expressions for the local currents. First of all, we define the local transition current

$$J_{mn}(x_k) \equiv P_m(x_k) \omega_{mn}(x_k) \ell_\Omega \geq 0, \quad (2.25)$$

by which we describe the current from level m to level n at the spatial position x_k .

Then the localized transition rates (2.19) are inserted into the transition current densities I_m as given by (2.18). Integration of the equation $\partial J_m / \partial x = I_m$ yields

$$J_m(x) = \bar{J}_m + \sum_{k=1}^K \Delta J_m(x_k) \theta(x - x_k) \quad (2.26)$$

with spatially independent coefficients \bar{J}_m and with the current discontinuities

$$\Delta J_m(x_k) \equiv \sum_{n, n \neq m} [-J_{mn}(x_k) + J_{nm}(x_k)]. \quad (2.27)$$

θ is Heaviside's step function,

$$\theta(x - x_k) = \begin{cases} 0 & \text{for } x < x_k \\ 1 & \text{for } x > x_k \end{cases}. \quad (2.28)$$

For the sum of the current discontinuities, we have $\sum_m \Delta J_m(x_k) = 0$ for all x_k , because the double sum over m and n again contains each term twice but with opposite sign. Therefore, summation of (2.26) over m leads to a total lateral current $J_{tot} = \sum_m J_m = \sum_m \bar{J}_m$.

According to (2.26), the currents $J_m(x)$ are piecewise constant functions of the spatial coordinate x . The local lateral current $J_m(x_k, x_{k+1})$ between position x_k and position x_{k+1} in level m is given by

$$\begin{aligned} J_m(x_k, x_{k+1}) &= \bar{J}_m + \sum_{q=1}^k \Delta J_m(x_q) \\ &= \bar{J}_m + \sum_{q=1}^k \sum_{n, n \neq m} [-J_{mn}(x_q) + J_{nm}(x_q)]. \end{aligned} \quad (2.29)$$

This relationship is equivalent to

$$J_m(x_k, x_{k+1}) = J_m(x_{k-1}, x_k) + \sum_{n, n \neq m} [-J_{mn}(x_k) + J_{nm}(x_k)], \quad (2.30)$$

which is an obvious consequence of (2.29) written down for $J_m(x_{k-1}, x_k)$.

In summary, we conclude that the systems we have introduced consist of a network of vertices (m, x_k) . These vertices are ordered pairs whose first components are given by the respective internal states m and whose second components are the corresponding spatial positions x_k . Neighbouring vertices are connected via local currents as suggested by (2.29). At each vertex, the sum of all local currents vanishes, which defines a knot rule similar to Kirchhoff's first rule in the case of electric currents.

The networks and their representations as graphs are the topic of the chapters 3 and 4. A listing of the terminology and the basic concepts of graph theory is provided in appendix C. Fig. 2.1 shows an overview of the vertices and their mutual connections via rates in a typical network. For fixed k , each pair of internal states, m and m' , can be connected by a pair of vertical transition rates $\omega_{mn}(x_k)$ and $\omega_{nm}(x_k)$. This means that a motor whose centre-of-mass is at location x_k in conformation $m = 1$ can change into conformation 2 with a certain probability, but also into conformation 3 or 4. This is an extension compared to other models with a fixed sequence of states [50, 51, 52]. Such fixed sequences of states correspond to a special path out of the total number of paths, which the motors can take along the networks in our models.

Now, we anticipate some expressions from the field of graph theory, compare appendix C, which will be used later on. A *graph* G is an ordered 2-tuple, $(V(G), E(G))$, which consists of a set $V(G)$ of vertices and a set $E(G)$ of edges. The arrows in fig. 2.1, which connect two vertices, are called directed edges of the network. A *walk* or an *edge train* in the network of fig. 2.1 is an

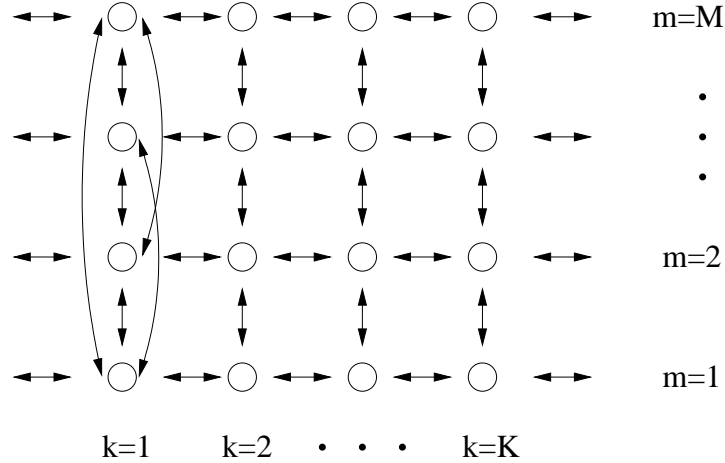


Figure 2.1: Network of discrete motor states represented by vertices (m, x_k) with $1 \leq m \leq M$ and $1 \leq k \leq K$. For fixed m , each pair of adjacent locations k and $k + 1$ is connected by a pair of horizontal rates (see chapter 4 for details concerning the horizontal rates). Since the network is periodic in the horizontal direction, the first column with $k = 1$ and the last column with $k = K$ are connected, too. For fixed k , each pair of internal states, m and m' , is connected by a pair of vertical transition rates $\omega_{mn}(x_k)$ and $\omega_{nm}(x_k)$. For $k = 1$, the representation indicates all vertical transition rates, while otherwise a limited subset is shown for simplicity.

edge sequence with multiplicity one for each edge. The *multiplicity* of an edge in an edge sequence is the number of times an edge appears in an edge sequence. A *path* is a walk for which no vertex occurs twice (the degree of each nonterminal vertex is two and the degree of each terminal vertex is one), and a *cycle* is a closed path [53, 54]. Because of the periodic boundary conditions, any path which starts at vertex $(k = 1, m)$, spans the whole network parallel to the x -direction, and ends at vertex $(k = K, m)$ can be supplemented with the di-edge between $(k = K, m)$ and $(k = 1, m)$ to form a *spanning-cycle* or short *s-cycle*.

In the field of enzyme reactions people talk about a main pathway which is the most important reaction pathway. In the context of our networks, the main pathway can be imagined as an s -cycle starting at $k = 1$ and carrying a maximum current across the network. Nevertheless, there is a certain possibility that the enzyme follows a different pathway. In our extended models we can also include non-chemical influences as defects of the filaments or pushes by other molecules. Furthermore, we can describe backward steps via paths which start at $k = K$. This will be discussed in more detail in chapter 4.

2.2.4 Current-resistance relationships

Now, we take a closer look at the general relations (2.21) which describe the probability densities P_m in terms of the currents J_m . The choice of $x = x_{k+1}$ and $x_* = x_k$ with $k = 1, 2, \dots, K - 1$ yields

$$P_m(x_k) e_m(x_k, x_{k+1}) - P_m(x_{k+1}) = J_m(x_k, x_{k+1}) \mathcal{E}_m(x_k, x_{k+1}). \quad (2.31)$$

The $\mathcal{E}_m(x, y)$ are defined by

$$\mathcal{E}_m(x, y) \equiv \frac{1}{D_m} \int_x^y dz e_m(z, y) = \frac{1}{D_m} \int_x^y dz \exp(V_m(z) - V_m(y)). \quad (2.32)$$

Since the effective force potentials $V_m(x)$ have the general form $V_m(x) = [U_m(x) - Fx]/T$ as indicated in (2.17), the \mathcal{E} -functions depend both on the molecular force potentials $U_m(x)$ and on the applied force F .

In 2.2.3 we have seen that the currents obey a knot rule. Now, we consider relation (2.31) and assume the difference $P_m(x_k) e_m(x_k, x_{k+1}) - P_m(x_{k+1})$ to be the local voltage and the function $\mathcal{E}_m(x_k, x_{k+1})$ to be the local resistance of the networks. The equations (2.31) thus are current-resistance relationships which resemble Ohm's law for electrical circuits. If a molecular interaction potential $U_m(x)$ has a high potential barrier within a given interval $x_k < x < x_{k+1}$, we derive from (2.32) that in this case we will find a large resistance $\mathcal{E}_m(x_k, x_{k+1})$ and, correspondingly, a small current $J_m(x_k, x_{k+1})$.

We consider a vertex (m, x_k) at which all local transition currents $J_{mn}(x_k)$, i.e., the vertical currents given by (2.25), vanish. We have $J_m(x_k, x_{k+1}) = J_m(x_{k-1}, x_k) \equiv J_m^k$. Considering a series combination of the corresponding two resistances $\mathcal{E}_m(x_{k-1}, x_k)$ and $\mathcal{E}_m(x_k, x_{k+1})$, the current-resistance relationships (2.31) with x_{k-1}, x_k and x_k, x_{k+1} , respectively, lead to the equation

$$P_m(x_{k-1}) e_m(x_{k-1}, x_{k+1}) - P_m(x_{k+1}) = J_m^k \mathcal{E}_m(x_{k-1}, x_{k+1}), \quad (2.33)$$

which contains the combined series resistance $\mathcal{E}_m(x_{k-1}, x_{k+1})$ which is calculated from (2.32) as

$$\mathcal{E}_m(x_{k-1}, x_{k+1}) = \mathcal{E}_m(x_{k-1}, x_k) e_m(x_k, x_{k+1}) + \mathcal{E}_m(x_k, x_{k+1}), \quad (2.34)$$

or, if we introduce the modified resistances

$$\mathcal{E}'_m(x, y) = \mathcal{E}_m(x, y) \exp(V_m(y)), \quad (2.35)$$

as

$$\mathcal{E}'_m(x_{k-1}, x_{k+1}) = \mathcal{E}'_m(x_{k-1}, x_k) + \mathcal{E}'_m(x_k, x_{k+1}). \quad (2.36)$$

Thus, the series combination of two modified resistances is the sum of the two single resistances as in the case of electric circuits.

2.2.5 Recursion relation for currents and densities

Now, our aim is to combine the vertex rules (2.30) for the local currents and the current-resistance relationships (2.31) into recursion relations for the local currents and densities.

At first, we consider the vertex rules (2.30) for the local currents and express the local transition currents $J_{mn}(x_k)$ in terms of the probability densities $P_m(x_k)$ as done in (2.25). This yields the recursion relation

$$\begin{aligned} J_m(x_k, x_{k+1}) &= J_m(x_{k-1}, x_k) \\ &+ \sum_{n, n \neq m} [-P_m(x_k) \omega_{mn}(x_k) + P_n(x_k) \omega_{nm}(x_k)] \ell_\Omega, \end{aligned} \quad (2.37)$$

which provides us with a possibility of calculating the outgoing lateral currents $J_m(x_k, x_{k+1})$ from position x_k to x_{k+1} in terms of the incoming lateral currents $J_m(x_{k-1}, x_k)$ and the probability densities $P_m(x_k)$ at location x_k .

We introduce the two transfer matrices \mathbf{T}^{JJ} with

$$T_{nm}^{JJ} \equiv \delta_{nm} \quad (2.38)$$

and $\mathbf{T}^{PJ}(x_k)$ which is given by

$$T_{nm}^{PJ}(x_k) \equiv -\delta_{nm} \sum_{p \neq m} \omega_{mp}(x_k) \ell_\Omega + (1 - \delta_{nm}) \omega_{nm}(x_k) \ell_\Omega. \quad (2.39)$$

In order to further simplify our writing, we define the row vectors $J \equiv (J_1, \dots, J_M)$ and $P \equiv (P_1, \dots, P_M)$. Using this short notation, the recursion relation for the currents (2.37) can be written in the compact form

$$J(x_k, x_{k+1}) = J(x_{k-1}, x_k) \mathbf{T}^{JJ} + P(x_k) \mathbf{T}^{PJ}(x_k) \quad (2.40)$$

where the first transfer matrix \mathbf{T}^{JJ} is equal to the unit matrix according to (2.38).

There is a second set of equations which can be obtained from the current-resistance relations (2.31) and which is needed for the recursion relation for the probability densities. We rewrite (2.31) as

$$P_m(x_{k+1}) = -J_m(x_k, x_{k+1}) \mathcal{E}_m(x_k, x_{k+1}) + P_m(x_k) e_m(x_k, x_{k+1}) \quad (2.41)$$

and obtain a way of calculating the densities $P_m(x_{k+1})$ at location x_{k+1} in terms of the outgoing currents $J_m(x_k, x_{k+1})$ from x_k to x_{k+1} and the densities $P_m(x_k)$ at the former location x_k .

As we want to use the row vectors J and P for a comprehensive formulation of this second set of recursion relations again, we further set up two diagonal matrices \mathbf{D}^{JP} and \mathbf{D}^{PP} with matrix elements

$$D_{nm}^{JP}(x_k, x_{k+1}) \equiv -\delta_{nm} \mathcal{E}_m(x_k, x_{k+1}) \quad (2.42)$$

and

$$D_{nm}^{PP}(x_k, x_{k+1}) \equiv \delta_{nm} e_m(x_k, x_{k+1}). \quad (2.43)$$

Besides, we define the additional transfer matrices

$$\mathbf{T}^{JP} \equiv \mathbf{T}^{JJ} \mathbf{D}^{JP} \quad (2.44)$$

and

$$\mathbf{T}^{PP} \equiv \mathbf{T}^{PJ} \mathbf{D}^{JP} + \mathbf{D}^{PP}. \quad (2.45)$$

With the help of these matrices, the recursion relations (2.41) can be rewritten in the compact form

$$\begin{aligned} P(x_{k+1}) &= J(x_k, x_{k+1}) \mathbf{D}^{JP}(x_k, x_{k+1}) + P(x_k) \mathbf{D}^{PP}(x_k, x_{k+1}) \\ &= J(x_{k-1}, x_k) \mathbf{T}^{JP}(x_k, x_{k+1}) + P(x_k) \mathbf{T}^{PP}(x_k, x_{k+1}), \end{aligned} \quad (2.46)$$

where we have reused (2.40) to obtain the second equation. In this way, we arrive at recursion relations which express the probability densities $P(x_{k+1})$ at x_{k+1} in terms of the incoming currents $J(x_{k-1}, x_k)$, which arrive at location x_k from x_{k-1} , and the probability densities $P(x_k)$ at location x_k .

Finally, the two recursion relations (2.40) and (2.46) for the outgoing currents and the new densities may be united in a single recursion relation given by

$$(J(x_k, x_{k+1}), P(x_{k+1})) = (J(x_{k-1}, x_k), P(x_k)) \mathbf{T}(x_k, x_{k+1}), \quad (2.47)$$

where we have defined the row vector (J, P) with $2M$ components and the $2M \times 2M$ transfer matrix \mathbf{T} which contains the four $M \times M$ transfer matrices \mathbf{T}^{JJ} , \mathbf{T}^{PJ} , \mathbf{T}^{JP} and \mathbf{T}^{PP} .

The system as described so far comprises a set of $2MK$ variables, which is made up of MK lateral currents $J(x_k, x_{k+1})$ and MK probability densities $P(x_k)$. As a result we have characterized a network consisting of MK discrete states.

Now, we focus on a further reduction of the number of variables. To do so, we use the recursion relation (2.47) and express all lateral currents and probability densities in terms of the densities $P_m(x_1)$ of location x_1 and the lateral currents which enter the system from $x < x_1$ (2.26).

Using the notation $\bar{J} \equiv (\bar{J}_1, \dots, \bar{J}_M)$, iteration of (2.47) leads to

$$(J(x_{k-1}, x_k), P(x_k)) = (\bar{J}, P(x_1)) \mathbf{T}^{(k)} \quad (2.48)$$

with the combined transfer matrices

$$\mathbf{T}^{(k)} \equiv \prod_{j=1}^{k-1} \mathbf{T}(x_j, x_{j+1}). \quad (2.49)$$

The combined transfer matrices $\mathbf{T}^{(k)}$ with $k = 2, \dots, K$ relate the local lateral currents $J_m(x_{k-1}, x_k)$ arriving at $x = x_k$ and the densities $P_m(x_k)$ to the average currents \bar{J}_m and the densities $P_m(x_1)$ at location x_1 . We supplement these matrices by the matrix $\mathbf{T}^{(1)}$ which is equal to the unit matrix.

Now, we take a closer look at the separate components of (2.48). The first M components of this equation determine the local lateral currents $J(x_{k-1}, x_k)$ via

$$J_m(x_{k-1}, x_k) = \sum_{i=1}^M \bar{J}_i T_{i,m}^{(k)} + \sum_{i=M+1}^{2M} P_{i-M}(x_1) T_{i,m}^{(k)} \quad (2.50)$$

where $T_{i,m}^{(k)}$ denotes the matrix element of $\mathbf{T}^{(k)}$ in the i th row and the m th column. $J_m(x_{k-1}, x_k)$ is calculated via the elements in column m of $\mathbf{T}^{(k)}$.

The remaining M components of the transfer matrix equation (2.48) determine the densities $P_m(x_k)$ via

$$P_m(x_k) = \sum_{i=1}^M \bar{J}_i T_{i,M+m}^{(k)} + \sum_{i=M+1}^{2M} P_{i-M}(x_1) T_{i,M+m}^{(k)}. \quad (2.51)$$

We notice that the densities $P_m(x_k)$ on the other hand depend on the matrix elements in the $(M+m)$ th column of $\mathbf{T}^{(k)}$.

2.2.6 Implementation of periodic boundary conditions

In 2.2.5 we have come to conclude that in order to solve our problem, we need $2M$ equations which define the $2M$ unknowns \bar{J}_m and $P_m(x_1)$. These equations are provided by the periodic boundary conditions together with the normalization condition. In this subsection we implement the periodic boundary conditions. The normalization condition is treated in 2.2.7.

The system is taken to be periodic in the spatial coordinates x with $0 \leq x < \ell$, see 2.2.2. This implies that the currents and densities satisfy the periodic boundary conditions $J_m(x + \ell) = J_m(x)$ and $P_m(x + \ell) = P_m(x)$ with $x_{K+1} \equiv x_1 + \ell$ per definition.

We start with the periodic boundary conditions for the lateral currents using $J_m(x) = \bar{J}_m + \sum_{k=1}^K \Delta J_m(x_k) \theta(x - x_k)$ as in (2.26). If we now choose $x > x_K$ with $J_m(x) = \bar{J}_m$, we obtain

$$\sum_{k=1}^K \Delta J_m(x_k) / \ell_\Omega = \sum_{k=1}^K \sum_{n, n \neq m} [-P_m(x_k) \omega_{mn}(x_k) + P_n(x_k) \omega_{nm}(x_k)] = 0 \quad \text{for } m = 1, \dots, M. \quad (2.52)$$

The above equation results from inserting (2.25).

Since $\sum_m \Delta J_m(x_k) = 0$ for any value of x_k as explained in 2.2.3, only $M - 1$ of the M equations given by (2.52) are linearly independent. In general, we can choose any subset which contains $(M - 1)$ equations from this set of M equations. However, we can always relabel the internal states so that the omitted equation corresponds to $m = M$. We will assume this to be done and therefore keep the first $(M - 1)$ equations from (2.52).

As announced, in these $(M - 1)$ equations we replace all densities $P_m(x_k)$ with $k \geq 2$ by the average currents \bar{J}_m and the densities $P_m(x_1)$ by using the transfer matrix equations (2.51). In this way, we arrive at a new set of equations as given by

$$\sum_{i=1}^M \bar{J}_i A_{i,m}^{(M,K)} + \sum_{i=M+1}^{2M} P_{i-M}(x_1) A_{i,m}^{(M,K)} = 0 \quad (2.53)$$

with $1 \leq m \leq M - 1$ which defines the first $(M - 1)$ columns of a new matrix $\mathbf{A}^{(M,K)}$ with matrix elements

$$A_{i,m}^{(M,K)} \equiv \sum_{k=1}^K \sum_{n, n \neq m} S(k, m, n) \quad (2.54)$$

and

$$S(k, m, n) \equiv -T_{i,M+m}^{(k)} \omega_{mn}(x_k) + T_{i,M+n}^{(k)} \omega_{nm}(x_k). \quad (2.55)$$

It is noteworthy that each term of the matrix elements $A_{i,m}^{(M,K)}$ in (2.54) contains one explicit factor $\omega_{mn}(x_k)$ or $\omega_{nm}(x_k)$, i.e., in the case of non-vanishing transfer matrix elements each term is proportional to one or more vertical transition rates. In fact, for $K \neq 1$ there is always at least one non-vanishing transfer matrix element $T_{i,j}^{(K)}$ since in a single row of $\mathbf{T}^{(K)}$ there are no M neighbouring columns which contain elements equal to zero.

Now, we take into account the periodic boundary conditions for the densities $P_m(x)$. First, we use equation (2.41) for $k = K$ which leads to

$$P_m(x_{K+1}) = -J_m(x_K, x_{K+1}) \mathcal{E}_m(x_K, x_{K+1}) + P_m(x_K) e_m(x_K, x_{K+1}) \quad (2.56)$$

with $x_{K+1} = x_1 + \ell$ as before. The periodic boundary conditions imply $P_m(x_{K+1}) = P_m(x_1 + \ell) = P_m(x_1)$ and $J_m(x_K, x_{K+1}) = \bar{J}_m$. If this is inserted into (2.56), we obtain, after rearranging the equation,

$$P_m(x_K) = \bar{J}_m \frac{\mathcal{E}_m(x_K, x_{K+1})}{e_m(x_K, x_{K+1})} + P_m(x_1) \frac{1}{e_m(x_K, x_{K+1})}. \quad (2.57)$$

On the other hand, it follows from (2.51) when inserting $k = K$ that

$$P_m(x_K) = \sum_{i=1}^M \bar{J}_i T_{i,M+m}^{(K)} + \sum_{i=M+1}^{2M} P_{i-M}(x_1) T_{i,M+m}^{(K)}. \quad (2.58)$$

Now, if we equate (2.57) and (2.58), we obtain another set of M equations given by

$$\sum_{i=1}^M \bar{J}_i A_{i,M+m-1}^{(M,K)} + \sum_{i=M+1}^{2M} P_{i-M}(x_1) A_{i,M+m-1}^{(M,K)} = 0 \quad (2.59)$$

with $m = 1, \dots, M$. The new elements of the matrix $\mathbf{A}^{(M,K)}$ are given by

$$A_{i,M+m-1}^{(M,K)} \equiv T_{i,M+m}^{(K)} - \delta_{i,m} \frac{\mathcal{E}_m(x_K, x_{K+1})}{e_m(x_K, x_{K+1})} \quad \text{for } 1 \leq i \leq M \quad (2.60)$$

and by

$$A_{i,M+m-1}^{(M,K)} \equiv T_{i,M+m}^{(K)} - \frac{\delta_{i-M,m}}{e_m(x_K, x_{K+1})} \quad \text{for } M+1 \leq i \leq 2M. \quad (2.61)$$

According to (2.49), the combined transfer matrix $\mathbf{T}^{(K)}$ is a product of transfer matrices $\mathbf{T}(x_j, x_{j+1})$ with $j \leq K-1$. The latter transfer matrices depend on the local transition currents $J_{mn}(x_k)$ with $k \leq K-1$ but are independent of the local transition currents $J_{mn}(x_K) \equiv P_m(x_K) \omega_{mn}(x_K) \ell_\Omega$. Therefore, the combined transfer matrix $\mathbf{T}^{(K)}$ is independent of these latter currents, too. This implies that the matrix elements $A_{i,M+m-1}^{(M,K)}$ in (2.60) and (2.61) do not depend on the vertical transition rates $\omega_{mn}(x_K)$.

2.2.7 Implementation of normalization condition

As we have shown in 2.2.6, the periodic boundary conditions lead to $2M-1$ linearly independent equations which are provided by (2.53) and (2.59). In order to determine the $2M$ variables \bar{J}_m and $P_m(x_1)$ unambiguously, we need one additional equation which is supplied by the normalization condition.

When the explicit form of the densities and currents is inserted into the normalization condition (2.24), we obtain the expression

$$1 = \sum_m \left[P_m(x_1) \bar{e}_m - \bar{J}_m \bar{\mathcal{E}}_m(x_1) - \sum_{k=1}^K \Delta J_m(x_k) \bar{\mathcal{E}}_m(x_k) \right], \quad (2.62)$$

which depends on the integrals

$$\bar{e}_m \equiv \int_{x_1}^{x_1+\ell} dx e_m(x_1, x) \quad (2.63)$$

and

$$\bar{\mathcal{E}}_m(x_k) \equiv \int_{x_k}^{x_1+\ell} dx \mathcal{E}_m(x_k, x). \quad (2.64)$$

The normalization condition (2.62) contains the current discontinuities $\Delta J_m(x_k)$ for all k . However, it follows from the relation (2.52) that

$$\Delta J_m(x_K) = - \sum_{k=1}^{K-1} \Delta J_m(x_k). \quad (2.65)$$

When this relation is inserted into (2.62), we obtain

$$\sum_m \left[-\bar{J}_m \bar{\mathcal{E}}_m(x_1) + P_m(x_1) \bar{e}_m - \sum_{k=1}^{K-1} \Delta J_m(x_k) \bar{\mathcal{D}}_m(x_k) \right] = 1 \quad (2.66)$$

with

$$\bar{\mathcal{D}}_m(x_k) \equiv \bar{\mathcal{E}}_m(x_k) - \bar{\mathcal{E}}_m(x_K). \quad (2.67)$$

Since this equation no longer involves the current discontinuities $\Delta J_m(x_K)$ at location x_K , it does not depend on the transition rate constants $\omega_{mn}(x_K)$.

The current discontinuities $\Delta J_m(x_k)$ with $1 \leq k \leq K-1$ can be expressed in terms of the densities $P_m(x_k)$ via (2.27) and (2.25). These densities on the other hand can be expressed in terms of the variables \bar{J}_m and $P_m(x_1)$ using the transfer matrix relations (2.51).

In this way we get the equation

$$\sum_{i=1}^M \bar{J}_i A_{i,2M}^{(M,K)} + \sum_{i=M+1}^{2M} P_{i-M}(x_1) A_{i,2M}^{(M,K)} = 1, \quad (2.68)$$

which defines the last or $2M$ th column of the matrix $\mathbf{A}^{(M,K)}$ with elements

$$A_{i,2M}^{(M,K)} \equiv -\bar{\mathcal{E}}_i(x_1) - \sum_{k=1}^{K-1} \sum_m \sum_{n, n \neq m} S(k, m, n) \bar{\mathcal{D}}_m(x_k) l_\Omega \quad \text{for } 1 \leq i \leq M \quad (2.69)$$

and

$$A_{i,2M}^{(M,K)} \equiv \bar{e}_{i-M} - \sum_{k=1}^{K-1} \sum_m \sum_{n, n \neq m} S(k, m, n) \bar{\mathcal{D}}_m(x_k) l_\Omega \quad \text{for } M+1 \leq i \leq 2M \quad (2.70)$$

with $S(k, n, m)$ as defined in (2.55).

2.2.8 Calculation of the total current

As all lateral currents and probability densities can be described in terms of the $2M$ densities $P_m(x_1)$ and the lateral currents \bar{J}_m which enter the system from $x < x_1$, we have

$$[\bar{J}, P(x_1)] = [0, \dots, 0, 1] \left(\mathbf{A}^{(M,K)} \right)^{-1} = [0, \dots, 0, 1] \frac{\mathbf{C}}{\det \mathbf{A}^{(M,K)}}, \quad (2.71)$$

where $\mathbf{A}^{(M,K)}$ is a $2M \times 2M$ matrix as explained in the preceding sections. The matrix elements of \mathbf{C} are the cofactors $C_{ij} \equiv (-1)^{i+j} \det \mathbf{A}^{(M,K)}[j, i]$, where $\mathbf{A}^{(M,K)}[j, i]$ is the $(2M-1) \times (2M-1)$

matrix obtained from $\mathbf{A}^{(M,K)}$ by erasing its j th row and i th column. Each of the first $M - 1$ columns of $\mathbf{A}^{(M,K)}$ corresponds to the periodic boundary condition for one lateral current J_m , each of the next M columns to the periodic boundary condition for one density P_m and the last one to the normalization condition. The total current $J_{tot}^{(M,K)} = \sum_{m=1}^M \bar{J}_m$ which determines the motor velocity $v^{(M,K)}$ via $v^{(M,K)} = \ell J_{tot}^{(M,K)}$ is

$$J_{tot}^{(M,K)} = \sum_{m=1}^M \bar{J}_m = \sum_{m=1}^M (-1)^{2M+m} \det \mathbf{A}^{(M,K)} [m, 2M] / \det \mathbf{A}^{(M,K)}. \quad (2.72)$$

As we use algebraic computer systems [55], which soon reach their limitations in complex matrix calculations, computing the complete inverse matrix $(\mathbf{A}^{(M,K)})^{-1}$ is often impossible so that we generally confine ourselves to the calculation of the elements contributing to $J_{tot}^{(M,K)}$ as explained above.

It is convenient to write

$$J_{tot}^{(M,K)} = \frac{Pol_1^{(M,K)}(\omega_{12}(x_1), \omega_{12}(x_2), \dots, \omega_{(M-1)M}(x_K))}{Pol_2^{(M,K)}(\omega_{12}(x_1), \omega_{12}(x_2), \dots, \omega_{(M-1)M}(x_K))} \quad (2.73)$$

with two polynomials $Pol_1^{(M,K)}$ and $Pol_2^{(M,K)}$ which depend on the vertical transition rates of the respective model. In chapter 3 we will calculate and characterize the total current and the two polynomials for various model systems.

Chapter 3

Results for various (M, K) -models and universal rules

In chapter 2 we have shown that our stochastic ratchets can be mapped onto stochastic networks of MK discrete states, which are represented by their respective vertices (m, x_k) , where m is the coordinate of the state or level, and x_k is the spatial coordinate.

Here, we present a detailed investigation of models with explicitly specified values of M and K [44]. The maximal number of states as well as the number of locations in these models varies between one and four. In this way we show that our general class of models has the advantage of comprising the possibility of describing the movements of a variety of different motor proteins. At first, we calculate the resulting total current $J_{tot}^{(M,K)}$ for each of these models, then we take a closer look at the various terms which contribute to the current and their dependence on the vertical transition rates of the model. We also discuss conceivable implications of these models in terms of the mechanochemical cycles of molecular motors and their structures. Several rules concerning the matrices $\mathbf{A}^{(M,K)}$ and the total current $J_{tot}^{(M,K)}$, which is calculated with the help of these matrices, can be derived. These rules impose constraints on the terms contributing to the current, so that if we have a network with a specified number of states and locations, we can list the combinations of vertical rates occurring in the terms of $J_{tot}^{(M,K)}$ without actually calculating the matrix $\mathbf{A}^{(M,K)}$ for this special case. Furthermore, we examine ratchets with several explicitly unbalanced transitions, which can arise from the enzymatic activity of the motor. With the help of the rules for the current we can predict possible simplifications in the dependence of the motor velocity on these unbalanced rates, too.

3.1 Examples of (M, K) -models

Here, we investigate models with different values of M and K . The inspected models comprise one to four states and one to four locations. We focus on the question of how the vertical transition rates enter the total current, which is the quotient of the two polynomials $Pol_1^{(M,K)}$ and $Pol_2^{(M,K)}$. Mainly, we centre on the terms of $Pol_1^{(M,K)}$ as they correspond to paths through the network, whereas $Pol_2^{(M,K)}$ provides a standardization of the total current with respect to the set of vertical rates which actually occur in the present model.

3.1.1 The special case of a single internal state

In the case of a *single internal state*, there are no vertical transition rates, i.e., the state is fixed. We have diffusion within this state, and there can be a periodic landscape described by the state's effective force potential, but no chemical reaction or conformational change. Without an external force the motor might find itself in a situation as the one depicted in fig. 1.5. The

single-state situation applies to a motor which is for some reason cut off its supply of fuel and whose conformation is fixed. The fixed conformation might be a consequence of the lack of fuel, but it can also result from a genetic defect.

The corresponding matrix $\mathbf{A}^{(1,K)}$ is a 2×2 matrix whose elements depend on the effective force potential $V_1(x)$, the small-scale diffusion coefficient D_1 and the spatial positions x_k . In the case of a single location, i.e., $K = 1$, $\mathbf{A}^{(1,1)}$ reads

$$\mathbf{A}^{(1,1)} = \begin{pmatrix} -\mathcal{E}_1(x_1, x_1 + \ell)/e_1(x_1, x_1 + \ell) & -\bar{\mathcal{E}}_1(x_1) \\ 1 - 1/e_1(x_1, x_1 + \ell) & \bar{e}_1 \end{pmatrix} \quad (3.1)$$

with $\mathcal{E}_1(x_1, x_1 + \ell)$, $e_1(x_1, x_1 + \ell)$, $\bar{\mathcal{E}}_1(x_1)$ and \bar{e}_1 as defined in chapter 2. The total current $J_{tot}^{(1,1)}$ is calculated as

$$J_{tot}^{(1,1)} = \frac{1 - e_1(x_1, x_1 + \ell)}{(e_1(x_1, x_1 + \ell) - 1)\bar{\mathcal{E}}_1(x_1) - \mathcal{E}_1(x_1, x_1 + \ell)\bar{e}_1}. \quad (3.2)$$

This current vanishes in the absence of an external force for all single state models, no matter what is the choice of K , as there cannot be a net current with a single fixed molecular interaction potential. This is obvious in 3.2, since in this case we have $e_1(x_1, x_1 + \ell) = \exp(U_1(x_1) - U_1(x_1)) = 1$.

If there is a finite external force, while the molecular interaction potential vanishes, the total current reads

$$J_{tot}^{(1,1)}(U_1 = 0) = \frac{FD_1}{\ell T}, \quad (3.3)$$

This relationship will be explained further in 4.1.1.

3.1.2 Results for two internal levels

A model with *two internal states* can describe a one-headed motor which has the chance to change between a state where its binding to the filament is strong and a state where this binding is weak or where it is even unbound, though still only free to move in the x -direction. Then we say that the motor is in state one, if its conformation is the conformation of strong binding, and in state two for the case of weak or no binding at all. As the labelling of the states is arbitrary, the two conformations might be classed with swapped numbers.

The two-state model also works for a simple two-headed motor with a strong cooperation so that the rebinding of the momentarily unbound head correlates with the ATP-adsorption of the bound head. In this case the two levels correspond to the first head unbound and the second head unbound, respectively.

Two states and one or two locations

For *two internal states* and *one spatial position*, the number of possible vertical transition rates is limited to two, namely $\omega_{12}(x_1)$ and $\omega_{21}(x_1)$. We might imagine a motor which binds ATP at location x_1 , changes its conformation to $m = 2$, but whose movement is blocked by an obstacle, so that it falls back into state $m = 1$ without having performed an effective movement in the second state. Of course, the two states might be swapped again.

In the following, $A_{ij}^{(M,K)}$ denotes the element in row i and in column j of the matrix $\mathbf{A}^{(M,K)}$. The vertical rates $\omega_{12}(x_1)$ and $\omega_{21}(x_1)$ occur in the matrix elements $A_{31}^{(2,1)}$ and $A_{41}^{(2,1)}$ of the 4×4 matrix $\mathbf{A}^{(2,1)}$. This means in a more general formulation that we have $\omega_{12}(x_1)$ in row $M + 1$ and $\omega_{21}(x_1)$ in row $M + 2$:

$$\begin{pmatrix} 0 & -\frac{\mathcal{E}_1(x_1, x_1 + \ell)}{e_1(x_1, x_1 + \ell)} & 0 & -\bar{\mathcal{E}}_1(x_1) \\ 0 & 0 & -\frac{\mathcal{E}_2(x_1, x_1 + \ell)}{e_2(x_1, x_1 + \ell)} & -\bar{\mathcal{E}}_2(x_1) \\ -\omega_{12}(x_1) & 1 - \frac{1}{e_1(x_1, x_1 + \ell)} & 0 & \bar{e}_1 \\ \omega_{21}(x_1) & 0 & 1 - \frac{1}{e_2(x_1, x_1 + \ell)} & \bar{e}_2 \end{pmatrix}. \quad (3.4)$$

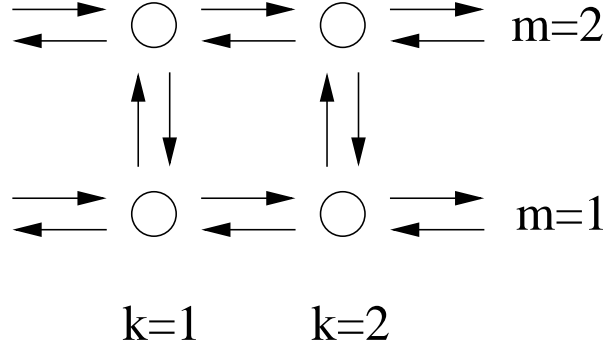


Figure 3.1: Network representation for $(M, K) = (2, 2)$. In this general model, there are four vertical transition rates connecting the two states.

If there is no external force, $F = 0$, the total current $J_{tot}^{(2,1)}$ vanishes as expected from the idea of the blocked motor above. There is no ratchet effect present, the switching back to the original state takes place at the same position.

For an external force $F \neq 0$, the polynomials $Pol_1^{(2,1)}$ and $Pol_2^{(2,1)}$ which enter the total current as explained in chapter 2, consist of terms containing a single vertical transition rate. Squares (or higher powers) or products of the two rates do not occur. Here, a net movement can occur because of the external force, which might even be effective against hindrances.

For **two states** and **two locations**, we have a maximum number of four possible vertical transition rates. The network situation is outlined in fig. 3.1, visualize fig. 2.1 for comparison, too. The matrix $\mathbf{A}^{(2,2)}$ reads

$$\left(\begin{array}{cccc}
 \mathcal{E}_1(x_1, x_2) \omega_{12}(x_2) & -\frac{\mathcal{E}_1(x_1, x_2)}{\mathcal{E}_1(x_2, x_1 + \ell)} & 0 & -\bar{\mathcal{E}}_1(x_1) \\
 -\mathcal{E}_2(x_1, x_2) \omega_{21}(x_2) & 0 & -\frac{\mathcal{E}_2(x_1, x_2)}{e_2(x_2, x_1 + \ell)} & -\bar{\mathcal{E}}_2(x_1) \\
 -\omega_{12}(x_2) [\omega_{12}(x_1) \ell_\Omega \cdot \mathcal{E}_1(x_1, x_2) + e_1(x_1, x_2)] - \omega_{12}(x_1) \ell_\Omega \cdot \mathcal{E}_2(x_1, x_2) & \omega_{12}(x_1) \ell_\Omega \cdot \mathcal{E}_1(x_1, x_2) + e_1(x_1, x_2) & -\omega_{12}(x_1) \ell_\Omega \cdot \mathcal{E}_2(x_1, x_2) & \bar{e}_1 + \omega_{12}(x_1) \cdot [\bar{\mathcal{E}}_1(x_1) - \bar{\mathcal{E}}_1(x_2)] \cdot \ell_\Omega - \omega_{12}(x_1) \cdot [\bar{\mathcal{E}}_2(x_1) - \bar{\mathcal{E}}_2(x_2)] \ell_\Omega \\
 \omega_{21}(x_2) [\omega_{21}(x_1) \ell_\Omega \cdot \mathcal{E}_2(x_1, x_2) + e_2(x_1, x_2)] + \omega_{21}(x_1) \ell_\Omega \cdot \mathcal{E}_1(x_1, x_2) & -\omega_{21}(x_1) \ell_\Omega \cdot \mathcal{E}_1(x_1, x_2) + e_2(x_1, x_2) & \omega_{21}(x_1) \ell_\Omega \cdot \mathcal{E}_2(x_1, x_2) + e_2(x_1, x_2) & \bar{e}_2 - \omega_{21}(x_1) \cdot [\bar{\mathcal{E}}_1(x_1) - \bar{\mathcal{E}}_1(x_2)] \cdot \ell_\Omega + \omega_{21}(x_1) \cdot [\bar{\mathcal{E}}_2(x_1) - \bar{\mathcal{E}}_2(x_2)] \ell_\Omega
 \end{array} \right) \quad (3.5)$$

Each term in the first column of $\mathbf{A}^{(2,2)}$ is proportional to at least one vertical transition rate. The incidence of $\omega_{12}(x_1)$ is restricted to the third row of the matrix $\mathbf{A}^{(2,2)}$, whereas $\omega_{21}(x_1)$ can only be found in row four. Vertical rates belonging to location x_K are restricted to the first column.

The terms of the polynomials $Pol_1^{(M,K)}$ and $Pol_2^{(M,K)}$, which are products containing the verticals transition rates, will be named \mathcal{T} in the following. The polynomials $Pol_1^{(2,2)}$ and $Pol_2^{(2,2)}$ for arbitrary F are found to be multilinear in the vertical transition rates $\omega_{mn}(x_k)$ with $m, n = 1, 2$

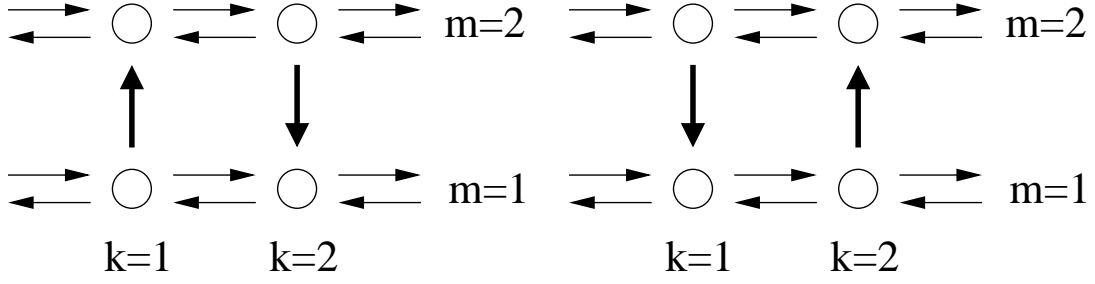


Figure 3.2: The two different combinations of vertical rates which occur in $Pol_1^{(2,2)}$ for $F = 0$ in the $(M, K) = (2, 2)$ -case, see (3.6). Left: the combination $\omega_{12}(x_1)\omega_{21}(x_2)$ (bold). In order to obtain complete paths, we have to add horizontal rates, compare 4.3 for details. The thin di-edges show the complete set of horizontal rates in the system. If we start at $x < x_1$ in state $m = 1$, follow the di-edge $\omega_{12}(x_1)$, take the horizontal rate leading from x_1 to x_2 in state $m = 2$ and then follow $\omega_{21}(x_2)$ back into state $m = 1$, the left combination belongs to a forward cycle in positive x -direction. Starting at $x > x_2$ in state $m = 2$, changing into state $m = 1$ with $\omega_{21}(x_2)$ and going from location x_2 to x_1 in the first state, we obtain a backward cycle. Right: the combination $\omega_{21}(x_1)\omega_{12}(x_2)$ (bold). This combination occurs in a forward and a backward-cycle, too.

and $k = 1, 2$, i.e., the rates occur as $\omega_{mn}^z(x_k)$ with $z = 0$ or $z = 1$. The degree of the polynomials in the $\omega_{mn}(x_k)$ with m, n and k as above varies between one and two, so that each term contains one or two vertical transition rates.

For $F \neq 0$, there are eight different combinations of vertical rates, the four one-rate combinations with $\omega_{12}(x_1)$, $\omega_{21}(x_1)$, $\omega_{12}(x_2)$ and $\omega_{21}(x_2)$ and then the four two-rate combinations $\omega_{12}(x_1)\omega_{21}(x_2)$, $\omega_{12}(x_1)\omega_{12}(x_2)$, $\omega_{21}(x_1)\omega_{12}(x_2)$ and $\omega_{21}(x_1)\omega_{21}(x_2)$. The two combinations $\omega_{12}(x_1)\omega_{21}(x_1)$ and $\omega_{12}(x_2)\omega_{21}(x_2)$ connecting the two states at one location do not occur.

We take a closer look at the numerator polynomial $Pol_1^{(2,2)}$ for $F = 0$. There are four terms with two different combinations of two vertical transition rates. These combinations are illustrated in fig. 3.2. We have

$$\begin{aligned}
 Pol_1^{(2,2)} &= a_1\omega_{12}(x_1)\omega_{21}(x_2) - a_2\omega_{12}(x_1)\omega_{21}(x_2) \\
 &\quad + b_1\omega_{12}(x_2)\omega_{21}(x_1) - b_2\omega_{12}(x_2)\omega_{21}(x_1)
 \end{aligned} \tag{3.6}$$

with coefficients a_i and b_i which contain the respective $e_m(x_k, x_l)$, $\mathcal{E}_m(x_k, x_l)$ and ℓ_Ω . The terms with a minus sign belong to backward combinations. Then the motor takes a step in the negative x -direction. The combination $\omega_{12}(x_1)\omega_{21}(x_2)$, e.g., describes a forward path starting in the first level (first term) and a backward path starting in level two at $x > x_2$ (second term).

The rest of the combinations of two rates, $\omega_{12}(x_1)\omega_{21}(x_1)$, $\omega_{12}(x_2)\omega_{21}(x_2)$, $\omega_{12}(x_1)\omega_{12}(x_2)$ and $\omega_{21}(x_1)\omega_{21}(x_2)$, vanish for $F = 0$ as well as the terms with a single vertical transition rate. The remaining terms in (3.6) contain the combinations $\omega_{12}(x_1)\omega_{21}(x_2)$ or $\omega_{21}(x_1)\omega_{12}(x_2)$. These two combinations of vertical rates can be supplemented with the accompanying horizontal rates to form s-cycles (see 2.2.3). This supplementation with horizontal rates will be tacitly assumed in the following. In section 4.3 the horizontal rates will be considered explicitly, too. We keep in mind that an s-cycle is a path of di-edges which starts at vertex $(k = 1, m)$, i.e., with an arbitrary conformation, spans the whole network parallel to the x -direction, and ends at vertex $(k = K, m)$ to be supplemented with the di-edge between $(k = K, m)$ and $(k = 1, m)$. Concentrating on the vertical di-edges of the term this means that we have a combination $\omega_{mn}(x_i)\omega_{no}(x_j)\dots\omega_{pq}(x_k)\omega_{qm}(x_l)$ leading from state m back to state m with at least to different locations i, j, \dots, k or l .

In a situation where we have no external force and no enzymatic activity, the corresponding vertical transition rates fulfill the condition of detailed balance,

$$\omega_{mn}^{db}(x_k) = e^{V_m(x_k) - V_n(x_k)} \omega_{nm}^{db}(x_k). \tag{3.7}$$

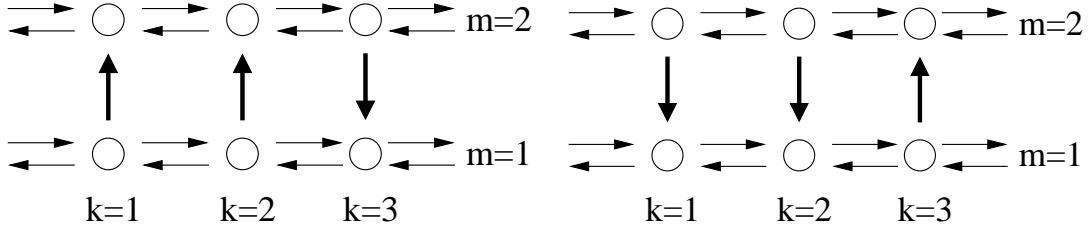


Figure 3.3: The six different three-rate combinations in $Pol_1^{(2,3)}$ for $F = 0$ can be derived from the above shown two combinations by cyclic permutations of the rates with respect to the locations. The three combinations derived from the left combination have two upward rates, the three derived from the right two downward rates. All of these combinations contain an s-cycle of the type $\omega_{12}(x_k)\omega_{21}(x_l)$ with $k \neq l$. As these are the terms for $F = 0$, the combination which contains only upward rates and the combination with three downward rates do not occur.

Then, each individual transition is balanced, and the incoming rates balance the outgoing rates for every vertex (m, x_k) of our network. In this case we obtain $Pol_1^{(2,2)} = 0$ for $F = 0$, i.e., the total current $J_{tot}^{(2,2)}$ vanishes. Terms in (3.6) which comprise $\omega_{12}(x_1)\omega_{21}(x_2)$ cancel with terms originally including the s-cycle $\omega_{21}(x_1)\omega_{12}(x_2)$ with opposite directionality. So if detailed balance is fulfilled, the first term in (3.6) cancels with the last one and the second one with the third.

Properties of $Pol_1^{(2,3)}$ and $Pol_2^{(2,3)}$

The elements of the matrix $\mathbf{A}^{(2,3)}$ for the case of *two internal states* and *three spatial positions* are listed in appendix A.1.

Altogether, there are six different vertical transition rates $\omega_{12}(x_k)$ and $\omega_{21}(x_k)$ with $k = 1, 2, 3$. For $F \neq 0$, the terms \mathcal{T} of the polynomials $Pol_1^{(2,3)}$ and $Pol_2^{(2,3)}$ comprise between one and three vertical transition rates.

There are 26 different combinations of vertical rates in the polynomials $Pol_1^{(2,3)}$ and $Pol_2^{(2,3)}$ for $F \neq 0$. These are the six combinations with a single rate, twelve combinations with two rates and eight with three rates. Again, combinations with rates connecting the two states in different directions at one location are missing.

For $F = 0$, the polynomial $Pol_1^{(2,3)}$ reduces to twelve different combinations of vertical rates, all of which include an s-cycle of the type $\omega_{mn}(x_k)\omega_{nm}(x_l)$ with $k \neq l$ and $m \neq n$, and six of these contain two vertical transition rates, the other six comprise three of them. The six three-rate combinations can be derived from the two combinations shown in fig. 3.3 by cyclic permutations of the rates with respect to the locations. The figure on the left provides us with the three combinations $\omega_{12}(x_1)\omega_{12}(x_2)\omega_{21}(x_3)$, $\omega_{12}(x_1)\omega_{21}(x_2)\omega_{12}(x_3)$ and $\omega_{21}(x_1)\omega_{12}(x_2)\omega_{12}(x_3)$.

Total current: properties of $Pol_1^{(2,4)}$ and $Pol_2^{(2,4)}$

For *two internal states* and *four spatial positions* the corresponding matrix $\mathbf{A}^{(2,4)}$ is given in appendix A.2.

The eight different vertical transition rates occur in $Pol_1^{(2,4)}$ and $Pol_2^{(2,4)}$ for arbitrary F in terms including one to four rates. We focus on summands with four vertical transition rates. There are $\binom{8}{4} = 70$ possibilities of choosing four rates out of a total number of eight. Actually, $Pol_1^{(2,4)}$ and $Pol_2^{(2,4)}$ contain the limited number of 16 different combinations of four vertical rates. These combinations consist of four rates at four different locations. There is one combination without an upward rate and a second one without a downward rate. There are four combinations each with one or three upward rates, and there are six combinations with two rates pointing upwards. Altogether this sums up to $1 + 1 + 4 + 4 + 6 = 16$ different combinations. In analogy to the

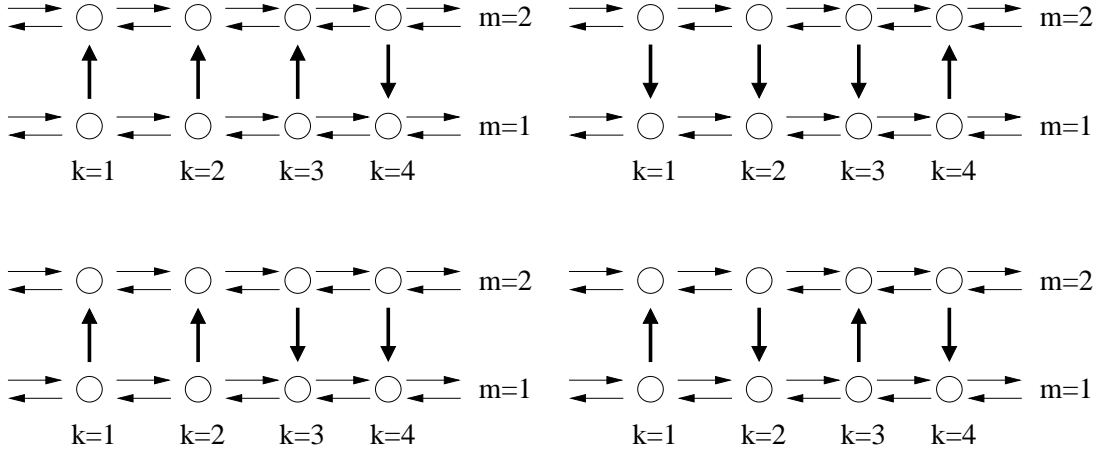


Figure 3.4: The 14 different four-rate combinations in $Pol_1^{(2,4)}$ for $F = 0$ can be derived from the above four combinations by cyclic permutations of the rates with respect to the locations. From the upper left combination we derive four combinations with three upward rates. The upper right combination leads to four combinations with three rates pointing downwards. The two combinations at the bottom imply three combinations each, all of them with two upward and two downward rates.

previous models we conclude that combinations with $\omega_{mn}(x_k)\omega_{nm}(x_k)$, i.e., two rates connecting the two states in opposite directions at one location, do not appear. Such a cycle of vertical rates restricted to a single location, whose extended form is $\omega_{mn}(x_k)\omega_{no}(x_k)\omega_{op}(x_k)\dots\omega_{rm}(x_k)$, will be called a *localized* or *l-cycle* in the following.

In the case of $F = 0$, the terms of two to four vertical transition rates which appear in $Pol_1^{(2,4)}$ can be mapped onto one or two s-cycles of the type $\omega_{mn}(x_k)\omega_{nm}(x_l)$ with $k \neq l$. For $F = 0$ the number of different combinations of four rates reduces to 14, as the combination with all four rates pointing upwards as well as the combination with all four rates pointing downwards do not occur, because they do not contain an s-cycle. The 14 different four-rate combinations in $Pol_1^{(2,4)}$ for $F = 0$ can be derived from the combinations displayed in fig. 3.4 if we use cyclic permutations of the rates with respect to the locations.

3.1.3 Model with three states

One interpretation of a model with *three internal states* is that of a two-headed motor with a doubly-bound state, in which both heads are bound to the filament, and two excited states with one of the two heads unbound, respectively. We might also imagine a motor with a single head and a state of strong binding, a loosely bound state and an unbound state, where nevertheless the movement is limited to the direction of the filament.

Three states and one or two locations

The polynomials $Pol_1^{(3,1)}$ and $Pol_2^{(3,1)}$ for arbitrary F in the case of *three internal states* and *one spatial position* contain two vertical transition rates per term. The total number of conceivable vertical rates in a certain network is in general $M(M-1)K$, which results in six in the present case, compare fig. 2.1. For $F = 0$, $Pol_1^{(3,1)}$ vanishes equal to zero.

For *three internal states* and *two spatial positions*, the elements of the matrix $\mathbf{A}^{(3,2)}$ are listed in appendix A.3. Concentrating on the vertical rates $\omega_{mn}(x_1)$ at the first location, we see that the occurrence of $\omega_{1n}(x_1)$ is restricted to row four, while $\omega_{2n}(x_1)$ occurs in row five (and nowhere else), and $\omega_{3n}(x_1)$ can only be found in row six. The rates $\omega_{12}(x_2)$ and $\omega_{21}(x_2)$ as well

as $\omega_{21}(x_2)$ and $\omega_{12}(x_2)$ are limited to the first two columns, $\omega_{31}(x_2)$ and $\omega_{13}(x_2)$ are restricted to column one, $\omega_{32}(x_2)$ and $\omega_{23}(x_2)$ to column two.

For arbitrary F , we have terms including two to four vertical transition rates in $Pol_1^{(3,2)}$ and $Pol_2^{(3,2)}$.

$Pol_1^{(3,2)}$ for $F = 0$ consists of terms of three and four vertical transition rates, each of which includes an s-cycle. If a product consists of four vertical transition rates, these four rates divide up equally in pairs of two rates belonging to the respective location. Four rates belonging to one location or three rates at a single location and the remaining one at the other do not appear. Any such non-occurring combination would either include two vertical rates rising from the same vertex as $\omega_{mn}(x_k)\omega_{mo}(x_k)$ or lead to an *l-cycle*.

Each location provides us with $\binom{6}{2} = 15$ possibilities of choosing two vertical rates out of a total number of six. In order to explain the four-rate combinations, we subtract the six combinations consisting of non-occurring products of rates and end up with $9 \cdot 9 = 81$ possibilities, a number which reduces further after subtracting the 9 cases of equal combinations at both locations and the 18 combinations which do not lead to s-cycles or which include vertical transition rates leading into a state from which no other vertical transition rate emanates, as these dead ends do not occur, too. Doing so, we can explain the $81 - 9 - 18 = 54$ different four-rate combinations which are actually observed. In the case of three vertical rates, there are $9 \cdot 6 \cdot 2 = 108$ combinations taking into account the nine possibilities of choosing two rates belonging to a single location which have already turned out to appear. Another 36 possibilities are dropped as they do not comprise an s-cycle or because the terminal vertices of vertical transitions belong to a state from which no other vertical rate rises, so that there are $108 - 2 \cdot 36 = 36$ possibilities left (the factor of two enters because of a possible swapping of locations). In summary, the 90 different combinations of vertical transition rates in $Pol_1^{(3,2)}$ for $F = 0$ are found by writing down all the combinations which are multilinear in these rates, contain $M = 3$ to $K(M - 1) = 4$ rates, do not include rates rising from identical vertices, ending in a dead end or forming l-cycles, but which can be mapped onto an s-cycle at the same time.

S-cycles for $(M, K) = (3, 2)$

In order to improve the understanding of the notion of s-cycles, we introduce a classification of the spanning cycles which can occur in the case of three states and two locations. Namely, we distinguish between five different types of s-cycles.

The simplest type of an s-cycle is **type 1**: Spanning cycles of this type do not contain more than two vertical transition rates. These two transition rates connect two states at different spatial positions in opposite directions, i.e., we have $\omega_{mn}(x_k)\omega_{nm}(x_l)$ with $m \neq n$ and $k \neq l$. As this type comprises two vertical rates and in this way less than the minimal number of three vertical rates in $Pol_1^{(3,2)}$ for $F = 0$, its occurrence requires one or two additional rates. The simple two-rate form is restricted to $(2, 2)$ -models. The additional rates always lead directly or in more extensive models via other additional rates into states occurring in the s-cycle, compare fig. 3.11. As they are not a part of the s-cycle, their task can be to empty or drain single states, as we will see in section 4.3. In this case, if one of the terms with additional rates stands on its own, the probabilities in the state affected by the emptying will be zero in the stationary state. In general, such an emptying will be compensated by other terms. In any case, the additional vertical rates do not violate the periodic boundary conditions of our systems.

The next type of s-cycles is **type 2**: Double spanning cycles of *type 2* consist of two s-cycles of *type 1* so that there are two pairs of vertical transition rate constants. This type of s-cycle comprises four-rate cycles. With its maximal number of vertical rates it actually can occur in $(3, 2)$ -models.

Fig. 3.5 shows s-cycles of the *types 1* and *2* which appear in a general network.

As in a $(3, 2)$ -model there are no four-rate s-cycles which are not of *type 2*, we now concentrate on combinations of three vertical rates, which set up s-cycles. Considering these s-cycles with

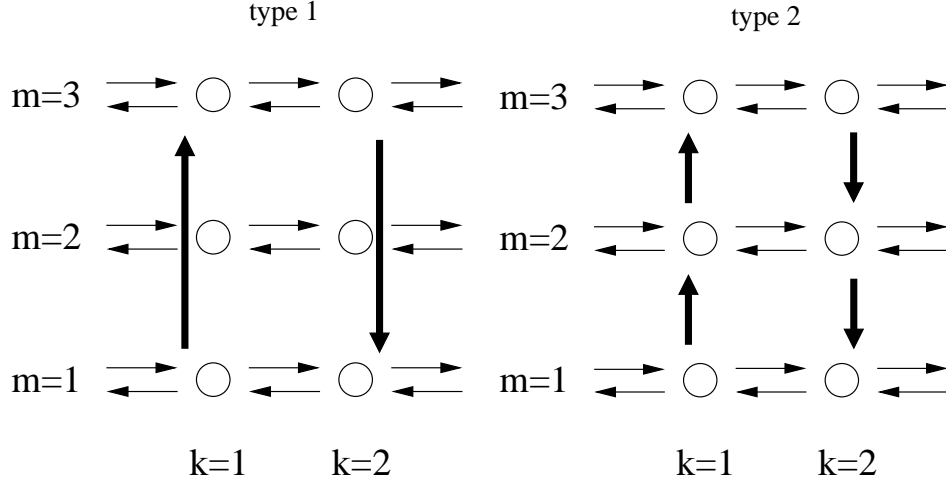


Figure 3.5: Left: s-cycle of *type 1* in $Pol_1^{(3,2)}$ for $F = 0$ given by $\omega_{13}(x_1)\omega_{31}(x_2)$. S-cycles of this type contain two vertical transition rates connecting two states at different spatial positions in opposite directions. Right: s-cycle of *type 2* with the vertical rates $\omega_{12}(x_1)\omega_{23}(x_1)\omega_{32}(x_2)\omega_{21}(x_2)$. This type consists of two s-cycles of *type 1*, so that there are two pairs of vertical transition rate constants. S-cycles of *type 2* are the only four-rate s-cycles in a $(3, 2)$ -system.

three rates, we come across three additional types of cycles as shown in fig. 3.6.

Type 3: S-cycles of *type 3* at one of the two locations contain a vertical rate which connects the states $m = 1$ and $m = 3$, i.e., the outer states in the present labelling of states. At the second location, there are two vertical rates coupling one of the outer states to the inner one. The direction of the rates at location two is the same. Both of them show either upwards or downwards.

Type 4: This type has a single vertical rate at one location which connects the inner state $m = 2$ and an outer state. At the second location we find one vertical rate coupling the states $m = 1$ and $m = 3$ and a second rate which starts from the terminal vertex of the first rate and leads into the inner state.

Type 5: This type is similar to *type 4* with the difference that here the second rate at the location with two rates arises from the inner state, and not from the terminal vertex of the first rate.

In the case of combinations with a total number of three vertical transition rates, there can be s-cycles of the *types 1, 3, 4* and *5*. Taking into account the rates forming the s-cycles and the possible additional rates, one finds that s-cycles of the *types 3* to *5* are not preserved under permutations of the symmetric group S_3 , which means that a permutation in the labelling of the states leads to an s-cycle of a different type. Nevertheless, it is sensible to distinguish between these types, as we will see in the following that there are rules of priority for these types so that we can determine the “right” s-cycle in four-rate combinations where there is no unique s-cycle.

As there are six different vertical transitions possible at each of the two locations in a system with three states, there are six different s-cycles of *type 1*. The missing or additional third rate can be chosen in four different ways, as each location provides us with two rates having a terminal vertex belonging to one of the states connected by the s-cycle. As a result, we find $6 \cdot 4 = 24$ different combinations. A fourth rate leads to another 24 combinations.

In the following we have a closer look at the s-cycle $\omega_{12}(x_1)\omega_{21}(x_2)$ which is of *type 1*. The four rates $\omega_{31}(x_1)$, $\omega_{32}(x_1)$, $\omega_{31}(x_2)$ and $\omega_{32}(x_2)$ can be chosen to complete this two-rate combination to a three- or, if we have two additional rates, to a four-rate combination, compare fig. 3.7. The possible number of three-rate-combinations is four. Besides, there are four combinations with four rates, as combinations with $\omega_{31}(x_k)$ and $\omega_{32}(x_k)$, i.e., with two rates rising from the same vertex, do not occur. In a $(3, 2)$ -system which contains only the above-mentioned six rates, the s-cycle $\omega_{12}(x_1)\omega_{21}(x_2)$ is unique. In the stationary state the factor $c_1\omega_{31}(x_1) + \dots + c_4\omega_{32}(x_2) +$

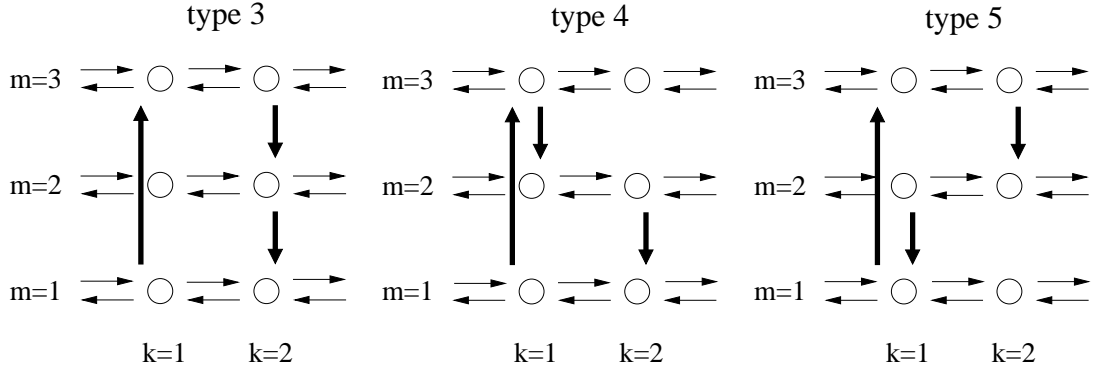


Figure 3.6: The remaining three types of s-cycles in $Pol_1^{(3,2)}$ for $F = 0$ (bold di-edges). Left: s-cycle of *type 3* with $\omega_{13}(x_1)\omega_{32}(x_2)\omega_{21}(x_2)$. Middle: s-cycle of *type 4* with $\omega_{13}(x_1)\omega_{32}(x_1)\omega_{21}(x_2)$. Right: s-cycle of *type 5* with $\omega_{13}(x_1)\omega_{21}(x_1)\omega_{32}(x_2)$. These types are not preserved under permutations of the states.

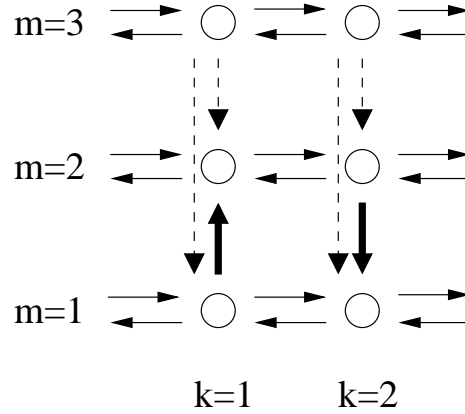


Figure 3.7: The s-cycle $\omega_{12}(x_1)\omega_{21}(x_2)$ (of *type 1*, bold lines) and the four rates $\omega_{31}(x_1)$, $\omega_{32}(x_1)$, $\omega_{31}(x_2)$ and $\omega_{32}(x_2)$ which occur in terms completing the two-rate s-cycle to a combination of three or four rates in $Pol_1^{(3,2)}$ for $F = 0$. None of the completed terms contains $\omega_{31}(x_k)$ and $\omega_{32}(x_k)$, i.e., two rates rising from the same vertex.

$c_{13}\omega_{31}(x_1)\omega_{31}(x_2) + \dots + c_{24}\omega_{31}(x_1)\omega_{32}(x_2)$ reduces from the numerator and denominator in the expression for $J_{tot}^{(3,2)}$ so that the result equals $J_{tot}^{(2,2)}$. Then we have an effective $(2, 2)$ -system. From this result it becomes clear why it makes sense to classify the eight combinations of three or four rates with respect to the s-cycle $\omega_{12}(x_1)\omega_{21}(x_2)$ as of *type 1*.

For s-cycles of *type 2* we consider the 15 different possibilities of choosing two rates at one location. Six of them lead to “forbidden” combinations, whereas three have equal terminal vertices, which cause a “forbidden” combination with two rates rising from the same initial vertex at the other location. In this context, “forbidden” means that these combinations have turned out to be non-occurring in our calculations, so it is not an outer constraint, but a result from the inherent properties of our systems. So there are $15 - 6 - 3 = 6$ different double s-cycles.

The *types 4* and *5* result in another four plus four different s-cycles. The four combinations forming s-cycles of *type 3* are displayed in fig. 3.8.

If we consider the three-rate s-cycles as parts of four-rate combinations of vertical rates, this results in another eight combinations per type. Table 3.1 summarizes how the total number of 90 combinations splits up among these five different types of s-cycles.

type 1	48
type 2	6
type 3	12
type 4	12
type 5	12
sum	90

Table 3.1: The number of different combinations of vertical rates in $Pol_1^{(3,2)}$ for $F = 0$ listed according to their corresponding types of s-cycles.

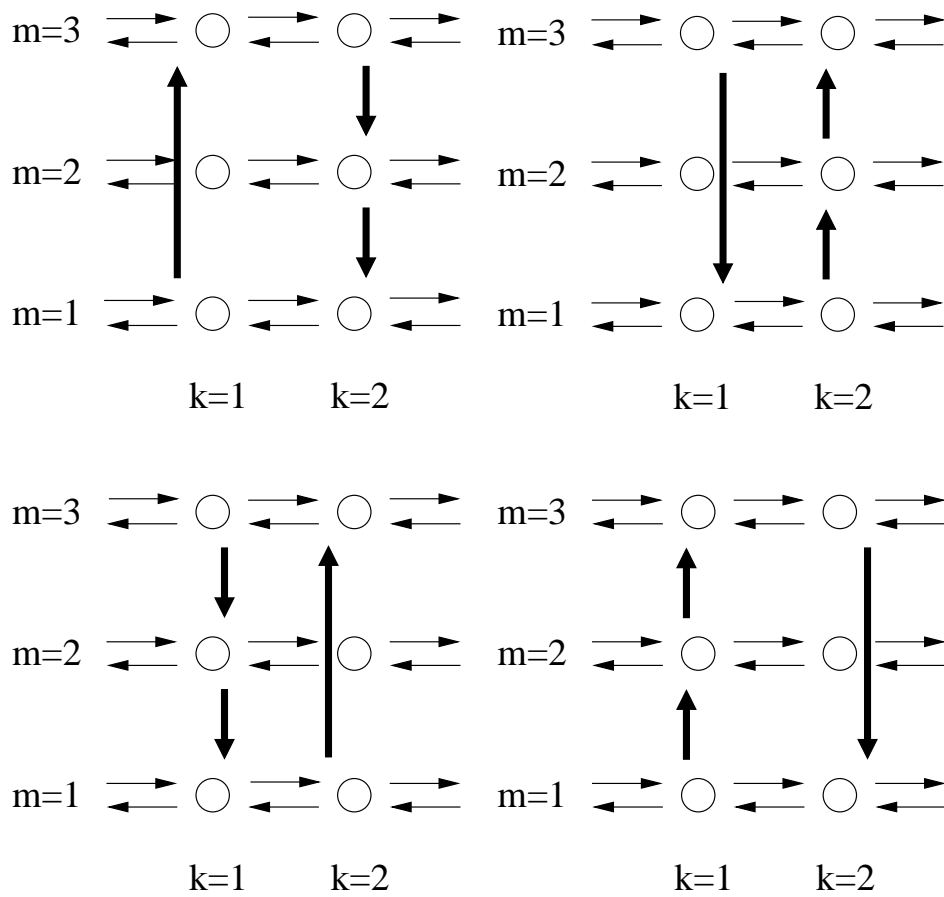


Figure 3.8: Different possibilities of s-cycles of *type 3* in $Pol_1^{(3,2)}$ for $F = 0$ (bold di-edges) in the case of terms with only three vertical transition rates and therefore without additional rates.

If the vertical rates fulfill the conditions of detailed balance, we end up with $v = 0$ and therefore $Pol_1^{(3,2)} = 0$. When using the conditions of detailed balance for $F = 0$, we find that pairs of terms sum up to zero. The two terms of such a pair contain the same set of vertical transition rates of the s-cycle except for their directions or orientations, which are opposed. The vertical transition rates which do not contribute to the s-cycle remain unchanged. These unchanged transition rates are the additional rates mentioned above. This result can be used for interpreting combinations of four vertical rates which allow for more than one s-cycle. In this case we say that the “right” s-cycle is the one which is contained with changed direction in the term summing up to zero with the original term, compare fig. 3.9. The additional rate has the same orientation as in the original term.

Now, we consider all combinations of four rates, which allow for more than one s-cycle of three rates. We take the term cancelling with the original one under conditions of detailed balance. In this way we identify the “right” s-cycle. Altogether, we obtain the following results of priority for the s-cycles in the $(M, K) = (3, 2)$ -case. We say that an s-cycle of a certain type has priority over another type, if a combination of vertical rates contains both a combination of the first and of the second kind, but detailed balance reveals that the first type, having priority, is the “right” one.

1. In case there is an s-cycle containing two rates and another one containing more than two rates, this other s-cycle is the “right” one (s-cycles of any type have priority over s-cycles of type 1).
2. S-cycles of type 4 have priority over s-cycles of type 3.
3. S-cycles of type 3 have priority over s-cycles of type 5.
4. Type 5 has priority over type 4 (fig. 3.9).

The rules of priority are easily understood when looking at examples. If we have a term with a combination of four rates where the “right” s-cycle cannot be identified straightaway, we draw both of the two possible s-cycles of three vertical rates. Then we change the orientations of the edges for both combinations. Together with the fourth rate, one of the two changed combinations with opposite directions of the rates will lead to a “forbidden” combination. For example, if we choose the s-cycle with the vertical rates $\omega_{21}(x_1)$, $\omega_{13}(x_2)$ and $\omega_{32}(x_2)$ in fig. 3.9 (type 4), the inversion of the s-cycle in order to find the corresponding combination for a cancellation in the case of detailed balance leads to the product $\omega_{13}(x_1)\omega_{12}(x_1)$ of two rates rising from the same vertex where $\omega_{13}(x_1)$ is the unchanged additional rate.

Three states and three or four locations

In the case of *three internal states* and *three spatial positions* there is a total number of $M(M-1)K = 18$ possible vertical transition rates. Combinations of two to six rates per term can occur. For $F = 0$, there are terms of three to six vertical transition rates in $Pol_1^{(3,3)}$, which belong to two or more spatial positions. Fig. 3.10 shows a representation of two terms with four vertical transition rates. These two terms cancel when detailed balance is assumed. They contain the s-cycles $\omega_{12}(x_1)\omega_{21}(x_2)$ and $\omega_{12}(x_2)\omega_{21}(x_1)$, respectively, and the additional rates $\omega_{31}(x_2)\omega_{13}(x_3)$. This example shows that the rules of priority for different types of s-cycles which we have found for the $(3, 2)$ -case do not hold for the $(3, 3)$ -model. In contrast to the first rule for the $(3, 2)$ -case, here the “right” s-cycle is a combination of two rates, not the four-rate combination with the two additional rates. This can be understood if we try to change the direction of the four-rate cycle $\omega_{13}(x_3)\omega_{31}(x_2)\omega_{21}(x_2)\omega_{12}(x_1)$, as in this case we obtain a “forbidden” combination with the rates $\omega_{13}(x_2)\omega_{12}(x_2)$ arising from the same vertex.

For *three states* and *four spatial positions* there are 24 vertical transition rates. $Pol_1^{(3,4)}$ and $Pol_2^{(3,4)}$ comprise two to eight vertical transition rates for arbitrary F . The $(M, K) = (3, 4)$ -models will be studied in the context of unbalanced vertical transition rates in section 3.3.

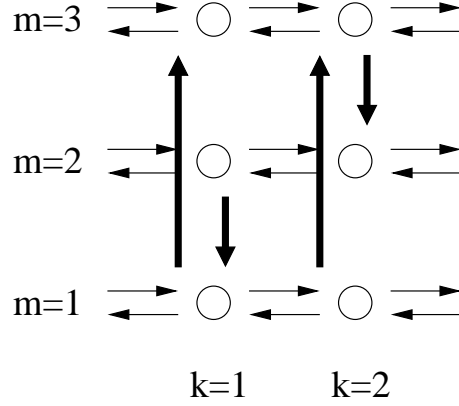


Figure 3.9: The “right” s-cycle in this combination from $Pol_1^{(3,2)}$ for $F = 0$ is given by the vertical transition rates $\omega_{13}(x_1)$, $\omega_{32}(x_2)$ and $\omega_{21}(x_1)$. This is an s-cycle of type 5. The combination $\omega_{13}(x_2)$, $\omega_{32}(x_2)$ and $\omega_{21}(x_1)$ represents an s-cycle of type 4. As type 5 has priority over type 4, we will see that under conditions of detailed balance this term is cancelled by a term which contains the s-cycle of type 5 with changed direction.

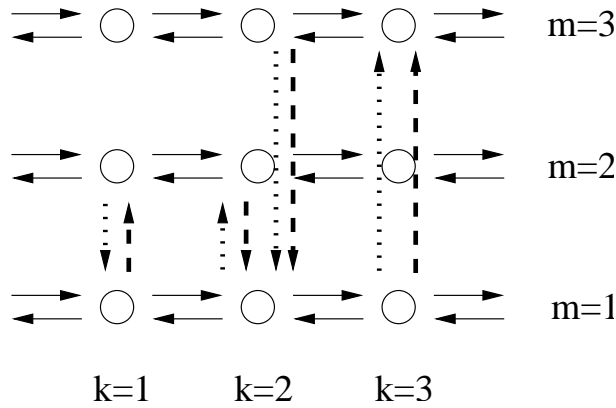


Figure 3.10: Representation of two combinations in $Pol_1^{(3,3)}$ for $F = 0$ with different vertical transition rates (marked by points and broken lines, respectively) which cancel when detailed balance is supposed; horizontal transition rates are not specified for simplicity.

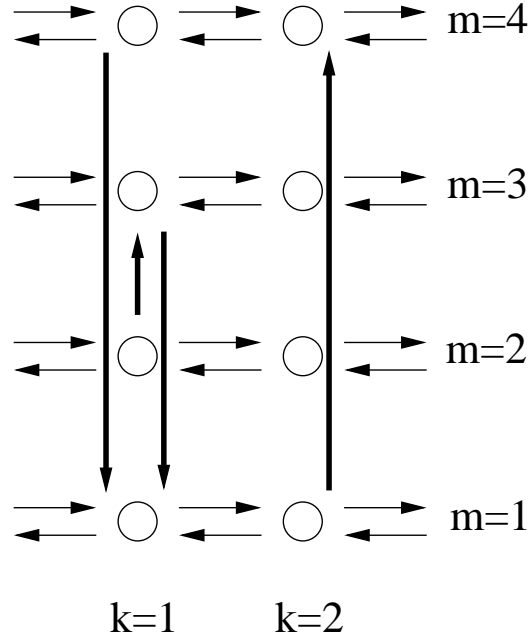


Figure 3.11: A combination of vertical transition rates occurring in $Pol_1^{(4,2)}$ for arbitrary F . The rates $\omega_{41}(x_1)\omega_{14}(x_2)$ form an s-cycle.

3.1.4 Four internal states

For a two-headed motor protein we need *four internal states* in order to distinguish between a conformation or state in which both heads are bound to the filament, a second conformation where one of the two heads is unbound, a third conformation where the situation is just the opposite and the other head is bound, whereas the first one is unbound, and a last fourth state in which both heads are unbound. These four conformations differ in the binding state of the motor with respect to its filament.

If we concentrate on the ATP hydrolysis instead, the conformations of the motor differ with respect to the adsorbed substrate. In this case we need four states for the description of a one-headed motor which is either in a state of no substrate, in a state of adsorbed ATP, adsorbed ADP/P or, as the last possibility, in a state of adsorbed ADP.

Four states and one or two locations

For *four states* and *one spatial position*, there are 12 different vertical transition rates. In the case of $F = 0$, $Pol_1^{(4,1)}$ is equal to zero as s-cycles are impossible with one location only. In order to obtain a net current, there has to be an external force $F \neq 0$. Then, the polynomials contain terms with $M - 1 = 3$ vertical transition rates each.

In the case of *four internal states* and *two spatial positions* there are 24 different vertical transition rates. $Pol_1^{(4,2)}$ for $F = 0$ contains combinations of four to six vertical transition rate constants. In the case $F \neq 0$, there are additional terms containing three vertical rates. Fig. 3.11 shows a combination of vertical transition rates in $Pol_1^{(4,2)}$. The labelling of the states is arbitrary, a change of direction, here in the additional vertical rates as given by $\omega_{23}(x_1)\omega_{31}(x_1)$, can occur at an inner state, too, here at $m = 3$.

Four states and three or four locations

The number of different vertical transition rates for *four internal states* and *three spatial positions* is 36. The minimal degree of the polynomials is 3, the maximal degree is 9. Fig. 3.12 shows a

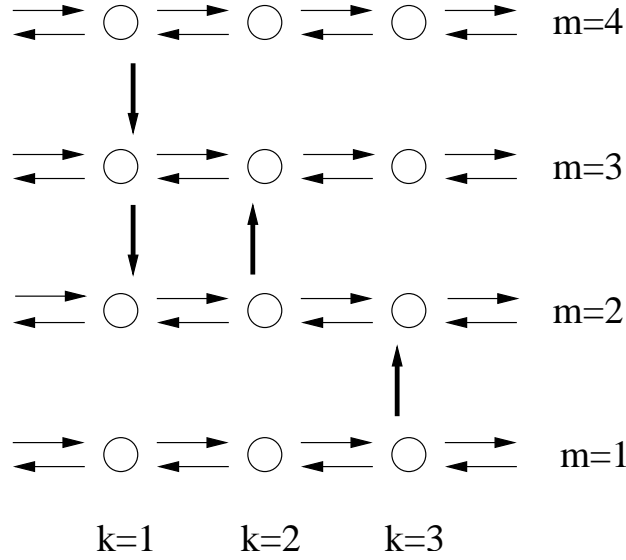


Figure 3.12: Example of a combination of vertical rates in $Pol_1^{(4,3)}$ for $F = 0$. The rates $\omega_{23}(x_2)\omega_{32}(x_1)$ determine an s-cycle.

combination with four vertical transition rates containing an s-cycle of the type $\omega_{mn}(x_k)\omega_{nm}(x_l)$ with $m \neq n$ and $k \neq l$.

For **four internal states** and **four spatial positions**, there are 48 different vertical transition rates. The degree of $Pol_1^{(4,4)}$ and $Pol_2^{(4,4)}$ varies between $M - 1 = 3$ and $(M - 1)K = 12$. Fig. 3.13 shows a combination of ten vertical transition rates with an s-cycle formed by five vertical rates.

3.2 Generic rules for the matrices and polynomials

Now, we summarize the general relationships we have drawn up in section 3.1 concerning the matrices $\mathbf{A}^{(M,K)}$ and the polynomials $Pol_1^{(M,K)}$ and $Pol_2^{(M,K)}$, which determine the total current $J_{tot}^{(M,K)}$ and the velocity of the motor particle. These relationships are direct consequences of the equations for the calculation of $\mathbf{A}^{(M,K)}$ for arbitrary values of M and K . They become obvious from the computations for the model systems. In the following, we repeat some of the results obtained in section 3.1 in order to illustrate the general properties and rules.

3.2.1 Matrix $\mathbf{A}^{(M,K)}$ and vertical transition rates

The dependence of the matrix $\mathbf{A}^{(M,K)}$ on the vertical transition rates $\omega_{mn}(x_k)$ shows the following general properties [43]:

For $(M, K) = (2, 1)$, the occurrence of $\omega_{12}(x_1)$ is restricted to the third row, while $\omega_{21}(x_1)$ can only be found in row four. This is also true in the case of $(M, K) = (2, 2)$. For $(M, K) = (3, 2)$, the occurrence of $\omega_{1n}(x_1)$ is limited to row four, the one of $\omega_{2n}(x_1)$ to row five, and $\omega_{3n}(x_1)$ can only be found in the last row. In summary, we derive

(A1): All matrix elements of $\mathbf{A}^{(M,K)}$, which depend on $\omega_{mn}(x_1)$, are located in the $(M + m)$ th row of $\mathbf{A}^{(M,K)}$.

The determinants $\det \mathbf{A}^{(M,K)}$ and the minor determinants $\det \mathbf{A}^{(M,K)}[j, i]$ can be calculated doing an expansion to the $(M + m)$ th row of $\mathbf{A}^{(M,K)}$, thus $\omega_{mn}(x_1)$ enters linearly in each summand according to (A1) and

(A2): The determinant $\det \mathbf{A}^{(M,K)}$ and the cofactors $C_{ij} \sim \det \mathbf{A}^{(M,K)}[j, i]$ are multilinear in the vertical transition rates $\omega_{mn}(x_1)$.

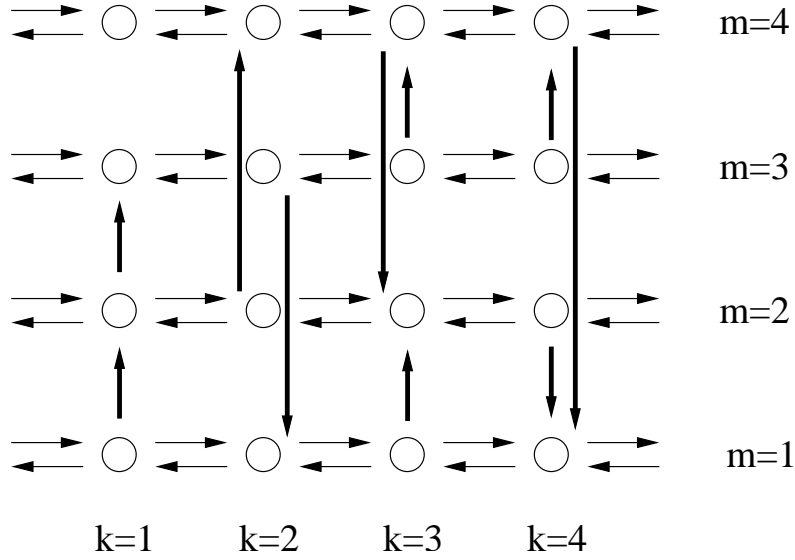


Figure 3.13: Combination of ten vertical transition rates for $F = 0$ in $Pol_1^{(4,4)}$. An s-cycle is given by $\omega_{12}(x_1)\omega_{23}(x_1)\omega_{34}(x_3)\omega_{42}(x_3)\omega_{21}(x_4)$.

When calculating the polynomials $Pol_1^{(M,K)}$ and $Pol_2^{(M,K)}$, we always observe multilinearity concerning the vertical rates $\omega_{mn}(x_k)$, irrespective of the value of k . As the total current must not depend on the labelling of the discrete set of states, it must be invariant under permutations of the labels m of the states and under a shift of the labels k of x_k using the periodic boundary conditions $x_{K+1} = x_1$. Together with (A1), this implies

(A3): Both the determinant $\det \mathbf{A}^{(M,K)}$ and the cofactor sum

$$\sum_{m=1}^M (-1)^{2M+m} \det \mathbf{A}^{(M,K)}[m, 2M] \quad (3.8)$$

are multilinear in the transition rates $\omega_{mn}(x_k)$ for all k .

For $(M, K) = (2, 2)$, we see that vertical rates at location x_K are restricted in their occurrence to the first column of $\mathbf{A}^{(2,2)}$. This is comparable to the case of $(M, K) = (3, 2)$ where the rates $\omega_{12}(x_2)$ as well as $\omega_{21}(x_2)$ are limited to the first two columns, $\omega_{31}(x_2)$ and $\omega_{13}(x_2)$ are restricted to column one, $\omega_{32}(x_2)$ and $\omega_{23}(x_2)$ to column two. In order to achieve the reduction to the $2M$ variables \bar{J}_m and $P_m(x_1)$, we need $(K - 1)$ transfer matrices $\mathbf{T}(x_k, x_{k+1})$ with $k \neq K$. For any pair of values for m and n , there is a set of $(M - 1)$ periodic boundary conditions which does not contain the periodic boundary condition for J_n . In this case, all elements depending on $\omega_{mn}(x_K)$ are in column m . We deduce

(A4): All matrix elements of $\mathbf{A}^{(M,K)}$ which depend on $\omega_{mn}(x_K)$ are located in the two columns of $\mathbf{A}^{(M,K)}$ corresponding to the two PBCs for J_m and J_n .

The examples of the matrices $\mathbf{A}^{(M,K)}$ show that

(A5): All terms occurring in the first $(M - 1)$ columns of $\mathbf{A}^{(M,K)}$ with $K > 1$ are proportional to at least one transition rate $\omega_{mn}(x_k)$.

The matrices $\mathbf{A}^{(M,K)}$ have the general form given in table 3.2.

3.2.2 Polynomials $Pol_i^{(M,K)}$ and vertical transition rates

The functional relationship between the total current $J_{tot}^{(M,K)}$ and the transition rates $\omega_{mn}(x_k)$ exhibits some universal features. In the following we will sometimes use the short-hand notation ω_r with $1 \leq r \leq N \equiv KM(M - 1)$ for $\omega_{mn}(x_k)$, where N equals the number of all vertical di-edges in the network of MK discrete states.

row\column	1	...	M-1	M	2M
1	K-1	K-1	K-1	K-2	K-2	K-2	K-2
...	K-1	K-1	K-1	K-2	K-2	K-2	K-2
M-1	K-1	K-1	K-1	K-2	K-2	K-2	K-2
M	K-1	K-1	K-1	K-2	K-2	K-2	K-2
...	K	K	K	K-1	K-1	K-1	K-1
...	K	K	K	K-1	K-1	K-1	K-1
2M	K	K	K	K-1	K-1	K-1	K-1

Table 3.2: General form of matrices $\mathbf{A}^{(M,K)}$. The elements of the table denote the maximum number of vertical transition rates found in a single term of the corresponding matrix element. For $K = 1$ the negative value of $K - 2$ is to be replaced with 0.

The generic features of the current-rate relationships can be summarized in terms of the following rules, compare [43]:

As $J_{tot}^{(M,K)}$ is calculated as

$$J_{tot}^{(M,K)} = \sum_{m=1}^M \bar{J}_m = \sum_{m=1}^M (-1)^{2M+m} \det \mathbf{A}^{(M,K)} [m, 2M] / \det \mathbf{A}^{(M,K)}, \quad (3.9)$$

we state

Rule 0: The dependence of the total current $J_{tot}^{(M,K)}$ on the transition rates ω_r has the form

$$J_{tot}^{(M,K)} = \frac{Pol_1^{(M,K)}(\omega_1, \omega_2, \dots, \omega_N)}{Pol_2^{(M,K)}(\omega_1, \omega_2, \dots, \omega_N)} \quad (3.10)$$

with two polynomials $Pol_1^{(M,K)}$ and $Pol_2^{(M,K)}$.

Due to (A3) we have

Rule 1: Both polynomials are multilinear in all ω_r , i.e., each term \mathcal{T} of both $Pol_1^{(M,K)}$ and $Pol_2^{(M,K)}$ reads as

$$\mathcal{T} \sim \omega_1^{z_1} \omega_2^{z_2} \dots \omega_N^{z_N} \quad \text{with } z_r = 0, 1, \quad (3.11)$$

i.e., it cannot contain powers ω_r^z with $z \geq 2$.

The polynomials are calculated via the determinants of the $\mathbf{A}^{(M,K)}$ and the minor determinants after erasing the last column. Together with (A5) we have

Rule 2: Each polynomial term \mathcal{T} contains at least $M - 1$ factors ω_r , i.e.,

$$\sum_r z_r \geq M - 1 \quad \text{for each } \mathcal{T}. \quad (3.12)$$

There is also an upper limit of vertical transition rates per term. For $(M, K) = (2, 2)$ we have found two, for $(2, 3)$ three and for $(2, 4)$ four. In the case of $(3, 2)$ we have come across four again, while for $(3, 3)$ the maximal number of vertical rates per term is six. In summary, each polynomial term \mathcal{T} contains at most $K(M - 1)$ factors ω_r , i.e.,

$$\sum_r z_r \leq K(M - 1) \quad \text{for each } \mathcal{T}. \quad (3.13)$$

This maximal number grows as $\sim M$, whereas the total number of rates in the general system grows as $\sim M^2$. This upper limit is a consequence of the following two rules.

The minimal number of factors in $Pol_1^{(M,K)}$ for $F = 0$ is found to be M . The vertices belonging to the vertical transition rates include every single internal state, while there has to be an s-cycle at the same time, see *rule 6*.

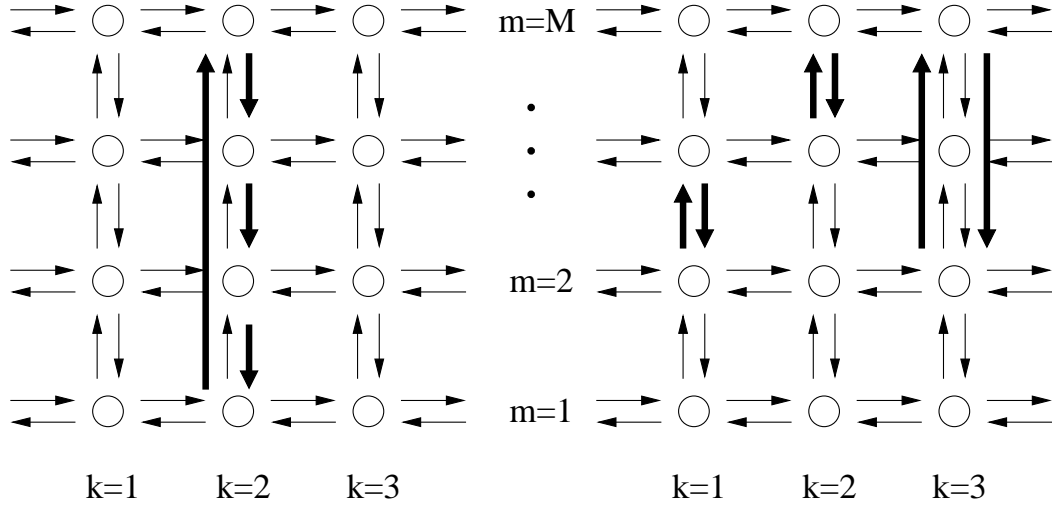


Figure 3.14: Left: a localized cycle or l-cycle at $k = 2$ marked by bold di-edges, compare *rule 4* in the text. Right: pair of opposite s-cycles (bold di-edges). These two s-cycles correspond to two terms in $Pol_1^{(M,K)}$ which cancel if the system satisfies detailed balance, see *rule 6* in the text. Since here the state $m = 1$ is not included in the s-cycle, there will be at least one additional vertical rate in each of the two terms (and identical in both terms) which connects this state to the s-cycle.

In the examples with two internal states, the polynomials $Pol_1^{(2,K)}$ and $Pol_2^{(2,K)}$ never contain the combinations $\omega_{12}(x_k)\omega_{21}(x_k)$ of vertical rates at identical locations. For three internal states, we never have $\omega_{12}(x_k)\omega_{13}(x_k)$ or $\omega_{12}(x_k)\omega_{23}(x_k)\omega_{31}(x_k)$. We deduce *rule 3* and *rule 4*:

Rule 3: No term \mathcal{T} contains a product of the form $\omega_{mn}(x_k)\omega_{mo}(x_k)$, or in words, there is no product of two vertical rates with the same starting vertex. This is a consequence of (A1).

Rule 4: No term \mathcal{T} contains a product of the form $\omega_{mn}(x_k)\omega_{nm}(x_k)$ (see (A4)). Such a product corresponds to the smallest l-cycle possible. Likewise, no term \mathcal{T} contains a product of the form

$$\omega_{mm'}(x_k)\omega_{m'm''}(x_k)\dots\omega_{nm}(x_k).$$

The latter products correspond to all possible l-cycles at $x = x_k$ with $1 \leq k \leq K$.

Rule 5: The combination of vertical rates in each term \mathcal{T} of $Pol_1^{(M,K)}$ or $Pol_2^{(M,K)}$ contains vertices of every single internal state m as starting or final vertices of vertical rates.

For example, for $M = 3$ and $K = 2$ and arbitrary F , the combination $\omega_{12}(x_1)\omega_{31}(x_2)$ occurs in $Pol_1^{(M,K)}$, whereas $\omega_{13}(x_1)\omega_{31}(x_2)$ does not appear. For $M = 4$ and $K = 2$, we find $\omega_{13}(x_1)\omega_{24}(x_1)\omega_{42}(x_2)$, but not $\omega_{12}(x_1)\omega_{24}(x_1)\omega_{41}(x_2)$, as in the second combination the third state does not contribute. A derivation using the structure of $\mathbf{A}^{(M,K)}$ is given in appendix B.

For $(M, K) = (2, 2)$ and $F = 0$, there are only two combinations of vertical rates left in the terms \mathcal{T} of $Pol_1^{(2,2)}$, namely $\omega_{12}(x_1)\omega_{21}(x_2)$ and $\omega_{21}(x_1)\omega_{12}(x_2)$. Likewise, for $(M, K) = (3, 2)$ and $F = 0$, $Pol_1^{(3,2)}$ contains $\omega_{12}(x_1)\omega_{23}(x_1)\omega_{32}(x_2)\omega_{21}(x_2)$, but not $\omega_{12}(x_1)\omega_{23}(x_1)\omega_{12}(x_2)\omega_{23}(x_2)$. We state

Rule 6: For $F = 0$, each term \mathcal{T} of $Pol_1^{(M,K)}$ can be mapped onto an s-cycle of the network. In general, this mapping is not one-to-one and several terms will be mapped onto the same s-cycle. The smallest such s-cycles involve a pair of transitions which connect two levels in opposite directions at two different x -locations. The latter s-cycles lead to polynomial terms of the form

$$\mathcal{T} \sim \omega_{mn}(x_k)\omega_{nm}(x_l) \quad \text{with } k \neq l. \quad (3.14)$$

This rule follows from the limiting case of detailed balance stated in the next rule.

Rule 7: If all the vertical transition rates satisfy detailed balance with $\omega_r = \omega_r^{db}$ as in (3.17), one has

$$J_{tot}^{(M,K)} \sim Pol_1^{(M,K)}(\omega_1^{db}, \omega_2^{db}, \dots) = 0 \text{ for } F = 0. \quad (3.15)$$

In fact, each term of $Pol_1^{(M,K)}$ corresponding to a certain s-cycle is cancelled by another term corresponding to the opposite s-cycle, i.e., to the cycle which contains the same vertices but has an opposite orientation of di-edges and an opposite sequence of vertices, see the right graph in fig. 3.14.

Rule 5 and the minimal number of factors in $Pol_1^{(M,K)}$ for $F = 0$ in *rule 2* have not been listed in [43].

3.3 Enzymatic activity - unbalanced transitions

Up to now we have not specified the vertical transition rates $\omega_{mn}(x_k)$. In this section we focus on the results for the total current in different models which contain vertical rates explicitly breaking the conditions of detailed balance. We limit ourselves to $(M, K) = (3, 4)$ -models.

In an $(M, K) = (3, 4)$ -model, there are 24 possible vertical transition rates. If there is no enzymatic activity and the applied force $F = 0$, the system obeys detailed balance (db) with

$$\Omega_{mn}^{db}(x) = e^{(U_m(x) - U_n(x))/T} \Omega_{nm}^{db}(x) = e^{V_m(x) - V_n(x)} \Omega_{nm}^{db}(x), \quad (3.16)$$

and the corresponding vertical transition rates $\omega_{mn}^{db}(x_k)$ satisfy equation (3.7),

$$\omega_{mn}^{db}(x_k) = e^{V_m(x_k) - V_n(x_k)} \omega_{nm}^{db}(x_k). \quad (3.17)$$

If all the vertical rates satisfy (3.17) and there is no external force, there will be no net current carried through the system. Here, we view a situation where the vertical transition rates are only partly balanced so that there can be a net current arising from the contributions of the unbalanced parts even if an external force is missing. In the context of molecular motors this will usually imply that the chemical equilibrium is broken. Then, the $\omega_{mn}(x_k)$ can be divided up into balanced parts ω_{mn}^{db} and unbalanced parts Δ_{mn} arising from the enzymatic activity,

$$\omega_{mn}(x_k) = \omega_{mn}^{db}(x_k) + \Delta_{mn}(x_k). \quad (3.18)$$

3.3.1 A single unbalanced vertical transition

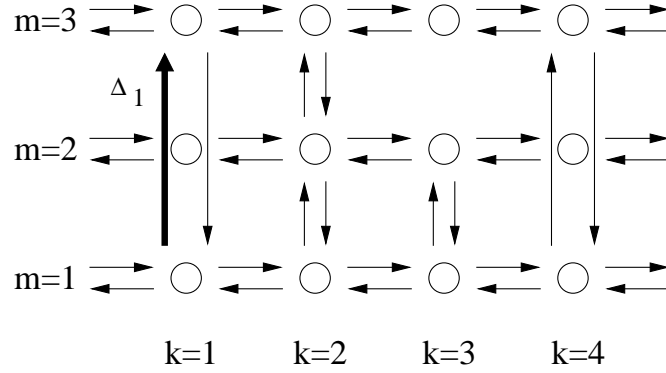
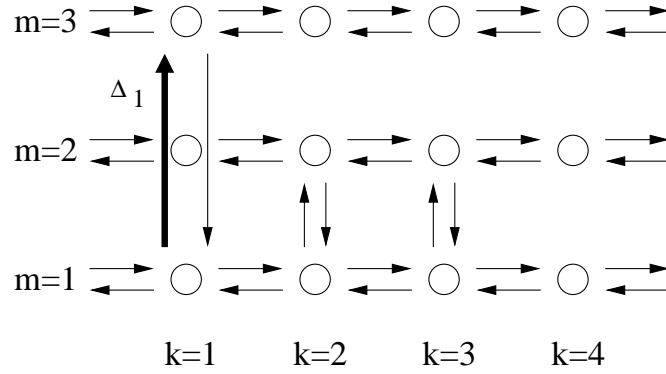
Fig. 3.15 shows an example of a ratchet with $Q = 1$ unbalanced vertical transition. In the following, Q is the total number of unbalanced transitions. At first, we consider a situation where the motor is one-headed. This head may bind to and unbind from the filament. Likewise, ATP can bind to the head, and ADP and/or the phosphate ion (P_i) can unbind from this head after the hydrolysis. It is also possible that there are reverse processes of ATP unbinding and ADP binding, too.

In order to simplify the situation, it is reasonable to confine the use of unbalanced transitions to those steps of the chemical reaction where actually a chemical bond is broken or rearranged. So in this approach, the binding of the motor to the filament, for example, is not described by an unbalanced transition. This approach is justified since the replacement of ATP by an analogue which can not be hydrolyzed, as, for example, AMP-PNP, leaves us with balanced adsorption and desorption processes only. Without the hydrolysis, the motor does not gain the energy it needs to perform a directed walk along the filament.

For cytoskeletal motors, the chemical reaction which changes the bonds is the hydrolysis of ATP. It obeys the simplified reaction scheme



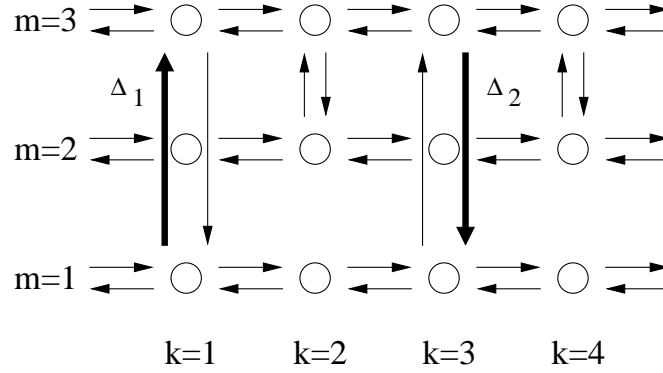
In this reaction scheme, P_i is a phosphate ion.

Figure 3.15: Ratchet with $Q = 1$ unbalanced transition at location $k = 1$ in a $(3, 4)$ -system.Figure 3.16: Ratchet with $Q = 1$ unbalanced transition as in fig. 3.15, but without the balanced vertical transition rates $\omega_{32}^{db}(x_2)$, $\omega_{23}^{db}(x_2)$ and $\omega_{31}^{db}(x_4)$, $\omega_{13}^{db}(x_4)$. This example no longer contains an s-cycle with the unbalanced rate Δ_1 .

Monomeric kinesin, for example, has a single enzymatic domain. In general, we expect that a single-headed motor undergoes one hydrolysis step per motor cycle. Here, a motor cycle is again defined as in 1.1.4 and belongs to one complete step of the motor. The hydrolysis step of the reaction is assigned with one location x_k at which we find one unbalanced transition rate $Q = 1$ as indicated in fig. 3.15. For the example in fig. 3.15 we define $\Delta_{13}(x_1) =: \Delta_{1,Q1}$. For $F = 0$, we find

$$J_{tot}^{(3,4)}(\Delta_{1,Q1}, F = 0) = \frac{a_1(F = 0) \Delta_{1,Q1}}{b_0(F = 0) + b_1(F = 0) \Delta_{1,Q1}} \quad (3.20)$$

with non-zero coefficients $a_1(F = 0)$, $b_0(F = 0)$ and $b_1(F = 0)$. By contrast with (3.6) these coefficients comprise, apart from the $e_m(x_k, x_l)$, $\mathcal{E}_m(x_k, x_l)$ etc., combinations of balanced parts ω_{mn}^{db} of vertical transition rates. Equation (3.20) is explainable as follows: The coefficient a_0 , which belongs to $(\Delta_1)^0$, vanishes equal to zero, since a combination of balanced rates without an external force leads to $Pol_1^{(3,4)} = 0$ according to *rule 7* in 3.2.2. The maximal power of $\Delta_{1,Q1}$ in both the numerator and the denominator is one because of *rule 1*, which states the multilinearity of the polynomials in the vertical transition rates. If there was no possibility of forming an s-cycle which included the unbalanced rate $\Delta_{1,Q1}$, the coefficient a_1 in the numerator of (3.20) would be equal to zero for $F = 0$ and we had $J_{tot}^{(3,4)}(\Delta_{1,Q1}, F = 0) = 0$. In the present situation this would happen if there were no balanced rates $\omega_{31}^{db}(x_4)$ and $\omega_{32}^{db}(x_2)$. This situation is depicted in fig. 3.16.

Figure 3.17: Ratchet with $Q = 2$ unbalanced transitions at the locations $k = 1$ and $k = 3$.

3.3.2 Two unbalanced vertical transitions

The ratchet in fig. 3.17 has $Q = 2$ unbalanced transitions. Such a model can be used for molecular motors such as dimeric kinesin, dynein, or myosin V which have two identical enzymatic domains or heads, so that within one motor cycle for a forward step of the motor protein there can be two locations with enzymatic activity at which one of these heads can be activated a time. In our example the unbalanced parts are $\Delta_{13}(x_1) =: \Delta_{1,Q2}$ and $\Delta_{31}(x_3) =: \Delta_{2,Q2}$. Using this notation, the total current for general F reads

$$J_{tot}^{(3,4)}(\Delta_{1,Q2}, \Delta_{2,Q2}, F) = \frac{a_0 + a_1\Delta_{1,Q1} + a_2\Delta_{2,Q2} + a_{12}\Delta_{1,Q1}\Delta_{2,Q2}}{b_0 + b_1\Delta_{1,Q1} + b_2\Delta_{2,Q2} + b_{12}\Delta_{1,Q1}\Delta_{2,Q2}} \quad (3.21)$$

with new coefficients a_i and b_i .

If we had $\Delta_{13}(x_1)$ and $\Delta_{31}(x_1)$ as the two unbalanced rates, the contributions with a_{12} and b_{12} would vanish because of *rule 4* about the l-cycles. So if we have two conformations in which enzymatic activity of the motor is possible at the same location and whose unbalanced rates connect to states as in $\Delta_{mn}(x_k)$ and $\Delta_{nm}(x_k)$, there are no terms with products of these two unbalanced rates contributing to the total current.

3.3.3 Four unbalanced vertical transitions

We still stick to the picture of a two-headed motor protein, but the situation is changed slightly in that respect that each head can make both forward and backward steps and, accordingly, it can be activated at both locations $k = 1$ and $k = 3$ in fig. 3.18. In summary, this leads to $Q = 4$ unbalanced transitions.

The total current is given by

$$J_{tot}^{(3,4)}(\Delta_{1,Q4}, \Delta_{2,Q4}, \Delta_{3,Q4}, \Delta_{4,Q4}, F) = \frac{a}{b} \quad (3.22)$$

with

$$\begin{aligned} a &:= a_0 + a_1\Delta_{1,Q4} + a_2\Delta_{2,Q4} + a_3\Delta_{3,Q4} + a_4\Delta_{4,Q4} + a_{13}\Delta_{1,Q4}\Delta_{3,Q4} \\ &\quad + a_{14}\Delta_{1,Q4}\Delta_{4,Q4} + a_{23}\Delta_{2,Q4}\Delta_{3,Q4} + a_{24}\Delta_{2,Q4}\Delta_{4,Q4} \\ b &:= b_0 + b_1\Delta_{1,Q4} + b_2\Delta_{2,Q4} + b_3\Delta_{3,Q4} + b_4\Delta_{4,Q4} + b_{13}\Delta_{1,Q4}\Delta_{3,Q4} \\ &\quad + b_{14}\Delta_{1,Q4}\Delta_{4,Q4} + b_{23}\Delta_{2,Q4}\Delta_{3,Q4} \end{aligned} \quad (3.23)$$

and with $\Delta_{23}(x_1) =: \Delta_{1,Q4}$, $\Delta_{21}(x_1) =: \Delta_{2,Q4}$, $\Delta_{23}(x_3) =: \Delta_{3,Q4}$, $\Delta_{21}(x_3) =: \Delta_{4,Q4}$ and once more with new coefficients a_i and b_i . Because of *rule 3*, the degree of the polynomials $Pol_1^{(3,4)}$ and $Pol_2^{(3,4)}$ in the unbalanced vertical transition rate parts is bounded from above by two, as the

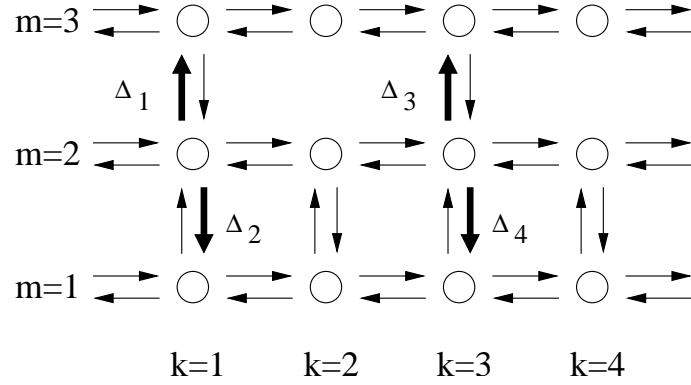


Figure 3.18: Example with $Q = 4$ unbalanced transitions arising from state 2 at the locations $k = 1$ and $k = 3$.

unbalanced parts split up into two pairs with the same starting vertex, respectively. The terms in $Pol_1^{(3,4)}$ for $F = 0$ with two unbalanced parts comprise $\Delta_{21}(x_1) \Delta_{21}(x_3)$, $\Delta_{21}(x_1) \Delta_{23}(x_3)$ and $\Delta_{23}(x_1) \Delta_{21}(x_3)$, whereas $\Delta_{21}(x_1) \Delta_{23}(x_1)$ and $\Delta_{21}(x_3) \Delta_{23}(x_3)$ do not occur due to *rule 3* and $\Delta_{23}(x_1) \Delta_{23}(x_3)$ does not appear because of *rule 4* about the l-cycles, as this last combination leads into state three, which must be left again, as according to *rule 5* these rates have to reach states of the s-cycle either directly or indirectly, which in the assumed situation cannot be done without just creating an l-cycle.

In summary, we have seen how a general (M, K) -model simplifies according to the rules in 3.2.2. There are further simplifications in the case where we have a limited number of unbalanced vertical transition rates, whereas the other vertical rates of the system fulfill the conditions of detailed balance. The reason for breaking detailed balance might be different from enzymatic activity, of course, for example, there could be physical influences. This can happen if there is another motor particle in the neighbourhood which approaches our motor and pushes it. If the cargo of this new motor is heavy, the push can even put the old motor in a conformation in which rebinding to the filament is impossible, maybe because of some damage done to it.

Nevertheless, if we focus on enzymatic activity as the background or reason for the occurrence of an unbalanced rate, the next step is to examine the connection between these unbalanced rates and the ATP concentration. This will be done in chapter 5.1. There we concentrate on the question of how the unbalanced rates depend on the concentration of fuel near the respective location in the motor's box and discuss several different models describing this dependence.

Chapter 4

Decoupled states, horizontal rates and networks

The models of the (M, K) -systems as examined in chapter 3 still have various restrictions or inconveniences. Here we show how to overcome them and introduce several new concepts, too.

We take a look at decoupled states or subsystems without a mutual coupling via vertical transition rates. The motor has a certain probability of being in these decoupled subsystems, but it cannot change between them. The reasons may be outer influences on the motor as a shortage of fuel or inner reasons as mutations of the motor protein. We explain why decoupled subsystems have not occurred in our previous calculations in chapter 3.

Furthermore, the horizontal rates in our systems are specified now, and active, unbalanced transitions in x -direction are introduced. From a discrete Master-equation approach we derive new rules for the total current, which now include the dependence on horizontal rates, too. Then we examine the time evolution for given initial probabilities on the way to a stationary state.

In the context of the idea of a main pathway and several other minor pathways in chemical reactions, we eventually focus on the different importance of single paths or pathways through a network of vertices.

Most of the concepts which we establish here are based on the network representation indicated in fig. 2.1. For a listing of the terminology and concepts of graph theory which are used in this chapter see appendix C.

4.1 Decoupled states

A decoupled state is a state which has no connection to any other state. There are no vertical rates starting from or ending in this state. Likewise, there can be subsystems of states which have no connections to states of the remaining system. With certain initial probabilities the motor can be in these decoupled states in the beginning, but it cannot leave them or their subsystem. This can be the case if, with a certain probability, we are dealing with a mutation of a motor which is unable to take part in the enzymatic reaction or if the binding sites of the motor's filament are blocked so that the motor still diffuses or even is driven by an external force, but its conformation is frozen.

The stationary state in such a decoupled system depends on the initial probability distribution, as the contribution of each of the decoupled subsystems to the total current depends on its part of the initial probability. For identical subsystems with a small or no coupling there can be bifurcations, so that the same "macroscopic" stationary total current belongs to different "microscopic" situations. Here, we at first consider a continuous x -direction. Then we return to network-based systems with localized vertical transitions.

4.1.1 Decoupled states and continuous x -direction

Here, the centre of interest is on analytic calculations of the total current for simple cases of decoupled states. Initially, we abstain from the idea of networks as presented in the chapters 2 and 3, but focus on the case of decoupled states with continuous coordinates in x -direction. At first, there is no molecular interaction potential, but a constant external force. Then we introduce a localized coupling between the states and consider situations with molecular interaction potentials, too.

In the restricted cases presented here the results for the currents and the probability distributions can be written down with their explicit coefficients. A straight decoupling of states has been impossible in the formalism of chapter 3 because of *rule 5* in 3.2.2 stating that vertices of every state have to occur in the combination of vertical rates of every term of the polynomials $Pol_i^{(M,K)}$.

Decoupled states, no potentials and constant force

We calculate the total current for a number of decoupled states under the conditions that the external force is an arbitrary constant, but there are no molecular interaction potentials. In this case the effective force potentials in (2.17) reduce to

$$V_m(x) \equiv -Fx/T. \quad (4.1)$$

Initially, we look at a single internal state. Without a molecular interaction potential U_m , the Smoluchowski equation (2.11) for this single state m reads

$$\frac{\partial P_m(x,t)}{\partial t} \equiv D_m \frac{\partial}{\partial x} \left[\frac{\partial}{\partial x} (-Fx)/T + \frac{\partial}{\partial x} \right] P_m(x,t) = -\frac{\partial J_m(x,t)}{\partial x}. \quad (4.2)$$

In the stationary state, the probability current $J_m(x,t)$ is constant with

$$J_m/D_m = (F/T) P_m - \partial P_m/\partial x. \quad (4.3)$$

The solution of (4.2) for the probability density of the stationary state is given by

$$P_m(x) = \exp(Fx/T) \left[C - J_m/D_m \int_0^x \exp(-Fx'/T) dx' \right] \quad (4.4)$$

with the integration constant C [47]. Although we have no molecular interaction potential, we still stick to the period ℓ . It is reasonable to assume that $P_m(x)$ is bounded for x large enough. We calculate the integral

$$\begin{aligned} \int_0^{\ell n+x} \exp(-Fx'/T) dx' &= \int_0^\ell \exp(-Fx'/T) dx' + \dots \\ &+ \int_{n\ell}^{\ell n+x} \exp(-Fx'/T) dx'. \end{aligned} \quad (4.5)$$

Because of $-F/T \cdot (x + \ell n) = -Fx/T - \ell nF/T$ we obtain

$$\begin{aligned} \int_0^{\ell n+x} \exp(-Fx'/T) dx' &= \int_0^\ell \exp(-Fx'/T) dx' \frac{1 - \exp(-\ell nF/T)}{1 - \exp(-\ell F/T)} \\ &= \exp(-\ell nF/T) \int_0^x \exp(-Fx'/T) dx'. \end{aligned} \quad (4.6)$$

This leads to

$$\begin{aligned} P_m(x + \ell n) &= \exp(Fx/T) \left[C - J_m \frac{I}{D_m (1 - \exp(-\ell F/T))} \right] \cdot \exp(\ell nF/T) \\ &+ \exp(Fx/T) \left[-J_m \frac{I}{D_m (1 - \exp(-\ell F/T))} + \frac{J_m}{D_m} \int_0^x \exp(-Fx'/T) dx \right]. \end{aligned} \quad (4.7)$$

In order to obtain a bounded expression in the limits $F > 0$, $n \rightarrow +\infty$ and $F < 0$, $n \rightarrow -\infty$ respectively, the first bracket has to vanish,

$$J_m I / D_m = C (1 - \exp(-\ell F / T)), \quad (4.8)$$

so that $P_m(x)$ is periodic in x with period ℓ , $P_m(x + \ell) = P_m(x)$. The distribution of the probability density is normalized in the interval from 0 to ℓ ,

$$\begin{aligned} \int_0^\ell P_m(x) dx &= C \int_0^\ell \exp(Fx/T) dx \\ &\quad - J_m / D_m \int_0^\ell \exp(Fx/T) \left(\int_0^x \exp(-Fx'/T) dx' \right) dx \\ &= 1. \end{aligned} \quad (4.9)$$

We solve (4.8) with respect to C and obtain

$$C = \frac{J_m T}{D_m F}. \quad (4.10)$$

This expression can then be inserted into (4.9) and supplies us with

$$J_m = \frac{F D_m}{\ell T}. \quad (4.11)$$

This is the same result obtained for J_m in equation (3.3).

Insertion of the preceding results into (4.4) yields $P_m(x) = 1/\ell$. This stationary solution is different from (2.14) to the effect that the above given P_m does not violate the periodic boundary conditions. Here, the current J_m is non-zero for $F \neq 0$, and the probability distribution is constant, as is to be expected in a periodic system without a molecular interaction potential.

The next step is to assume a situation where we look at a set of an arbitrary number M internal states, each without any molecular interaction potential. The external force stays constant. The M states are considered to be completely decoupled.

In this case we have to solve M Smoluchowski equations (4.2). The normalization of the distribution is then given by

$$\int_0^\ell (P_1^{multi}(x) + P_2^{multi}(x) + \dots + P_M^{multi}(x)) dx = 1, \quad (4.12)$$

where the index ‘‘multi’’ refers to the multi-state system we consider now. If we assume equidistribution of the probability densities in the initial configuration, we have to choose a normalization which is weighted by $1/M$ for each single state. The current in state m of the multi-state system is then accordingly given by

$$J_m^{multi} = \frac{F D_m}{M \ell T}, \quad (4.13)$$

while the total current reads

$$J_{tot}^{multi} = \frac{F D_1}{M \ell T} + \frac{F D_2}{M \ell T} + \dots + \frac{F D_M}{M \ell T}. \quad (4.14)$$

By choosing different small-scale diffusion coefficients D_m , a specific hindrance or promotion against or in favour of moving in the horizontal direction, which might be inherent to a certain conformation of the protein, can easily be modelled.

It is also possible that the initial weights of the internal states vary. This is the case if the conformations refer to defects or mutations of the motor protein which in general occur with different probabilities. Then we have

$$\frac{1}{M_1} + \frac{1}{M_2} + \dots + \frac{1}{M_M} = 1 \quad (4.15)$$

and, accordingly,

$$J_{tot}^{multi} = \frac{FD_1}{M_1\ell T} + \frac{FD_2}{M_2\ell T} + \dots + \frac{FD_M}{M_M\ell T}. \quad (4.16)$$

In this situation of decoupled levels the resulting lateral currents J_m^{multi} depend on the initial probability distribution of our system. In the special case that the motor can be localized in a certain state at time $t = 0$, the weights of the other states are zero.

Connection to coupling between states

Now, we reintroduce a coupling between the states. This coupling is attained by vertical transition rates ω_{mn} , which enter the transition current densities I_m as explained in chapter 2. If all these transition rates are chosen to be equal to ω , $\omega_{mn}(x_k) =: \omega$, for any values of m , n and k , they fulfill the conditions of detailed balance, as up to now we still do not have any potentials, but $U_m(x) =: 0$ for all m , and therefore $\exp(V_m(x_k) - V_n(x_k)) = 1$, irrespective of the choices of m , n or k .

The vertical rates drop out from the total current J_{tot}^{multi} and we obtain equipartition with $1/M$ as in (4.14). If the small-scale diffusion coefficients fulfill $D_1 + D_2 + \dots + D_M = MD_1$, this means that the same value of the total current might result either from a single-state system or from the above-mentioned M -state system. The number of locations where vertical transitions can occur is arbitrary, as a different choice does not change the result.

In a next step, we consider a situation with two states and two locations where vertical transitions can take place. The vertical transition rates are completely unbalanced,

$$\omega_{mn}(x_k) = \Delta_{mn}(x_k), \quad (4.17)$$

compare equation (3.18). The upward rates are chosen to be $\omega_{12}(x_1) = \omega_{12}(x_2) =: \Delta_1$, the downward rates are $\omega_{21}(x_1) = \omega_{21}(x_2) =: \Delta_2$. For $\Delta_1 := \Delta_2$ and $\Delta_2 := \Delta$, the total lateral current reads

$$J_{tot}^{multi} = \frac{F\Delta(D_1 + D_2)}{2\ell T\Delta} = \frac{F(D_1 + D_2)}{2\ell T}. \quad (4.18)$$

If we have $\Delta_1 \neq \Delta_2$, the symmetry between the states is broken. In this general case, J_{tot}^{multi} is calculated as

$$J_{tot}^{multi} = \frac{FD_1\Delta_2}{\ell T(\Delta_1 + \Delta_2)} + \frac{FD_2\Delta_1}{\ell T(\Delta_1 + \Delta_2)}, \quad (4.19)$$

where the first summand belongs to the lateral current in the first state, the second one accordingly to the current in state two. The contribution of one single state to the total current J_{tot}^{multi} grows with the share the rates leading into this state have of the sum of all rates.

If $D_1 = D_2$ and $D_2 =: D$, J_{tot}^{multi} yields for arbitrary values of Δ_1 and Δ_2

$$J_{tot}^{multi} = \frac{FD}{\ell T}. \quad (4.20)$$

As Δ_1 and Δ_2 can take arbitrary values, the contributions of the respective states to the total lateral current might be considerably distinct, whereas the total lateral current J_{tot}^{multi} itself remains unchanged.

Result with potential

Here, we consider a situation where we have non-zero molecular interaction potentials. The one or more states are uncoupled or either coupled by balanced vertical transition rates again.

At first, m is the only state the motor can attain. The Smoluchowski equation with an effective force potential $V(x) = [U(x) - Fx]/T$ is given by

$$\frac{\partial P_m(x, t)}{\partial t} \equiv D_m \frac{\partial}{\partial x} \left[\frac{\partial}{\partial x} V_m(x) + \frac{\partial}{\partial x} \right] P_m(x, t) = -\frac{\partial J_m(x, t)}{\partial x}. \quad (4.21)$$

Here, the solution for the probability density reads

$$P_m(x) = \exp(V_m(x)) \left[C' - J_m/D_m \int_0^x \exp(-V_m(x')) dx' \right] \quad (4.22)$$

with the new integration constant C' . Because of $V_m(x + \ell n) = V_m(x) - \ell n F$ we obtain

$$\begin{aligned} \int_0^{\ell n+x} \exp(V_m(x')) dx' &= \int_0^\ell \exp(V_m(x)) dx \frac{1 - \exp(-\ell n F/T)}{1 - \exp(-\ell F/T)} \\ &\quad + \exp(-\ell n F/T) \int_0^x \exp(V_m(x')) dx'. \end{aligned} \quad (4.23)$$

Again, we impose the normalization condition and the condition that we must get a bounded expression for $P_m(x + \ell n)$ in the limits $F > 0$, $n \rightarrow +\infty$ and $F < 0$, $n \rightarrow -\infty$. This yields

$$C' = \frac{J_m}{D_m} \int_0^\ell \exp(V(x)) dx / (1 - \exp(-F\ell/T)) \quad (4.24)$$

for the integration constant. The current results as

$$\begin{aligned} J_m &= D_m \left[\int_0^\ell \exp(V_m(x)) dx \int_0^\ell \exp(-V_m(x)) dx / (1 - \exp(-F\ell/T)) \right. \\ &\quad \left. - \int_0^\ell \exp(-V_m(x)) \left(\int_0^x \exp(V_m(x')) dx' \right) dx \right]^{-1}, \end{aligned} \quad (4.25)$$

which is in general a non-zero expression. In terms of a $(M, K) = (1, 1)$ -model as in 3.1.1, we have $J_1 = J_{tot}$. Then (4.25) is equal to

$$J_{tot} = \frac{1 - e_1(0, \ell)}{(e_1(0, \ell) - 1) \bar{\mathcal{E}}_1(0) - \mathcal{E}_1(0, \ell) \bar{e}_1}, \quad (4.26)$$

which follows from (3.2) for $x_1 = 0$.

The distribution $P_m(x)$ reads

$$\begin{aligned} P_m(x) &= J_m/D_m (\exp(-V(x))) \left[\int_0^\ell \exp(V(x)) dx / (1 - \exp(-F\ell/T)) \right. \\ &\quad \left. - \int_0^x \exp(V(x')) dx' \right]. \end{aligned} \quad (4.27)$$

As we have used the same considerations as in the context of (4.7), we have $P_m(x + \ell n) = P_m(x)$ for all n . The probability distribution shows the same periodicity as the underlying molecular interaction potentials.

If the external force F is zero, we have

$$\begin{aligned} P_m(x + \ell n) &= \exp(-U(x)/T) \left[C'' - \frac{J_m}{D_m} \int_0^{x+\ell n} \exp(U(x')/T) dx' \right] \\ &= \exp(-U(x)/T) \left[C'' - n \frac{J_m}{D_m} \int_0^\ell \exp(U(x')/T) dx' + \right. \\ &\quad \left. \frac{J_m}{D_m} \int_0^x \exp(U(x')/T) dx' \right]. \end{aligned} \quad (4.28)$$

In order to receive a bounded expression for $P_m(x + \ell n)$ in the limits $n \rightarrow +\infty$ and $n \rightarrow -\infty$, the condition

$$n \frac{J_m}{D_m} \int_0^\ell \exp(U(x')/T) dx' = 0 \quad (4.29)$$

has to be fulfilled. Therefore we can conclude that in a one-state system in the case of an arbitrary exponentially integrable molecular interaction potential, but no external force we have $J_m = 0$ as in 3.1.1.

In a multi-state system with M states and arbitrary constant force F we impose the normalization (4.12). For a balanced coupling between the states this leads to the total current

$$J_{tot}^{multi} = J_1^{multi} + J_2^{multi} + \dots + J_M^{multi} \quad (4.30)$$

with the single-state currents $J_m^{multi} = J_m/M$ and J_m as in (4.25). The same is true for the probability densities P_m^{multi} ,

$$P_{tot}^{multi} = P_1^{multi} + P_2^{multi} + \dots + P_M^{multi} \quad (4.31)$$

with $P_m^{multi} = P_m/M$ and P_m as in (4.27). In this way we have shown that in a multi-state system with an external force in which all transitions fulfill the conditions of detailed balance the currents J_m^{multi} are in general finite with $J_m \neq 0$ due to F , and the probability densities P_m^{multi} reflect the periodicity of the molecular interaction potentials. The conditions of detailed balance are fulfilled in a model without active processes as enzymatic activity.

In this subsection we have treated the decoupling of states for special simple systems. For more complex systems, we return to the network-based approach, compare 4.1.2.

4.1.2 Decoupled levels and localized transitions

The calculation of the total current with the use of linear algebra as in (3.9) fails in the presence of decoupled levels, as in this case we have $\det \mathbf{A}^{(M,K)} = 0$. Here we show how the network-based approach used in chapter 3 has to be modified so that more comprehensive systems with decoupling of states or subsystems can be dealt with, too. We remember that a decoupled state is defined as a level without any non-zero vertical rates connecting it to another state. The matrices $\mathbf{A}^{(M,K)}$ as calculated in chapter 2 and their submatrices are singular. The corresponding graph is disconnected, which means that there are vertices which are not connected by a path. No vertex belonging to the states one and two in fig. 4.1 can be reached by a path from a vertex of state three or the other way round. In the following, the decoupled level is taken to be M . As the labelling of the states is arbitrary, we can choose any level to be the decoupled one without a loss of generality. In contrast to chapter 4.1.1, here decoupled levels are treated in the discrete network approach.

Decoupled states: algebraic approach

Single decoupled state

In the following, $\mathbf{A}^{(M,K),\{1,2,\dots,M-1\},\{M\}}$ denotes the $2M \times 2M$ -matrix, which is obtained from $\mathbf{A}^{(M,K)}$ by neglecting the vertical rates between state M and other states, i.e., we set $\omega_{Mm}(x_k) = 0$ and $\omega_{mM}(x_k) = 0$ for arbitrary m and k . The first braces in the exponent refer to the subsystem with the states $1, 2, \dots, M-1$, the second braces to the subsystem with the single state M .

We consider an example with $(M, K) = (3, 2)$, where we decouple the third state $M = 3$ as in fig. 4.1.

The resulting matrix $\mathbf{A}^{(3,2),\{1,2\},\{3\}}$ is given in appendix A.4. The general matrix $\mathbf{A}^{(2,2)}$ as in (3.5) is regained from $\mathbf{A}^{(3,2),\{1,2\},\{3\}}$ if we cross out the second and the fifth column and the third and sixth row. Similarly, the $\mathbf{A}^{(1,1)}$ matrix is obtained from the matrix $\mathbf{A}^{(2,1),\{1\},\{2\}}$ by eliminating the first and third column as well as the second and fourth row, and the $\mathbf{A}^{(3,1)}$ matrix can be obtained from the $\mathbf{A}^{(4,1),\{1,2,3\},\{4\}}$ -matrix by cancelling the columns three and seven and the rows four and eight. $\mathbf{A}^{(2,3)}$ results from $\mathbf{A}^{(3,3),\{1,2\},\{3\}}$ when we cross out the columns two and five as well as the rows three and six.

In summary, we obtain the matrix $\mathbf{A}^{(M-1,K)}$ from $\mathbf{A}^{(M,K),\{1,2,\dots,M-1\},\{M\}}$ by erasing the $(M-1)$ th and the $(2M-1)$ th column as well as the M th and $2M$ th row. The elements of the $(2M-1)$ th column and the M th and $2M$ th row of $\mathbf{A}^{(M,K),\{1,2,\dots,M-1\},\{M\}}$ are equal to zero or

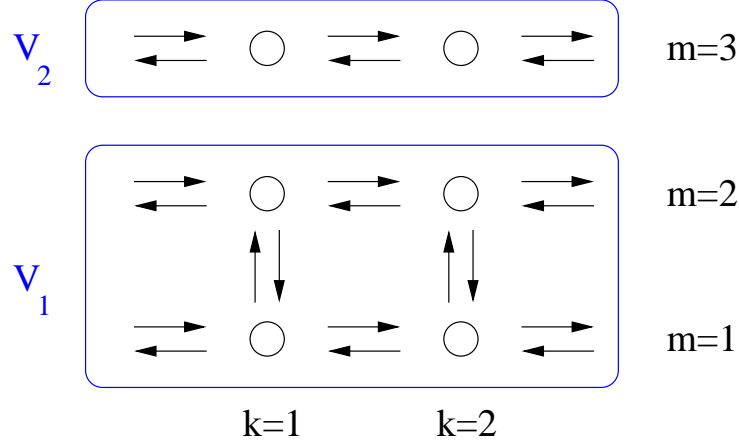


Figure 4.1: The third state in this system of three states and two locations is decoupled and the graph disintegrates into two parts whose vertices belong to the subsets of vertices V_1 and V_2 , respectively. V_1 contains the vertices of the states $m = 1$ and $m = 2$, V_2 the vertices of $m = 3$. There are no rates connecting V_1 and V_2 .

refer to state M . The elements of the $(M - 1)$ th column are, except for a change of sign, contained in the elements of the preceding columns.

The lateral current in the decoupled state is zero if the external force F is zero. Otherwise we have

$$J_m = \frac{FD_m}{M_M \ell T}, \quad (4.32)$$

as in section 4.1.1, where $1/M_M$ is the probability weight of state M . Subject to these considerations the total lateral current in the case of one decoupled state is calculated easily from $\mathbf{A}^{(M-1, K)}$ and its submatrices. The probability weight $1/M_M$ is one if the motor is frozen in this state. In this way we can describe situations when a motor has certain defects as the ones leading to the syndromes mentioned in section 1.1. If our motor is an “ill” one, it is in state M at the beginning and cannot produce net movement without an external force. If it is “healthy” its starting conformation will belong to the other $M - 1$ states with probability one and it will move regularly.

Arbitrary number of decoupled states

Now, we view a situation where we have a set of vertically decoupled states, in general more than one, forming a subsystem. The graph divides into two parts whose vertices belong to different subsets V_1 and V_2 with $V_1 = \{(m_1, k), (n_1, k), \dots\}$ and $V_2 = \{(m_2, k), (n_2, k), \dots\}$ for all $k \in \{1, \dots, K\}$ and $m_1 \neq n_1 \neq m_2 \neq n_2 \neq \dots$. The graph is disconnected in such a way that there are no di-edges connecting any two vertices v_1 and v_2 with $v_1 \in V_1$ and $v_2 \in V_2$. The $2M_1 \times 2M_1$ -matrix $\mathbf{A}^{(\{m_1, n_1, \dots\}, K)(M_1, K)_{eff}}$, where M_1 is the number of states comprised in the first subset of vertices V_1 , describes the subnetwork belonging to V_1 . The m_1, n_1, \dots are the states in this subset V_1 , and K is, as usual, the total number of locations where transitions into other states are possible. The matrix $\mathbf{A}^{(\{m_1, n_1, \dots\}, K)(M_1, K)_{eff}}$ is obtained from the matrix $\mathbf{A}^{(M, K)}$ of the complete (M, K) -network by erasing the rows m_2, n_2, \dots and $M + m_2, M + n_2, \dots$ as well as the columns $m_2 - 1, n_2 - 1, \dots$ and $M - 1 + m_2, M - 1 + n_2, \dots$ for all m_2, n_2, \dots with $(m_2, k), (n_2, k), \dots \in V_2$. If $m_2 - 1 = 0$ or $n_2 - 1 = 0$, the columns m_2 and n_2 are crossed out instead. This is a generalization of the procedure described in the case of a single decoupled state before. In an analogous way, $\mathbf{A}^{(\{m_2, n_2, \dots\}, K)(M_2, K)_{eff}}$ is obtained by cancelling the rows m_1, n_1, \dots and $M + m_1, M + n_1, \dots$ as well as the columns $m_1 - 1, n_1 - 1, \dots$ and $M - 1 + m_1, M - 1 + n_1, \dots$ for all m_1, n_1, \dots with $(m_1, k), (n_1, k), \dots \in V_1$.

Fig. 4.2 shows a $(4, 2)$ -network which decouples into two $(2, 2)$ -networks. The decoupling is achieved by limiting the vertical rates to the altogether eight rates $\omega_{12}(x_k)$, $\omega_{21}(x_k)$ and $\omega_{34}(x_k)$,

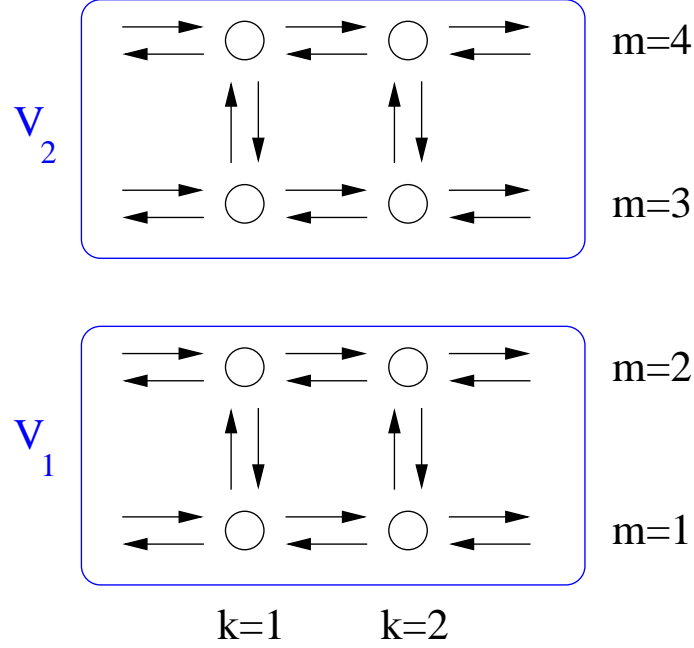


Figure 4.2: $(M, K) = (4, 2)$ -network which decouples into two $(2, 2)$ -networks. The first subset of vertices, V_1 , comprises all the vertices in the states $m = 1$ and $m = 2$. The subset V_2 comprises the vertices of the states $m = 3$ and $m = 4$. There is no rate which connects the two subsets V_1 and V_2 , they are completely decoupled.

$\omega_{43}(x_k)$. Appendix A.5 shows in detail the elements of the matrix $\mathbf{A}^{(4,2),\{1,2\},\{3,4\}}$, i.e., the matrix $\mathbf{A}^{(4,2)}$ without the vertical rates connecting the different subsets of vertices, and how the submatrices $\mathbf{A}^{\{1,2\},(2,2)}_{eff}$ and $\mathbf{A}^{\{3,4\},(2,2)}_{eff}$ describing the $(M, K) = (2, 2)$ -subsystem formed by the states $m = 1, 2$ and $m = 3, 4$, respectively, are derived. Fig. 4.3 provides a schematic overview of this example with $\mathbf{A}^{\{1,2\},(2,2)}_{eff}$ denoted by \blacksquare and $\mathbf{A}^{\{3,4\},(2,2)}_{eff}$ by \blacksquare . The total current is calculated from the submatrices $\mathbf{A}^{\{1,2\},(2,2)}_{eff}$ and $\mathbf{A}^{\{3,4\},(2,2)}_{eff}$ after adapting the normalization condition for the probability densities.

4.1.3 Numerical approach to decoupled levels

Singular value decomposition methods

If we consider an example where we know all the quantities which enter the elements of a numerical matrix $\mathbf{A}_{num}^{(M,K)}$ and want to calculate the numerical value of the total current, we can use standard singular value decomposition methods and compute the pseudo-inverse of $\mathbf{A}_{num}^{(M,K)}$.

Singular value decomposition (SVD) methods are based on the theorem that any quadratic matrix, which in particular includes any $2M \times 2M$ matrix $\mathbf{A}_{num}^{(M,K)}$, whose number of rows, in our case $2M$, is equal to its number of columns, can be written as the product of an $2M \times 2M$ column-orthogonal matrix \mathbf{U} , an $2M \times 2M$ diagonal matrix \mathbf{W} with positive or zero elements (the singular values), and the transpose of an $2M \times 2M$ orthogonal matrix \mathbf{V} [56], i.e., $\mathbf{A}_{num}^{(M,K)} = \mathbf{U} \cdot \mathbf{W} \cdot \mathbf{V}^T$. A proof of this theorem by induction can be found in [57].

The matrices \mathbf{U} and \mathbf{V} are orthogonal in the sense that their columns are orthonormal,

$$\sum_{i=1}^{2M} U_{ik} U_{in} = \delta_{kn}, \quad \text{for } 1 \leq k \leq 2M, 1 \leq n \leq 2M, \quad (4.33)$$

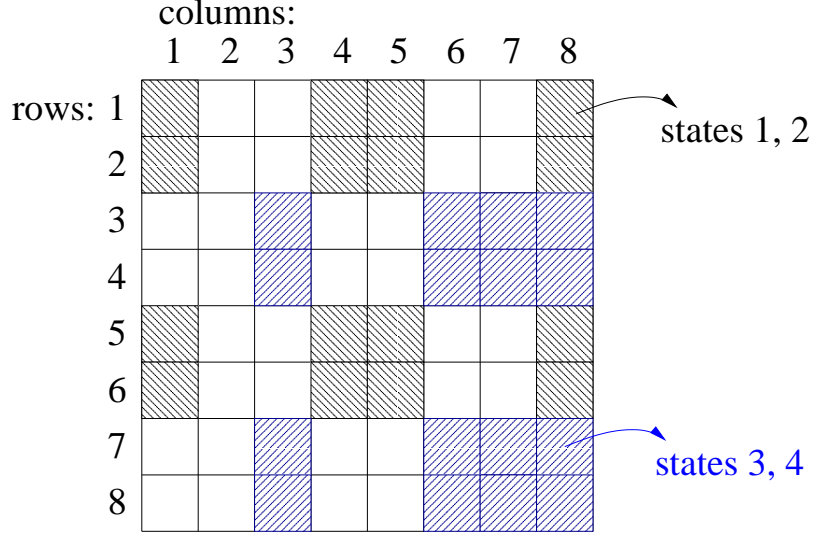


Figure 4.3: Scheme of the 8×8 -matrix $\mathbf{A}^{(4,2),\{1,2\},\{3,4\}}$ showing the position of $\mathbf{A}^{\{1,2\},2,(2,2)}_{eff}$ (black) and $\mathbf{A}^{\{3,4\},2,(2,2)}_{eff}$ (blue). $\mathbf{A}^{(4,2),\{1,2\},\{3,4\}}$ is the matrix of the $(M, K) = (4, 2)$ -system which decomposes into the two subsets V_1 with the states $m = 1, 2$ and V_2 with $m = 3, 4$ as shown in fig. 4.2. $\mathbf{A}^{\{1,2\},2,(2,2)}_{eff}$ is the effective $(M, K) = (2, 2)$ -matrix belonging to the states $m = 1, 2$, and $\mathbf{A}^{\{3,4\},2,(2,2)}_{eff}$ the effective $(M, K) = (2, 2)$ -matrix belonging to $m = 3, 4$. The white squares in this scheme of matrix elements refer to elements which are either zero or proportional to other elements, compare appendix A.5.

$$\sum_{j=1}^{2M} V_{jk} V_{jn} = \delta_{kn}, \quad \text{for } 1 \leq k \leq 2M, 1 \leq n \leq 2M. \quad (4.34)$$

\mathbf{V} is square and therefore also row-orthonormal.

The decomposition is unique up to making the same permutation of the columns of \mathbf{U} , elements of \mathbf{W} , and columns of \mathbf{V} , or forming linear combinations of any columns of \mathbf{U} and \mathbf{V} whose corresponding elements of \mathbf{W} happen to be exactly equal.

As the matrix $\mathbf{A}_{num}^{(M,K)}$ is square, \mathbf{U} , \mathbf{V} , and \mathbf{W} are square matrices of the same size. The inverses of \mathbf{U} and \mathbf{V} are equal to their transposes, because \mathbf{U} and \mathbf{V} are orthogonal. The inverse of \mathbf{W} is the diagonal matrix whose elements are the reciprocals of the elements w_j . So the pseudo-inverse of $\mathbf{A}_{num}^{(M,K)}$ is given by

$$\left(\mathbf{A}_{num}^{(M,K)}\right)^{-1} = \mathbf{V} \cdot [diag(1/w_j)] \cdot \mathbf{U}^T. \quad (4.35)$$

In this construction it is possible that one or more than one of the w_j 's are zero or numerically so small that their values are dominated by roundoff error.

The condition number of a matrix is defined as the ratio of the largest in magnitude of the w_j 's to the smallest of the w_j 's. A matrix is singular if its condition number is infinite, and it is ill-conditioned if its condition number is too large, i.e., if its reciprocal approaches the machine's floating-point precision.

If the matrix $\mathbf{A}_{num}^{(M,K)}$ is nonsingular, then its range will be, for $\mathbf{A}_{num}^{(M,K)} \cdot \mathbf{x} = \mathbf{b}$, all of the vector space \mathbf{b} , so its rank is $2M$. If $\mathbf{A}_{num}^{(M,K)}$ is singular, then the rank will be less than $2M$ according to "rank plus nullity equals $2M$ ".

SVD explicitly constructs orthonormal bases for the nullspace and range of a matrix. The columns of \mathbf{U} whose same-numbered elements w_j are non-zero are an orthonormal set of basis vectors that span the range. The columns of \mathbf{V} whose same-numbered elements w_j are zero are an orthonormal basis for the nullspace.

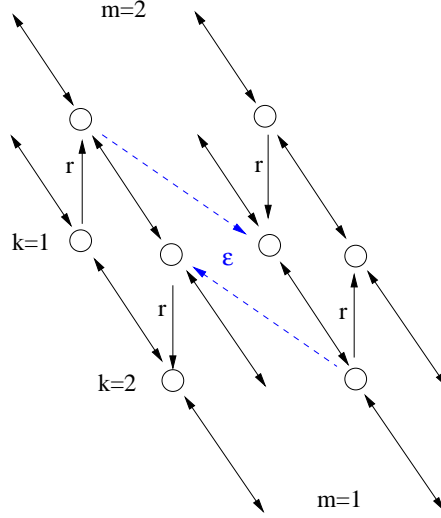


Figure 4.4: Two (2,2)-ratchet systems with coupling parameter ϵ . The perspective view illustrates that in this system there are two identical conformations $m = 1$ and two states $m = 2$. The rates connecting $m = 1$ and $m = 2$ are given by r .

Application: $(M, K) = (2, 2)$ as limiting case of $(M, K) = (3, 2)$

Now, we consider an example where we use SVD. The general outline is that of the single decoupled state in 4.1.2, i.e., we take a look at the case $(M, K) = (3, 2)$. We assume $F = 0$ and imply the additional restriction that we only allow vertical transition rates which directly connect the first two states, i.e., we have the set of vertical rates established by $\omega_{12}(x_1)$, $\omega_{21}(x_1)$, $\omega_{12}(x_2)$ and $\omega_{21}(x_2)$. $\mathbf{A}_{num}^{(3,2),\{1,2\},\{3\}}$ is singular and a numerical matrix. The pseudo-inverse $(\mathbf{A}_{num}^{(3,2),\{1,2\},\{3\}})^{-1}$ can be calculated with the help of SVD, which in turn can be used in order to calculate the total current J_{tot} . We choose fixed values for the four vertical rates $\omega_{12}(x_1)$, $\omega_{21}(x_1)$, $\omega_{12}(x_2)$ and $\omega_{21}(x_2)$, respectively and the remaining parameters of the system. From the pseudo-inverse $(\mathbf{A}_{num}^{(3,2),\{1,2\},\{3\}})^{-1}$ we calculate the total current J_{tot} .

As we have $F = 0$, the current in the third state is zero. So for comparison we calculate the inverse $(\mathbf{A}_{num}^{(2,2)})^{-1}$ for a genuine system with two states. The calculation of the total current yields approximately the same value for J_{tot} again. The difference between the both exact results is in the range of a numerical error and very small compared to J_{tot} .

So if we have a numerical matrix $\mathbf{A}_{num}^{(M,K)}$, we can use SVD and do not have to bother about the details of decoupling discussed in 4.1.2. In our general models, however, the parameters are usually not known in detail.

4.1.4 Coupling parameter and bifurcations

Now, we consider two identical subsystems with a coupling between them. It is imaginable that for certain values of the coupling parameter one and the same “macroscopic” value of the total current is created by different “microscopic” situations. The introduction of the decoupling of states supplies us with a method to discuss such kinds of bifurcations in specially defined networks.

Here, we take into consideration a situation similar to that illustrated by fig. 4.2, but with the essential difference that now we have a variable coupling of strength ϵ instead of no coupling, compare fig. 4.4. In addition, the states one and three and two and four are assumed to be pairwise identical, so that we have two states $m = 1$ and two states $m = 2$. The pairwise identical states can be explained as belonging to identical conformations of the motor protein. The model of

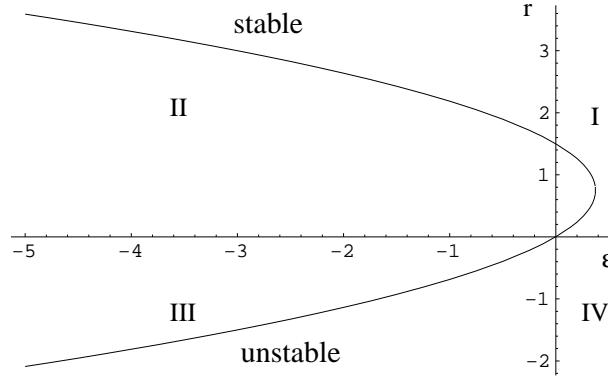


Figure 4.5: Parabola of a saddle-node bifurcation with system parameters as pointed out in the text. The first quadrant *I* refers to non-negative transition rates and therefore includes the physical solutions.

fig. 4.4 contains four vertical transition rates apart from the coupling parameter ε . The value of those four vertical rates is considered to be r . The system for $J_{tot} = 0$ then has the two solutions

$$\begin{aligned}
 r_1 &= \left[(-1+a) \cdot b - a \cdot c + a^2 \cdot c - \left((b+a \cdot c) \left((-1+a)^2 \right. \right. \right. \\
 &\quad \left. \left. \left. (b+a \cdot c) - 4 \cdot \varepsilon \cdot a \cdot b \cdot c \cdot \ell_\Omega \right)^{1/2} \right) / (2 \cdot a \cdot b \cdot c \cdot \ell_\Omega), \\
 r_2 &= \left[(-1+a) \cdot b - a \cdot c + a^2 \cdot c + \left((b+a \cdot c) \left((-1+a)^2 \right. \right. \right. \\
 &\quad \left. \left. \left. (b+a \cdot c) - 4 \cdot \varepsilon \cdot a \cdot b \cdot c \cdot \ell_\Omega \right)^{1/2} \right) / (2 \cdot a \cdot b \cdot c \cdot \ell_\Omega)
 \end{aligned} \tag{4.36}$$

with the corresponding system parameters $a := e_2(x_1, x_2)$, $b := \mathcal{E}_2(x_1, x_2)$, and $c := \mathcal{E}_2(x_2, x_1 + \ell)$, which depend on the effective force potentials as introduced in chapter 2. In order to examine the stability of the solutions r_1 and r_2 , we calculate the Jacobian. In the following we choose numerical values for the parameters. As a result, we find a saddle-node bifurcation, see fig. 4.5 [58, 59]. The parameters are $a = 2$ and $b = c = \ell_\Omega = 1$ and assumed to be dimensionless. r_2 , which belongs to the upper branch, yields stable nodes as solutions, r_1 unstable saddle points. The model system of fig. 4.4 can adopt two different stationary states for identical values of the coupling ε . When we look at the case of zero external force, the trivial solution for $J_{tot} = 0$ is obtained if $r = 0$ and $\varepsilon = 0$. This is the case of complete decoupling of all four states and free diffusion in every single one of these states, which does not lead to a net current without an external force. The bifurcation ceases to exist independently of the value of the coupling ε if $b = -ac$ or if $4\varepsilon abc \ell_\Omega = 0$. This is the case for zero external force and free diffusion in state two. For $a = 1$, the vertex of the parabola is shifted to $(\varepsilon, r) = (0, 0)$. As dynamic variables and control parameters are real, this means that either b or c have to be negative in this case to ensure the real values. In general, r and ε will be non-negative as transition rates, and we will only take into account the first quadrant of fig. 4.5.

4.2 Distorted networks

Up to now, our networks have been constrained in so far as the horizontal rates have to implicitly fulfill the conditions of detailed balance, which means that the transport in the horizontal direction is not actively hindered or promoted. Such an active transport can be integrated into our systems via distortion of the underlying networks. An alternative approach will be discussed in 4.3 and 4.4.

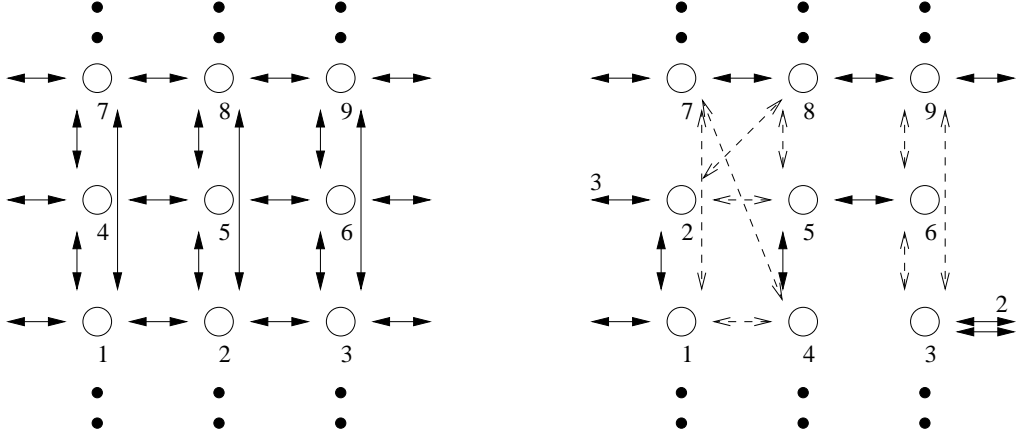


Figure 4.6: Left-hand side: detail of a large network with vertices $i = 1, \dots, 9$. The network extends further in vertical (indicated by the dots) and horizontal direction. Right-hand side: the same detail, but now the network has been distorted by transferring vertex 2 to the former location of vertex 4 and vice versa; broken di-edges correspond to mappings of vertical transition rates. These rates can be unbalanced. The numbers at two of the horizontal edges denote the numbers of the terminal vertices of the corresponding edges.

4.2.1 Concepts of distortion and unbalanced transitions in x -direction

Our networks are defined completely by their graphs, i.e., by their respective sets of vertices and edges. In graph theory, isomorphic graphs are usually not distinguished [60], and one just talks about different representations of the same graph. In the case of our networks this means that they might be distorted and obtain different shapes, in particular, if several transition rates are set equal to zero. In order to guarantee the periodic boundary conditions, we apply the distortions to larger networks. It is possible to distort the networks in such a way that the resulting networks contain active elements given by unbalanced transition rates whose direction is no longer vertical.

4.2.2 Application and rules

The left-hand side of fig. 4.6 shows a detail of a network with the vertices $i = 1, \dots, 9$, which might be a part of a large-scale network. The right-hand side shows the mapping of this network onto a distorted network which originates from transferring vertex 2 to the former location of vertex 4 and vice versa. Broken di-edges correspond to mappings of vertical transition rates. In the distorted network it is possible to have an unbalanced transition between the vertices 1 and 4, which are now connected in the horizontal x -direction. Here, we concentrate on distortions which are generated by effectively swapping the locations of pairs of vertices. The transition rates are denoted by $\omega_{mn}(x_k, x_l)$, where m, n are the apparent states, and x_k and x_l are the new locations, i.e. we assume that the past of the rates is unknown and their labelling is determined by their present occurrence. The labelling of the states and locations follows the scheme used in fig. 4.7. At first, we concentrate on one pair of possibly unbalanced transitions in x -direction, $\omega_{11}(x_1, x_2)$ and $\omega_{11}(x_2, x_1)$. The other horizontal and diagonal transition rates which might be unbalanced are set to zero. The resulting network is shown on the left-hand side of fig. 4.7. Now, the total current contains combinations of possibly unbalanced rates as displayed on the right-hand side of fig. 4.7. Here, we have an active displacement from location x_m to x_n in state m .

For $F = 0$, each term of the numerator polynomial of the total current in a distorted network can be mapped onto a generalized s-cycle of the network. A generalized s-cycle is a closed path of the type

$$\omega_{mn}(x_k, x_k) \omega_{no}(x_l, x_l) \omega_{rr}(x_o, x_p) \omega_{pm}(x_q, x_q). \quad (4.37)$$

The horizontal rate $\omega_{rr}(x_o, x_p)$ is connected to the preceding vertical rate via the destination

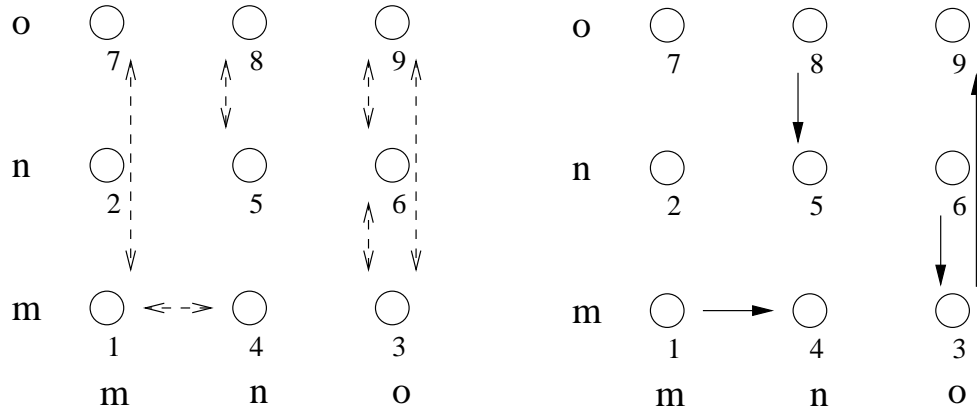


Figure 4.7: Left-hand side: detail of a network resulting from the distorted network as shown in fig. 4.6. Diagonal rates and the horizontal rates between the vertices 2 and 5 have been set to zero, so that we have a single pair of unbalanced transitions in x -direction. Transitions which have to be balanced are not shown for simplicity. The letters denote the respective states and locations. Right-hand side: combination of possibly unbalanced rates in a term of the numerator polynomial of the corresponding total current.

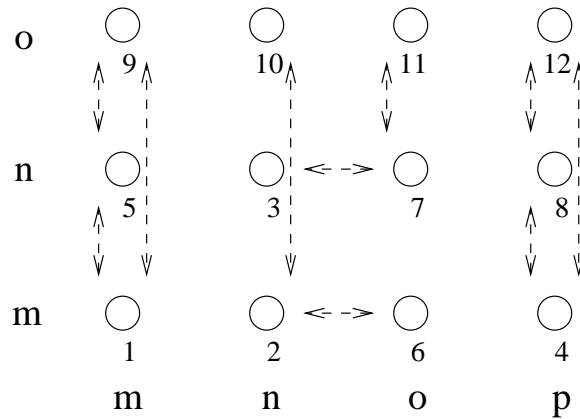


Figure 4.8: Detail of a larger network. For the three states and four locations of this distorted part we consider two possibly unbalanced horizontal transition rates.

index o of the first location, the second location x_p provides the starting state of the succeeding vertical rate. If we have more than one active or unbalanced horizontal transition in our network, the generalized s -cycles might contain more than one horizontal rate, too.

There can also be diagonal rates, e.g. $\omega_{om}(x_m, x_n)$ in fig. 4.6. These diagonal rates enter the generalized s -cycles via these two of their four indices which do not occur twice. For example, the rate $\omega_{om}(x_m, x_n)$ comprises the four indices o, m, m and n . The index m occurs twice, so o and n are the relevant indices for the generalized s -cycle. The rate might be preceded by a vertical rate leading into state o , while a succeeding vertical rate might originate from state n . Of course, this index rule holds for mere horizontal or vertical rates, too.

Fig. 4.8 shows a detail of a larger network which contains two possibly unbalanced horizontal transition rates resulting from the exchange of the positions of the vertices 3 and 6. In general, we can introduce an arbitrary number of unbalanced horizontal transitions into our networks by swapping the positions of vertices. If we are starting from a situation where we only know the present shape of the network, which includes possibly unbalanced horizontal transitions, but not the original network, we are still able to list the terms of the total current by taking into account

generalized s-cycles.

4.3 Master equation and horizontal rates

In this section we introduce a discrete Master-equation approach to our system. This approach explicitly comprises the horizontal forward and backward rates. With the help of these horizontal rates we are able to determine uniquely complete s-cycles, which contribute to the total current in our network, rather than only contributions by vertical rates. In this way it becomes clear whether a combination of rates belongs to the motor taking a forward or a backward step. Furthermore, with this additional piece of information we can determine for sure which conformation can be associated with the motor entering the network from the left, or, in the case of a backward step, with the motor entering it from the right. In the Master-equation approach it is possible to abstain from the original definition of the horizontal rates, so that we can break the conditions of detailed balance for these rates, too, and have active horizontal elements. Besides, we derive extensions to the rules in 3.2.2, since now the polynomials depend on the vertical and also on the horizontal rates. The Master equation has been introduced in [43], but this is the first time that this approach is used to perform calculations for general model systems.

4.3.1 General outline

At first, we introduce several changes in our notation as compared to chapter 2.

Now, the probabilities of finding the motor in the discrete states (m, k) are denoted by

$$P(m, k) \equiv P_m(x_k) \ell_\Omega \quad (4.38)$$

We introduce the forward transition rate

$$W(m, k | m, k + 1) \equiv \frac{e_m(x_k, x_{k+1})}{\mathcal{E}_m(x_k, x_{k+1}) \ell_\Omega}, \quad (4.39)$$

which belongs to the motor moving from location x_k in state m to location x_{k+1} in the same state. The rate for a backward move in level m from position x_{k+1} to x_k is accordingly denoted as

$$W(m, k + 1 | m, k) \equiv \frac{1}{\mathcal{E}_m(x_k, x_{k+1}) \ell_\Omega}. \quad (4.40)$$

Here, the horizontal rates show a pairwise dependence,

$$\begin{aligned} W(m, k | m, k + 1) &= \frac{e_m(x_k, x_{k+1})}{\mathcal{E}_m(x_k, x_{k+1}) \ell_\Omega} \\ &= e_m(x_k, x_{k+1}) W(m, k + 1 | m, k), \end{aligned} \quad (4.41)$$

and accordingly fulfill the conditions of detailed balance. As $e_m(x_k, x_{k+1}) \neq 0$ for every choice of m and k , a horizontal forward rate can never vanish equal to zero. The same is true for backward rates, $W(m, k + 1 | m, k) \equiv 1/\mathcal{E}_m(x_k, x_{k+1}) \ell_\Omega$, as their numerators are constant and equal to one. Nevertheless, the horizontal rates might attain small values and approach zero, if the corresponding $\mathcal{E}_m(x_k, x_{k+1})$ are large. The interlevel current $J_{mn}(x_k)$ as given by (2.25) is rewritten in the form

$$J_{mn}(x_k) \equiv P(m, k) W(m, k | n, k), \quad (4.42)$$

where we have adapted the notation for the vertical transition rates to

$$W(m, k | n, k) \equiv \omega_{mn}(x_k). \quad (4.43)$$

Now, equation (2.41) reads

$$P(m, k + 1) = -J(m, k | m, k + 1) \frac{1}{W(m, k + 1 | m, k)} + P(m, k) \frac{W(m, k | m, k + 1)}{W(m, k + 1 | m, k)} \quad (4.44)$$

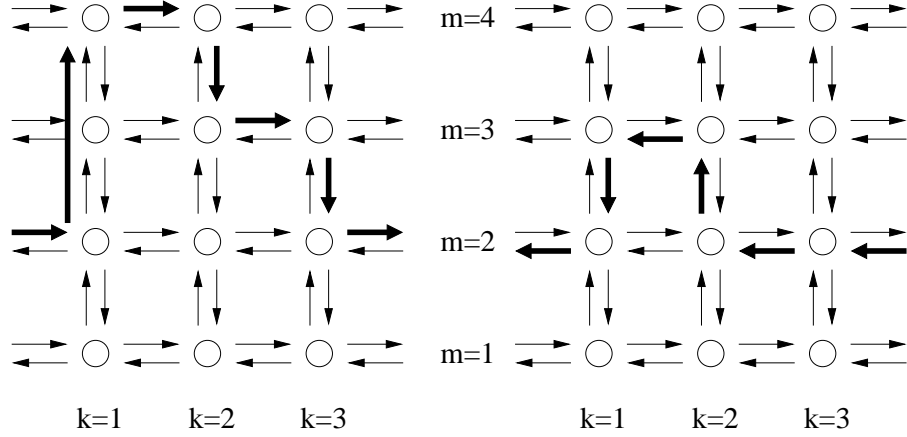


Figure 4.9: Complete spanning cycles in the directed graph of a network with four states and three locations. The s-cycles are indicated by sequences of bold arrows. Left: forward or positive s-cycle containing the three vertical rates $W(2, 1|4, 1)$, $W(4, 2|3, 2)$ and $W(3, 3|2, 3)$. Right: negative s-cycle with the two vertical rates $W(2, 2|3, 2)$ and $W(3, 1|2, 1)$. Note that beyond the s-cycles the representation of the vertical rates is restricted to rates connecting adjacent states for simplicity. Because at least one state of the network is not included in these s-cycles, there will be additional vertical rates in the respective terms of $\overline{Pol}_1^{(4,3)}$ or otherwise the network will be decoupled and the rates joining these states will vanish.

with the outgoing local lateral currents from x_k to x_{k+1} as introduced in (2.29).

The relations (4.42) and (4.44) (after conversion) are inserted into the local conservation law (2.30), which yields

$$\begin{aligned}
0 = & \sum_{n, n \neq m} [-P(m, k) W(m, k|n, k) + P(n, k) W(n, k|m, k)] \\
& -P(m, k) W(m, k|m, k+1) + P(m, k+1) W(m, k+1|m, k) \\
& -P(m, k) W(m, k|m, k-1) + P(m, k-1) W(m, k-1|m, k).
\end{aligned} \tag{4.45}$$

The parts which enter with a minus sign are the transition currents flowing out of the vertex (m, k) , those with a plus sign are the ones flowing into this vertex. In (4.45) we see that the stationary solutions of the stochastic ratchets considered here are identical to the stationary solutions of the Master equation

$$\begin{aligned}
\frac{\partial P(m, k)}{\partial t} = & \sum_{n, n \neq m} [-P(m, k) W(m, k|n, k) + P(n, k) W(n, k|m, k)] \\
& -P(m, k) W(m, k|m, k-1) + P(m, k+1) W(m, k+1|m, k) \\
& -P(m, k) W(m, k|m, k-1) + P(m, k-1) W(m, k-1|m, k),
\end{aligned} \tag{4.46}$$

which describes the temporal change of the probability of finding the motor in a state associated with the vertex (m, k) in terms of the various transition currents. The effective force potentials are no longer contained explicitly. Starting from the Master equation (4.46) and not considering its derivation, there is no need for the horizontal rates to fulfill the conditions of detailed balance.

The local lateral current between location k and $k+1$ in state m is given by

$$J(m, k|m, k+1) = P(m, k) W(m, k|m, k+1) - P(m, k+1) W(m, k+1|m, k). \tag{4.47}$$

By transforming (4.47), we obtain the probability at location $k + 1$,

$$P(m, k + 1) = -J(m, k | m, k + 1) \frac{1}{W(m, k + 1 | m, k)} + P(m, k) \frac{W(m, k | m, k + 1)}{W(m, k + 1 | m, k)}. \quad (4.48)$$

We introduce the diagonal matrices $\overline{\mathbf{D}}^{JP}$ and $\overline{\mathbf{D}}^{PP}$ with matrix elements

$$\overline{D}_{nm}^{JP}(k, k + 1) \equiv -\delta_{nm} \frac{1}{W(m, k + 1 | m, k)} \quad (4.49)$$

and

$$\overline{D}_{nm}^{PP}(k, k + 1) \equiv \delta_{nm} \frac{W(m, k | m, k + 1)}{W(m, k + 1 | m, k)}. \quad (4.50)$$

The bar above the symbols refers to the Master-equation approach which is used here in contrast to chapter 2. Besides, we define the additional transfer matrices

$$\overline{\mathbf{T}}^{JP} \equiv \overline{\mathbf{T}}^{JJ} \overline{\mathbf{D}}^{JP} \quad (4.51)$$

and

$$\overline{\mathbf{T}}^{PP} \equiv \overline{\mathbf{T}}^{PJ} \overline{\mathbf{D}}^{JP} + \overline{\mathbf{D}}^{PP} \quad (4.52)$$

where $\overline{\mathbf{T}}^{JJ}$ is equal to the unit matrix and $\overline{\mathbf{T}}^{PJ}(k)$ is given by

$$\overline{\mathbf{T}}_{nm}^{PJ}(k) \equiv -\delta_{nm} \sum_{p \neq m} W(m, k | p, k) + (1 - \delta_{nm}) W(n, k | m, k). \quad (4.53)$$

With the help of these additional matrices we obtain

$$\begin{aligned} P(m, k + 1) &= J(k, k + 1) \overline{\mathbf{D}}^{JP}(k, k + 1) + P(k) \overline{\mathbf{D}}^{PP}(k, k + 1) \\ &= J(k - 1, k) \overline{\mathbf{T}}^{JP}(k, k + 1) + P(k) \overline{\mathbf{T}}^{PP}(k, k + 1). \end{aligned} \quad (4.54)$$

This relation and (4.47) can be combined into the recursion relation

$$(J(k, k + 1), P(k + 1)) = (J(k - 1, k), P(k)) \overline{\mathbf{T}}(k, k + 1). \quad (4.55)$$

We proceed by analogy to the procedure described in section 2.2 and take into account that the normalization for the discrete probability distribution is now given by

$$\sum_k \sum_m P(m, k) \equiv 1. \quad (4.56)$$

Doing so, we obtain new matrices $\overline{\mathbf{A}}^{(M, K)}$ which explicitly contain all the horizontal and vertical rates of the system.

4.3.2 Complete s-cycles and horizontal rates

Spanning cycles or s-cycles have already been introduced in 2.2.3 and examined later in chapter 3. We remember that an s-cycle starts at vertex $(k = 1, m)$, spans the whole network parallel to the x -direction, and then ends at vertex $(k = K, m)$, i.e., in the same state m it started in. An s-cycle has to contain vertical rates. In the preceding chapters, we have identified these s-cycles via their vertical rates. Because of the Master-equation approach, we now have the possibility of determining complete paths of vertical and horizontal rates. Note, that here we do not refer to the generalized s-cycles of 4.2.2 for distorted networks, but to complete s-cycles explicitly containing all their horizontal and vertical rates. Furthermore, we extend the original definition provided in 2.2.3 in such a way that we distinguish between *positive spanning-cycles* or *positive s-cycles*, which traverse the network in positive x -direction, in fig. 4.9 to the right, and *negative s-cycles* traversing it in negative x -direction. Accordingly, positive spanning-cycles are associated with a forward stepping of the motor, negative ones with a backward stepping. Usually, there is a main direction of movement for a certain motor protein. Conventional kinesin, for example, most of the time steps in the direction of the plus end of its microtubule. We define this main direction to be the positive x -direction with respect to a special motor protein.

Networks with two states

Two locations

Here, we discuss complete s-cycles in the context of different two-state networks. At first, we consider a general $(M, K) = (2, 2)$ -network with the maximal number of four vertical rates and eight horizontal rates. Four of these eight horizontal rates directly connect the two locations x_1 and x_2 , the remaining warrant the periodic boundary conditions. We calculate the total current $\overline{J}_{tot}^{(2,2)}$ using the new matrix $\overline{\mathbf{A}}^{(2,2)}$,

$$\left(\begin{array}{cccc} \frac{W(1,2|2,2)}{W(1,2|1,1)} & -\frac{1}{W(1,2|1,1)} & 0 & -\frac{1}{W(1,2|1,1)} \\ & -\frac{1}{W(1,2|1,K+1)} & & \\ -\frac{W(2,2|1,2)}{W(2,2|2,1)} & 0 & -\frac{1}{W(2,2|2,1)} & -\frac{1}{W(2,2|2,1)} \\ & & -\frac{1}{W(2,2|2,K+1)} & \\ -W(1,1|2,1) - W(1,2|2,2) & \frac{W(1,1|2,1)}{W(1,2|1,1)} & & \frac{W(1,1|2,1)}{W(1,2|1,1)} \\ \cdot \left[\frac{W(1,1|2,1)}{W(1,2|1,1)} + \frac{W(1,1|1,2)}{W(1,2|1,1)} \right] & +\frac{W(1,1|1,2)}{W(1,2|1,1)} & -\frac{W(1,1|2,1)}{W(2,2|2,1)} & +\frac{W(1,1|1,2)}{W(1,2|1,1)} \\ -\frac{W(1,1|2,1)W(2,2|1,2)}{W(2,2|2,1)} & -\frac{W(1,K+1|1,2)}{W(1,2|1,K+1)} & & -\frac{W(1,1|2,1)}{W(2,2|2,1)} \\ W(2,1|1,1) + W(2,2|1,2) & & \frac{W(2,1|1,1)}{W(2,2|2,1)} & -\frac{W(2,1|1,1)}{W(1,2|1,1)} \\ \cdot \left[\frac{W(2,1|1,1)}{W(2,2|2,1)} + \frac{W(2,1|2,2)}{W(2,2|2,1)} \right] & -\frac{W(2,1|1,1)}{W(1,2|1,1)} & +\frac{W(2,1|2,2)}{W(2,2|2,1)} & +\frac{W(2,1|1,1)}{W(2,2|2,1)} \\ +\frac{W(1,2|2,2)W(2,1|1,1)}{W(1,2|1,1)} & & -\frac{W(2,K+1|2,2)}{W(2,2|2,K+1)} & +\frac{W(2,1|2,2)}{W(2,2|2,1)} \end{array} \right), \quad (4.57)$$

and view the numerator polynomial $\overline{Pol}_1^{(2,2)}$. The terms of $\overline{Pol}_1^{(2,2)}$ contain only vertical or horizontal rates. Altogether, there are two positive and two negative complete s-cycles in $\overline{Pol}_1^{(2,2)}$, which contribute to $\overline{J}_{tot}^{(2,2)}$. The existence of two positive and of two negative s-cycles has already been assumed in the context of equation (3.6) because of the signs of the terms, but now the complete paths with vertical and horizontal rates are given explicitly in $\overline{Pol}_1^{(2,2)}$. We obtain one positive combination with $W(1,1|2,1)$, $W(2,1|2,2)$, $W(2,2|1,2)$ and $W(1,2|1,K+1)$, and a second one with the rates $W(2,1|1,1)$, $W(1,1|1,2)$, $W(1,2|2,2)$ and $W(2,2|2,K+1)$, see fig. 4.10, both of which are complete s-cycles of horizontal and vertical rates, but in the first case the motor is in conformation $m = 1$ on entering the network from the left, in the second case in conformation $m = 2$. Usually one of these paths can be assumed to carry a by far larger current across the network than the other one. The rates in one of the s-cycles will be quite low, if its sequence of conformations and locations hinders enzymatic activity. Without the specification of the horizontal rates, the direction of the s-cycles is ambiguous. The left-hand positive

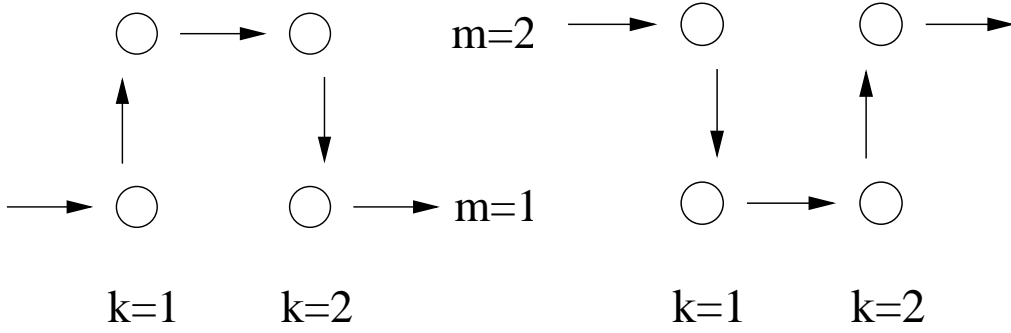


Figure 4.10: The two forward or positive complete s-cycles in $\overline{Pol}_1^{(2,2)}$ for $(M, K) = (2, 2)$. On the left, the starting conformation of the motor is $m = 1$, on the right it is $m = 2$. Usually, one of the two cycles will be strongly favoured and carry a large current across the network.

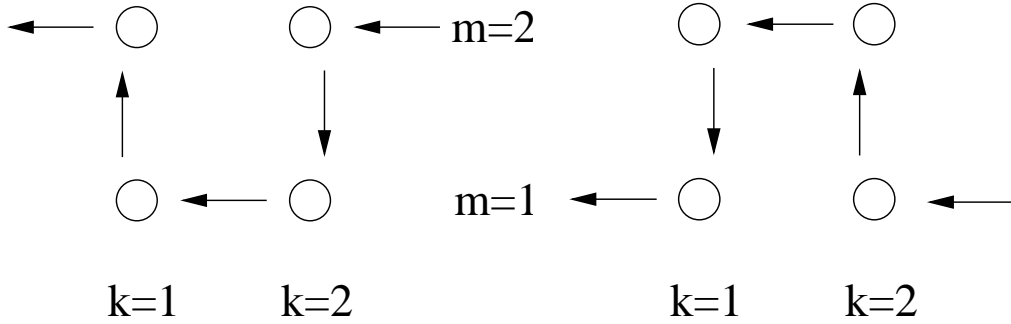


Figure 4.11: The two backward or negative complete s-cycles in the first polynomial for $(M, K) = (2, 2)$. On the left, the starting conformation of the motor is $m = 2$, on the right it is $m = 1$.

s-cycle in fig. 4.10, for example, could have been mistaken for the backward cycle with the rates $W(2, K+1|2, 2)$, $W(2, 2|1, 2)$, $W(1, 2|1, 1)$ and $W(1, 1|2, 1)$, if only the vertical rates had been taken into consideration.

The above listed backward cycle is one of the two backward cycles which are possible in a $(2, 2)$ -model. The second negative s-cycle is described by the rate combination $W(1, K+1|1, 2)$, $W(1, 2|2, 2)$, $W(2, 2|2, 1)$ and $W(2, 1|1, 1)$. In this case the motor is in conformation $m = 1$ on entering the network from the right. Fig. 4.11 displays the two negative s-cycles. If the system's rates fulfill the conditions of detailed balance, the left-hand side complete backward s-cycle cancels with the right-hand side combination in fig. 4.10.

If we now forget about the definition of the forward horizontal rates as given in (4.39), we can consider arbitrary forward rates, whose values might be equal to zero, too. This is justified as our approach here uses the Master equation as its starting point. In the context of (4.39) the forward rates have been non-zero as the numerator in the definition is a special exponential function. If we now have $W(1, 1|1, 2) = 0$ the number of forward s-cycles reduces to one, as the combination on the right in fig. 4.10 vanishes. The zero horizontal rate can be thought of to represent an obstacle in the positive x -direction of the filament which cannot be overcome by the motor while it is in conformation $m = 1$. Meanwhile, the backward s-cycles are unchanged.

The backward horizontal rates cannot be set to zero, as they appear as divisors in the calculation. In the same way the forward rates $W(m, K|m, K+1)$, which realize the periodic boundary conditions, cannot vanish. In summary, horizontal rates equal to zero in the context of this changed transfer matrix formalism are restricted to horizontal forward rates at inner locations.

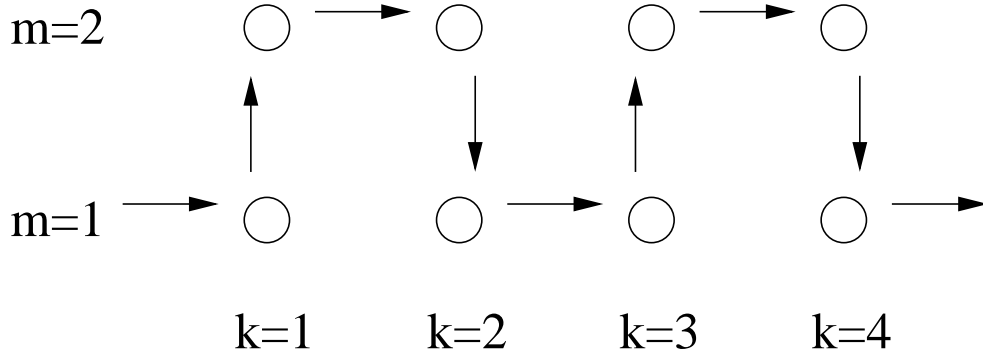


Figure 4.12: Complete forward s-cycle with four vertical transition rates in $\overline{Pol}_1^{(2,4)}$ in a limited (2,4)-system containing only the four vertical rates occurring here.

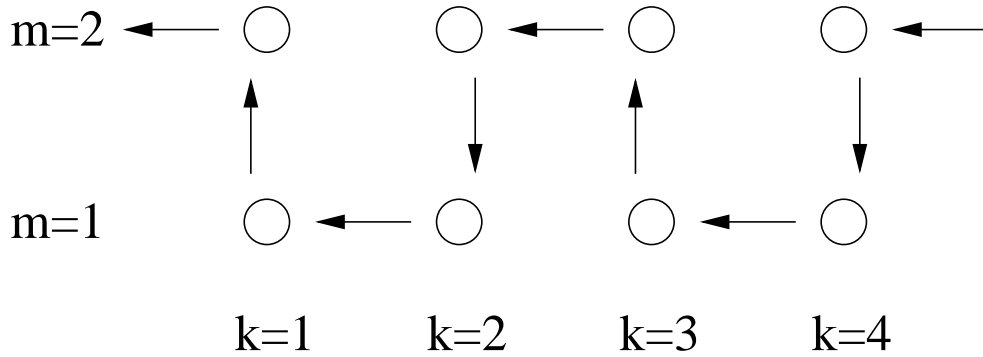


Figure 4.13: Complete backward s-cycle in $\overline{Pol}_1^{(2,4)}$ in a system with the same four vertical transition rates as in fig. 4.12.

Four locations

In the case of $(M, K) = (2, 4)$ we consider the restricted case of four vertical transition rates, namely $W(1, 1 | 2, 1)$, $W(2, 2 | 1, 2)$, $W(1, 3 | 2, 3)$ and $W(2, 4 | 1, 4)$. The other four vertical transition rates of the general system vanish equal to zero. As the number of vertical rates is restricted to four, there is a single combination with four vertical transition rates in the numerator polynomial $\overline{Pol}_1^{(2,4)}$. This combination occurs twice in $\overline{Pol}_1^{(2,4)}$, once in a term corresponding to a forward s-cycle, and a second time in a negative s-cycle belonging to a backward term. The complete forward combination is shown in fig. 4.12, the backward combination in fig. 4.13. As the forward and backward cycle belong to different internal states or conformations at the boundaries of our system box, we can predict whether the motor is about to take a forward or a backward step if we catch it in a certain conformation in this region.

Now, we have a look at fig. 4.14. It shows all six combinations in $\overline{Pol}_1^{(2,4)}$ which contain exactly the two vertical transition rates $W(1, 1 | 2, 1)$ and $W(2, 2 | 1, 2)$. If the bottom right combination was the only one in a model system, the rates $W(1, 3 | 1, 2)$ and $W(1, 4 | 1, K + 1)$ would empty the vertices (1, 3) and (1, 4) which would then lead to $P(1, 3) = 0$ and $P(1, 4) = 0$ in the stationary state, i.e., there would be no actual current flowing from the vertices (1, 3) and (1, 4) in the stationary state.

As in the example with two vertical rates the number of vertical rates has decreased by two compared to the previous combinations with four rates, the number of horizontal rates has been raised by two on the other hand. The total number of vertical and horizontal rates is constant and equal to $MK = 8$. Note that in the figures for clarity the horizontal rates belonging to the periodic boundary conditions for s-cycles are depicted twice, once on entering and once on leaving

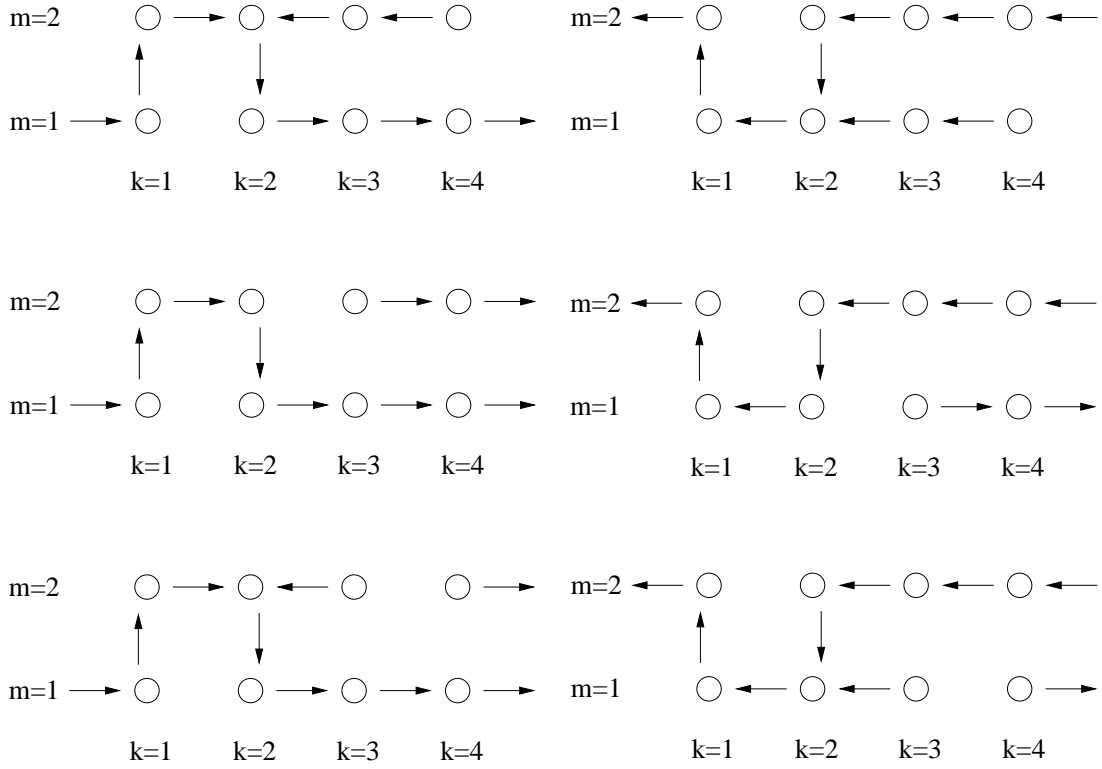


Figure 4.14: The six different combinations in $\overline{Pol}_1^{(2,4)}$ which contain exactly the two vertical transition rates $W(1,1|2,1)$ and $W(2,2|1,2)$. The first three combinations belong to the same complete positive s-cycle, the next three combinations describe the same complete negative s-cycle. Combinations with the same positive or negative s-cycle differ in the additional horizontal rates. The horizontal rates for the boundary conditions in the cycle are drawn twice.

the network, nevertheless they have to be counted as one rate each.

Network with three states and two locations

Fig. 4.15 shows terms of $\overline{Pol}_1^{(3,2)}$, which include positive s-cycles. Horizontal backward rates do not occur in these combinations. Again we observe an emptying of single vertices under the assumption that these combinations are on their own. In general there will be additional combinations of rates emptying other vertices or states and balancing the effect in this way.

The total number of rates is the same in all the terms in $\overline{Pol}_1^{(M,K)}$ in a certain (M, K) -system. In the $(3, 2)$ -system this number is 6. So in a combination with 3 vertical rates there are 3 horizontal rates, and in a combination with 4 vertical rates there are 2 horizontal rates.

4.3.3 Rules: dependence of the total current on vertical and horizontal rates

From our calculations for several specific systems we derive rules as in 3.2.2 which now relate the polynomials $\overline{Pol}_1^{(M,K)}$ and $\overline{Pol}_2^{(M,K)}$ to the vertical and horizontal transition rates.

Rule 0: The dependence of the total current $\overline{J}_{tot}^{(M,K)}$ on the system's transition rates W_r has

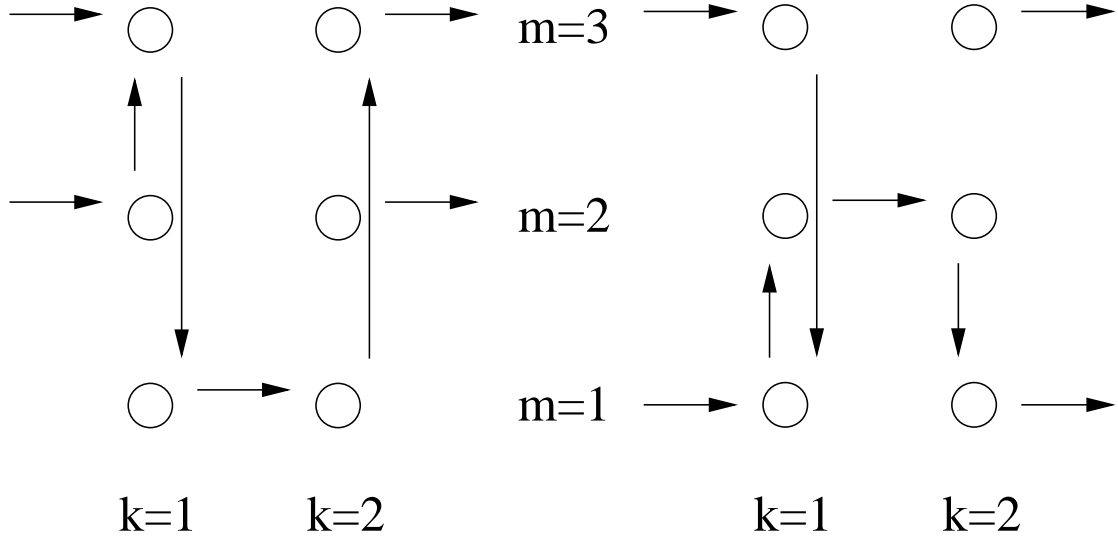


Figure 4.15: Examples of complete combinations of vertical and horizontal rates in $\overline{Pol}_1^{(3,2)}$ which include forward s-cycles. The horizontal rates maintaining the periodic boundary conditions are drawn twice.

the form

$$\overline{J}_{tot}^{(M,K)} = \frac{\overline{Pol}_1^{(M,K)}(W_1, W_2, \dots, W_N)}{\overline{Pol}_2^{(M,K)}(W_1, W_2, \dots, W_N)} \quad (4.58)$$

with two polynomials $\overline{Pol}_1^{(M,K)}$ and $\overline{Pol}_2^{(M,K)}$.

Rule 1: Both polynomials are multilinear in all the rates $W(m, k | m, k+1)$, $W(m, k+1 | m, k)$, $W(m, k | n, k)$ and $W(n, k | m, k)$ with $m \neq n$, i.e., they are multilinear in all the vertical and horizontal transition rates. Each term \mathcal{T} of both $\overline{Pol}_1^{(M,K)}$ and $\overline{Pol}_2^{(M,K)}$ reads as

$$\mathcal{T} \sim W_1^{z_1} W_2^{z_2} \dots W_N^{z_N} \quad \text{with } z_r = 0, 1, \quad (4.59)$$

i.e., it cannot contain powers W_i^z with $z \geq 2$. The index i indicates an arbitrary numbering of the rates.

Rule 2: Each polynomial term \mathcal{T} in $\overline{Pol}_1^{(M,K)}$ contains at least K factors $W(m, k | m, l)$ of horizontal rates and $M-1$ factors $W(m, k | n, k)$ of vertical rates, i.e.,

$$\sum_{r, hor.} z_r \geq K \quad \text{for each } \mathcal{T} \quad (4.60)$$

and

$$\sum_{r, ver.} z_r \geq M-1 \quad \text{for each } \mathcal{T}. \quad (4.61)$$

The upper limit of vertical transition rates per term is given by

$$\sum_{r, ver.} z_r \leq K(M-1) \quad \text{for each } \mathcal{T}, \quad (4.62)$$

and for horizontal transition rates by

$$\sum_{r, hor.} z_r \leq M(K-1) + 1 \quad \text{for each } \mathcal{T}. \quad (4.63)$$

Here, the sum over r is the sum over all the rates of the same alignment, either vertical or horizontal.

The total number of vertical and horizontal rates in $\overline{Pol}_1^{(M,K)}$ is MK .

Rule 3: No term \mathcal{T} contains a product of the form $W(m, j | n, k)W(m, j | o, l)$, or, in words, there is no product of two rates with the same starting vertex. As there are MK vertices in a general network, this limits the total number of rates per term to MK as stated in *rule 2*.

Rule 4: No term \mathcal{T} contains a product of the form $W(m, k | n, k)W(n, k | m, k)$ for vertical or $W(m, k | m, l)W(m, l | m, k)$ for horizontal rates or any other 1-cycles. Horizontal 1-cycles are localized with respect to the state.

Rule 5: The combination of vertical rates in each term \mathcal{T} contains vertices of every single internal state m , the one of horizontal rates vertices of every single location k . In $\overline{Pol}_1^{(M,K)}$ the horizontal rates irrespective of their states connect the locations 1 and 2, the locations 2 and 3 and so on until K and the first location are connected again. Because here the periodic boundary conditions have to be included, this explains the minimal number of K (instead of $K-1$) horizontal rates per term in $\overline{Pol}_1^{(M,K)}$.

Rule 6: For $F = 0$ and the horizontal rates fulfilling the conditions of detailed balance, each term \mathcal{T} of $\overline{Pol}_1^{(M,K)}$ can be mapped onto a complete s-cycle of the network, which contains vertical and horizontal rates. In general, this mapping is not one-to-one and several terms will be mapped onto the same s-cycle.

Rule 7: If all the transition rates satisfy detailed balance with $W_i = W_i^{db}$, one has

$$\overline{J}_{tot}^{(M,K)} \sim \overline{Pol}_1^{(M,K)} (W_1^{db}, W_2^{db}, \dots) = 0 \text{ for } F = 0. \quad (4.64)$$

In fact, each term of $\overline{Pol}_1^{(M,K)}$ corresponding to a certain complete s-cycle is cancelled by another term corresponding to the opposite complete s-cycle.

In summary, we have shown that the Master-equation approach leads to a comprehensive understanding of the many terms of $\overline{Pol}_1^{(M,K)}$ concerning their associated paths. This is only possible with explicit horizontal rates.

4.4 Time evolution of initial probability distributions

In this section we view the time evolution of several networks on their way to their respective stationary states and its dependence on the initial probability distribution. At first, we integrate the Master equation as given by (4.46). In this way we obtain results which can be checked by means of a Markov-chain approach. We consider systems with a larger number of locations where we have remarkable hindrances at locations or special transport properties of certain states. From that we can judge the importance of such changes. Apart from a detailed stepping scheme, an application for systems with a large number of locations is to describe genetic defects in filaments occurring with a period larger than the pseudorepeat or the stepping distance of a motor.

4.4.1 Integration of the Master equation

The discrete master equation as given by (4.46) can be integrated by numerical methods. In this way we obtain information about the dynamics of the systems. Using a numerical approach, we can view larger systems than before. Here, we examine systems with up to 16 locations. Now, arbitrary rates can be zero, in particular horizontal backward rates, as we do not refer to the original derivation of the Master equation. Such arbitrary horizontal are related to active elements in horizontal direction as discussed recently in the context of molecular motors [61, 62], compare the sections 4.2 and 4.3. Clearly, the active elements are not restricted to the horizontal or vertical direction, as our networks are uniquely determined by their vertices and the di-edges connecting them. The actual direction of an edge can be quite different from the zero or ninety degree angle

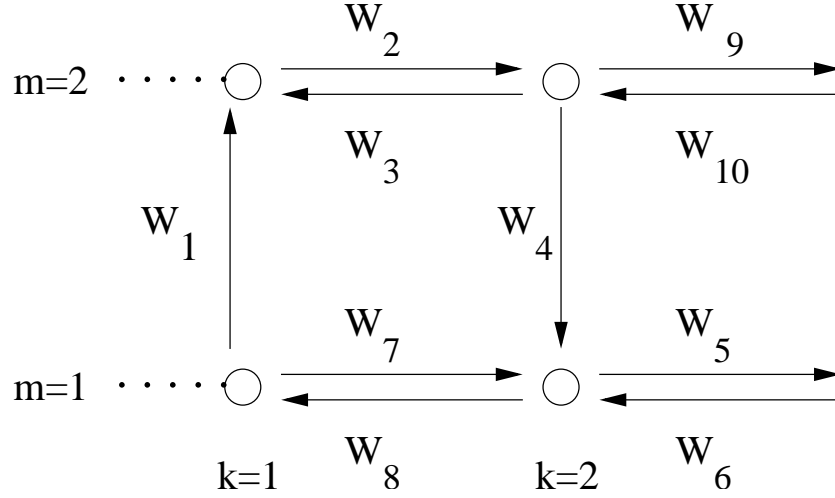


Figure 4.16: Network with two states and locations and two vertical and eight horizontal transition rates connecting its vertices. The W_i refer to the values of the transition rates.

with respect to the filament direction. In spite of this we still continue to use the terms vertical and horizontal for simplicity.

Different initial probability distributions are examined in order to determine the time evolutions of the system until the stationary state is reached. We determine the current carried through the network and the changes of the probability distributions.

Limited (2,2)-network

The starting point for our examination of the time evolution is a model network of two states and two locations with two vertical and eight horizontal transition rates, compare fig. 4.16, where the values of the transition rates are referred to as W_i with $i = 1, \dots, 10$. In this numerical approach the horizontal rates $W(m, k | m, k + 1)$ and $W(m, k + 1 | m, k)$ can be chosen arbitrarily. This will be done in the following. To start with we choose an example where the rates take on the values $W_1 = W_4 = 0.5$, $W_2 = W_5 = W_8 = W_{10} = 1.0$ and $W_3 = W_6 = W_7 = W_9 = 0.25$ which is the first example in table 4.1. In the following, the rates will be defined by dimensionless values for simplicity.

Fig. 4.17 and 4.18 show the time evolution of the system for two different initial probability distributions. The probabilities $P(m, k, t_0)$ of finding the motor in the state (m, k) at time t_0 are given by $P(m, k, t_0) = 0.25$ for $m = 1, 2$ and $k = 1, 2$ in fig. 4.17 and by $P(m, k, t_0) = 1.0$ for $m = 1$ and $k = 1$ and $P(m, k, t_0) = 0.0$ for the remaining states for the development shown in fig. 4.18. In this second case the motor is localized in vertex $(1, 1)$ at the beginning. The solid lines in the figures correspond to $P(m, k) = 0.25$, which is the uniform distribution for four vertices.

Of course, the stationary states which are reached in these two examples are identical, as any vertex of the system is connected to every other vertex either directly or via other vertices. The probabilities in the stationary state are $P(1, 1) = P(2, 2) = 1/3$ and $P(1, 2) = P(2, 1) = 1/6$ which is clear from the preceding choice of the rates. With the uniform initial probability distribution, there are only minor changes in the probability distribution after 100 timesteps, compare fig. 4.17, although the final stationary state is reached only after almost 400 timesteps. In the case of the localized a priori probability distribution, the system is still far from the stationary state after 100 timesteps. After 400 timesteps the configuration is similar to the stationary one, but still it takes about 1500 timesteps until the stationary state of the system is finally reached.

Usually, the initial probability distribution is localized in one vertex, if the period of the system corresponds to one or more steps of the motor and there are few locations and ample different conformations. In situations with many locations and a number of similar conformations, however,

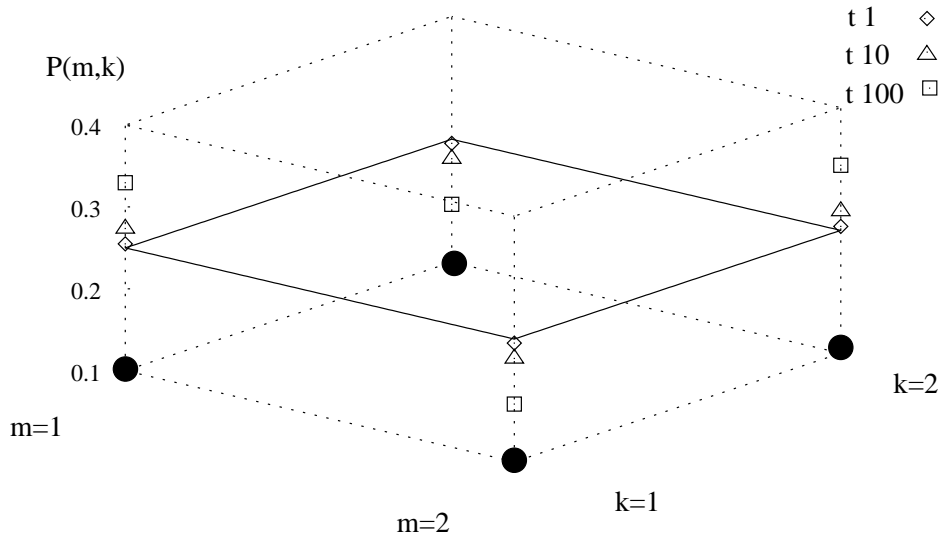


Figure 4.17: Time development of $P(m, k)$ for a uniform a priori probability distribution in a system of two states and two locations. The rates are chosen as in the first example in table 4.1. The black circles indicate the position of the vertices. The solid lines refer to the plane belonging to $P(m, k) = 0.25$. We see snapshots taken after 1, 10 and 100 timesteps.

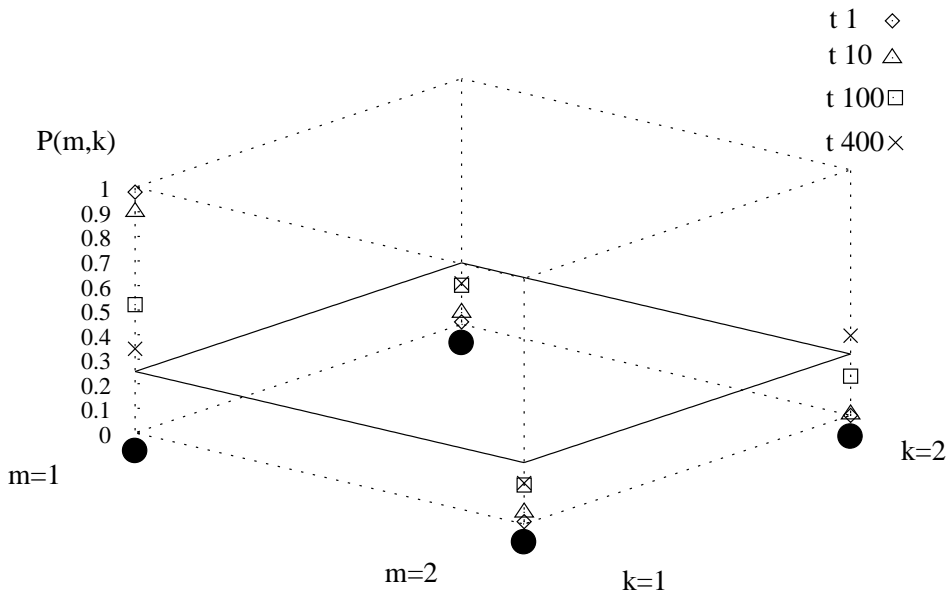


Figure 4.18: Time-dependent behaviour of $P(m, k)$ for an initial probability distribution which is localized in vertex $(1, 1)$. The system has two states and two locations and its rates are listed in the first example in table 4.1. The plane $P(m, k) = 0.25$ is marked by solid lines again. The snapshots are taken after 1, 10, 100 and 400 timesteps.

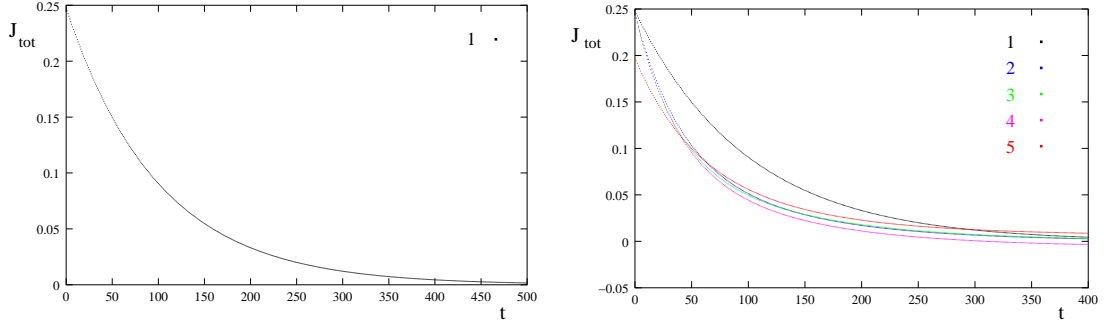


Figure 4.19: Time evolution of the total current J_{tot} for the initially $(1,1)$ -localized probability distribution in the $(2,2)$ -system. The examples are specified in table 4.1. The left-hand side displays the curve corresponding to example 1, the right-hand side shows all five curves for the examples 1 to 5. The curves for the examples 2 and 3 show a very similar course. The stationary states are not yet reached. The stationary currents are given in the text.

example \ rates	W_1	W_2	W_3	W_4	W_5	W_6	W_7	W_8	W_9	W_{10}
1	0.5	1.0	0.25	0.5	1.0	0.25	0.25	1.0	0.25	1.0
2	0.2	1.0	0.25	0.8	1.0	0.25	0.25	1.0	0.25	1.0
3	0.2	0.8	0.2	0.8	1.0	0.25	0.25	1.0	0.2	0.8
4	0.2	0.8	0.2	0.8	1.0	0.25	0.25	1.0	0.25	1.0
5	0.2	1.0	0.25	0.8	1.0	0.25	0.2	0.8	0.25	1.0

Table 4.1: Values of the rates W_i as defined in fig. 4.16 for the examples 1 to 5.

it can be difficult to localize the motor “frozen” in one vertex, and it makes sense to assume a different initial probability distribution.

The time evolution of the total current J_{tot} in the case of the $(1,1)$ -localized a priori probability distribution for the first example in table 4.1 is shown for up to 500 timesteps on the left-hand side of fig. 4.19. In this region, we observe an exponential decay of the total current according to $J_{tot}(t) \approx \exp(-0.01t - 1.4)$. The current is zero in the stationary state.

The right-hand side of fig. 4.19 shows this curve again and also four other curves of different examples 2 to 5 for initially $(1,1)$ -localized probability distributions. Table 4.1 specifies these new examples. The faster decrease for the examples 2 to 4 is mainly caused by the new choice of the vertical transition rates. The changed vertical rates result in a stationary distribution where the probability for vertex $(1,1)$ is still high. In example 5 the current is lower at the beginning compared to the other curves, because of a small current in the first state. This is due to W_7 rising from the vertex $(1,1)$, where the initial probability is localized, hindering a redistribution.

The stationary states in these examples are reached after between 1000 and 1500 timesteps. The stationary currents are $J_{tot}^{1stat} = J_{tot}^{2stat} = J_{tot}^{3stat} = 0$ for the examples 1, 2 and 3 and $J_{tot}^{4stat} = -J_{tot}^{5stat} \approx -6 \cdot 10^{-3}$ in the remaining examples. The network as shown in fig. 4.16 comprises the forward path given by the rates W_5 , W_1 , W_2 , and W_4 as well as the backward path with W_{10} , W_4 , W_8 and W_1 . Pairs of horizontal rates connecting vertices in opposite directions result in effective horizontal rates. Although in a strict sense the detailed balance condition is broken for the vertical rates in all of these examples, as one of the vertical rates connecting a pair of vertices in opposite direction is set to zero, while on the other hand the exponential factor of the detailed-balance relation is different from zero, the total current J_{tot}^{stat} in the stationary state vanishes for the first three examples. Of course, this does not violate our previous *rule 7* in 3.2.2, because there we only state that $J_{tot}^{stat} = 0$ without an external force if the vertical and horizontal rates fulfill detailed balance. Obviously, we can also have $J_{tot}^{stat} = 0$ if the conditions of detailed balance are broken. In our examples 1, 2 and 3 the total current vanishes, as the above mentioned forward and backward paths contribute partial currents to the states whose absolute values are

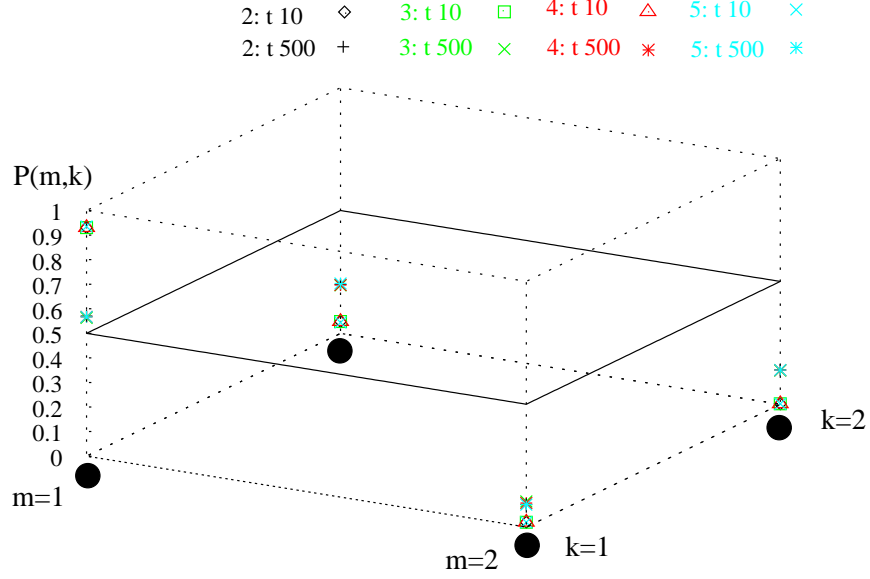


Figure 4.20: Probability distributions at $t = 10$ and $t = 500$ of the examples 2-5 with two states and two locations. The numbers preceding the colons are the numbers of the examples introduced in table 4.1. The plane $P(m, k) = 0.5$ is set off by solid lines.

equal, but which differ in their direction. In example 4, the total current is directed in the negative x -direction, since the forward contribution is reduced by the effective horizontal contribution of the rates W_2 and W_3 . The combination of W_7 and W_8 in example 5 however leads to a resulting positive current.

The corresponding probability distributions at times $t = 10$ and $t = 500$ are shown in fig. 4.20 for the examples 2 to 5. The stationary distributions are similar. The values we find for the stationary state for example 5 are $P^{5\text{ stat}}(1, 1) \approx .56$, $P^{5\text{ stat}}(1, 2) \approx .20$, $P^{5\text{ stat}}(2, 1) \approx .09$ and $P^{5\text{ stat}}(2, 2) \approx .14$.

The general (2, 2)-network

The stationary probability distributions for the general (2, 2)-system, i.e., the network of two states and two locations with four vertical and eight horizontal rates as shown in fig. D.1, are given in appendix D. The solution of the homogeneous system of equations is given in such a way that three of the stationary probability distributions $P^{\text{stat}}(m, k)$ depend on the remaining fourth. Taking into consideration the normalization condition for the probability distribution, the solution is unique and unambiguous for a non-specified choice of the rates W_i numbered as indicated in fig. D.1.

If, however, all the vertical rates W_1 , W_4 , W_{11} and W_{12} vanish equal to zero, there is an infinite set of solutions, as there is no exchange between the two states, once the initial probability distribution has been specified. In this case we have

$$\begin{aligned}
 P^{\text{stat}}(1, 1) &= P^{\text{stat}}(1, 2)(W_5 + W_8) / (W_6 + W_7), \\
 P^{\text{stat}}(2, 1) &= P^{\text{stat}}(2, 2)(W_3 + W_9) / (W_{10} + W_2) \\
 &\text{for } W_1 = W_4 = W_{11} = W_{12} = 0.
 \end{aligned} \tag{4.65}$$

Note that in (4.65) we still have to take into account the normalization condition for the probabilities. Here, we tacitly extend the discussion of decoupled states compared to section 4.1.2, as the explicit initial probability distributions in this approach replace the somewhat artificial probability weights we have used before.

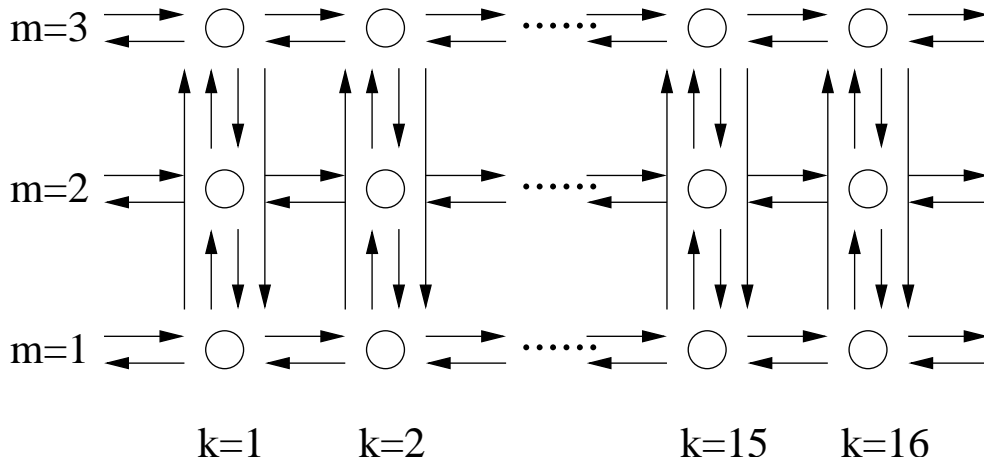


Figure 4.21: Part of a large system with three states and sixteen locations at which the motor might undergo conformational changes. Since the period of this system includes a considerably larger number of locations for vertical transitions, the motor might take several steps within this spatial interval. The choice of the number of the locations is arbitrary.

Time evolution in larger systems

The numerical integration provides us with a tool for dealing with larger model systems than the ones examined in chapter 3. Here, we concentrate on systems with more than the previous maximal number of four locations for transitions into other conformations. The period of such a large system might comprise more than one step of the motor. The motor's track might show periodic irregularities on a larger scale than just one step. There can be defects or obstacles as other bound molecules attached to the filament, which occur on average after a given number of steps of the motor. Therefore we have a look at the behaviour of systems with a larger number of locations and imagine that within the given spatial interval the motor bridges a distance of a hundred nm or more. Then we watch the localized initial probability distribution spread along the horizontal direction under a variety of different circumstances.

Three states

Our example is a system of three states with a total number of sixteen locations for conformational changes, compare fig. 4.21. The number of sixteen is chosen arbitrarily. Fig. 4.22 shows the time evolution of the total current J_{tot} for the case of an initial probability distribution which is localized in vertex (1, 1). In this example we have inserted all the 192 vertical and horizontal rates as indicated by the detail in fig. 4.21. The curve on the left-hand side shows a system where we have assumed that all rates have equal absolute values. Due to this choice of rates we have $J_{tot}^{stat} = 0$ in the stationary state. The right-hand side curves show the time evolution of J_{tot} if the horizontal rates between the sites in state three are gradually decreased from a value of 0.5 to 0.00001. As we still do not have directed transport, the total current is zero in the stationary state for all these examples. In the low-time regime small horizontal rates in state three lead to a faster decrease of the total current after the influence of the starting position of the motor in state one has weakened. The transport of the motor along its track is effectively slowed down while the stationary state is still in the distant future. Such a choice of state three as presented above might describe a situation where the motor from time to time attains a conformation in which it is weakly bound or even unbound from its filament or which from a steric point of view is unfavourable with respect to its horizontal transport, so that its arriving at a neighbouring site is seriously impeded. The regime of increased times shows a different situation. Our system more and more approaches its stationary state. Due to the previously higher current the stationary distribution is nearly reached in the

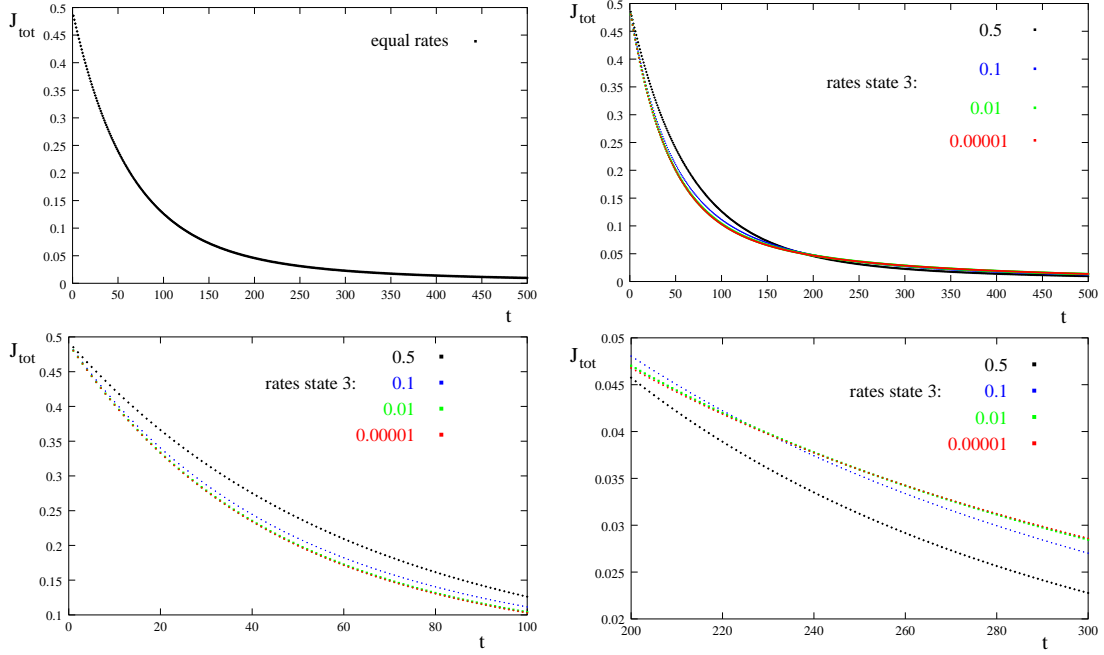


Figure 4.22: Time evolution of J_{tot} for the initially $(1, 1)$ -localized probability distribution in the $(3, 16)$ -system for cases which have different horizontal rates in the third state. Top left: all rates are equal. Top right: horizontal rates in state 3 are gradually decreased. Bottom: details of the top right curve for different time ranges. There is no directed transport in the systems, so there are no net currents in the stationary states.

case of high horizontal rates in all three states, whereas the low horizontal rates in state three still induce a remarkable current, because there the rearranging of the probabilities is not yet finished. It takes longer to reach the stationary state if the horizontal rates in one state are extraordinarily low. In all of these examples, the above given choice of the rates leads to a vanishing current in the stationary states, $J_{tot}^{stat} = 0$, since we have no directed transport.

Hindrances

In the next step we consider a situation with a built-in hindrance or defect at one location. We choose location nine and decrease the horizontal rates leading into the corresponding vertices $(m, 9)$. For the motor particle reaching this location is difficult, maybe because another molecule is bound there and blocks the stepping of the motor irregardless of its conformation.

Here we have a directed transport and the total current J_{tot}^{stat} in the stationary state is different from zero. As shown on the right in fig. 4.23, the hindrance at location nine noticeably reduces the stationary current, and with that the speed of the motor. The left side of fig. 4.23 shows the total probability, which is the sum of all single-state probabilities, for the case of a large obstacle. The total probability at location is almost zero. The resulting net current in the stationary state in our example is positive. The obstacle at location nine hinders the transport in the forward as well as in the backward direction so that the contributions by forward and backward paths will be reduced by a similar amount. The net current still has the same orientation, but its absolute value is lower. But the reduction of the current is not linear in the size or amount of the hindrance, as for a large obstacle the effects of the breaking of the detailed balance conditions slacken. Accordingly, the difference in J_{tot}^{stat} between a smaller and a greater hindrance on the right-hand side of fig. 4.23 is small compared to the difference between no hindrance and a small hindrance.

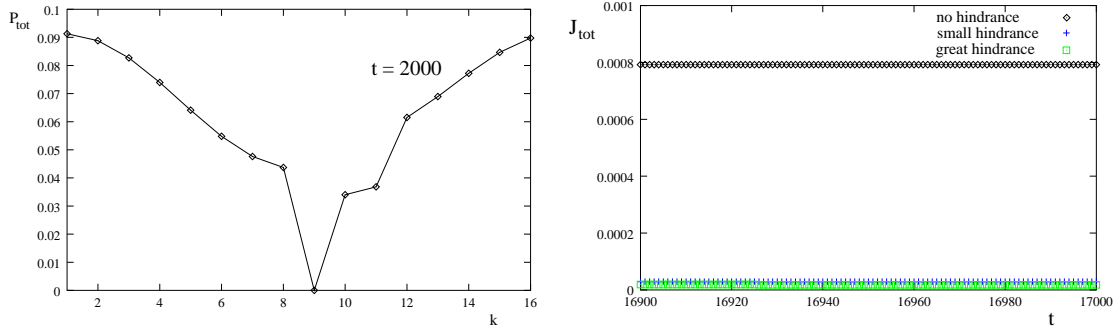


Figure 4.23: Left: the total probability P_{tot} at time $t = 2000$ for a $(3, 16)$ -system with directed transport and a hindrance at location nine. Right: the stationary current J_{tot}^{stat} of the system for different degrees of the built-in hindrance at location nine.

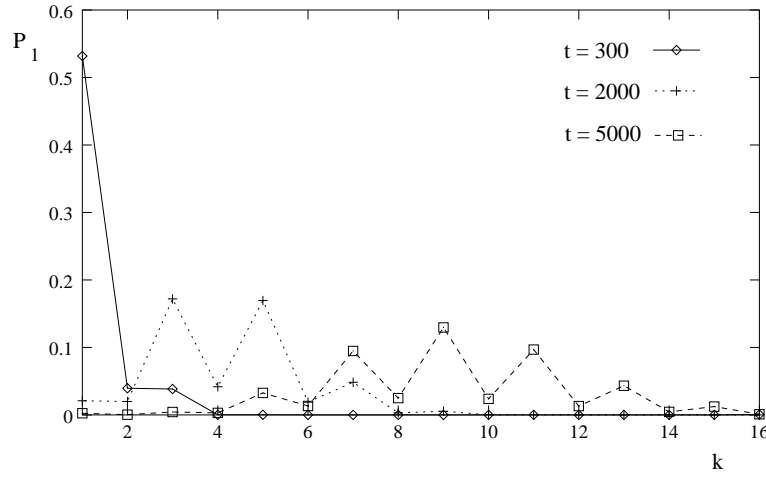


Figure 4.24: Probability distribution P_1 for state 1 in a system of two states and sixteen locations at different times from $t = 300$ to $t = 5000$. Transport in the positive x -direction is favoured.

Two states again

Now, we reduce the system by one state, but keep the number of sixteen locations. Fig. 4.24 shows the time evolution of the probability P_1 in state 1 at the sixteen different locations k for a case where transport in the positive horizontal direction is favoured. Because the horizontal rates do not have to fulfill the conditions of detailed balance any longer, there can be active processes driving the horizontal transport.

The horizontal rates are chosen in such a way that small and large rates alternate for one state, and this sequence is shifted in the second state, so that a switching between the conformations is favoured. The choice of the locations is arbitrary, in particular it is not necessary to choose equidistant k . If the horizontal rate $W(m, k | m, k + 1)$ between location k and $k + 1$ is large, it corresponds to a favoured movement of the motor. Difficult transitions against hindrances on the other hand correspond to low rates.

In the beginning, the probability distribution is localized in vertex $(1, 1)$. The value of P_1 at location 1 is still larger than 0.5 after 300 timesteps. With ongoing time the probability distribution wanders to the right and flattens more and more as can be seen in fig. 4.24. The zigzag form with local maxima and minima of the curves occurs due to the underlying sequence of small and large rates in one state.

The left-hand side of fig. 4.25 displays a comparison of P_1 and P_2 at the same time $t = 5000$. The local minima of the probability distributions correspond to locations with large effective rates

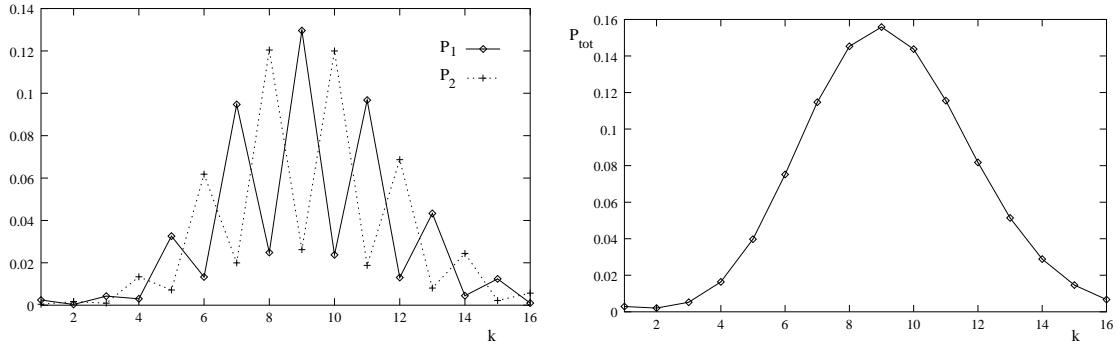


Figure 4.25: Left-hand side: the probabilities distributions P_1 for the first state and P_2 for the second state at time $t = 5000$. Right-hand side: the total probability P_{tot} at time $t = 5000$. The probability distributions belong to a $(2, 16)$ -system with directed transport.

leading out of these locations, the local maxima occur at locations which are difficult to leave. If the motor is at such a location, it stays there with a high probability. The rate for conformational changes, however, is not changed. Because of the shifted sequences of the horizontal rates in the two states, the behaviour of the two probability distributions concerning the alternation of the minima and maxima is opposed. On the right-hand side in fig. 4.25 the total probability for the states one and two after the same number of timesteps is displayed. It shows the expected smooth behaviour, as the effects of the shifted minima and maxima level.

Up to now, the vertical rates in the $(2, 16)$ -system have had equal values. Now, the vertical rates will be adapted to the idea of a directed transport, too. On the left-hand side of fig. 4.26 the probability distributions P_1 are compared for the cases that all the vertical rates have the same value (case a) or that the vertical rates for leaving the state are smaller if transport in positive x -direction is favoured in the present state. In this way directed transport in this direction is actively supported by the vertical rates. Accordingly we see that the probability distribution in case (b) has advanced further within the same interval of time. Its maximum value is attained at location 11, while for (a) the maximum is at location 9.

The right-hand side of fig. 4.26 demonstrates the effects of varying the large vertical transition rates. If their values are increased, this leads to probability distributions which have advanced further in the positive x -direction. We can imagine that to every favoured horizontal rate there is an underlying active process supporting this transition.

There is a certain value of the large transition rate which minimizes the fluctuations in the single-state probability distributions arising from the sequence of small and large horizontal rates. This effect reproduces itself in the stationary probability distributions. The case of minimum fluctuations occurs when the effective landscape arising from the rates is flat.

Adding different third states

We take the above system and add a third state again. The horizontal rates in the states 1 and 2 are chosen in such a way that transport in the positive x -direction is favoured, again the vertical rates leading out of the state have a small values if transport in positive x -direction is favoured in the present state and a large value otherwise. As far as the involvement and the transport properties of state 3 are concerned, we make a distinction between five different cases (3a)-(3e) as listed in table 4.2. The number 3 in the naming refers to the total number of states. In the cases (3a), (3b), (3d) and (3e), there are transitions into state 3 which are realized by the four rates $W(1, 1 | 3, 1)$, $W(1, 5 | 3, 5)$, $W(1, 9 | 3, 9)$ and $W(1, 13 | 3, 13)$. These four rates are assumed to be equal. Case (3a) might describe a situation where the motor particle has a possibility of “losing” its track or strictly speaking its sense of direction at certain equidistant locations. Then it attains conformation 3 without a directed transport in x -direction. Forward or backward movement are equally likely with a certain probability until the motor finally reaches state 1 or 2 again and its

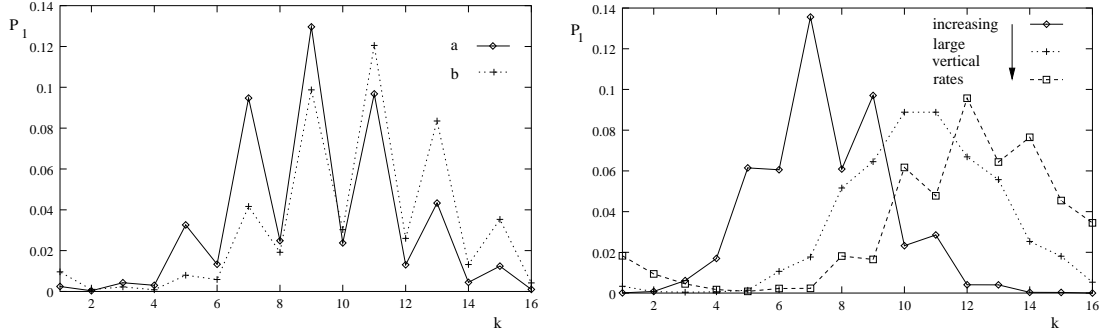


Figure 4.26: Left-hand side: Probability P_1 after the same number of timesteps in a system with two states (a) if all vertical rates have equal values, and (b) if the vertical rates leading into the other states have a small value if in the present state transport in positive x -direction is favoured. The other vertical rates have the same value for the cases (a) and (b). Right-hand side: P_1 at the same time for three cases with small and large vertical rates as in (b) of the left figure. The values of the large vertical rates are increased.

(3a)	state 3: horizontal rates left/right identical
(3b)	state 3: horizontal rates right large, left small
(3c)	as in b, but no (vertical) transitions into state 3
(3d)	as in a, but no transitions from state 3 into the states 1 and 2
(3e)	as in b, but no transitions from state 3 into the states 1 and 2

Table 4.2: Differences between the cases (3a)-(3e) in a system with three states and sixteen locations. The system of the states one and two remains unchanged. The number 3 in the naming of the cases refers to the total number of states and is chosen in order to avoid confusion with the two-state systems.

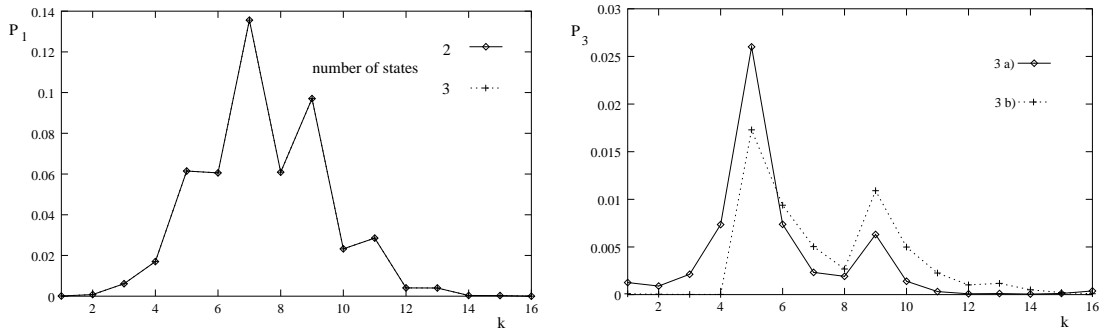


Figure 4.27: Left: the probability distribution P_1 at time $t = 2000$ of a system of two states and of a system of three states without transitions into the third state as in case (3c). As the rates belonging to the states 1 and 2 are identical in both cases, the probability distributions for the first state are identical, too. Right: the probability distributions P_3 at time $t = 1500$ for the cases (3a) and (3b) as given in table 4.2.

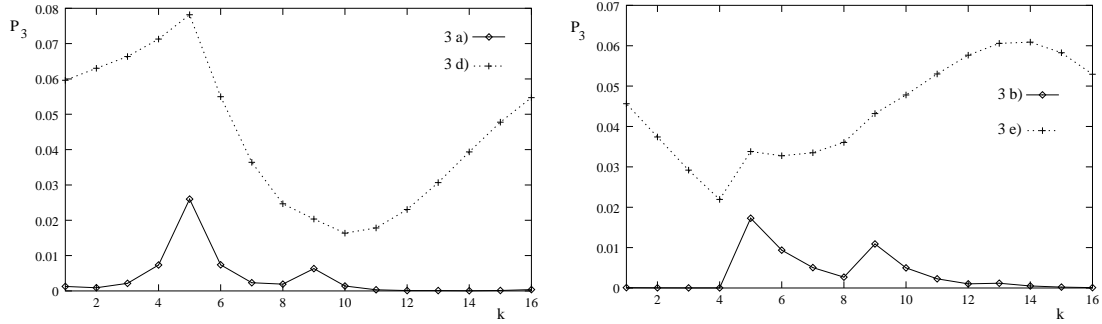


Figure 4.28: Left: the probability distributions P_3 at time $t = 1500$ for the cases (3a) and (3d) as explained in table 4.2. Right: P_3 at time $t = 1500$ for the cases (3b) and (3e). The systems have three states and sixteen locations.

directed transport can be restarted.

In case (3b) the transport in state 3 is directed in the positive x -direction. State 3 provides an alternative and fast way of transport. This fast active transport might require a certain conformation of the motor protein which is not reached easily due to energetic or steric restrictions.

Case (3c) describes a system where an existing state 3 can never be reached. The motor can be imagined to be a mutation or “faulty” compared to other motors of its family or subfamily. A possible lack of fuel can also prevent the motor from reaching the conformation 3.

(3d) and (3e) are variants of (3a) and (3b) where the conformation belonging to state 3 does not offer a way back into the states 1 or 2. This can happen because the motor is unable to “find” its track again or because its conformational change is irreversible, as it is damaged or just due to the underlying reaction kinetics.

As we start with a probability distribution which is localized in $(m, k) = (1, 1)$, case (3c) is equivalent to a system of two states, as the probability in state 3 remains zero. Accordingly, the probability distribution P_1 for the first state at time $t = 2000$ is identical to the one of the corresponding system of two states, see the left-hand side of fig. 4.27. The total probability distribution for (3c) advances faster in the positive x -direction than for case (3a), where the equal horizontal rates in state 3 hinder directed transport, but slower than for (3b), where state 3 plays the role of a fast track.

The right-hand side of fig. 4.27 shows the probability distributions P_3 of state 3 after the same number of timesteps for the cases (3a) and (3b). As for (3b) the transport in state 3 is directed into the positive x -direction, there is hardly a non-zero probability left at the first locations 1 to 4. The probability at the locations > 5 on the other hand is larger compared to case (3a).

The left side of fig. 4.28 shows how the probability in state 3 for case (3d) has already started accumulating at time $t = 1500$ compared to case (3a), as there are no rates leading from state 3 back into the states 1 or 2 again. We remember that the transitions into conformation 3 occur at the locations 1, 5, 9 and 13. The maximum of the probability distributions of the states 1 and 2 is located between the locations 5 and 9 at $t = 1500$. This explains why the maxima in fig. 4.28 occur at the second transition location 5. For (3a) there is also a distinct second maximum at location 9, which is superimposed by the ground-level probability for (3d). This ground-level probability is caused by the already widely spread probability density which came into state 3 with the first transition at location 1. The accumulation in state 3 is also obvious if we compare P_3 at $t = 1500$ for (3e) to (3b), see the right side of fig. 4.28. Here, the transport in state 3 is directed which increases the overall velocity of the motor. The influence of the last transition location 13 shows up in a small local maximum for (3b). The peaks are asymmetric because of the directed transport which causes the global maximum at location 14 for (3e). Fig. 4.29 shows the evolution in time of the total current J_{tot} for the cases (3a), (3b) and (3c) on the left and (3d) and (3e) on the right. The total currents J_{tot} undergo weakening fluctuations before approaching the stationary value. The curve for case (3b) reaches the maxima and minima at earlier times due

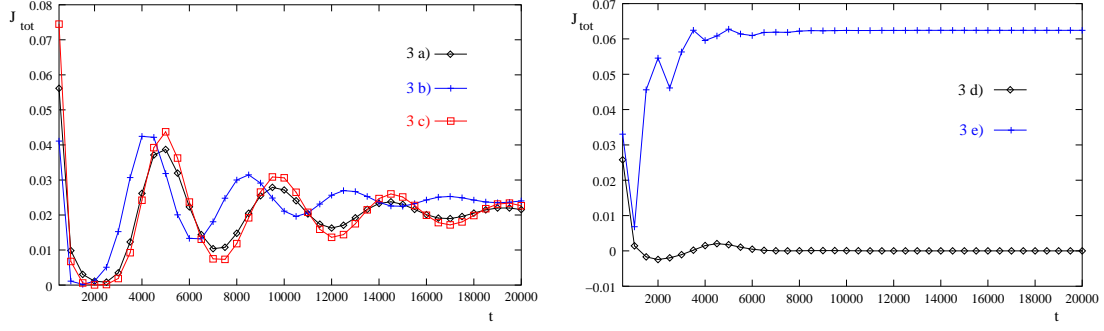


Figure 4.29: Left: time evolution of the total current J_{tot} for (3a), (3b) and (3c). Right: evolution of J_{tot} for (3d) and (3e). These three-state examples are listed in table 4.2.

to the influence of the fast directed transport in state 3. The stationary value of J_{tot} is larger in this case than for (3a) or (3c) for the same reason. The stationary value in case (3a) is the lowest of the three, because the transport in state three is not directed. In the cases (3d) and (3e) the probabilities accumulate in state 3 and the stationary current is reached fast. It is zero for the undirected transport in (3d) and high for the directed transport in state 3 which underlies (3e). The oscillations of J_{tot} are caused by the interplay of noticeably directed horizontal transport in several states which transiently creates unfavourable probability distributions. This results in high redistribution currents. There are also transient distributions nearer to the stationary one resulting in low currents. For (3d) directed horizontal transport is only effective in the states 1 and 2 whose influence weakens soon, so that we find one small maximum. When this maximum is reached the curve for (3e) has almost reached its third maximum because of the fast-lane transport in state 3.

4.4.2 Markov chains in continuous time

An alternative way of looking at our systems provides their description as Markov chains. Here we show how the time evolution of a Markov chain in continuous time can be calculated and compare the results of this approach to the results obtained in 4.4.1 where we have used discrete timesteps because of the numerical integration. In the Markov approach the initial probability distribution is localized in single states, and the resulting probability matrices of the transition functions display the time evolution for any possible vertex of the system as the vertex in which the initial probability is localized. Because of this we can directly compare how a different starting vertex of the motor in a special system influences its probable positions at present time.

Markov property and steady state distribution

In general, the states of our systems can change at arbitrary points of time. If we know the present state of the system, the future development is independent of the past of the process. Therefore, the underlying stochastic process $X(t)$ fulfills the Markov property

$$P(X(t_n) = (m_n, k_n) | X(t_1) = (m_1, k_1), \dots, X(t_{n-1}) = (m_{n-1}, k_{n-1})) = P(X(t_n) = (m_n, k_n) | X(t_{n-1}) = (m_{n-1}, k_{n-1})), \quad (4.66)$$

where P denotes the conditional probability that the motor is in state (m_n, k_n) at time t_n if it has been in state (m_{n-1}, k_{n-1}) at time t_{n-1} [63, 64, 65]. The distribution of the residence times is the exponential distribution, a continuous distribution fulfilling the Markov property.

The transition functions $p(m, k | m', k')(t)$ are defined as

$$p(m, k | m', k')(t) = P(X(t) = (m', k') | X(0) = (m, k)). \quad (4.67)$$

The infinitesimal generator $\mathbf{Q}^{(M,K)}$ is a matrix whose elements are infinitesimal transition rates $q(m, k | m', k')$. The $q(m, k | m', k')$ denote the average number of transitions from state (m, k) to state (m', k') per unit of time. The residence times of the single states follow an exponential distribution so that the average residence time is $1/q(m, k)$. The average number of jumps from state (m, k) per unit of time is $q(m, k)$. If the residence time in state (m, k) is expired, there is a jump to another state (m', k') which is different from (m, k) . The infinitesimal probability of this jump leading into state (m', k') is

$$p(m, k | m', k') = \frac{q(m, k | m', k')}{q(m, k)} \quad (4.68)$$

with $(m', k') \neq (m, k)$. The $q(m, k | m', k')$ are the elements of the secondary diagonal of $\mathbf{Q}^{(M,K)}$. Summing up the $q(m, k | m', k')$ leads to

$$\sum_{(m', k') \neq (m, k)} q(m, k | m', k') = q(m, k) \quad \sum_{(m', k') \neq (m, k)} P(m, k | m', k') = q(m, k), \quad (4.69)$$

because $\sum_{(m', k') \neq (m, k)} P(m, k | m', k') = 1$. The elements of the primary diagonal of $\mathbf{Q}^{(M,K)}$ are given by $-q(m, k)$. The elements of a single row of $\mathbf{Q}^{(M,K)}$ sum up to 0.

The first derivative of the transition functions measures the change of the transition functions. The differential equation of Kolmogorov reads

$$p'(t) = p(t) \mathbf{Q}^{(M,K)}. \quad (4.70)$$

$p(t)$ is the row vector of the unconditional probabilities,

$$p(t) = (p(1, 1)(t), p(1, 2)(t), \dots), \quad (4.71)$$

with $p(m, k)(t) = P(X(t) = (m, k))$ and $p'(t) = (p'(1, 1)(t), p'(1, 2)(t), \dots)$. The quadratical matrix $\mathbf{P}^{(M,K)}(t)$ contains the transition functions,

$$\mathbf{P}^{(M,K)}(t) = (p(m, k | m', k')(t)), \quad (4.72)$$

and is called the transition matrix of the process $X(t)$. Using this matrix we obtain

$$\mathbf{P}'^{(M,K)}(t) = \mathbf{P}^{(M,K)}(t) \mathbf{Q}^{(M,K)} \quad (4.73)$$

with the initial condition

$$\mathbf{P}^{(M,K)}(0) = \mathbf{I} \quad (4.74)$$

where \mathbf{I} is the identity matrix. The solution of (4.73) is found with the help of the ansatz

$$\mathbf{P}^{(M,K)}(t) = \exp(\mathbf{Q}^{(M,K)}t). \quad (4.75)$$

The exponential matrix function is defined by its Taylor series

$$\exp(\mathbf{Q}^{(M,K)}t) = I + \mathbf{Q}^{(M,K)} \frac{t}{1!} + (\mathbf{Q}^{(M,K)})^2 \frac{t^2}{2!} + (\mathbf{Q}^{(M,K)})^3 \frac{t^3}{3!} + \dots \quad (4.76)$$

The Markov process X_t has a steady state distribution only if it is irreducible and if all of its states are positive recurrent. $T(m', k' | m', k')$ is the recurrence time from (m', k') to (m', k') . If $E(T(m', k' | m', k')) < \infty$, the state or vertex (m', k') is positive recurrent. The steady state distribution is given by the left-hand-side eigenvector p belonging to the eigenvalue 0,

$$0 = p \mathbf{Q}^{(M,K)}. \quad (4.77)$$

p satisfies the normalization condition

$$pe = 1. \quad (4.78)$$

e is a vector with one column all of whose elements are equal to one.

Application to model systems and time evolution

We consider a situation with $M = 4$ states and transitions which take place at a single location x_1 . The infinitesimal generator $\mathbf{Q}^{(4,1)}$ reads

$$\mathbf{Q}^{(4,1)} = \begin{pmatrix} -q(1,1) & q(1,1|2,1) & q(1,1|3,1) & q(1,1|4,1) \\ q(2,1|1,1) & -q(2,1) & q(2,1|3,1) & q(2,1|4,1) \\ q(3,1|1,1) & q(3,1|2,1) & -q(3,1) & q(3,1|4,1) \\ q(4,1|1,1) & q(4,1|2,1) & q(4,1|3,1) & -q(4,1) \end{pmatrix}. \quad (4.79)$$

The situation displayed in fig. 4.31 is described by

$$\mathbf{Q}_{example}^{(4,1)} = \begin{pmatrix} -q(1,1|2,1) & q(1,1|2,1) & 0 & 0 \\ q(2,1|1,1) & -q(2,1|1,1) & 0 & 0 \\ 0 & 0 & 0 & 0 \\ 0 & q(4,1|2,1) = \varepsilon & q(4,1|3,1) & -\varepsilon - q(4,1|3,1) \end{pmatrix} \quad (4.80)$$

where ε is taken to be small. The infinitesimal transition rate ε couples state $(4,1)$ to the states $(2,1)$ and $(1,1)$.

Time evolution without coupling

First, we have a look at a situation where state $(4,1)$ is not coupled to $(2,1)$ and therefore not to $(1,1)$, too. For $q(1,1|2,1) = 0.5$, $q(2,1|1,1) = 0.5$, $q(4,1|3,1) = 0$ and $q(4,1|2,1) = \varepsilon = 0$, the time evolution of the probability matrix $\mathbf{P}^{(4,1)}(t)$ contains

$$\mathbf{P}_{uncoupled}^{(4,1)}(1) = \begin{pmatrix} 0.68394 & 0.31606 & 0 & 0 \\ 0.31606 & 0.68394 & 0 & 0 \\ 0 & 0 & 1 & 0 \\ 0 & 0 & 0 & 1 \end{pmatrix}, \quad (4.81)$$

$$\mathbf{P}_{uncoupled}^{(4,1)}(2) = \begin{pmatrix} 0.567668 & 0.432332 & 0 & 0 \\ 0.432332 & 0.567668 & 0 & 0 \\ 0 & 0 & 1 & 0 \\ 0 & 0 & 0 & 1 \end{pmatrix} \quad (4.82)$$

and

$$\mathbf{P}_{uncoupled}^{(4,1)}(10) = \begin{pmatrix} 0.500023 & 0.499977 & 0 & 0 \\ 0.499977 & 0.500023 & 0 & 0 \\ 0 & 0 & 1 & 0 \\ 0 & 0 & 0 & 1 \end{pmatrix}. \quad (4.83)$$

If the particle is momentarily in state $(1,1)$ or $(2,1)$, it will still or again be in this state after $t = 10$ with a probability of 0.500023, it will be in state $(2,1)$ (if it was in $(1,1)$ at $t = 0$) or in $(1,1)$ (if it was in $(2,1)$ at $t = 0$), respectively, with probability 0.499977. If the particle is in state $(3,1)$ or $(4,1)$, it stays there with probability 1.

Master equation versus Markov approach

To make a comparison between the Master-equation and the Markov approach, we compute the time evolution of this same example with a particle which in its initial configuration is localized in state $(1,1)$ via the method of the integration of the master equation as explained in 4.4.1. We use timesteps of length $\Delta t = 0.01$ in the integration and compare the time evolution of the probabilities. The results are shown in table 4.3. If n is the number of the timesteps, the actual time in the integration of the master equation is $t = n\Delta t$. In this way we see that the correspondence between the two approaches is very good.

probability matrix	timesteps
$P_{1,i}^{(4,1)}(1)$	99
$P_{1,i}^{(4,1)}(2)$	198
$P_{1,i}^{(4,1)}(3)$	298
$P_{1,i}^{(4,1)}(4)$	397
$P_{1,i}^{(4,1)}(5)$	496
$P_{1,i}^{(4,1)}(6)$	596
$P_{1,i}^{(4,1)}(7)$	696

Table 4.3: This table shows how many timesteps are needed for a (1, 1)-localized particle in the integration of the master equation as explained in 4.4.1 in order to reach a conformation which is approximately equal to the one given by the i elements in the first row of the transition matrix $\mathbf{P}^{(4,1)}(t)$.

probability matrix	timesteps
$P_{1,i}^{(2,2)}(1)$	99
$P_{1,i}^{(2,2)}(2)$	198
$P_{1,i}^{(2,2)}(3)$	298
$P_{1,i}^{(2,2)}(4)$	398
$P_{1,i}^{(2,2)}(5)$	499
$P_{1,i}^{(2,2)}(6)$	599
$P_{1,i}^{(2,2)}(7)$	698

Figure 4.30: Example of a (2, 2)-system with four rates. The table lists the number of timesteps needed for a (1, 1)-localized particle in the integration of the master equation as explained in 4.4 in order to reach a conformation which is nearly equal to the one given by the i elements in the first row of the transition matrix $\mathbf{P}^{(2,2)}(t)$

As a second example we have a look at a (2, 2)-system with four rates as shown in fig. 4.30. In our example the values of the rates are not equal. The agreement is again very good. In those cases where two conformations arising from the Master-equation approach are very close to the respective row matrix, we have chosen the first conformation with the lower number of timesteps. This explains why the number of timesteps tends to be slightly lower than expected.

Time evolution with coupling

We go back to the (4, 1)-system. With the choice $q(1, 1 | 2, 1) = 0.5$, $q(2, 1 | 1, 1) = 0.5$, $q(4, 1 | 3, 1) = 0.1$ and $\varepsilon = 0.01$, we obtain the time evolution

$$P^{(4,1)}(1) = \begin{pmatrix} 0.68394 & 0.31606 & 0 & 0 \\ 0.31606 & 0.68394 & 0 & 0 \\ 0 & 0 & 1 & 0 \\ 0.00176877 & 0.00770085 & 0.0946962 & 0.895834 \end{pmatrix}, \quad (4.84)$$

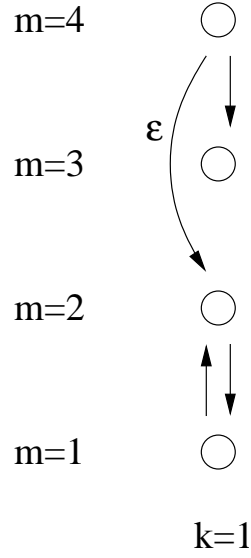


Figure 4.31: Example of a system with four states and a coupling ε between the states 4 and 2. The system contains two rates rising from the same vertex (4, 1) and the rates connecting the vertices (2, 1) and (1, 1) in opposite directions.

$$P^{(4,1)}(2) = \begin{pmatrix} 0.567668 & 0.432332 & 0 & 0 \\ 0.432332 & 0.567668 & 0 & 0 \\ 0 & 0 & 1 & 0 \\ 0.0052282 & 0.0127246 & 0.179528 & 0.802519 \end{pmatrix} \quad (4.85)$$

and

$$P^{(4,1)}(10) = \begin{pmatrix} 0.500023 & 0.499977 & 0 & 0 \\ 0.499977 & 0.500023 & 0 & 0 \\ 0 & 0 & 1 & 0 \\ 0.0284542 & 0.0321938 & 0.606481 & 0.332871 \end{pmatrix}. \quad (4.86)$$

The probability that a particle in state (4, 1) remains there, decreases as time goes on. State (4, 1) is emptied and therefore not positive recurrent.

Steady state behaviour for the (4, 1)-example

For arbitrary values of ε and the $q(m, k | m', k')$, the corresponding eigenvector $p_{(1)}^{(4,1)}$ in (4.77) describing the possible steady state behaviour is given by

$$p_{(1)}^{(4,1)} = \left(\frac{q(2, 1 | 1, 1)}{q(1, 1 | 2, 1)} p_{2, p_2, 1} - \frac{q(1, 1 | 2, 1) + q(2, 1 | 1, 1)}{q(1, 1 | 2, 1)} p_{2, 0} \right). \quad (4.87)$$

In the case of $\varepsilon = 0$ and $q_{43} = 0$, there is a second solution,

$$p_{(2)}^{(4,1)} = \left(\frac{q_{21}}{q_{12}} p_{2, p_2, p_3, 1} - \frac{q_{12} + q_{21}}{q_{12}} p_2 - p_3 \right). \quad (4.88)$$

Both cases are “pathological” as state (4, 1) is not positive recurrent. The choice of $p_2 = 0.4$ leads to $p_{(1)}^{(4,1)} = (0.4, 0.4, 0.2, 0)$. The second solution with $p_2 = 0.4$ and $p_3 = 0.1$ leads to $p_{(2)}^{(4,1)} = (0.4, 0.4, 0.1, 0.1)$. The solution $p_{(2)}^{(4,1)}$ isolates state (3, 1) and state (4, 1) from the remaining system. There is no unique steady state.

In the context of the systems of chapter 3 the calculation of $(\mathbf{A}^{(M,K)})^{-1}$ for this example after adding the periodic boundary conditions would have been impossible as in the (4, 1)-case there the minimal number of vertical rates in the polynomials is 3, which here is impossible due to the problem of creating l-cycles or having to vertices rising from the same vertex.

The Markov approach is helpful for estimating the influences of differently localized initial probability distributions. The time evolution is obtained for the initial probability localized in any of the system's vertices. The results here confirm the results obtained in 4.4.1. For larger systems the calculations for Markov chains are resource- and time-consuming, though.

4.5 Maximum flow and shortest paths

In general, there are many paths across a certain network. Molecular motors are enzymes, and in the field of enzyme kinetics, one usually distinguishes one special cycle of chemical reactions which is then called the main pathway of the enzyme. In the context of our networks, the main pathway can be imagined to be a positive s-cycle carrying a maximum current across the network. Here, we use the concept of a main pathway and search for paths with s-cycles in flow networks which carry large flows. We focus on the question of what is the maximum flow which can be gained from a set of possible pathways. This is the question of an optimal utilization of a given network with limited capacities. It is sensible to assume upper boundaries for the capacities, as in cells there are chemical and physical limitations to transport processes, e.g. given by the concentration of ATP. If the flow is fixed in our networks, we look for the path with the lowest costs or fees. Here, costs can refer to energetic considerations, for example.

4.5.1 The main pathway in unspecified networks

As stated in rule 1 in 3.2.2, the total current along a model network is the quotient of two polynomials $Pol_i(\omega_1, \omega_2, \dots, \omega_N)$ which depend on the vertical transition rates ω_i . The contribution a certain path along the network gives to the total current is judged by its occurrence in Pol_1 . The assignment of a path to a term with a combination of vertical rates can be achieved for complete paths of vertical and horizontal rates as outlined in section 4.3. The different paths, which contribute to the total current in our systems, actually do have a right to exist. Recent simulations have shown that chemical reactions do not necessarily follow the minimum energy pathway, if vibrational and kinetic energy effects of finite temperature are taken into account [66]. In other words, the stochasticity in our models is not artificial, but on the contrary a characteristic of chemical reactions.

In a first step we assume a very simple criterion in judging the value of the contribution of a path. The small-scale diffusion coefficients D_m are taken to be the small parameters of the system as we are in an over-damped regime. Then the directed walk of the motor is "diffusion-limited" according to the basic idea of diffusion-based transport in the horizontal direction, which is of course not a necessary prerequisite as we have pointed out before. The $\mathcal{E}_m(x_k, x_{k+1})$ are proportional to D_m^{-1} . A term \mathcal{T} containing n vertical transition rates implies the factor D_m^{-n} . According to this reasoning the path carrying the maximum flow across the network will contain $K(M-1)$ vertical rates. If the external force F is negligibly small, the contribution of certain paths with s-cycles will be more important as they in general contain horizontal forward rates belonging to different states and with shifted locations. This can result in a number of considerable factors if the interplay of state and location fits the respective shift of the molecular interaction potentials. For example, we have a look at fig. 4.10 again, where the two forward s-cycles in a general (2, 2)-network are depicted. In a situation where the molecular interaction potential in state 1 impedes the motor particle reaching vertex $(m, k) = (1, 2)$ if it presently is in vertex $(1, 1)$, whereas the potential of state 2 favours a transition from $(2, 1)$ to $(2, 2)$, the left-hand forward s-cycle is the main pathway. But of course this can only be true if the effect is supported by the corresponding vertical rates $W(1, 1|2, 1)$ and $W(2, 2|1, 2)$, since if we, for example, had $W(1, 1|2, 1) = 0$, the path would not contribute to the current at all.

4.5.2 Maximum flow and cut-sets

Now, we consider a graph $G = (V(G), E(G))$, which is directed and connected. A graph is connected if there is a path between any two distinct vertices of graph, see appendix C. A directed graph or digraph is strongly connected if there is at least one directed path from every vertex to every other vertex, and weakly connected if the underlying undirected graph is connected. By removing several edges, a connected graph might split up into distinct parts. A set of edges is said to be a cut-set if its removal splits a weakly connected directed graph into two separate parts, G_s and G_t . We define a flow network with a source and a destination node in which G_s and G_t contain the source and destination nodes, respectively. The subset of edges in the cut-set that are incident from the vertices in G_s to vertices in G_t define a cut [67]. The directed edge (v_i, v_j) that is incident on vertex v_j from vertex v_i has a capacity c_{ij} which can be associated with a corresponding maximum rate $W_{max}(m, k | m', k')$ if $i = (m, k)$ and $j = (m', k')$. Of course, capacities are not identical to rates, as they define an upper limit to the flow between two vertices. The capacity implies a constraint on the flow along edge (v_i, v_j) in such a way that its value has to be non-negative and either less than or equal to c_{ij} . The source and terminal vertices are labelled as $v_1 = s$ and $v_{|V|} = t$, respectively, where $|V|$ is the cardinality of the set of vertices. We distinguish between the set $A(v_i)$, which denotes the set of those vertices $v_j \in V$ for which a directed edge (v_i, v_j) exists in G , and the set $A^{-1}(v_i)$ of those vertices $v_k \in V$ for which a directed edge (v_k, v_i) exists in G . A set of numbers q_{ij} sets up a valid flow when satisfying the conditions

$$\sum_{v_j \in A(v_i)} q_{ij} - \sum_{v_k \in A^{-1}(v_i)} q_{ki} = \begin{cases} j_{tot} & \text{if } v_i = s \\ -j_{tot} & \text{if } v_i = t \\ 0 & \text{if } v_i \neq s, t \end{cases}, \quad (4.89)$$

where j_{tot} units are the total flow from source s to the sink t . We say that a cut-set $G_s \rightarrow G_t$ has a value, which is given by the sum $\sum_{i,j} c_{ij}$ for $(v_i, v_j) \in G_s \rightarrow G_t$ of the capacities of all edges of the associated cut. The minimum cut-set is the one with the smallest value.

According to the maximum-flow minimum-cut theorem the value of the maximum flow from the source vertex s to the terminal vertex t equals the minimum value over all the cut-sets separating s from t .

The proof is given as follows: The maximum flow from s to t cannot become larger than the value of the minimum cut-set, because each edge, directed from G_s toward G_t in the cut which is associated with this cut-set, connects the two separate parts G_s , containing s , and G_t , containing t , and the flow along such an edge cannot be negative.

4.5.3 Flow carried along motor networks

Now, we concentrate on our motor networks again and introduce a source vertex s and a terminal vertex t which do not belong to a labelled location. The source and terminal vertices emulate the periodic boundary conditions via their edges whose respective second endpoints are vertices at location 1, $(m, 1)$, and location K , (m, K) . The boundary conditions are preserved by the choices $c_{s(m,1)} = c_{(m,K)t}$. By defining the source and terminal vertices, we define a direction of possible paths, as the source vertex cannot be the endpoint of an edge, whereas the terminal vertex cannot be the starting point of an edge. This direction is positive if the locations of the source and terminal vertices fulfill $l_s < 1$ and $l_t > K$. The rest of the vertices are denoted by $v_i = (m, k)$ with $v_1 = (1, 1)$, $v_2 = (2, 1), \dots, v_{M \cdot K} = (M, K)$. Fig. 4.32 displays this new situation for the general network with $(M, K) = (3, 3)$.

4.5.4 Search for paths

At first, we want to gain information about the maximum flow which can be carried across a model network if we have a look at the sum of various flows along different paths. A general network for $(M, K) = (2, 2)$ with the corresponding capacities is shown in fig. 4.33. We start at the source vertex and check the vertices which are endpoints of edges originating from the source, where the

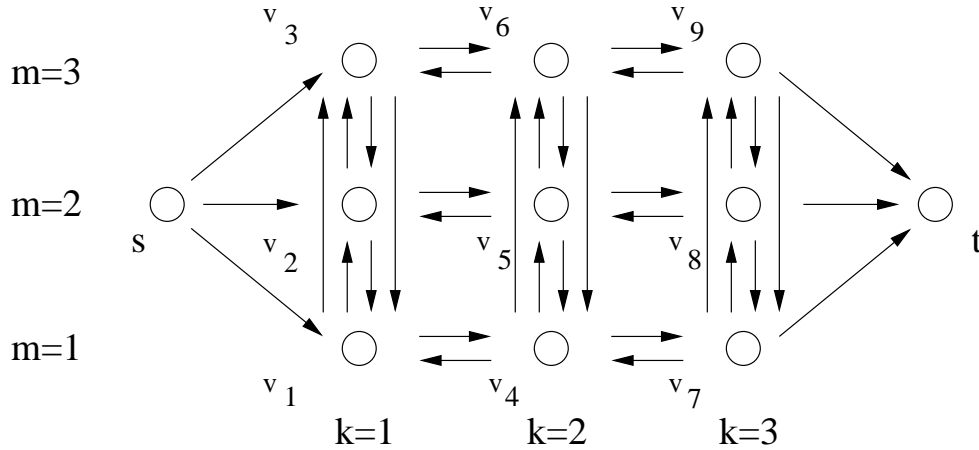


Figure 4.32: Complete flow network for $(M, K) = (3, 3)$ with source vertex s and terminal vertex t . The vertices v_i are numbered as explained in the text. The di-edges refer to the capacities c_{ij} between v_i and v_j .

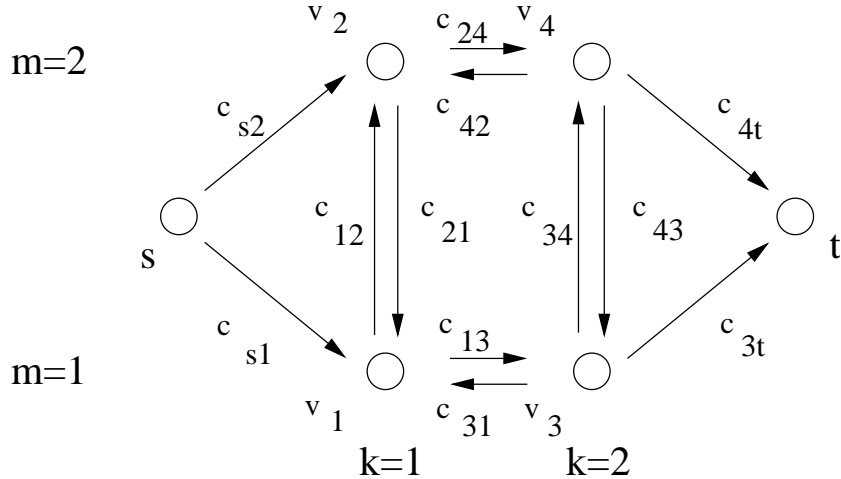


Figure 4.33: General network for $(M, K) = (2, 2)$ with capacities c_{ij} .

sequence of the vertices v_i is determined by increasing indices i . Before an edge is chosen as a part of a path, it is examined with respect to leading to a dead end, which of course can happen in the case of a weakly connected graph. As mentioned in section 4.4, the horizontal rates in the original general networks cannot be zero, which of course prevents dead ends. Here, we permit the leaving out of horizontal capacities in order to introduce a guidance of paths. The numbering of the vertices as explained above is chosen in such a way that a vertical connection is preferred against a horizontal forward connection in the decision about the next edge in a path. This is even sensible if we have an in the vertical direction “reaction-limited” case as we still need at least a couple of vertical contributions to cause the motor to walk without an external force and active horizontal elements. In general, it will not be favourable to have backward substeps in a forward step, so backward capacities can be set to zero. We are looking for paths, i.e. for walks in which no vertex occurs twice. Therefore we exclude inner cycles, which means that we exclude l-cycles if we are in a case where we do not have backward capacities. By this we fulfill the rules 1, 3 and 4 as listed in 3.2.2 for the paths in our flow networks. Of course, by doing so we do not exclude s-cycles, as s-cycles in a flow network start at the source vertex s , end at the terminal vertex t and are in this way different from inner cycles. In contrast to the calculations that led to the rules in

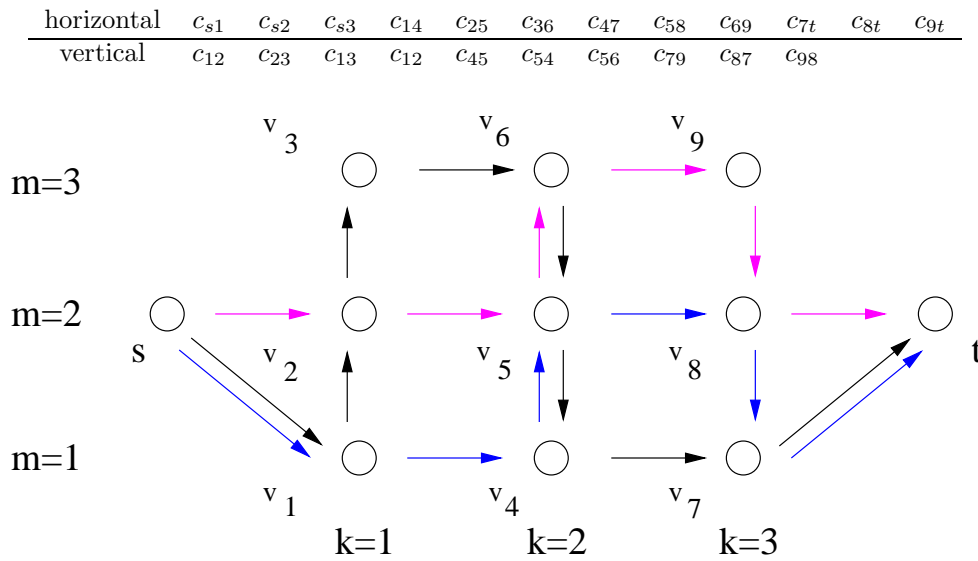


Figure 4.34: Three paths realizing maximum flow in a (3, 3)-network with the above listed capacities. The paths are marked by edge trains of different colours. Path 2 (blue) and 3 (magenta) refer to an effective two-state network.

3.2.2, the paths considered here do not have to span the network in vertical direction, but might belong to effective subnetworks so that the maximal number of vertical contributions is reduced accordingly.

To provide an example, we take a (2, 2)-network as in fig. 4.33 and specify the capacities c_{s1} , c_{s2} , c_{12} , c_{21} , c_{13} , c_{24} , c_{34} , c_{43} , c_{3t} and c_{4t} in such a way that from the considerations in 4.5.1 we expect a path with a sequence of edges corresponding to the sequence of rates in the left-hand side in fig. 4.10 to form the main pathway. This expectation is confirmed if c_{s2} , c_{13} and $c_{4t} = c_{s2}$ are small compared to c_{s1} , c_{24} and $c_{3t} = c_{s1}$, and c_{12} and c_{43} are bigger than c_{21} and c_{34} . Paths which do not contain horizontal contributions contradict rule 2 for rates in 3.2.2 and do not carry flow along the network in the absence of an external force. Therefore they are rejected. So the only paths to be listed finally correspond to the two in fig. 4.10 for rates, and the maximum flow across the network is the sum of the flows of these two paths.

Fig. 4.34 shows the result realizing maximum flow for a (3, 3)-network where we have introduced 22 non-zero capacities in such a way that the vertical capacities are small compared to the horizontal capacities which are taken to be identical in this example. Here, the maximum flow through the network is three units. Each of the three paths contributes one unit of flow. Paths without vertical contributions are neglected as they do not occur in our original models. In this simple example with identical values for horizontal and vertical capacities, respectively, the choice of the three paths is not unique. The main pathway carries the maximum flow along the network. In general, it cannot be found by listing flow-augmenting paths as every occurrence of an edge reduces its actual capacity in following paths. So if we want to obtain the main pathway instead of the paths realizing maximum flow, the flow of one path is calculated, then all the flows are set to zero again and the next path is looked for. The numbering of the vertices causes the main pathway to be found as one of the first paths if the general considerations as explained above hold. Usually, the paths realizing maximum flow will be important paths carrying large flows because of the rules used for their determination. So it is probable that at least for the first conformation a “local” main pathway with respect to the conformation will be found.

horizontal low	f_{s1}	f_{25}	f_{69}						
horizontal high	f_{s2}	f_{s3}	f_{14}	f_{36}	f_{47}	f_{58}	f_{8t}	f_{9t}	
vertical low	f_{12}	f_{23}	f_{45}	f_{54}	f_{56}	f_{65}	f_{98}	f_{87}	
vertical high	f_{13}	f_{79}							
state 1	s	v_1	v_2	v_5	v_6	v_9	v_8	v_7	t
state 2	s	v_2	v_5	v_6	v_9	v_8	t		
state 3 - hor.	s	v_3	v_6	v_9	t				
state 3 - s-cyc.	s	v_3	v_6	v_5	v_4	v_7	v_9	t	

Table 4.4: Top: list of costs or fees f_{ij} for edges in a $(3, 3)$ -network and resulting shortest paths. For each of the two classes of edges (horizontal or vertical) we make a differentiation between low and high costs. Bottom: resulting low-cost paths grouped according to their starting states. The path for state 1 realizes the absolute path of lowest costs for the network. The relative low-cost path for state 3 does not contain vertical contributions, so the second lowest is listed, too.

4.5.5 Paths with minimal costs

In a way very similar to the one presented above for the capacities c_{ij} , we can associate costs or fees f_{ij} to the edges of our networks. These costs among other points imply losses or gains of physical or chemical energy or even a reduction of the lifetime of the protein or an increase in stability. For simplicity the single costs are taken to be non-negative.

Algorithms which minimize the costs of transport along a network are usually called shortest-path algorithms and named after Dijkstra. Since the name is misleading, we want to stress that the shortest path along a network is not, as one might imagine, the path with the minimum number of edges or vertices, but the one with the lowest costs. In our variant of the algorithm, we make a distinction between shortest paths for various starting conformations of the motor, i.e., depending on the state the particle is in when it enters the network on the left-hand side, we search for respective shortest paths starting and ending in this state. If there are distinct differences in the costs of horizontal transport vertical transitions between the states are favoured as in the case of the idea of shifted potential barriers associated with the different levels. The shortest-path algorithm of Dijkstra is a labelling algorithm which includes backtracking in order to actually list the shortest path afterwards. A description is given in appendix E. Of course, l-cycles do not occur, as they always increase the costs. Tab. 4.4 shows a list of costs and resulting paths for a $(3, 3)$ -network with 22 edges. Here we come across a situation where the lowest-cost path starting with conformation 3 does not contain vertical contributions. This can happen in a situation where the motor in this conformation experiences an effective potential which drives it in the positive direction, whereas a change of conformation is sumptuous in contrast to our general assumptions. In this way we can describe an situation which can occur in experiments, where a motor gets caught in a certain conformation, it is practically “frozen” in its state, and then it is pulled along its track.

When we determine the shortest pathway carrying a given fixed flow, we can call this a main pathway in an alternative definition based on energetic considerations. The lowest-cost pathway for a given fixed flow is favourable since walking along this way is possible without using up too many resources, so it will be used with a high probability and, as a result, possibly carry a large total current across the network. Of course, this simple dependence holds only as long as the capacities for this lowest-cost path are large enough. If this is not the case and the lowest-cost path is reached only from a rare starting conformation, it can be of little importance in spite of its low costs.

Chapter 5

ATP-concentration and transport properties

In this chapter we at first examine the dependence of the motor's velocity on the ATP concentration. The energy for the movement of the molecular motor is released in the hydrolysis of ATP, which is an enzymatic reaction. When the motor shows enzymatic activity, we have unbalanced rates in our system describing the deviation from equilibrium and detailed balance. In order to relate the unbalanced rates to the concentration of ATP, we discuss the underlying reaction kinetics, compare section 5.1. The dependence of the velocity of the motor on the ATP-concentration varies with the number of centres of enzymatic activity and the type of the assumed reaction kinetics.

In section 5.2 we have a look at an alternative stochastic two-state model. This model has a continuous x -direction and uses finite vertical transition widths, which we change gradually. We determine transport coefficients and consider different explicit molecular interaction potentials. The numerical solution provides us with a time evolution of the probabilities. This last section is based on [73].

5.1 Reaction kinetics

In section 3.3 we have shown that the enzymatic activity of the motor proteins enters our (M, K) -systems via breaking the conditions of detailed balance. If there is enzymatic activity for the motor taking on a certain conformation at a specified location, the corresponding transition rate has an unbalanced part. Without a loss of generality, we assume that the unbalanced rates are vertical rates leading to conformational changes. Nevertheless, it is not clear yet how the unbalanced rates are connected to the chemical reaction, the hydrolysis of ATP. This connection is established by including the underlying reaction kinetics into our systems, which determine the dependence of the unbalanced transition rates on the fuel or ATP concentration.

5.1.1 Michaelis-Menten equation

Just as many other intra- and extracellular proteins, molecular motors are enzymes [68]. They are biological catalysts, which raise the speed of chemical reactions by influencing the energy of activation. Enzymes have active sites which are crucial for their catalytic activity and their specific reaction. Besides, they need specific binding bags in which they bind their substrates.

The enzyme reaction in the case of linear molecular motors is the hydrolysis of ATP, so ATP is the motors' substrate. The chemical equilibrium in the simplified reaction scheme



would be reached if

$$\kappa_1 \Gamma_{ATP} = \kappa_2 \Gamma_{ADP} \Gamma_P \quad (5.2)$$

with the reaction rate constants κ_1 and κ_2 and the respective concentrations Γ of ATP, ADP and phosphate P [43].

In actual experiments where the motor runs processively along its filament and produces a net movement, the chemical equilibrium is broken, as will be explained later. In the following, we consider the motor's deviation from the equilibrium state, which here is described by the deviation of the vertical transition rates from the conditions of detailed balance.

If the motor is in state (o, k) before, and in state (p, k) after the hydrolysis, the corresponding unbalanced transition rates connecting the two vertices are

$$\Delta_{op}(x_k) = \exp(V_o(x_k)) \kappa_1(F) \Gamma_{ATP} \equiv \hat{\kappa}_1(F) \Gamma_{ATP} \quad (5.3)$$

and

$$\Delta_{po}(x_k) = \exp(V_p(x_k)) \kappa_2(F) \Gamma_{ADP} \Gamma_P \equiv \hat{\kappa}_2(F) \Gamma_{ADP} \Gamma_P. \quad (5.4)$$

Because in experimental situations the concentration of ATP will usually be high in the beginning, and the concentration of ADP very low at the same time, the state of the system is far from chemical equilibrium for small concentrations of motors within the time scale of the experiment. There is almost no ADP, Γ_{ADP} is low so that $\Delta_{po}(x_k) \approx 0$. In this case we need a single unbalanced vertical rate to describe the movement of a motor with one hydrolysis step in its motor cycle.

Strictly speaking, the hydrolysis of motor proteins as kinesin (K), which we have summarized in (5.1), comprises several substeps. Kinesin binds to a microtubule (M), until ATP arrives and binds to the kinesin molecule. Then the actual hydrolysis follows, in the course of which K/ADP unbinds and phosphate is released,



The common way of describing the reaction kinetics in this sequence is to assume the simplest case of an enzymatic catalyzed reaction, namely a reaction using a single molecule of the substrate at a time. The unbalanced transition rate $\Delta_{op}(x_k)$ is then given by the Michaelis-Menten equation

$$\Delta_{op}(x_k) = \frac{\tilde{\kappa}_2(F) \Gamma_{ATP}}{\tilde{\kappa}_2(F) / \tilde{\kappa}_1(F) + \Gamma_{ATP}}, \quad (5.6)$$

with reaction rate constants $\tilde{\kappa}_1$ and $\tilde{\kappa}_2$ [69].

5.1.2 Allosteric effects

The Michaelis-Menten equation as stated in 5.1.1 is valid for simple systems. In the case of molecular motors however, there might be allosteric centres which bind regulatory molecules so that the dependence of the unbalanced rates $\Delta_{op}(x_k)$ on the ATP-concentration Γ_{ATP} is changed. This discussion is new compared to [43].

Concept

If an effector, a ligand which influences the binding characteristics, binds to a regulatory binding domain, which is in this case not identical with that of the substrate, there will be a conformational change of the enzyme influencing the enzymatic activity. In such a situation the unbalanced parts of the transition rates can show a sigmoidal dependence on Γ_{ATP} . In the simplest case the Δ_{op} obey

$$\Delta_{op}^{sigm.}(x_k) = \frac{\tilde{\mu}_2(F) n \Gamma_{ATP}^n}{\tilde{\mu}_2(F) / \tilde{\mu}_1(F) + \Gamma_{ATP}^n} \quad (5.7)$$

with constants $\tilde{\mu}_1(F)$, $\tilde{\mu}_2(F)$ and a number n , which denotes the number of identical units of the allosteric enzyme. The number n will be called the Hill coefficient in the following. The abbreviation "sigm." refers to "sigmoidal".

Equation (5.7) is derived from the Hill equation which describes the binding of n molecules of the substrate to the enzyme. Schnitzer and Block have suggested a Hill coefficient of one for

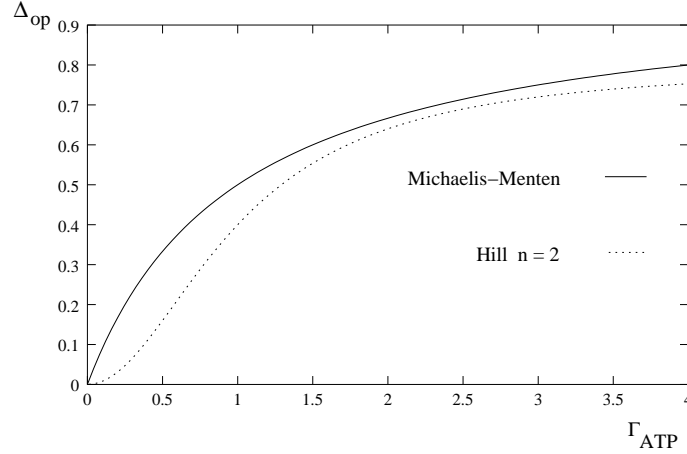


Figure 5.1: Unbalanced part Δ_{op} of the vertical transition rate as given by (5.6) for a Michaelis-Menten dependence on Γ_{ATP} and by (5.7) for a Hill dependence with $n = 2$. The reaction constants are chosen in such a way that the resulting curves are in a similar range. For small Γ_{ATP} , the Michaelis-Menten curve increases linearly, whereas the Hill curve shows a sigmoidal behaviour.

kinesin [10], which means that one molecule of ATP is used per step of the motor. In the case of myosin people usually assume one to be the right coefficient, too, though there has been a controversial discussion [70, 71]. Although we do not rule out a binding of more than one molecule of the substrate, we want to focus on allosteric effects as the reason for a sigmoidal dependence on Γ_{ATP} in the following.

Fig. 5.1 shows the dependence of the unbalanced part Δ_{op} of the vertical transition rate on Γ_{ATP} for a Michaelis-Menten case and for a Hill case with $n = 2$. We keep in mind that the dependence of the unbalanced part Δ_{op} on Γ_{ATP} is determined by the underlying enzymatic reaction and does not yet imply any statement about the dependence of the motor velocity on Γ_{ATP} . The velocity of the motor protein will be calculated later on.

A further stage is the development of a sequential model where the binding sites of the macromolecule are used one after the other. Binding of a ligand induces a conformational change and the transition takes place step after step in a sequential manner. G. S. Adair has developed an equation which takes into account these single steps of binding. The constants of the partial steps are assumed to be different, so that we effectively look at a more detailed version of (5.7). The unbalanced rates are now assumed to be given by

$$\Delta_{op}^{det.}(x_k) = \frac{\frac{\Gamma_{ATP}}{\rho_1} + \frac{2\Gamma_{ATP}^2}{\rho_1\rho_2} + \dots + \frac{n\Gamma_{ATP}^n}{\rho_1\rho_2\dots\rho_n}}{1 + \frac{\Gamma_{ATP}}{\rho_1} + \frac{\Gamma_{ATP}^2}{\rho_1\rho_2} + \dots + \frac{\Gamma_{ATP}^n}{\rho_1\rho_2\dots\rho_n}}. \quad (5.8)$$

The short form “det.” refers to “detailed”, and the $\tilde{\rho}_i$ are reaction constants again.

Application: Example of a Ratchet

Now, we study the influence a change in the assumed reaction kinetics has on the velocity of the motor molecule in our models. We consider the case $(M, K) = (3, 3)$ with one single unbalanced transition rate $\Delta_1 = \Delta_{13}(x_1)$ (fig. 5.2).

If the sequence (5.5) follows Michaelis-Menten kinetics the unbalanced vertical transition rate is given by

$$\Delta_1^{-1} = (\tilde{\kappa}_1(F)\Gamma_{ATP})^{-1} + (\tilde{\kappa}_2(F))^{-1} \quad (5.9)$$

with rate constants $\tilde{\kappa}_1$ and $\tilde{\kappa}_2$ which may depend on the external force F . The velocity of the

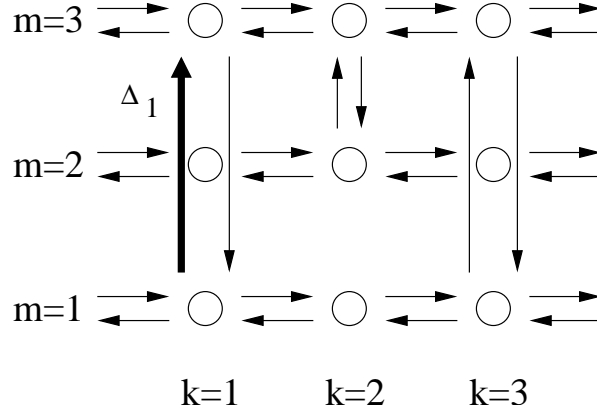


Figure 5.2: Example of an $(M, K) = (3, 3)$ -ratchet with one unbalanced transition $\Delta_1 = \Delta_{13}(x_1)$.

molecular motor then results as

$$v(\Gamma_{ATP}) = \frac{g_0(F) + g_1(F)\Gamma_{ATP}}{h_0(F) + h_1(F)\Gamma_{ATP}} \quad (5.10)$$

with force-dependent coefficients g_i and h_i . (5.10) yields a Michaelis-Menten-type relation between velocity v and Γ_{ATP} as suggested by [15, 10], compare (1.1). There is a linear increase in v for small values of Γ_{ATP} and a saturation regime for large values of Γ_{ATP} .

In the general case, the use of Michaelis-Menten kinetics for several unbalanced transition rates leads to the motor velocity

$$v(\Gamma_{ATP}) = \frac{\sum_{l=0}^Q \tilde{g}_l(F)\Gamma_{ATP}^l}{\sum_{l=0}^Q \tilde{h}_l(F)\Gamma_{ATP}^l} \quad (5.11)$$

where $Q \leq K(M-1)$ is the number of unbalanced rates, and \tilde{g}_l and \tilde{h}_l are coefficients which depend on the external force F [43]. This relationship can simplify again for symmetry reasons, e.g., for a motor with two identical heads.

If the motor contains allosteric domains binding regulatory molecules, the vertical transition rate Δ_1 exhibits a sigmoidal dependence on Γ_{ATP} as in (5.7).

We insert the sigmoidal dependence (5.7) into the expression for the motor velocity in our model system. Then, the motor velocity is found to be

$$v(\Gamma_{ATP}) = \frac{p_0(F) + p_1(F)\Gamma_{ATP}^n + p_2(F)n\Gamma_{ATP}^n}{q_0(F) + q_1(F)\Gamma_{ATP}^n + q_2(F)n\Gamma_{ATP}^n} \quad (5.12)$$

with coefficients p_i and q_i , which depend on the external force again and the Hill coefficient n . The general case for arbitrary Q is calculated as

$$v(\Gamma_{ATP}) = \frac{\sum_{l=0}^Q \tilde{p}_l(F, n)\Gamma_{ATP}^{ln}}{\sum_{l=0}^Q \tilde{q}_l(F, n)\Gamma_{ATP}^{ln}} \quad (5.13)$$

with coefficients \tilde{p}_l and \tilde{q}_l which depend on F and n .

The left-hand side of fig. 5.3 shows plots of velocities where the single unbalanced rate is treated according to Michaelis-Menten kinetics or otherwise fulfills the sigmoidal dependence as in (5.7). The coefficients are $g_1 = h_0 = h_1 = 1$, $g_0 = 0.1$ and $p_1 = p_2 = q_0 = q_1 = q_2 = 1$, $p_0 = 0.1$ and $n = 2$. The sigmoidal dependence of the unbalanced rate on the ATP-concentration Γ_{ATP} results in a sigmoidal dependence of the velocity v on Γ_{ATP} on the other hand.

Now, we consider a restricted case of (5.8) with terms up to quadratic order in Γ_{ATP} and insert

$$\Delta_{op}^{det.}(x_k) = \frac{\hat{\rho}_2\Gamma_{ATP} + 2\epsilon\Gamma_{ATP}^2}{\hat{\rho}_1\hat{\rho}_2 + \hat{\rho}_2\Gamma_{ATP} + \Gamma_{ATP}^2} \quad (5.14)$$

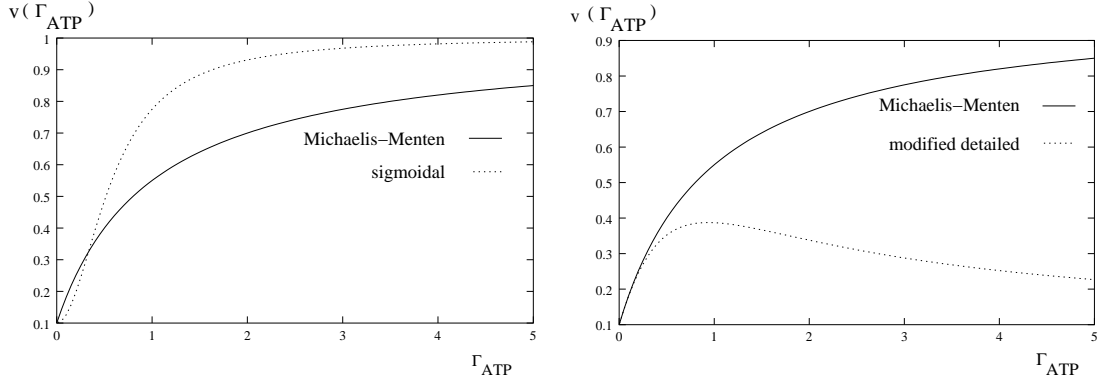


Figure 5.3: Left-hand side: the velocity as a function of Γ_{ATP} in the Michaelis-Menten and the sigmoidal case. Right-hand side: comparison between a Michaelis-Menten dependence and a modified detailed case as in (5.14). These are qualitative curves, as we have inserted trial values for the reaction constants; the absolute values are not expressive.

with a small parameter $\varepsilon < 0.5$ and constants $\hat{\rho}_1$ and $\hat{\rho}_2$. The resulting motor velocity is now given by

$$v(\Gamma_{ATP}) = \frac{s_0(F) + s_1(F)\Gamma_{ATP} + s_2(F)\varepsilon\Gamma_{ATP}^2 + s_3(F)\Gamma_{ATP}^2}{t_0(F) + t_1(F)\Gamma_{ATP} + t_2(F)\varepsilon\Gamma_{ATP}^2 + t_3(F)\Gamma_{ATP}^2} \quad (5.15)$$

with coefficients s_i and t_i . A general case with Q unbalanced transition rates will then result in

$$v(\Gamma_{ATP}) = \frac{\sum_{l=0}^Q \sum_{m=0}^n \tilde{s}_l(F, n) \Gamma_{ATP}^{lm}}{\sum_{l=0}^Q \sum_{m=0}^n \tilde{t}_l(F, n) \Gamma_{ATP}^{lm}}. \quad (5.16)$$

As there are more terms contributing to $t_2(F)$ in the denominator than to $s_3(F)$ in the numerator of (5.15), we can normally make the approximation that $t_2(F) > j s_3(F)$ where j is an integer number larger than one. In this case the velocity has a maximum and decreases after reaching this maximum. We might also assume that $s_3(F)$ equals zero so that the numerator does not contain terms in Γ_{ATP}^2 without the small parameter ε , whereas $t_2(F)$ will still be different from zero in general. The right-hand side of fig. 5.3 shows a comparison between a Michaelis-Menten dependence and this limited detailed sigmoidal case. The coefficients are $g_1 = h_0 = h_1 = 1$, $g_0 = 0.1$ and $s_1 = s_2 = t_0 = t_1 = t_2 = t_3 = 1$, $s_0 = 0.1$ and $s_3 = 0$ and $\varepsilon = 0.1$. The corresponding curve in the limited detailed sigmoidal case has a maximum instead of showing a saturation behaviour.

This curve resembles curves which have been measured in experiments for the velocity of kinesin as a function of the concentration of various cofactors [72]. In this case one also has a maximum, not a saturation regime.

Concerning the dependence of the velocity v on the ATP-concentration, experimental groups fit Michaelis-Menten curves [72, 15, 10]. Nevertheless, the number of data points, especially in the saturation regime, is usually not very large, and within the error bars it is in any way possible that there is a sigmoidal behaviour or a maximum of the velocity in these curves. If the reaction kinetics differ from the simple Michaelis-Menten case in the above discussed ways, our systems yield such deviations of the velocity.

Even if we use Michaelis-Menten kinetics, the Michaelis-Menten-type behaviour for the velocity is just the simplest relationship of a whole family of relationships as given by (5.16). It applies to motors with a single forward pathway involving one hydrolysis process. In general, it is sensible to assume several pathways, more than one process of hydrolysis of ATP and backward steps, too. Then the more general relationships should apply.

5.2 Potentials and transport coefficients

Up to now, the details of the molecular interaction potentials $U_m(x)$ have not been specified. In this chapter, we examine different explicit examples of molecular interaction potentials $U_m(x)$ in the context of a two-state model. The starting point here is a Fokker-Planck equation for each of the states [40], so that the x -coordinate is taken to be continuous again, and active processes are limited to vertical transitions. Using a numerical integration (T. Harms [73]), we study the effects changing the width of the transition interval between the states has on the transport coefficients. We also vary the molecular interaction potentials $U_m(x)$ with respect to the shape and the height of the barrier and consider snapshots of the probabilities in the time evolution of the system.

5.2.1 Fokker-Planck equation and integration

We consider a system with two states $m = 1, 2$. As before, the stochastic motion of the motor in each of the two states is taken to be described by the Fokker-Planck equation

$$\frac{\partial}{\partial t} P_m = D_m \frac{\partial}{\partial x} \left(\frac{\partial V_m(x)}{\partial x} + \frac{\partial}{\partial x} \right) P_m + I_m(x, t), \quad (5.17)$$

where $P_m(x, t)$ again denotes the probability that the motor is in state m at location x at time t . The transition current densities I_m depend on the transition rate functions $\Omega_{mn}(x)$ as in (2.18). In contrast to section 2.1, the transition rate functions are not parameterized in terms of delta functions now, but are given by $\Omega_{mn}(x) = \omega_{mn}(x)$. The transition rates $\omega_{mn}(x)$ are piecewise constant and placed around the minima of the corresponding potential with a finite width, see (5.19).

The numerical solution of the above set of two partial differential equations is obtained with the use of a finite differencing method. The $P_m(x, t)$ are represented by their values at the discrete set of points

$$\begin{aligned} x_j &= x_0 + j\Delta, \quad j = 0, 1, \dots, J, \\ t_n &= t_0 + n\Delta, \quad n = 0, 1, \dots, N. \end{aligned} \quad (5.18)$$

A combination of an implicit and an explicit FTCS (Forward Time Centered Space) scheme is used in order to combine the stability of an implicit method with the second-order accuracy in space and time [56]. In an explicit scheme, P_j^{n+1} can be calculated explicitly from known values for each j . The implicit scheme requires the solution of implicit equations which couple the P_j^{n+1} for different j .

5.2.2 Localizing transitions

As the transition rates $\omega_{mn}(x)$ are piecewise constant and localized around the minima x_m of the corresponding molecular interaction potential, they are chosen as

$$\begin{aligned} \omega_{mn}(x) &= \omega_m \quad \text{for } x_m - \varepsilon \leq x \leq x_m + \varepsilon, \\ &= 0 \quad \text{otherwise.} \end{aligned} \quad (5.19)$$

The molecular interaction potentials of the two states are of type (c) as displayed on the right in fig. 5.6, but the position of the maximum is shifted to lower values of x then in the figure. The potential in the second state is shifted for half a period compared to the first one. As one result of the integration, we obtain the effective transport coefficients velocity and diffusion, for details compare [73]. Fig. 5.4 shows the dependence of the effective velocity v_{eff} and the diffusion coefficient D_{eff} on the transition rate ω , where we have chosen $\omega := \omega_1 = \omega_2$. The curves refer to transition widths of 0.2 and smaller. Here and in the following our parameters are dimensionless, as we concentrate on qualitative results. Decreasing the transition width by decreasing ε shifts the

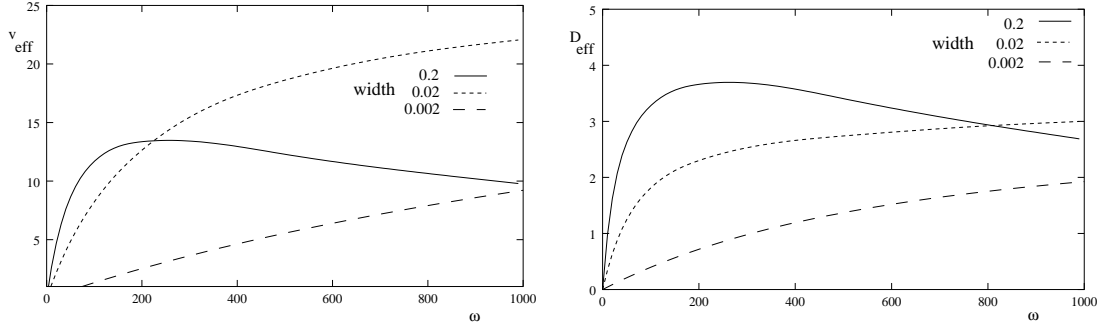


Figure 5.4: Effective transport coefficients v_{eff} and D_{eff} for different transition widths depending on the rate ω .

location of the maxima to larger and larger values of ω . The slope in the linear regime decreases with decreasing ε . A completely localized transition is the limiting case of the crossover from a resonant to a saturation regime as favoured by the Michaelis-Menten type velocity curves.

If the transition rates are low, the stationary distribution of each state in the effective medium approximation is a Boltzmann distribution [73]. The transition rates of the states determine the weight of the respective state. For small values of ω_{12} and ω_{21} , the leading term of the drift velocity is

$$\begin{aligned}
 v_{eff} &\approx \ell \left(\frac{2}{\ell} \int_{I_1} \omega_{12}(x) dx \int_{I_2} \omega_{21}(x) dx \right) / \int_{I_{1,2}} (\omega_{12}(x) + \omega_{21}(x)) dx \\
 &\cdot \int_0^\ell \frac{1}{\ell} \left(\frac{\exp(U_1(x)/T)}{\langle \exp(U_1/T) \rangle} - \frac{\exp(U_2(x)/T)}{\langle \exp(U_2/T) \rangle} \right) dx \\
 &\cdot \int_0^x \frac{1}{\ell} \left(\frac{\exp(-U_1(y)/T)}{\langle \exp(-U_1/T) \rangle} - \frac{\exp(-U_2(y)/T)}{\langle \exp(-U_2/T) \rangle} \right) dy
 \end{aligned} \tag{5.20}$$

with $\langle f \rangle = \int_0^\ell dx f(x) / \ell$. I_1 , I_2 and $I_{1,2}$ denote the splitting up of the interval $I = [0, \ell]$ into regions where the respective integrands are steady. If we insert $\omega_1 = \omega_2 = \omega$, the weight of the states results as $2\varepsilon\omega/\ell$. The ℓ is the period of our potentials.

For the choice $\varepsilon = \ell/2$, this pre-factor is given by ω again. In this way we confirm the linear dependence of v_{eff} on ω , which has been calculated for the case of transition rates which do not depend on the spatial coordinate x [73]. The slope of the linear regime as given by $2\varepsilon\omega/\ell$ decreases for decreasing ε as indicated by the numerical results on the left-hand side of fig. 5.4. The left of fig. 5.5 shows the curves for the widths 0.02 and 0.002 in the region of small ω as well as the straight lines given by $\varepsilon\omega c$, where ε is the width and c a constant arising from (5.20). The correspondence between the numerically obtained curves and the straight lines is very good and also holds in the case of smaller transition widths. For $\varepsilon = 0.2$, however, the actual slope is about four times smaller than the one suggested by the straight line, because the width is now in the range of the potential period ℓ where the influence of the actual form of the potentials gains in importance compared to the transition width.

The diffusion coefficient is given by

$$\begin{aligned}
 D_{eff} &\approx \frac{T}{D_1} \frac{2}{\ell} \int_{I_1} \omega_{12}(x) dx / \int_{I_{1,2}} (\omega_{12}(x) + \omega_{21}(x)) dx \frac{1}{\langle \exp(U_1/T) \rangle \langle \exp(-U_1/T) \rangle} \\
 &+ \frac{T}{D_2} \frac{2}{\ell} \int_{I_2} \omega_{21}(x) dx / \int_{I_{1,2}} (\omega_{12}(x) + \omega_{21}(x)) dx \frac{1}{\langle \exp(U_2/T) \rangle \langle \exp(-U_2/T) \rangle},
 \end{aligned} \tag{5.21}$$

which is the average of the diffusion coefficients of the single states weighted by the transition rates. As $\omega_1 = \omega_2 = \omega$, the dependence on ω as well as on ε drops out, so that the diffusion

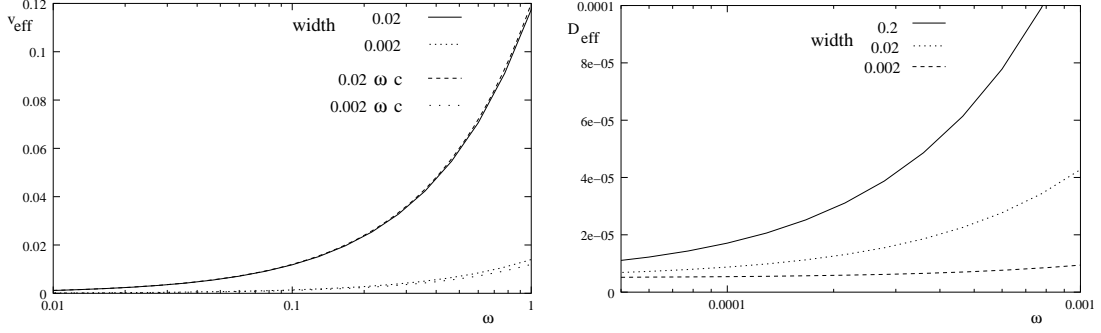


Figure 5.5: Transport coefficients v_{eff} and D_{eff} in the region of small ω for varying transition widths. Left: v_{eff} for the widths $\varepsilon = 0.02$ and 0.002 in the region of small ω as well as the straight lines given by $\varepsilon\omega c$.

coefficient starts with a constant and in general non-zero value for small ω . However, this is a very rough estimate, as for larger values of ω a regime of linear increase in ω is reached soon [73].

If the transition rates are large, the switching between the states is much faster than the transport in a single state. The particle experiences one effective potential U_{eff} , and v_{eff} becomes

$$v_{eff} \approx \frac{T}{D_1 + D_2} D_{eff} \frac{2}{\ell} \left(\int_{I_1} \omega_{12}(x) dx \int_{I_2} \omega_{21}(x) dx \right) / \int_{I_{1,2}} (\omega_{12}(x) + \omega_{21}(x))^3 dx \cdot \int_0^L \frac{1}{\ell} \left(\frac{dU_1/T}{dx} - \frac{dU_2/T}{dx} \right)^2 \frac{dU_{eff}/T}{dx} dx \quad (5.22)$$

with

$$U_{eff} \approx \frac{2}{\ell} \left(\int_{I_1} \omega_{12}(x) dx U_1 + \int_{I_2} \omega_{21}(x) dx U_2 \right) / \left(\int_{I_{1,2}} (\omega_{12}(x) + \omega_{21}(x)) dx \right). \quad (5.23)$$

The weight factor concerning the transition rates is

$$\begin{aligned} & \frac{2}{\ell} \left(\int_{I_1} \omega_{12}(x) dx \int_{I_2} \omega_{21}(x) dx \right) / \int_{I_{1,2}} (\omega_{12}^3(x) + \dots + \omega_{21}^3(x)) dx \\ &= \frac{2}{\ell} (4\varepsilon^2\omega^2) / (2\varepsilon\omega^3 + \dots + 2\varepsilon\omega^3) = O(\varepsilon/\omega). \end{aligned} \quad (5.24)$$

The relationship in $O(\varepsilon/\omega)$ shows that, for large values of ω , v_{eff} decreases with ε . If ε is very small, the effect of variations in ω minimizes for comparable large values of ω , so that we observe a saturation-like behaviour as indicated by the numerical results on the left-hand side of fig. 5.4. For $\omega_1 = \omega_2 = \omega$, the diffusion coefficient in the regime of large transition rates is accordingly given by

$$D_{eff} \approx \frac{T}{D_1 + D_2} \frac{1}{\langle \exp(U_{eff}/T) \rangle \langle \exp(-U_{eff}/T) \rangle}, \quad (5.25)$$

which leads to a constant again, as the dependence on ω drops out.

5.2.3 Molecular interaction potentials

In the following, we compare the transport coefficients we obtain for different molecular interaction potentials. Fig. 5.6 shows the three different types of potentials where U is given by $U \equiv U_1(x/\ell)$. (c) shows a standard sawtooth potential, whereas the steep barriers of the potentials (a) and (b) reflect the limited extensibility of the molecule [40]. The underlying idea is that we consider a two-headed motor protein, e.g. kinesin. Besides, we imagine a situation where one tries to displace

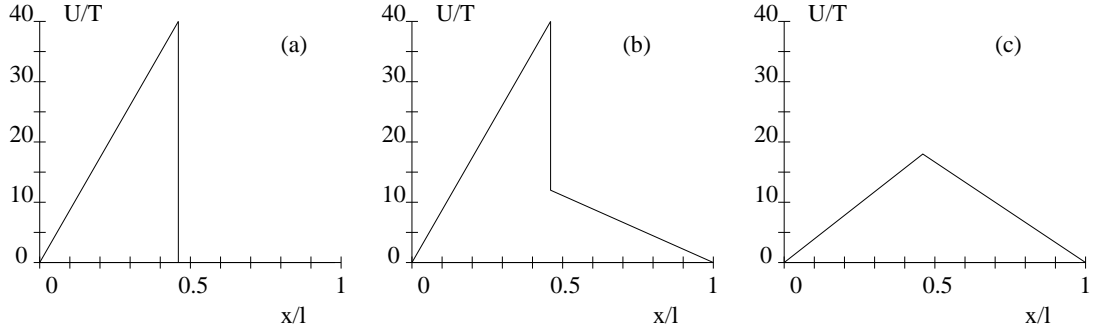


Figure 5.6: Periodic molecular interaction potentials of types (a), (b) and (c).

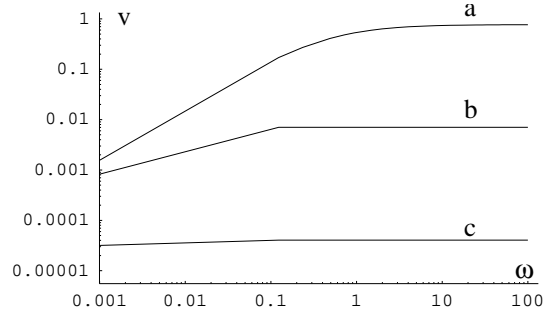


Figure 5.7: Velocities of the motor particle as a function of the unbalanced vertical rate for the model potentials (a), (b) and (c) as shown in fig. 5.6. The calculation has been done using the results obtained in 3.1.2.

the unbound head. If it is displaced for about 16 nm this corresponds to a displacement of the motor protein's centre of mass of about 8 nm . A displacement in this range is possible because of the flexibility of the neck region of the protein. If one causes an even further displacement, this will result in an over-stretching or a considerable distortion.

The ramp in the models of fig. 5.6 represents those values of displacements of the motor protein which can be reached under "normal" circumstances. The barrier on the other hand belongs to the forbidden region of displacements. The total area over one period of the geometric shapes in the cases (a) and (c) is equal.

Fig. 5.7 shows the velocities of the motor particles as a function of a single unbalanced vertical rate in the case of the three different model molecular interaction potentials. The calculation has been done by inserting the potential shapes into the results as obtained in 3.1.2 for a system with two states and here with localized transitions again. The potentials in the two states are shifted by half a potential period, 0.5ℓ . The unbalanced transition is $\omega_{12}(x_1) =: \omega$ located at $x_1 = 0$. There is no external force, but a passive relaxation back into the first state with rate $\omega_{21}(x_2)$ at $x_2 = 0.5\ell$. The resulting curve for the velocity for model potential (a) lies above curve (b), which again shows a higher saturation value than in the case of model (c). Example (a) with its single ramp leads to the highest velocities within the complete range of values of ω . The single ramp together with the high barrier prevent the motor from stepping back. Backward steps are most likely in the potential landscape (c), accordingly the velocity is lowest for case (c).

In the next step, we have a look at the transport coefficients in dependence on the different values of the external force F . We use the numerical approach as in 5.2.1 and 5.2.2, which in particular means that the transition rates have finite widths again. The transport coefficients are displayed in fig. 5.8.

In the case of a steep barrier as given by (b), the velocity is positive for large values of the external force and approaches zero as F is reduced further and further. There is no change in sign

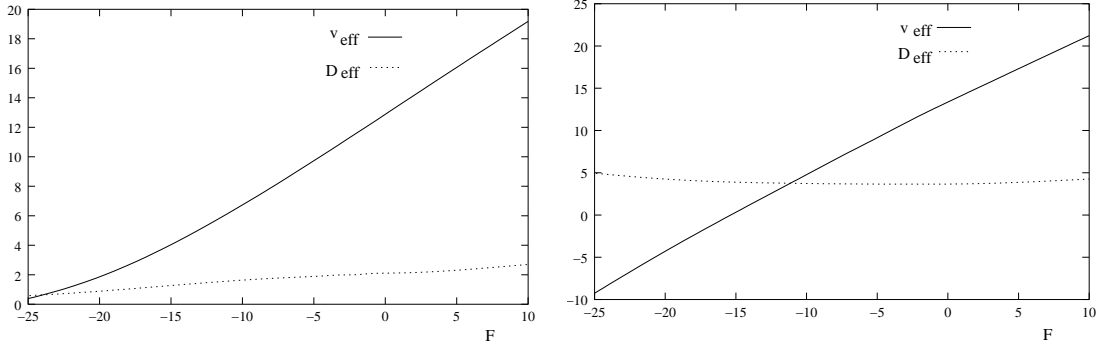


Figure 5.8: Transport coefficients v_{eff} and D_{eff} depending on the external force F for molecular interaction potentials (b) on the left and (c) on the right, respectively.

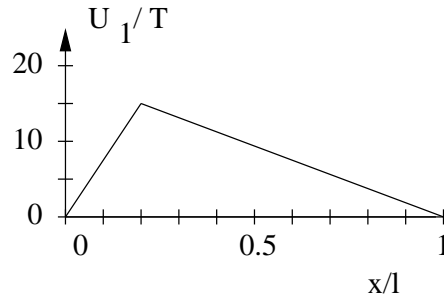


Figure 5.9: Potential $U_1(x)$ inserted in 5.2.4.

for the velocity. Correspondingly, the diffusion coefficient decreases and its curve can be fitted by a straight line.

Molecular interaction potentials of the simple sawtooth type as (c) lead to a change of the sign of the velocity if the external force F decreases beyond a certain value. Over the whole range of values of F , the velocity increases monotonically with the external force. The change of sign in the velocity is coupled to a minimum of the diffusion. As the transition rates have finite widths, the advantage of the steep barrier in preventing backward movement is partly lost, and the velocities in the cases (b) and (c) are comparable.

5.2.4 Free diffusion

The molecular interaction potentials can be different in each state. Now, we compare the case $U_2(x) = U_1(x - \ell/2)$ to $U_2(x) = 0$. In the second example we have free diffusion in state two. The potentials $U_1(x)$ are inserted as depicted in fig. 5.9.

Fig. 5.10 shows how free diffusion in the second state influences the transport coefficients by reducing the velocity and raising diffusion as expected, i.e., directed transport is hindered.

Snapshots of the local distribution of the total probability $P_{tot} = P_1 + P_2$ show that the maximal values of P_{tot} are higher in the case of free diffusion in state 2 compared to the case of two shifted potentials. At the same time the fluctuations are larger, too, compare fig. 5.11. This is easily explained as the particles tend to stay near the minima of the respective potentials. The minima and maxima are lacking in the case of $U_2(x) = 0$, so that the local probability in state 2 does not attain any sharp peaks, which, in the case of shifted potentials, are opposed to the peaks of state 1. For shifted potentials we compare an extinction of the minima and maxima of the probabilities similar to fig. 4.25.

If the frequency ω of switching between the two states is increased, this leads to a probability distribution which is advanced further in the x -direction compared to a distribution with a lower

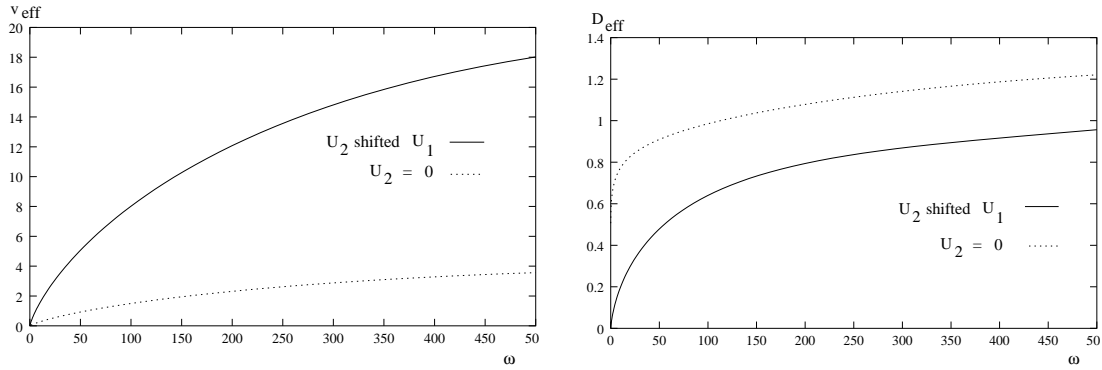


Figure 5.10: Left-hand side: the velocity reduces remarkably in the case of free diffusion in the second state. Right-hand side: diffusion for shifted potentials (solid curve) compared to free diffusion (dotted curve) in state two.

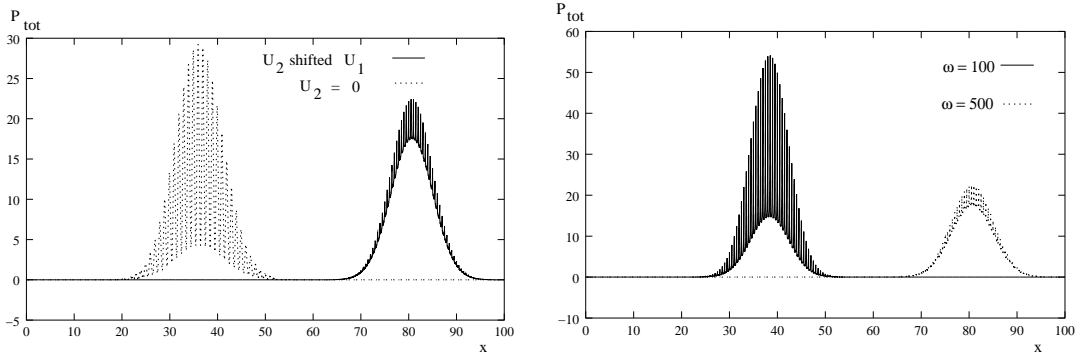


Figure 5.11: Left: The total probability P_{tot} depending on the x - coordinate for shifted potentials versus no potential in state 2 for $\omega = 500$ at $t = 10$. Right: The total probability for shifted potentials for $\omega = 100$ and $\omega = 500$ at $t = 10$.

value of ω at the same time, as in this regime of ω larger values promote the directed transport. The fluctuations in the probability distribution are smaller for larger ω . Comparing this result to the result from the discrete Master-equation computation displayed in fig. 4.26, we conclude that we find a comparable behaviour with an "optimal" value of the rates in order to minimize the effects of the potential maxima and minima here.

The examples show that the approach with a continuous x -direction and finite transitions widths on the one hand and the discrete Master-equation approach presented in 4.4 on the other hand lead to qualitatively similar results. This is a good confirmation for the network-based approach.

Chapter 6

Conclusions And Outlook

Linear molecular motors use the energy released in the hydrolysis of ATP to move other molecules, their cargoes, along filamental tracks. Coupled to the hydrolysis of ATP is a cycle of conformational changes of the motor protein. Such a motor cycle leads to a single step along the filament.

Here, we have examined stochastic models for these motor cycles, which determine the transport properties for the directed walks of the motor along its filament. In the short time regime of conformational changes and motor cycles, the motor performs single steps in the range of about 10 nm , and the corresponding stepping times are of the order of 10 ms , if there is a sufficient amount of ATP around. This short time regime determines the regime of directed walks where the motor takes up to several hundred steps along its track.

The main ingredients of our stochastic models as introduced in chapter 2 are a spatial coordinate x describing the displacement of the motor along the filament, a set of M states or conformations the motor particle can attain as well as a set of K locations at which transitions between these different states take place.

The ratchet models can be solved analytically using a transfer matrix formalism as described in chapter 2. Besides, we have shown that they can be mapped onto stochastic networks with MK discrete states or vertices. Finally, we obtain a general solution scheme by which the total current can be calculated.

In chapter 3 we have calculated explicit solutions for stochastic systems with up to four states or conformations and with one to four locations for transitions between the states. The total current which is carried along such a network is the quotient of two polynomials which depend on the transitions between the states via the corresponding vertical transition rates. The current is proportional to the motor's velocity. From the explicit solutions and from the general properties of the matrices used for the computations, we derive a number of universal rules which impose restrictions on the dependence of the velocity on the vertical transition rates connecting the states. The terms in the numerator polynomial of the total current are shown to be connected to paths through the networks if corresponding implicit horizontal rates are added. If we do not apply an external force, every such term of the first polynomial can be mapped onto an s-cycle spanning the network in horizontal direction.

If a given motor follows a stepping scheme with a known number of different conformations and locations, the above-mentioned rules enable us to derive combinations of vertical rates which contribute to its velocity via certain paths entering the numerator polynomial. Furthermore, we are able to exclude those combinations which do not contribute, even if we have not explicitly calculated the solution of this special model.

In principle, our models are not limited as far as the number of their states or locations is concerned. In this way, quite a variety of different stepping mechanisms for different motors can be described and new findings about how a specific motor walks can be integrated. As more and more experiments are performed, people frequently identify new substeps in the stepping schemes of motors. These substeps can easily be modelled in our approach.

In the first section of chapter 4 we have shown how decoupled states or subsystems can be

handled. Although for decoupled states a straightforward calculation as used for the model systems in the preceding chapter fails due to the singularity of the underlying matrices, the subsystems are inherent in these matrices. States or subsystems without a direct or indirect connection to the remaining system play a role if the motor can, with a certain probability, attain conformations which exclude transitions into certain other conformations, which might be the case if there is, for example, no possibility of the motor binding ATP. Likewise, in a system with decoupling we can include additional states which are needed for the description of certain mutants of the motor or faulty motor proteins. In addition to the “normal” or “healthy” stepping, we then have alternative paths if such a special situation occurs. The introduction of a control parameter coupling two identical subsystems reveals bifurcations with different branches for the internal rates of the subsystems, while the total current in the stationary state is fixed, so that the “macroscopic” appearance corresponds to different “microscopic” configurations.

In the sections 4.2 and 4.3 we introduce active elements or unbalanced rates in other than the vertical and, in particular, in the horizontal direction. One way of achieving this is by distortion of the networks as done in 4.2. The new approach in 4.3 is based on a discrete Master equation. This no longer requires horizontal transition rates fulfilling the conditions of detailed balance, but allows us to view arbitrary horizontal rates, if we start from the Master equation without considering its former derivation. The unbalanced rates drive the transport in horizontal direction or any other direction obtained by distorting the underlying networks.

Now, the total current obtained from the Master-equation calculations explicitly depends on the vertical and also on the horizontal rates of the systems. Its numerator polynomial contains terms with complete paths of vertical and horizontal rates along the network. From calculations in model systems we derive universal rules for the dependence of the total current on all the transition rates of the system. The results of the model systems relate one and the same combination of vertical rates to several forward and backward paths with possible additional horizontal rates fulfilling rules analogous to the ones derived before for vertical rates.

By integrating the discrete Master equation numerically, it is possible to take into account larger systems where the spatial periodicity comprises a number of steps as shown in section 4.4. Beginning with a certain probability distribution, we look at how the stationary state is reached with ongoing time. Doing so, we examine the hindrance of the transport by a defect or obstacle on its track reducing the total current. The dependence of the motor’s transport on a single conformation, which is attained in the course of a multi-state stepping process, can be significant, if this conformation allows for fast directed transport or otherwise for no directed transport at all and if there are few possibilities of leaving this conformation again. Several results concerning the time evolution of the systems are confirmed in a Markov-chain approach.

In the field of enzyme kinetics, one usually distinguishes one special cycle of chemical processes which is then called the main pathway of the enzyme. In our system this is the positive s-cycle carrying the largest current along the network.

In section 4.5 we have discussed how possible “candidates” for this main pathway can be identified in a special system. If we have maximum rates given in a system, these rates correspond to an upper limit of transport. The systems are then associated with flow networks with certain capacities for the edges. A number of paths realizing maximum flow along the network is determined. If the flow is fixed, a preferred pathway will be one with low costs. From our models we suggest that the main pathway irregardless of its importance is not the only pathway through the network. Furthermore, there are other pathways whose contributions might be smaller, but still existent. This view is already accepted for a number of chemical reactions, and it can be interesting to examine such alternative pathways for molecular motors, too.

The network-oriented approach to the movements of molecular motors has turned out to offer a simple picture for the motor cycles which nevertheless comprises many details of motor transport. This can be an impulse to further models.

The underlying reaction kinetics of the hydrolysis of ATP or other chemical processes enters our models via the dependence of the unbalanced rates on the respective concentrations, here the concentration of ATP. We have shown in section 5.1 that if we assume different reaction kinetics for the dependence on the concentration of ATP, this leads to velocities whose dependence on the

ATP-concentration can differ from the usually assumed Michaelis-Menten type behaviour. Apart from the Michaelis-Menten curves for the simple case of Michaelis-Menten kinetics and a single unbalanced rate, we obtain curves with sigmoidal courses or maxima. These differences can occur due to allosteric effects when the motor binds regulatory molecules. The tolerances and the low number of data points in the present experimental results still offer possibilities for such deviating dependences which might be determined in future experiments.

In section 5.2 we have looked at the influences different choices of the molecular interaction potentials have on the transport properties in systems without active horizontal transport. Besides, we have examined the effects of localized vertical transitions as used in our networks compared to other models with finite transition widths, where the horizontal direction is continuous again. If the widths are small, the maxima of the transport coefficients are shifted to large rates and we approach the crossover to a saturation regime. Some of the qualitative results obtained from our network models as, for example, for the time evolution of the probabilities, are comparable to the results of these alternative models. In this way we have been able to elucidate the characteristics of our models as well as the results when inserting experimental data.

Our stochastic models can be mapped onto networks, which simplifies the calculations and offers possibilities for approaches from the field of graph theory. The models are meant to qualitatively describe a variety of different features of motor transport rather than to fit data for the stepping process of a certain motor construct. In the context of our models we can handle backward steps and substeps, transient conformations, faulty motors and mutants, periodic defects of the filament, active elements in vertical, horizontal or any distorted direction as well as the idea of a main and a couple of minor pathways. The future challenge will be the building in of newly discovered properties and characteristics of the motors and their tracks.

Appendix A

Matrices $\mathbf{A}^{(M,K)}$

In the following sections A.1-A.3 we list the matrix elements $A_{ij}^{(M,K)}$, where i indicates the corresponding row and j the column, for the general model systems $(M, K) = (2, 3)$, $(M, K) = (2, 4)$ and $(M, K) = (3, 2)$.

The sections A.4 and A.5 show the derivation of matrices describing subsystems of an $(M, K) = (3, 2)$ and an $(M, K) = (2, 4)$ -system, respectively.

A.1 Matrix $\mathbf{A}^{(2,3)}$

Here, we list the matrix elements of $\mathbf{A}^{(2,3)}$. The notation is as given in chapter 2.

$$\begin{aligned}
 A_{11}^{(2,3)} &= \mathcal{E}_1(x_1, x_2) \omega_{12}(x_2) - (-\mathcal{E}_1(x_2, x_3) - \mathcal{E}_1(x_1, x_2) (e_1(x_2, x_3) + \mathcal{E}_1(x_2, x_3) \\
 &\quad \ell_{\Omega} \omega_{12}(x_2))) \omega_{12}(x_3) + \mathcal{E}_1(x_1, x_2) \mathcal{E}_2(x_2, x_3) \ell_{\Omega} \omega_{12}(x_2) \omega_{21}(x_3) \\
 A_{12}^{(2,3)} &= -\mathcal{E}_1(x_2, x_3) - \mathcal{E}_1(x_3, x_1 + \ell) / e_1(x_3, x_1 + \ell) - \mathcal{E}_1(x_1, x_2) \\
 &\quad (e_1(x_2, x_3) + \mathcal{E}_1(x_2, x_3)) \ell_{\Omega} \omega_{12}(x_2) \\
 A_{13}^{(2,3)} &= \mathcal{E}_1(x_1, x_2) \mathcal{E}_2(x_2, x_3) \ell_{\Omega} \omega_{12}(x_2) \\
 A_{14}^{(2,3)} &= -\bar{\mathcal{E}}_1(x_1) - \mathcal{E}_1(x_1, x_2) (\bar{\mathcal{E}}_1(x_2) - \bar{\mathcal{E}}_1(x_3)) \ell_{\Omega} \omega_{12}(x_2) \\
 &\quad + \mathcal{E}_1(x_1, x_2) (\bar{\mathcal{E}}_2(x_2) - \bar{\mathcal{E}}_2(x_3)) \ell_{\Omega} \omega_{21}(x_2) \\
 A_{21}^{(2,3)} &= -(\mathcal{E}_2(x_1, x_2) \omega_{21}(x_2) - \mathcal{E}_1(x_2, x_3) \mathcal{E}_2(x_1, x_2) \ell_{\Omega} \omega_{12}(x_3) \omega_{21}(x_2) \\
 &\quad + (-\mathcal{E}_2(x_2, x_3) \mathcal{E}_2(x_1, x_2) (e_2(x_2, x_3) + \mathcal{E}_2(x_2, x_3) \ell_{\Omega} \omega_{21}(x_2))) \omega_{21}(x_3) \\
 A_{22}^{(2,3)} &= \mathcal{E}_1(x_2, x_3) \mathcal{E}_2(x_1, x_2) \ell_{\Omega} \omega_{21}(x_2) \\
 A_{23}^{(2,3)} &= -\mathcal{E}_2(x_2, x_3) - \mathcal{E}_2(x_3, x_1 + \ell) / e_2(x_3, x_1 + \ell) - \mathcal{E}_2(x_1, x_2) \\
 &\quad (e_2(x_2, x_3) + \mathcal{E}_2(x_2, x_3) \ell_{\Omega} \omega_{21}(x_2)) \\
 A_{24}^{(2,3)} &= -\bar{\mathcal{E}}_2(x_1) + \mathcal{E}_2(x_1, x_2) (\bar{\mathcal{E}}_1(x_2) - \bar{\mathcal{E}}_1(x_3)) \ell_{\Omega} \omega_{21}(x_2) \\
 &\quad - \mathcal{E}_2(x_1, x_2) (\bar{\mathcal{E}}_2(x_2) - \bar{\mathcal{E}}_2(x_3)) \ell_{\Omega} \omega_{21}(x_2) \\
 A_{31}^{(2,3)} &= -\omega_{12}(x_1) - (e_1(x_1, x_2) + \mathcal{E}_1(x_1, x_2) \ell_{\Omega} \omega_{12}(x_1)) \omega_{12}(x_2) \\
 &\quad - \mathcal{E}_2(x_1, x_2) \ell_{\Omega} \omega_{12}(x_1) \omega_{21}(x_2) - \omega_{12}(x_3) (\mathcal{E}_1(x_2, x_3) \ell_{\Omega} \omega_{12}(x_1) \\
 &\quad + (e_1(x_1, x_2) + \mathcal{E}_1(x_1, x_2) \ell_{\Omega} \omega_{12}(x_1)) (e_1(x_2, x_3) + \mathcal{E}_1(x_2, x_3) \ell_{\Omega} \omega_{12}(x_2)) \\
 &\quad + \mathcal{E}_1(x_2, x_3) \mathcal{E}_2(x_1, x_2) \ell_{\Omega}^2 \omega_{12}(x_1) \omega_{21}(x_2)) + (-\mathcal{E}_2(x_2, x_3) \ell_{\Omega} \omega_{12}(x_1)) \\
 &\quad - \mathcal{E}_2(x_2, x_3) \ell_{\Omega} (e_1(x_1, x_2) + \mathcal{E}_1(x_1, x_2) \ell_{\Omega} \omega_{12}(x_1)) \omega_{12}(x_2) \\
 &\quad - \mathcal{E}_2(x_1, x_2) \ell_{\Omega} \omega_{12}(x_1) (e_2(x_2, x_3) + \mathcal{E}_2(x_2, x_3) \ell_{\Omega} \omega_{21}(x_2))) \omega_{21}(x_3) \\
 A_{32}^{(2,3)} &= -1/e_1(x_3, x_4) + \mathcal{E}_1(x_2, x_3) \ell_{\Omega} \omega_{12}(x_1)
 \end{aligned}$$

$$\begin{aligned}
& + (e_1(x_1, x_2) + \mathcal{E}_1(x_1, x_2) \ell_\Omega \omega_{12}(x_1)) (e_1(x_2, x_3) + \mathcal{E}_1(x_2, x_3) \ell_\Omega \omega_{12}(x_2)) \\
& + \mathcal{E}_1(x_2, x_3) \mathcal{E}_2(x_1, x_2) \ell_\Omega^2 \omega_{12}(x_1) \omega_{21}(x_2) \\
A_{33}^{(2,3)} & = -(\mathcal{E}_2(x_2, x_3) \ell_\Omega \omega_{12}(x_1)) - \mathcal{E}_2(x_2, x_3) \ell_\Omega (e_1(x_1, x_2) + \mathcal{E}_1(x_1, x_2) \ell_\Omega \omega_{12}(x_1)) \\
& \omega_{12}(x_2) - \mathcal{E}_2(x_1, x_2) \ell_\Omega \omega_{12}(x_1) (e_2(x_2, x_3) + \mathcal{E}_2(x_2, x_3) \ell_\Omega \omega_{21}(x_2)) \\
A_{34}^{(2,3)} & = \bar{e}_1 + (\bar{\mathcal{E}}_1(x_1) - \bar{\mathcal{E}}_1(x_3)) \ell_\Omega \omega_{12}(x_1) - (\bar{\mathcal{E}}_2(x_1) - \bar{\mathcal{E}}_2(x_3)) \ell_\Omega \omega_{12}(x_1) \\
& - (\bar{\mathcal{E}}_1(x_2) - \bar{\mathcal{E}}_1(x_3)) \ell_\Omega (-((e_1(x_1, x_2) + \mathcal{E}_1(x_1, x_2) \ell_\Omega \omega_{12}(x_1)) \omega_{12}(x_2)) \\
& - \mathcal{E}_2(x_1, x_2) \ell_\Omega \omega_{12}(x_1) \omega_{21}(x_2)) - (\bar{\mathcal{E}}_2(x_2) - \bar{\mathcal{E}}_2(x_3)) \ell_\Omega \\
& ((e_1(x_1, x_2) + \mathcal{E}_1(x_1, x_2) \ell_\Omega \omega_{12}(x_2)) \omega_{12}(x_1) + \mathcal{E}_2(x_1, x_2) \ell_\Omega \omega_{12}(x_1) \omega_{21}(x_2)) \\
A_{41}^{(2,3)} & = \omega_{21}(x_1) + \mathcal{E}_1(x_1, x_2) \ell_\Omega \omega_{12}(x_2) \omega_{21}(x_1) + (e_2(x_1, x_2) + \mathcal{E}_2(x_1, x_2) \ell_\Omega \omega_{21}(x_1)) \\
& \omega_{21}(x_2) - \omega_{12}(x_3) (-(\mathcal{E}_1(x_2, x_3) \ell_\Omega \omega_{21}(x_1)) - \mathcal{E}_1(x_1, x_2) \ell_\Omega \\
& (e_1(x_2, x_3) + \mathcal{E}_1(x_2, x_3) \ell_\Omega \omega_{12}(x_2)) \omega_{21}(x_1) - \mathcal{E}_1(x_2, x_3) \ell_\Omega \\
& (e_2(x_1, x_2) + \mathcal{E}_2(x_1, x_2) \ell_\Omega \omega_{21}(x_1)) \omega_{21}(x_2)) + \\
& (\mathcal{E}_2(x_2, x_3) \ell_\Omega \omega_{21}(x_1) + \mathcal{E}_1(x_1, x_2) \mathcal{E}_2(x_2, x_3) \ell_\Omega^2 \omega_{12}(x_2) \omega_{21}(x_1) \\
& + (e_2(x_1, x_2) + \mathcal{E}_2(x_1, x_2) \ell_\Omega \omega_{21}(x_1)) + (e_2(x_2, x_3) + \mathcal{E}_2(x_2, x_3) \ell_\Omega \omega_{21}(x_2))) \\
& \omega_{21}(x_3) \\
A_{42}^{(2,3)} & = -\mathcal{E}_1(x_2, x_3) \ell_\Omega \omega_{21}(x_1) - \mathcal{E}_1(x_1, x_2) \ell_\Omega (e_1(x_2, x_3) + \mathcal{E}_1(x_2, x_3) \ell_\Omega \omega_{12}(x_2)) \\
& \omega_{21}(x_1) - \mathcal{E}_1(x_2, x_3) \ell_\Omega (e_2(x_1, x_2) + \mathcal{E}_2(x_1, x_2) \ell_\Omega \omega_{21}(x_1)) \omega_{21}(x_2) \\
A_{43}^{(2,3)} & = -1/e_2(x_3, x_4) + \mathcal{E}_2(x_2, x_3) \ell_\Omega \omega_{21}(x_1) \\
& + \mathcal{E}_1(x_1, x_2) \mathcal{E}_2(x_2, x_3) \ell_\Omega^2 \omega_{12}(x_2) \omega_{21}(x_1) + (e_2(x_1, x_2) + \mathcal{E}_2(x_1, x_2) \ell_\Omega \omega_{21}(x_1)) \\
& (e_2(x_2, x_3) + \mathcal{E}_2(x_2, x_3) \ell_\Omega \omega_{21}(x_2)) \\
A_{44}^{(2,3)} & = \bar{e}_2 - (\bar{\mathcal{E}}_1(x_1) - \bar{\mathcal{E}}_1(x_3)) \ell_\Omega \omega_{21}(x_1) + (\bar{\mathcal{E}}_2(x_1) - \bar{\mathcal{E}}_2(x_3)) \ell_\Omega \omega_{21}(x_1) \\
& - (\bar{\mathcal{E}}_2(x_2) - \bar{\mathcal{E}}_2(x_3)) \ell_\Omega (-(\mathcal{E}_1(x_1, x_2) \ell_\Omega \omega_{12}(x_2) \omega_{21}(x_1)) \\
& - (e_2(x_1, x_2) + \mathcal{E}_2(x_1, x_2) \ell_\Omega \omega_{21}(x_1)) \omega_{21}(x_2)) \\
& - (\bar{\mathcal{E}}_1(x_2) - \bar{\mathcal{E}}_1(x_3)) \ell_\Omega (\mathcal{E}_1(x_1, x_2) \ell_\Omega \omega_{12}(x_2) \omega_{21}(x_1) \\
& + (e_2(x_1, x_2) + \mathcal{E}_2(x_1, x_2) \ell_\Omega \omega_{21}(x_1)) \omega_{21}(x_2))
\end{aligned} \tag{A.1}$$

A.2 Matrix $\mathbf{A}^{(2,4)}$

In the following the elements of the 4×4 -matrix $\mathbf{A}^{(2,4)}$ as used for calculations in 3.1.2 are listed.

$$\begin{aligned}
A_{11}^{(2,4)} & = \mathcal{E}_1(x_1, x_2) \omega_{12}(x_2) - (-\mathcal{E}_1(x_2, x_3) - \mathcal{E}_1(x_1, x_2) (e_1(x_2, x_3) \\
& + \mathcal{E}_1(x_2, x_3) \ell_\Omega \omega_{12}(x_2))) \omega_{12}(x_3) + \mathcal{E}_1(x_1, x_2) \mathcal{E}_2(x_2, x_3) \ell_\Omega \\
& \omega_{12}(x_2) \omega_{21}(x_3) - \omega_{12}(x_4) (-(\mathcal{E}_1(x_3, x_4) (1 + \mathcal{E}_1(x_1, x_2) \ell_\Omega \omega_{12}(x_2))) \\
& + (-\mathcal{E}_1(x_2, x_3) - \mathcal{E}_1(x_1, x_2) (e_1(x_2, x_3) + \mathcal{E}_1(x_2, x_3) \ell_\Omega \omega_{12}(x_2))) \\
& (e_1(x_3, x_4) + \mathcal{E}_1(x_3, x_4) \ell_\Omega \omega_{12}(x_3)) - \mathcal{E}_1(x_1, x_2) \mathcal{E}_1(x_3, x_4) \mathcal{E}_2(x_2, x_3) \\
& \ell_\Omega^2 \omega_{12}(x_2) \omega_{21}(x_3)) + (\mathcal{E}_1(x_1, x_2) \mathcal{E}_2(x_3, x_4) \ell_\Omega \omega_{12}(x_2) - \mathcal{E}_2(x_3, x_4) \ell_\Omega \\
& (-\mathcal{E}_1(x_2, x_3) - \mathcal{E}_1(x_1, x_2) (e_1(x_2, x_3) + \mathcal{E}_1(x_2, x_3) \ell_\Omega \omega_{12}(x_2))) \\
& \omega_{12}(x_3) + \mathcal{E}_1(x_1, x_2) \mathcal{E}_2(x_2, x_3) \ell_\Omega \omega_{12}(x_2) (e_2(x_3, x_4) \\
& + \mathcal{E}_2(x_1, x_3) \ell_\Omega \omega_{21}(x_3))) \omega_{21}(x_4) \\
A_{12}^{(2,4)} & = -\mathcal{E}_1(x_4, x_1 + \ell) / e_1(x_4, x_1 + \ell) - \mathcal{E}_1(x_3, x_4) (1 + \mathcal{E}_1(x_1, x_2) \ell_\Omega \omega_{12}(x_2)) \\
& + (-\mathcal{E}_1(x_2, x_3) - \mathcal{E}_1(x_1, x_2) (e_1(x_2, x_3) + \mathcal{E}_1(x_2, x_3) \ell_\Omega \omega_{12}(x_2))) \\
& (e_1(x_3, x_4) + \mathcal{E}_1(x_3, x_4) \ell_\Omega \omega_{12}(x_3)) - \mathcal{E}_1(x_1, x_2) \mathcal{E}_1(x_3, x_4) \mathcal{E}_2(x_2, x_3)
\end{aligned}$$

$$\begin{aligned}
& \ell_\Omega^2 \omega_{12}(x_2) \omega_{21}(x_3) \\
A_{13}^{(2,4)} &= \mathcal{E}_1(x_1, x_2) \mathcal{E}_2(x_3, x_4) \ell_\Omega \omega_{12}(x_2) - \mathcal{E}_2(x_3, x_4) \ell_\Omega (-\mathcal{E}_1(x_2, x_3) - \mathcal{E}_1(x_1, x_2) \\
& \quad (e_1(x_2, x_3) + \mathcal{E}_1(x_2, x_3) \ell_\Omega \omega_{12}(x_2))) \omega_{12}(x_3) + \mathcal{E}_1(x_1, x_2) \mathcal{E}_2(x_2, x_3) \\
& \quad \ell_\Omega \omega_{12}(x_2) (e_2(x_3, x_4) + \mathcal{E}_2(x_3, x_4) \ell_\Omega \omega_{21}(x_3)) \\
A_{14}^{(2,4)} &= -\bar{\mathcal{E}}_1(x_1) - \mathcal{E}_1(x_1, x_2) (\bar{\mathcal{E}}_1(x_2) - \bar{\mathcal{E}}_1(x_4)) \ell_\Omega \omega_{12}(x_2) + \mathcal{E}_1(x_1, x_2) \\
& \quad (\bar{\mathcal{E}}_2(x_2) - \bar{\mathcal{E}}_2(x_4)) \ell_\Omega \omega_{12}(x_2) - (\bar{\mathcal{E}}_2(x_3) - \bar{\mathcal{E}}_2(x_4)) \ell_\Omega \\
& \quad ((-\mathcal{E}_1(x_2, x_3) - \mathcal{E}_1(x_1, x_2) (e_1(x_2, x_3) + \mathcal{E}_1(x_2, x_3) \ell_\Omega \omega_{12}(x_2)))) \omega_{12}(x_3) \\
& \quad - \mathcal{E}_1(x_1, x_2) \mathcal{E}_2(x_2, x_3) \ell_\Omega \omega_{12}(x_2) \omega_{21}(x_3) - (\bar{\mathcal{E}}_1(x_3) - \bar{\mathcal{E}}_1(x_4)) \ell_\Omega \\
& \quad (-((-\mathcal{E}_1(x_2, x_3) - \mathcal{E}_1(x_1, x_2) (e_1(x_2, x_3) + \mathcal{E}_1(x_2, x_3) \ell_\Omega \omega_{12}(x_2)))) \omega_{12}(x_3)) \\
& \quad \mathcal{E}_1(x_1, x_2) \mathcal{E}_2(x_2, x_3) \ell_\Omega \omega_{12}(x_2) \omega_{21}(x_3)) \\
A_{21}^{(2,4)} &= -\mathcal{E}_2(x_1, x_2) \omega_{21}(x_2) - \mathcal{E}_1(x_2, x_3) \mathcal{E}_2(x_1, x_2) \ell_\Omega \omega_{12}(x_3) \omega_{21}(x_2) \\
& \quad + (-\mathcal{E}_2(x_2, x_3) - \mathcal{E}_2(x_1, x_2) (e_2(x_2, x_3) + \mathcal{E}_2(x_2, x_3) \ell_\Omega \omega_{21}(x_2))) \omega_{21}(x_3) \\
& \quad - \omega_{12}(x_4) (\mathcal{E}_1(x_3, x_4) \mathcal{E}_2(x_1, x_2) \ell_\Omega \omega_{21}(x_2) + \mathcal{E}_1(x_2, x_3) \mathcal{E}_2(x_1, x_2) \ell_\Omega \\
& \quad (e_1(x_3, x_4) + \mathcal{E}_1(x_3, x_4) \ell_\Omega \omega_{12}(x_3)) \omega_{21}(x_2) - \mathcal{E}_1(x_3, x_4) \ell_\Omega (-\mathcal{E}_2(x_2, x_3) \\
& \quad - \mathcal{E}_2(x_1, x_2) (e_2(x_2, x_3) + \mathcal{E}_2(x_2, x_3) \ell_\Omega \omega_{21}(x_2))) \omega_{21}(x_3)) \\
& \quad + ((-\mathcal{E}_1(x_2, x_3) \mathcal{E}_2(x_1, x_2) \mathcal{E}_2(x_3, x_4) \ell_\Omega^2 \omega_{12}(x_3) \omega_{21}(x_2)) - \mathcal{E}_2(x_3, x_4) \\
& \quad (1 + \mathcal{E}_2(x_1, x_2) \ell_\Omega \omega_{21}(x_2)) + (-\mathcal{E}_2(x_2, x_3) - \mathcal{E}_2(x_1, x_2) \\
& \quad (e_2(x_2, x_3) + \mathcal{E}_2(x_2, x_3) \ell_\Omega \omega_{21}(x_2))) (e_2(x_3, x_4) + \mathcal{E}_2(x_3, x_4) \ell_\Omega \omega_{21}(x_3))) \\
& \quad \omega_{21}(x_4) \\
A_{22}^{(2,4)} &= \mathcal{E}_1(x_3, x_4) \mathcal{E}_2(x_1, x_2) \ell_\Omega \omega_{21}(x_2) + \mathcal{E}_1(x_2, x_3) \mathcal{E}_2(x_1, x_2) \ell_\Omega (e_1(x_3, x_4) \\
& \quad + \mathcal{E}_1(x_3, x_4) \ell_\Omega \omega_{12}(x_3)) \omega_{21}(x_2) - \mathcal{E}_1(x_3, x_4) \ell_\Omega (-\mathcal{E}_2(x_2, x_3) - \mathcal{E}_2(x_1, x_2) \\
& \quad (e_2(x_2, x_3) + \mathcal{E}_2(x_2, x_3) \ell_\Omega \omega_{21}(x_2))) \omega_{21}(x_3) \\
A_{23}^{(2,4)} &= -\mathcal{E}_2(x_4, x_1 + \ell) / e_2(x_4, x_1 + \ell) - \mathcal{E}_1(x_2, x_3) \mathcal{E}_2(x_1, x_2) \mathcal{E}_2(x_3, x_4) \ell_\Omega^2 \omega_{12}(x_3) \\
& \quad \omega_{21}(x_2) - \mathcal{E}_2(x_3, x_4) (1 + \mathcal{E}_2(x_1, x_2) \ell_\Omega \omega_{21}(x_2)) + (-\mathcal{E}_2(x_2, x_3) - \mathcal{E}_2(x_1, x_2) \\
& \quad (e_2(x_2, x_3) + \mathcal{E}_2(x_2, x_3) \ell_\Omega \omega_{21}(x_2))) (e_2(x_3, x_4) + \mathcal{E}_2(x_3, x_4) \ell_\Omega \omega_{21}(x_3)) \\
A_{24}^{(2,4)} &= -\bar{\mathcal{E}}_2(x_1) + \mathcal{E}_2(x_1, x_2) (\bar{\mathcal{E}}_1(x_2) - \bar{\mathcal{E}}_1(x_4)) \ell_\Omega \omega_{21}(x_2) - \mathcal{E}_2(x_1, x_2) \\
& \quad (\bar{\mathcal{E}}_2(x_2) - \bar{\mathcal{E}}_2(x_4)) \ell_\Omega \omega_{21}(x_2) - (\bar{\mathcal{E}}_2(x_3) - \bar{\mathcal{E}}_2(x_4)) \ell_\Omega \\
& \quad (\mathcal{E}_1(x_2, x_3) \mathcal{E}_2(x_1, x_2) \ell_\Omega \omega_{12}(x_3) \omega_{21}(x_2) - (\mathcal{E}_2(x_2, x_3) - \mathcal{E}_2(x_1, x_2) (e_2(x_2, x_3) \\
& \quad + \mathcal{E}_2(x_2, x_3) \ell_\Omega \omega_{21}(x_2))) \omega_{21}(x_3)) - (\bar{\mathcal{E}}_1(x_3) - \bar{\mathcal{E}}_1(x_4)) \ell_\Omega \\
& \quad (-\mathcal{E}_1(x_2, x_3) \mathcal{E}_2(x_1, x_2) \ell_\Omega \omega_{12}(x_3) \omega_{21}(x_2)) + (-\mathcal{E}_2(x_2, x_3) - \mathcal{E}_2(x_1, x_2) \\
& \quad (e_2(x_2, x_3) + \mathcal{E}_2(x_2, x_3) \ell_\Omega \omega_{21}(x_2))) \omega_{21}(x_3)) \\
A_{31}^{(2,4)} &= -\omega_{12}(x_1) - (e_1(x_1, x_2) + \mathcal{E}_1(x_1, x_2) \ell_\Omega \omega_{12}(x_1)) \omega_{12}(x_2) - \mathcal{E}_2(x_1, x_2) \ell_\Omega \omega_{12}(x_1) \\
& \quad \omega_{21}(x_2) - \omega_{12}(x_3) (\mathcal{E}_1(x_2, x_3) \ell_\Omega \omega_{12}(x_1) + (e_1(x_1, x_2) + \mathcal{E}_1(x_1, x_2) \ell_\Omega \omega_{12}(x_1)) \\
& \quad (e_1(x_2, x_3) + \mathcal{E}_1(x_2, x_3) \ell_\Omega \omega_{12}(x_2)) + \mathcal{E}_1(x_2, x_3) \mathcal{E}_2(x_1, x_2) \ell_\Omega^2 \omega_{12}(x_1) \omega_{21}(x_2)) \\
& \quad + (-\mathcal{E}_2(x_2, x_3) \ell_\Omega \omega_{12}(x_1)) - \mathcal{E}_2(x_2, x_3) \ell_\Omega (e_1(x_1, x_2) + \mathcal{E}_1(x_1, x_2) \ell_\Omega \omega_{12}(x_1)) \\
& \quad \omega_{12}(x_2) - \mathcal{E}_2(x_1, x_2) \ell_\Omega \omega_{12}(x_1) (\mathcal{E}_2(x_2, x_3) + \mathcal{E}_2(x_2, x_3) \ell_\Omega \omega_{21}(x_2))) \omega_{21}(x_3) \\
& \quad - \omega_{12}(x_4) (-\mathcal{E}_1(x_3, x_4) (-\ell_\Omega \omega_{12}(x_1)) - \ell_\Omega (e_1(x_1, x_2) + \mathcal{E}_1(x_1, x_2) \ell_\Omega) \\
& \quad \omega_{12}(x_2) - \mathcal{E}_2(x_1, x_2) \ell_\Omega^2 \omega_{12}(x_1) \omega_{21}(x_2)) + (e_1(x_3, x_4) + \mathcal{E}_1(x_3, x_4) \ell_\Omega \omega_{12}(x_3)) \\
& \quad (\mathcal{E}_1(x_2, x_3) \ell_\Omega \omega_{12}(x_1) + (e_1(x_1, x_2) + \mathcal{E}_1(x_1, x_2) \ell_\Omega \omega_{12}(x_1)) (e_1(x_2, x_3) \\
& \quad + \mathcal{E}_1(x_2, x_3) \ell_\Omega \omega_{12}(x_2)) + \mathcal{E}_1(x_2, x_3) \mathcal{E}_2(x_1, x_2) \ell_\Omega^2 \omega_{12}(x_1) \omega_{21}(x_2)) - \mathcal{E}_1(x_3, x_4) \\
& \quad \ell_\Omega (-\mathcal{E}_2(x_2, x_3) \ell_\Omega \omega_{12}(x_1)) - \mathcal{E}_2(x_2, x_3) \ell_\Omega (e_1(x_1, x_2) + \mathcal{E}_1(x_1, x_2) \ell_\Omega \omega_{12}(x_1)) \\
& \quad \omega_{12}(x_2) - \mathcal{E}_2(x_1, x_2) \ell_\Omega \omega_{12}(x_1) (e_2(x_2, x_3) + \mathcal{E}_2(x_2, x_3) \ell_\Omega \omega_{21}(x_2))) \omega_{21}(x_3)
\end{aligned}$$

A.3 Matrix $\mathbf{A}^{(3,2)}$

The matrix $\mathbf{A}^{(3,2)}$ as used for computations in 3.1.3 is a 6×6 -matrix.

$$\begin{aligned}
A_{11}^{(3,2)} &= \mathcal{E}_1(x_1, x_2) \omega_{12}(x_2) + \mathcal{E}_1(x_1, x_2) \omega_{13}(x_2), \\
A_{12}^{(3,2)} &= -\mathcal{E}_1(x_1, x_2) \omega_{12}(x_2), \\
A_{13}^{(3,2)} &= -\mathcal{E}_1(x_1, x_2) - \mathcal{E}_1(x_2, x_1 + \ell) / e_1(x_2, x_1 + \ell), \\
A_{14}^{(3,2)} &= 0, \\
A_{15}^{(3,2)} &= 0, \\
A_{16}^{(3,2)} &= -\bar{\mathcal{E}}_1(x_1), \\
A_{21}^{(3,2)} &= -\mathcal{E}_2(x_1, x_2) \omega_{21}(x_2), \\
A_{22}^{(3,2)} &= \mathcal{E}_2(x_1, x_2) \omega_{21}(x_2) + \mathcal{E}_2(x_1, x_2) \omega_{23}(x_2), \\
A_{23}^{(3,2)} &= 0, \\
A_{24}^{(3,2)} &= -\mathcal{E}_2(x_1, x_2) - \mathcal{E}_2(x_2, x_1 + \ell) / e_2(x_2, x_1 + \ell), \\
A_{25}^{(3,2)} &= 0, \\
A_{26}^{(3,2)} &= -\bar{\mathcal{E}}_2(x_1), \\
A_{31}^{(3,2)} &= -\mathcal{E}_3(x_1, x_2) \omega_{31}(x_2), \\
A_{32}^{(3,2)} &= -\mathcal{E}_3(x_1, x_2) \omega_{32}(x_2), \\
A_{33}^{(3,2)} &= 0, \\
A_{34}^{(3,2)} &= 0, \\
A_{35}^{(3,2)} &= -\mathcal{E}_3(x_1, x_2) - \mathcal{E}_3(x_2, x_1 + \ell) / e_3(x_2, x_1 + \ell), \\
A_{36}^{(3,2)} &= -\bar{\mathcal{E}}_3(x_1), \\
A_{41}^{(3,2)} &= -\omega_{12}(x_1) - \omega_{13}(x_1) - \omega_{12}(x_1) \omega_{12}(x_2) \ell_{\Omega} \mathcal{E}_1(x_1, x_2) - \omega_{13}(x_1) \omega_{12}(x_2) \ell_{\Omega} \mathcal{E}_1(x_1, x_2) \\
&\quad - \omega_{12}(x_2) e_1(x_1, x_2) - \omega_{12}(x_1) \omega_{21}(x_2) \ell_{\Omega} \mathcal{E}_2(x_1, x_2) - \omega_{12}(x_1) \omega_{13}(x_2) \ell_{\Omega} \mathcal{E}_1(x_1, x_2) \\
&\quad - \omega_{13}(x_1) \omega_{13}(x_2) \ell_{\Omega} \mathcal{E}_1(x_1, x_2) - \omega_{13}(x_2) e_1(x_1, x_2) - \omega_{13}(x_1) \omega_{31}(x_2) \ell_{\Omega} \mathcal{E}_3(x_1, x_2), \\
A_{42}^{(3,2)} &= \omega_{12}(x_1) + \omega_{12}(x_1) \omega_{21}(x_2) \ell_{\Omega} \mathcal{E}_2(x_1, x_2) + \omega_{12}(x_1) \omega_{12}(x_2) \ell_{\Omega} \mathcal{E}_1(x_1, x_2) \\
&\quad + \omega_{13}(x_1) \omega_{12}(x_2) \ell_{\Omega} \mathcal{E}_1(x_1, x_2) + \omega_{12}(x_2) e_1(x_1, x_2) + \omega_{12}(x_1) \omega_{23}(x_2) \ell_{\Omega} \mathcal{E}_2(x_1, x_2) \\
&\quad - \omega_{13}(x_1) \omega_{32}(x_2) \ell_{\Omega} \mathcal{E}_3(x_1, x_2), \\
A_{43}^{(3,2)} &= \omega_{12}(x_1) \ell_{\Omega} \mathcal{E}_1(x_1, x_2) + \omega_{13}(x_1) \ell_{\Omega} \mathcal{E}_1(x_1, x_2) + e_1(x_1, x_2) - 1 / e_1(x_2, x_1 + \ell), \\
A_{44}^{(3,2)} &= -\omega_{12}(x_1) \ell_{\Omega} \mathcal{E}_2(x_1, x_2), \\
A_{45}^{(3,2)} &= -\omega_{13}(x_1) \ell_{\Omega} \mathcal{E}_3(x_1, x_2), \\
A_{46}^{(3,2)} &= \bar{e}_1 + \omega_{12}(x_1) (\bar{\mathcal{E}}_1(x_1) - \bar{\mathcal{E}}_1(x_2)) \ell_{\Omega} + \omega_{13}(x_1) (\bar{\mathcal{E}}_1(x_1) - \bar{\mathcal{E}}_1(x_2)) \ell_{\Omega} \\
&\quad - \omega_{12}(x_1) (\bar{\mathcal{E}}_2(x_1) - \bar{\mathcal{E}}_2(x_2)) \ell_{\Omega} - \omega_{13}(x_1) (\bar{\mathcal{E}}_3(x_1) - \bar{\mathcal{E}}_3(x_2)) \ell_{\Omega}, \\
A_{51}^{(3,2)} &= \omega_{21}(x_1) + \omega_{21}(x_1) \omega_{12}(x_2) \ell_{\Omega} \mathcal{E}_1(x_1, x_2) + \omega_{21}(x_1) \omega_{21}(x_2) \ell_{\Omega} \mathcal{E}_2(x_1, x_2) \\
&\quad + \omega_{23}(x_1) \omega_{21}(x_2) \ell_{\Omega} \mathcal{E}_2(x_1, x_2) + \omega_{21}(x_2) e_2(x_1, x_2) + \omega_{21}(x_1) \omega_{13}(x_2) \ell_{\Omega} \mathcal{E}_1(x_1, x_2) \\
&\quad - \omega_{23}(x_1) \omega_{31}(x_2) \ell_{\Omega} \mathcal{E}_3(x_1, x_2), \\
A_{52}^{(3,2)} &= -\omega_{21}(x_1) - \omega_{23}(x_1) - \omega_{21}(x_1) \omega_{21}(x_2) \ell_{\Omega} \mathcal{E}_2(x_1, x_2) - \omega_{23}(x_1) \omega_{21}(x_2) \ell_{\Omega} \mathcal{E}_2(x_1, x_2) \\
&\quad - \omega_{21}(x_2) e_2(x_1, x_2) - \omega_{21}(x_1) \omega_{12}(x_2) \ell_{\Omega} \mathcal{E}_1(x_1, x_2) - \omega_{21}(x_1) \omega_{23}(x_2) \ell_{\Omega} \mathcal{E}_2(x_1, x_2) \\
&\quad - \omega_{23}(x_1) \omega_{23}(x_2) \ell_{\Omega} \mathcal{E}_2(x_1, x_2) - \omega_{23}(x_2) e_2(x_1, x_2) - \omega_{23}(x_1) \omega_{32}(x_2) \ell_{\Omega} \mathcal{E}_3(x_1, x_2), \\
A_{53}^{(3,2)} &= -\omega_{21}(x_1) \ell_{\Omega} \mathcal{E}_1(x_1, x_2),
\end{aligned}$$

$$\begin{aligned}
A_{54}^{(3,2)} &= \omega_{21}(x_1) \ell_{\Omega} \mathcal{E}_2(x_1, x_2) + \omega_{23}(x_1) \ell_{\Omega} \mathcal{E}_2(x_1, x_2) + e_2(x_1, x_2) - 1/e_2(x_2, x_1 + \ell), \\
A_{55}^{(3,2)} &= -\omega_{23}(x_1) \ell_{\Omega} \mathcal{E}_3(x_1, x_2), \\
A_{56}^{(3,2)} &= \bar{e}_2 - \omega_{21}(x_1) (\bar{\mathcal{E}}_1(x_1) - \bar{\mathcal{E}}_1(x_2)) \ell_{\Omega} + \omega_{21}(x_1) (\bar{\mathcal{E}}_2(x_1) - \bar{\mathcal{E}}_2(x_2)) \ell_{\Omega} \\
&\quad + \omega_{23}(x_1) (\bar{\mathcal{E}}_2(x_1) - \bar{\mathcal{E}}_2(x_2)) \ell_{\Omega} - \omega_{23}(x_1) (\bar{\mathcal{E}}_3(x_1) - \bar{\mathcal{E}}_3(x_2)) \ell_{\Omega}, \\
A_{61}^{(3,2)} &= \omega_{31}(x_1) + \omega_{31}(x_1) \omega_{12}(x_2) \ell_{\Omega} \mathcal{E}_1(x_1, x_2) - \omega_{32}(x_1) \omega_{21}(x_2) \ell_{\Omega} \mathcal{E}_2(x_1, x_2) \\
&\quad + \omega_{31}(x_1) \omega_{13}(x_2) \ell_{\Omega} \mathcal{E}_1(x_1, x_2) + \omega_{31}(x_1) \omega_{31}(x_2) \ell_{\Omega} \mathcal{E}_3(x_1, x_2) \\
&\quad + \omega_{32}(x_1) \omega_{31}(x_2) \ell_{\Omega} \mathcal{E}_3(x_1, x_2) + \omega_{31}(x_2) e_3(x_1, x_2), \\
A_{62}^{(3,2)} &= \omega_{32}(x_1) + \omega_{32}(x_1) \omega_{21}(x_2) \ell_{\Omega} \mathcal{E}_2(x_1, x_2) - \omega_{31}(x_1) \omega_{12}(x_2) \ell_{\Omega} \mathcal{E}_1(x_1, x_2) \\
&\quad + \omega_{32}(x_1) \omega_{23}(x_2) \ell_{\Omega} \mathcal{E}_2(x_1, x_2) + \omega_{31}(x_1) \omega_{32}(x_2) \ell_{\Omega} \mathcal{E}_3(x_1, x_2) \\
&\quad + \omega_{32}(x_1) \omega_{32}(x_2) \ell_{\Omega} \mathcal{E}_3(x_1, x_2) + \omega_{32}(x_2) e_3(x_1, x_2), \\
A_{63}^{(3,2)} &= -\omega_{31}(x_1) \ell_{\Omega} \mathcal{E}_1(x_1, x_2), \\
A_{64}^{(3,2)} &= -\omega_{32}(x_1) \ell_{\Omega} \mathcal{E}_2(x_1, x_2), \\
A_{65}^{(3,2)} &= \omega_{31}(x_1) \ell_{\Omega} \mathcal{E}_3(x_1, x_2) + \omega_{32}(x_1) \ell_{\Omega} \mathcal{E}_3(x_1, x_2) + e_3(x_1, x_2) \\
&\quad - 1/e_3(x_2, x_1 + \ell), \\
A_{66}^{(3,2)} &= \bar{e}_3 - \omega_{31}(x_1) (\bar{\mathcal{E}}_1(x_1) - \bar{\mathcal{E}}_1(x_2)) \ell_{\Omega} - \omega_{32}(x_1) (\bar{\mathcal{E}}_2(x_1) - \bar{\mathcal{E}}_2(x_2)) \ell_{\Omega} \\
&\quad + \omega_{31}(x_1) (\bar{\mathcal{E}}_3(x_1) - \bar{\mathcal{E}}_3(x_2)) \ell_{\Omega} + \omega_{32}(x_1) (\bar{\mathcal{E}}_3(x_1) - \bar{\mathcal{E}}_3(x_2)) \ell_{\Omega}. \tag{A.3}
\end{aligned}$$

A.4 The elements of $\mathbf{A}^{(2,2)}$ derived from a (3, 2)-matrix

$\mathbf{A}^{(3,2),\{1,2\},\{3\}}$ denotes the matrix, which is obtained from $\mathbf{A}^{(3,2)}$ by neglecting the vertical rates between state M and other states. Its elements are compared to the elements of $\mathbf{A}^{(2,2)}$.

$$\begin{aligned}
A_{11}^{(3,2),\{1,2\},\{3\}} &= \mathcal{E}_1(x_1, x_2) \omega_{12}(x_2) = A_{11}^{(2,2)}, \\
A_{12}^{(3,2),\{1,2\},\{3\}} &= -\mathcal{E}_1(x_1, x_2) \omega_{12}(x_2), \\
A_{13}^{(3,2),\{1,2\},\{3\}} &= -\mathcal{E}_1(x_1, x_2) - \mathcal{E}_1(x_2, x_1 + \ell) / e_1(x_2, x_1 + \ell) = A_{12}^{(2,2)}, \\
A_{14}^{(3,2),\{1,2\},\{3\}} &= 0 = A_{13}^{(2,2)}, \\
A_{15}^{(3,2),\{1,2\},\{3\}} &= 0, \\
A_{16}^{(3,2),\{1,2\},\{3\}} &= -\bar{\mathcal{E}}_1(x_1) = A_{14}^{(2,2)}, \\
A_{21}^{(3,2),\{1,2\},\{3\}} &= -\mathcal{E}_2(x_1, x_2) \omega_{21}(x_2) = A_{21}^{(2,2)}, \\
A_{22}^{(3,2),\{1,2\},\{3\}} &= \mathcal{E}_2(x_1, x_2) \omega_{21}(x_2), \\
A_{23}^{(3,2),\{1,2\},\{3\}} &= 0 = A_{22}^{(2,2)}, \\
A_{24}^{(3,2),\{1,2\},\{3\}} &= -\mathcal{E}_2(x_1, x_2) - \mathcal{E}_2(x_2, x_1 + \ell) / e_2(x_2, x_1 + \ell) = A_{23}^{(2,2)}, \\
A_{25}^{(3,2),\{1,2\},\{3\}} &= 0, \\
A_{26}^{(3,2),\{1,2\},\{3\}} &= -\bar{\mathcal{E}}_2(x_1) = A_{24}^{(2,2)}, \\
A_{31}^{(3,2),\{1,2\},\{3\}} &= 0, \\
A_{32}^{(3,2),\{1,2\},\{3\}} &= 0, \\
A_{33}^{(3,2),\{1,2\},\{3\}} &= 0, \\
A_{34}^{(3,2),\{1,2\},\{3\}} &= 0, \\
A_{35}^{(3,2),\{1,2\},\{3\}} &= -\mathcal{E}_3(x_1, x_2) - \mathcal{E}_3(x_2, x_1 + \ell) / e_3(x_2, x_1 + \ell), \\
A_{36}^{(3,2),\{1,2\},\{3\}} &= -\bar{\mathcal{E}}_3(x_1),
\end{aligned}$$

$$\begin{aligned}
A_{41}^{(3,2),\{1,2\},\{3\}} &= -\omega_{12}(x_1) - \omega_{12}(x_1)\omega_{12}(x_2)\ell_{\Omega}\mathcal{E}_1(x_1, x_2) \\
&\quad -\omega_{12}(x_2)e_1(x_1, x_2) - \omega_{12}(x_1)\omega_{21}(x_2)\ell_{\Omega}\mathcal{E}_2(x_1, x_2) = A_{31}^{(2,2)}, \\
A_{42}^{(3,2),\{1,2\},\{3\}} &= \omega_{12}(x_1) + \omega_{12}(x_1)\omega_{21}(x_2)\ell_{\Omega}\mathcal{E}_2(x_1, x_2) + \omega_{12}(x_1)\omega_{12}(x_2) \\
&\quad \ell_{\Omega}\mathcal{E}_1(x_1, x_2) + \omega_{12}(x_2)e_1(x_1, x_2), \\
A_{43}^{(3,2),\{1,2\},\{3\}} &= \omega_{12}(x_1)\ell_{\Omega}\mathcal{E}_1(x_1, x_2) + e_1(x_1, x_2) - 1/e_1(x_2, x_1 + \ell) = A_{32}^{(2,2)}, \\
A_{44}^{(3,2),\{1,2\},\{3\}} &= -\omega_{12}(x_1)\ell_{\Omega}\mathcal{E}_2(x_1, x_2) = A_{33}^{(2,2)}, \\
A_{45}^{(3,2),\{1,2\},\{3\}} &= 0, \\
A_{46}^{(3,2),\{1,2\},\{3\}} &= \bar{e}_1 + \omega_{12}(x_1)(\bar{\mathcal{E}}_1(x_1) - \bar{\mathcal{E}}_1(x_2))\ell_{\Omega} \\
&\quad -\omega_{12}(x_1)(\bar{\mathcal{E}}_2(x_1) - \bar{\mathcal{E}}_2(x_2))\ell_{\Omega} = A_{34}^{(2,2)}, \\
A_{51}^{(3,2),\{1,2\},\{3\}} &= \omega_{21}(x_1) + \omega_{21}(x_1)\omega_{12}(x_2)\ell_{\Omega}\mathcal{E}_1(x_1, x_2) + \omega_{21}(x_1)\omega_{21}(x_2) \\
&\quad \ell_{\Omega}\mathcal{E}_2(x_1, x_2) + \omega_{21}(x_2)e_2(x_1, x_2) = A_{41}^{(2,2)}, \\
A_{52}^{(3,2),\{1,2\},\{3\}} &= -\omega_{21}(x_1) - \omega_{21}(x_1)\omega_{21}(x_2)\ell_{\Omega}\mathcal{E}_2(x_1, x_2) \\
&\quad -\omega_{21}(x_2)e_2(x_1, x_2) - \omega_{21}(x_1)\omega_{12}(x_2)\ell_{\Omega}\mathcal{E}_1(x_1, x_2), \\
A_{53}^{(3,2),\{1,2\},\{3\}} &= -\omega_{21}(x_1)\ell_{\Omega}\mathcal{E}_1(x_1, x_2) = A_{42}^{(2,2)}, \\
A_{54}^{(3,2),\{1,2\},\{3\}} &= \omega_{21}(x_1)\ell_{\Omega}\mathcal{E}_2(x_1, x_2) + e_2(x_1, x_2) - 1/e_2(x_2, x_1 + \ell) = A_{43}^{(2,2)}, \\
A_{55}^{(3,2),\{1,2\},\{3\}} &= 0, \\
A_{56}^{(3,2),\{1,2\},\{3\}} &= \bar{e}_2 - \omega_{21}(x_1)(\bar{\mathcal{E}}_1(x_1) - \bar{\mathcal{E}}_1(x_2))\ell_{\Omega} + \omega_{21}(x_1) \\
&\quad (\bar{\mathcal{E}}_2(x_1) - \bar{\mathcal{E}}_2(x_2))\ell_{\Omega} = A_{44}^{(2,2)}, \\
A_{61}^{(3,2),\{1,2\},\{3\}} &= 0, \\
A_{62}^{(3,2),\{1,2\},\{3\}} &= 0, \\
A_{63}^{(3,2),\{1,2\},\{3\}} &= 0, \\
A_{64}^{(3,2),\{1,2\},\{3\}} &= 0, \\
A_{65}^{(3,2),\{1,2\},\{3\}} &= e_3(x_1, x_2) - 1/e_3(x_2, x_1 + \ell), \\
A_{66}^{(3,2),\{1,2\},\{3\}} &= \bar{e}_3. \tag{A.4}
\end{aligned}$$

A.5 Decoupling of a (4, 2)-network into two (2, 2)-networks

As explained in 4.1.2, the (M, K) -networks can be decoupled into subnetworks by limiting the number of vertical rates so that the corresponding graph is disconnected. Here, we show how the $\mathbf{A}^{(2,2)}$ -matrices $\mathbf{A}^{\{1,2\},2(2,2)_{eff}}$ and $\mathbf{A}^{\{3,4\},2(2,2)_{eff}}$, which describe the subnetworks with the states $m = 1, 2$ and $m = 3, 4$, respectively, are obtained from the matrix $\mathbf{A}^{(4,2),\{1,2\},\{3,4\}}$, i.e., the matrix $\mathbf{A}^{(4,2)}$ without the vertical rates connecting the two subsets of vertices.

$$\begin{aligned}
A_{11}^{(4,2),\{1,2\},\{3,4\}} &= \mathcal{E}_1(x_1, x_2)\omega_{12}(x_2) = A_{11}^{\{1,2\},2(2,2)_{eff}}, \\
A_{12}^{(4,2),\{1,2\},\{3,4\}} &= -\mathcal{E}_1(x_1, x_2)\omega_{12}(x_2), \\
A_{13}^{(4,2),\{1,2\},\{3,4\}} &= 0, \\
A_{14}^{(4,2),\{1,2\},\{3,4\}} &= -\mathcal{E}_1(x_1, x_2) - \mathcal{E}_1(x_2, x_1 + \ell)/e_1(x_2, x_1 + \ell) = A_{12}^{\{1,2\},2(2,2)_{eff}}, \\
A_{15}^{(4,2),\{1,2\},\{3,4\}} &= 0 = A_{13}^{\{1,2\},2(2,2)_{eff}}, \\
A_{16}^{(4,2),\{1,2\},\{3,4\}} &= 0, \\
A_{17}^{(4,2),\{1,2\},\{3,4\}} &= 0,
\end{aligned}$$

$$\begin{aligned}
A_{18}^{(4,2),\{1,2\},\{3,4\}} &= -\bar{\mathcal{E}}_1(x_1) = A_{14}^{(\{1,2\},2)(2,2)_{eff}}, \\
A_{21}^{(4,2),\{1,2\},\{3,4\}} &= -\mathcal{E}_2(x_1, x_2) \omega_{21}(x_2) = A_{21}^{(\{1,2\},2)(2,2)_{eff}}, \\
A_{22}^{(4,2),\{1,2\},\{3,4\}} &= \mathcal{E}_2(x_1, x_2) \omega_{21}(x_2), \\
A_{23}^{(4,2),\{1,2\},\{3,4\}} &= 0, \\
A_{24}^{(4,2),\{1,2\},\{3,4\}} &= 0 = A_{22}^{(\{1,2\},2)(2,2)_{eff}}, \\
A_{25}^{(4,2),\{1,2\},\{3,4\}} &= -\mathcal{E}_2(x_1, x_2) - \mathcal{E}_2(x_2, x_1 + \ell) / e_2(x_2, x_1 + \ell) = A_{23}^{(\{1,2\},2)(2,2)_{eff}}, \\
A_{26}^{(4,2),\{1,2\},\{3,4\}} &= 0, \\
A_{27}^{(4,2),\{1,2\},\{3,4\}} &= 0, \\
A_{28}^{(4,2),\{1,2\},\{3,4\}} &= -\bar{\mathcal{E}}_2(x_1) = A_{24}^{(\{1,2\},2)(2,2)_{eff}}, \\
A_{31}^{(4,2),\{1,2\},\{3,4\}} &= 0, \\
A_{32}^{(4,2),\{1,2\},\{3,4\}} &= 0, \\
A_{33}^{(4,2),\{1,2\},\{3,4\}} &= \mathcal{E}_3(x_1, x_2) \omega_{34}(x_2) = A_{11}^{(\{3,4\},2)(2,2)_{eff}}, \\
A_{34}^{(4,2),\{1,2\},\{3,4\}} &= 0, \\
A_{35}^{(4,2),\{1,2\},\{3,4\}} &= 0, \\
A_{36}^{(4,2),\{1,2\},\{3,4\}} &= -\mathcal{E}_3(x_1, x_2) - \mathcal{E}_3(x_2, x_1 + \ell) / e_3(x_2, x_1 + \ell) = A_{12}^{(\{3,4\},2)(2,2)_{eff}}, \\
A_{37}^{(4,2),\{1,2\},\{3,4\}} &= 0 = A_{13}^{(\{3,4\},2)(2,2)_{eff}}, \\
A_{38}^{(4,2),\{1,2\},\{3,4\}} &= -\bar{\mathcal{E}}_3(x_1) = A_{14}^{(\{3,4\},2)(2,2)_{eff}}, \\
A_{41}^{(4,2),\{1,2\},\{3,4\}} &= 0, \\
A_{42}^{(4,2),\{1,2\},\{3,4\}} &= 0, \\
A_{43}^{(4,2),\{1,2\},\{3,4\}} &= -\mathcal{E}_4(x_1, x_2) \omega_{43}(x_2) = A_{21}^{(\{3,4\},2)(2,2)_{eff}}, \\
A_{44}^{(4,2),\{1,2\},\{3,4\}} &= 0, \\
A_{45}^{(4,2),\{1,2\},\{3,4\}} &= 0, \\
A_{46}^{(4,2),\{1,2\},\{3,4\}} &= 0 = A_{22}^{(\{3,4\},2)(2,2)_{eff}}, \\
A_{47}^{(4,2),\{1,2\},\{3,4\}} &= -\mathcal{E}_4(x_1, x_2) - \mathcal{E}_4(x_2, x_1 + \ell) / e_4(x_2, x_1 + \ell) = A_{23}^{(\{3,4\},2)(2,2)_{eff}}, \\
A_{48}^{(4,2),\{1,2\},\{3,4\}} &= -\bar{\mathcal{E}}_4(x_1) = A_{24}^{(\{3,4\},2)(2,2)_{eff}}, \\
A_{51}^{(4,2),\{1,2\},\{3,4\}} &= -\omega_{12}(x_1) - \omega_{12}(x_2) (e_1(x_1, x_2) + \mathcal{E}_1(x_1, x_2) \ell_{\Omega} \omega_{12}(x_1)) \\
&\quad - \mathcal{E}_2(x_1, x_2) \ell_{\Omega} \omega_{12}(x_1) \omega_{21}(x_2) = A_{31}^{(\{1,2\},2)(2,2)_{eff}}, \\
A_{52}^{(4,2),\{1,2\},\{3,4\}} &= \omega_{12}(x_1) + \omega_{12}(x_2) (e_1(x_1, x_2) + \mathcal{E}_1(x_1, x_2) \ell_{\Omega} \omega_{12}(x_1)) \\
&\quad + \mathcal{E}_2(x_1, x_2) \ell_{\Omega} \omega_{12}(x_1) \omega_{21}(x_2), \\
A_{53}^{(4,2),\{1,2\},\{3,4\}} &= 0, \\
A_{54}^{(4,2),\{1,2\},\{3,4\}} &= e_1(x_1, x_2) - 1/e_1(x_2, x_3) + \mathcal{E}_1(x_1, x_2) \ell_{\Omega} \omega_{12}(x_1) \\
&= A_{32}^{(\{1,2\},2)(2,2)_{eff}}, \\
A_{55}^{(4,2),\{1,2\},\{3,4\}} &= -\mathcal{E}_2(x_1, x_2) \ell_{\Omega} \omega_{12}(x_1) = A_{33}^{(\{1,2\},2)(2,2)_{eff}}, \\
A_{56}^{(4,2),\{1,2\},\{3,4\}} &= 0, \\
A_{57}^{(4,2),\{1,2\},\{3,4\}} &= 0, \\
A_{58}^{(4,2),\{1,2\},\{3,4\}} &= \bar{e}_1 + (\bar{\mathcal{E}}_1(x_1) - \bar{\mathcal{E}}_1(x_2)) \ell_{\Omega} \omega_{12}(x_1) - (\bar{\mathcal{E}}_2(x_1) - \bar{\mathcal{E}}_2(x_2)) \ell_{\Omega} \omega_{12}(x_1)
\end{aligned}$$

$$\begin{aligned}
&= A_{34}^{(\{1,2\},2)(2,2)_{eff}} \\
A_{61}^{(4,2),\{1,2\},\{3,4\}} &= \omega_{21}(x_1) + \mathcal{E}_1(x_1, x_2) \ell_{\Omega} \omega_{12}(x_2) \omega_{21}(x_1) + \omega_{21}(x_2) \\
&\quad (e_2(x_1, x_2) + \mathcal{E}_2(x_1, x_2) \ell_{\Omega} \omega_{21}(x_1)) = A_{41}^{(\{1,2\},2)(2,2)_{eff}} \\
A_{62}^{(4,2),\{1,2\},\{3,4\}} &= -\omega_{21}(x_1) - \mathcal{E}_1(x_1, x_2) \ell_{\Omega} \omega_{12}(x_2) \omega_{21}(x_1) - \omega_{21}(x_2) \\
&\quad (e_2(x_1, x_2) + \mathcal{E}_2(x_1, x_2) \ell_{\Omega} \omega_{21}(x_1)) \\
A_{63}^{(4,2),\{1,2\},\{3,4\}} &= 0 \\
A_{64}^{(4,2),\{1,2\},\{3,4\}} &= -\mathcal{E}_1(x_1, x_2) \ell_{\Omega} \omega_{21}(x_1) = A_{42}^{(\{1,2\},2)(2,2)_{eff}} \\
A_{65}^{(4,2),\{1,2\},\{3,4\}} &= e_2(x_1, x_2) - 1/e_2(x_2, x_3) + \mathcal{E}_2(x_1, x_2) \ell_{\Omega} \omega_{21}(x_1) \\
&= A_{43}^{(\{1,2\},2)(2,2)_{eff}} \\
A_{66}^{(4,2),\{1,2\},\{3,4\}} &= 0 \\
A_{67}^{(4,2),\{1,2\},\{3,4\}} &= 0 \\
A_{68}^{(4,2),\{1,2\},\{3,4\}} &= \bar{e}_2 - (\bar{\mathcal{E}}_1(x_1) - \bar{\mathcal{E}}_1(x_2)) \ell_{\Omega} \omega_{21}(x_1) + (\bar{\mathcal{E}}_2(x_1) - \bar{\mathcal{E}}_2(x_2)) \ell_{\Omega} \omega_{21}(x_1) \\
&= A_{44}^{(\{1,2\},2)(2,2)_{eff}} \\
A_{71}^{(4,2),\{1,2\},\{3,4\}} &= 0 \\
A_{72}^{(4,2),\{1,2\},\{3,4\}} &= 0 \\
A_{73}^{(4,2),\{1,2\},\{3,4\}} &= -\omega_{34}(x_1) - (e_3(x_1, x_2) + \mathcal{E}_3(x_1, x_2) \ell_{\Omega} \omega_{34}(x_1)) \omega_{34}(x_2) \\
&\quad - \mathcal{E}_4(x_1, x_2) \ell_{\Omega} \omega_{34}(x_1) \omega_{43}(x_2) = A_{31}^{(\{3,4\},2)(2,2)_{eff}} \\
A_{74}^{(4,2),\{1,2\},\{3,4\}} &= 0 \\
A_{75}^{(4,2),\{1,2\},\{3,4\}} &= 0 \\
A_{76}^{(4,2),\{1,2\},\{3,4\}} &= e_3(x_1, x_2) - 1/e_3(x_2, x_3) + \mathcal{E}_3(x_1, x_2) \ell_{\Omega} \omega_{34}(x_1) \\
&= A_{32}^{(\{3,4\},2)(2,2)_{eff}} \\
A_{77}^{(4,2),\{1,2\},\{3,4\}} &= -\mathcal{E}_4(x_1, x_2) \ell_{\Omega} \omega_{34}(x_1) = A_{33}^{(\{3,4\},2)(2,2)_{eff}} \\
A_{78}^{(4,2),\{1,2\},\{3,4\}} &= \bar{e}_3 - (\bar{\mathcal{E}}_3(x_1) - \bar{\mathcal{E}}_3(x_2)) \ell_{\Omega} \omega_{34}(x_1) - (\bar{\mathcal{E}}_4(x_1) - \bar{\mathcal{E}}_4(x_2)) \\
&\quad \ell_{\Omega} \omega_{34}(x_1) = A_{34}^{(\{3,4\},2)(2,2)_{eff}} \\
A_{81}^{(4,2),\{1,2\},\{3,4\}} &= 0 \\
A_{82}^{(4,2),\{1,2\},\{3,4\}} &= 0 \\
A_{83}^{(4,2),\{1,2\},\{3,4\}} &= \omega_{43}(x_1) + \mathcal{E}_3(x_1, x_2) \ell_{\Omega} \omega_{34}(x_2) \omega_{43}(x_1) + \omega_{43}(x_2) \\
&\quad (e_4(x_1, x_2) + \mathcal{E}_4(x_1, x_2) \ell_{\Omega} \omega_{43}(x_1)) = A_{41}^{(\{3,4\},2)(2,2)_{eff}} \\
A_{84}^{(4,2),\{1,2\},\{3,4\}} &= 0 \\
A_{85}^{(4,2),\{1,2\},\{3,4\}} &= 0 \\
A_{86}^{(4,2),\{1,2\},\{3,4\}} &= -\mathcal{E}_3(x_1, x_2) \ell_{\Omega} \omega_{43}(x_1) = A_{42}^{(\{3,4\},2)(2,2)_{eff}} \\
A_{87}^{(4,2),\{1,2\},\{3,4\}} &= e_4(x_1, x_2) - 1/e_4(x_2, x_3) + \mathcal{E}_4(x_1, x_2) \ell_{\Omega} \omega_{43}(x_1) \\
&= A_{43}^{(\{3,4\},2)(2,2)_{eff}} \\
A_{88}^{(4,2),\{1,2\},\{3,4\}} &= \bar{e}_4 - (\bar{\mathcal{E}}_3(x_1) - \bar{\mathcal{E}}_3(x_2)) \ell_{\Omega} \omega_{43}(x_1) + (\bar{\mathcal{E}}_4(x_1) - \bar{\mathcal{E}}_4(x_2)) \ell_{\Omega} \omega_{43}(x_1) \\
&= A_{44}^{(\{3,4\},2)(2,2)_{eff}} \tag{A.5}
\end{aligned}$$

Appendix B

Polynomials and vertices of every state

Rule 5 in 3.2.2 states that the combination of vertical rates in each term \mathcal{T} of $Pol_1^{(M,K)}$ or $Pol_2^{(M,K)}$ contains vertices of every single internal state m as starting or final vertices of vertical rates.

For $K = 1$ the derivation of this rule is trivial, as there is no way of choosing the minimal number of $M - 1$ (compare **rule 2**) vertical rates at one location and not reaching vertices of every single state without at the same time violating at least one of the other rules about forming an l-cycle (**rule 4**) or having two vertical rates starting from the same vertex (**rule 3**).

For $K > 1$ we have to take into account the explicit structure of the matrix $\mathbf{A}^{(M,K)}$ as shown in table B.1. An entry $1_{2..K}$ in a certain field of the table means that each term of the respective element of $\mathbf{A}^{(M,K)}$ is proportional to at least one vertical rate $\omega_{1m}(x_2), \omega_{1m}(x_3), \dots, \omega_{1m}(x_K)$ where m is a non-specified other state, so that each term contains at least one rate starting from state 1, and this rate is located at $x_2, x_3, \dots, \text{ or } x_K$. The capital number in the table entries denotes the starting state, the indices refer to the possible locations of the rate.

If we now calculate the determinants and subdeterminants of $\mathbf{A}^{(M,K)}$ which enter the numerator or denominator polynomials $Pol_1^{(M,K)}$ or $Pol_2^{(M,K)}$ of the total current, the structure of the matrix as shown in table B.1 enforces the occurrence of every state in every term contributing to these determinants. No matter how we start developing the determinants in our calculation, it is unavoidable to find factors of every state in every resulting term.

row\col.	1	...	$M - 1$	M	$M + 1$	$M + 2$...	$2M$
1	$1_{2..K}$	$1_{2..K}$	$1_{2..K}$	/	$1_{2..K-1}$	$1_{2..K-1}$	$1_{2..K-1}$	/
2	$2_{2..K}$	$2_{2..K}$	$2_{2..K}$	$2_{2..K-1}$	/	$2_{2..K-1}$	$2_{2..K-1}$	/
3	$3_{2..K}$	$3_{2..K}$	$3_{2..K}$	$3_{2..K-1}$	$3_{2..K-1}$	/	$3_{2..K-1}$	/
...
M	$M_{2..K-1}$	$M_{2..K-1}$	$M_{2..K-1}$	$M_{2..K-1}$	$M_{2..K-1}$	$M_{2..K-1}$	/	/
$M + 1$	$1_{2..K-1}$	$1_{2..K-1}$	$1_{2..K-1}$	/	$1_{2..K-1}$	$1_{2..K-1}$	$1_{2..K-1}$	/
$M + 2$	$2_{2..K-1}$	$2_{2..K-1}$	$2_{2..K-1}$	$2_{2..K-1}$	/	$2_{2..K-1}$	$2_{2..K-1}$	/
$M + 3$	$3_{2..K-1}$	$3_{2..K-1}$	$3_{2..K-1}$	$3_{2..K-1}$	$3_{2..K-1}$	/	$3_{2..K-1}$	/
...
$2M$	$M_{2..K-1}$	$M_{2..K-1}$	$M_{2..K-1}$	$M_{2..K-1}$	$M_{2..K-1}$	$M_{2..K-1}$	/	/

Table B.1: The entries $m_{2..K-1}$ of the table indicate that every term of the corresponding element of the matrix $\mathbf{A}^{(M,K)}$ is proportional to at least one vertical rate $\omega_{mn}(x_i)$ starting from state m at one of the locations x_i with $i = 2, 3, \dots, K - 1$.

Appendix C

Terminology and basics on graph theory

In this appendix we summarize important terms and relationships from the field of graph theory. For a detailed overview see [53, 67].

A *graph* G is an ordered 2-tuple, $(V(G), E(G))$, which consists of a set $V(G)$ of vertices and a set $E(G)$ of edges.

A *vertex* can be imagined as a point, node or 0-simplex.

An *edge* can be referred to as a line, an arc or a 1-simplex.

A *directed graph* is a graph whose edges have an orientation.

If $V(G)$ and $E(G)$ are finite sets, the graph is said to be *finite*.

The *degree* of a vertex is given by the number of edges having that vertex for one of their endpoints.

A graph in which every vertex is of even degree belongs to the class of *Euler graphs*.

An *edge sequence* is a graph or subgraph whose edges can be ordered in such a way that each edge with the exclusion of the initial edge and the final edge has a vertex in common with the preceding edge in the ordered sequence and the other vertex in common with the succeeding edge.

The *multiplicity* of an edge in an edge sequence is the number of times an edge appears in an edge sequence.

If the multiplicity of each edge in an edge sequence is one, the edge sequence is called an *edge train* or *walk*.

The *terminal vertices* of the edge sequence are the initial and final vertices.

In the case of coinciding terminal vertices the edge train is a *closed edge train*.

An edge train is a *path* if the degree of each nonterminal vertex is two and the degree of each terminal vertex is one.

In a *connected graph* there is a path between any two distinct vertices of the graph.

A digraph is *strongly connected* if there is at least one directed path from every vertex to every other vertex.

A digraph is *weakly connected* if the underlying undirected graph is connected.

A graph without self-loops and parallel edges is a *simple* graph.

Self-loops are edges with identical endpoints.

A *cut set* is a set of edges whose removal splits a weakly connected directed graph into two separate parts.

An edge train that contains more than one edge, is closed and only has vertices of degree two is a *loop*, *circuit* or *cycle*.

A *spanning-cycle* or short *s-cycle* starts at vertex $(m, k = 1)$, spans the whole network parallel to the x -direction, ends at vertex $(m, k = K)$ and can be supplemented with the di-edge between $(m, k = K)$ and $(m, k = 1)$ to form a cycle, see fig. 2.1. If the horizontal di-edges are not known explicitly the s-cycle shows as an edge train of vertical rates starting and ending in state m where

each edge with the exclusion of the initial edge and the final edge has a state in common with the preceding edge and the other state in common with the succeeding edge.

A *localized* or *l-cycle* is a cycle of vertical di-edges at a single location.

A *self-loop* is a closed edge train with only one edge.

A *subgraph* H of a graph G consists of subsets of vertices and edges of G such that the endpoints of every edge in H are in H , too.

A *spanning tree* is any connected subgraph of a graph over the same set of nodes which does not comprise loops.

Appendix D

Stationary probabilities for general (2, 2)-networks

In the following we list the stationary values of the probabilities $P^{stat}(1, 1)$, $P^{stat}(1, 2)$ and $P^{stat}(2, 1)$ depending on the probability $P^{stat}(2, 2)$ in state 2 at location 2. This solution is true for a general (2, 2)-network with rates as depicted in fig. D.1. The non-negativity and the normalization of the probabilities determine the value of $P^{stat}(2, 2)$.

$$\begin{aligned}
 P^{stat}(1, 1) &= - (P^{stat}(2, 2) ((W_3 + W_9) / W_1 - ((-W_{10} - W_{11} - W_2) \\
 &\quad (- (W_1 (-W_{12} - W_5 - W_8) (-W_3 - W_4 - W_9)) \\
 &\quad + W_{12} (W_1 W_4 - (W_6 + W_7) (W_3 + W_9)))) / \\
 &\quad (W_1 (- (W_{12} (-W_{10} - W_{11} - W_2) (W_6 + W_7)) \\
 &\quad - W_1 (W_{10} + W_2) (-W_{12} - W_5 - W_8))))), \\
 P^{stat}(1, 2) &= - (P^{stat}(2, 2) ((-W_3 - W_4 - W_9) / W_{12} \\
 &\quad - ((W_{10} + W_2) (- (W_1 (-W_{12} - W_5 - W_8) (-W_3 - W_4 - W_9)) \\
 &\quad + W_{12} (W_1 W_4 - (W_6 + W_7) (W_3 + W_9)))) / \\
 &\quad (W_{12} (- (W_{12} (-W_{10} - W_{11} - W_2) (W_6 + W_7)) \\
 &\quad - W_1 (W_{10} + W_2) (-W_{12} - W_5 - W_8))))), \\
 P^{stat}(2, 1) &= - ((P^{stat}(2, 2) (- (W_1 (-W_{12} - W_5 - W_8) (-W_3 - W_4 - W_9)) \\
 &\quad + W_{12} (W_1 W_4 - (W_6 + W_7) (W_3 + W_9)))) / \\
 &\quad (- (W_{12} (-W_{10} - W_{11} - W_2) (W_6 + W_7)) \\
 &\quad - W_1 (W_{10} + W_2) (-W_{12} - W_5 - W_8)))
 \end{aligned} \tag{D.1}$$

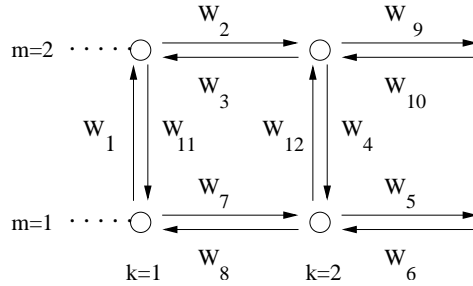


Figure D.1: Naming of vertical and horizontal rates W_i in the general (2, 2)-network as used in 4.4.1.

Appendix E

Algorithms for path problems

E.1 Maximum-flow problem

Every edge connecting a pair of vertices v_i and v_j has a certain capacity c_{ij} . Before starting a new cycle of the algorithm with the starting vertex $v_s = s$, the actual flow q_{ij} for each edge is updated. In the beginning, all the edge flows are zero. Then a label is attached to a vertex in a possible flow-augmenting path which is the minimum of the label of the preceding vertex and the difference between edge capacity and momentary flow. This process of labelling is continued until either no additional labels can be placed and the algorithm stops or the terminal vertex becomes the new starting vertex and the path is completed. Backtracking is necessary in order to update the actual flows, before the next flow-augmenting path is looked for.

E.2 Shortest-path problem

Every edge between a pair of vertices v_i and v_j has a certain cost or fee f_{ij} associated with it.

We start in state 1. The source vertex receives the label 0 which is set permanent. The other vertices are labelled with ∞ or, in an actual implementation with a number which is very large compared to the system costs. The temporary labels $lab(v_j)$ of the vertices which are terminal vertices of edges originating from the starting vertex v_s are updated according to $lab(v_j) = \min(lab(v_j), lab(v_s) + f_{sj})$. The minimum label of the vertices with temporary labels is then marked as permanent. The choice is not necessarily unambiguous. The vertex with the new permanent label is the new starting vertex v_s . The updating is repeated until the terminal vertex is set the starting vertex. Its label gives the costs for the shortest path. The corresponding path is found by backtracking from the terminal vertices as the difference of the labels between the current vertex and the preceding vertex of the path equals the cost of the respective edge. If the shortest path does not include horizontal edges, we search for an alternative path whose costs are higher, but which forms a proper s-cycle.

Then the operation is continued with the search for the shortest path of the next state. The procedure is repeated until the shortest path for the last level M is found.

List of symbols

- $\mathbf{A}^{(M,K)}$ is a $2M \times 2M$ matrix describing a system of M states and K locations
- $\mathbf{A}^{(M,K),\{m_1,n_1,\dots\},\{m_2,n_2,\dots\}}$ is the matrix of the (M, K) -system which decomposes into the two subsets V_1 with the states m_1, n_1, \dots and V_2 with m_2, n_2, \dots
- $\mathbf{A}^{(\{m_1,n_1,\dots\},K)(M_1,K)_{eff}}$ the effective (M_1, K) matrix where M_1 is the number of states comprised in the first subset of vertices V_1 belonging to the states m_1, n_1, \dots ; describes the subnetwork belonging to V_1
- c_{ij} capacity of directed edge (v_i, v_j)
- D_m diffusion coefficient in lateral currents J_m
- $\Delta_{mn}(x_k)$ unbalanced parts of transition rates
- $e_m(y, z)$ exponential functions given by $\exp(V_m(y) - V_m(z))$
- ε coupling parameter, in 5.2 transition width
- $\mathcal{E}_m(x, y)$ integral defined by $\frac{1}{D_m} \int_x^y dz e_m(z, y)$
- f_{ij} costs or fees for edges
- F applied (tangential) force; a load force corresponds to $F < 0$
- $G = (V(G), E(G))$ directed connected graph with corresponding set of vertices $V(G)$ and set of edges $E(G)$
- Γ concentration of fuel molecules such as *ATP*
- Γ_* characteristic intermediate concentration
- I_m transition current density for internal state m
- J_m lateral current for internal state m
- \bar{J}_m average currents
- $J_{tot}^{(M,K)}$ total lateral current in an (M, K) -system
- $\bar{J}_{tot}^{(M,K)}$ total current in the Master-equation approach
- ΔJ_m current discontinuities
- K number of locations for transitions between internal states
- ℓ period of molecular force potentials
- ℓ_Ω molecular “localization” length for transition rates

- M total number of internal motor states
- M_i^{-1} probability weight of state i
- Ω_{mn} spatially dependent transition rate from state m to state n
- ω_{mn} transition rate from state m to state n
- ω_{mn}^{db} part of transition rate fulfilling detailed balance
- $p(m, k | m', k')(t)$ time-dependent transition functions
- P_m probability density for internal state m
- $Pol_i^{(M,K)}$ polynomial in the numerator ($i = 1$) or denominator ($i = 2$) of the expression for $J_{tot}^{(M,K)}$
- $\overline{Pol}_i^{(M,K)}$ polynomials in the Master-equation approach
- P_{tot} total probability density
- $\mathbf{P}^{(M,K)}(t)$ quadratical matrix of the transition functions
- $q(m, k | m', k')$ infinitesimal transition rates
- Q number of unbalanced transition rates
- $\mathbf{Q}^{(M,K)}$ infinitesimal generator
- s source vertex
- t time, in 4.5 terminal vertex
- T temperature in energy units
- \mathcal{T} term of polynomial $Pol_i^{(M,K)}$
- U_m molecular interaction potential for internal state m
- V_i subsets of vertices
- V_m effective force potential
- v motor velocity
- v_i with $v_i = (m, k)$ vertex of the network in state m at location k
- $W(m, k | m', k')$ transition rate from state (m, k) into state (m', k')
- x spatial coordinate for motor position
- x_k position at which motor undergoes localized transition
- $X(t)$ stochastic process

Bibliography

- [1] B. Alberts, A. Johnson, J. Lewis, M. Raff, K. Roberts, and P. Walter, *Molekularbiologie der Zelle*, 3. Auflage (VCH, 1995), and *Molecular Biology of the Cell*, 4th edition (Garland, 2002).
- [2] J. Howard, *Mechanics of Motor Proteins and the Cytoskeleton*, 1 ed. (Sinauer, New York, 2001).
- [3] M. Schliwa and G. Woehlke, *Nature* (London) **422**, 759 (2003).
- [4] <http://home19.inet.tele.dk/griscellisynndrome>.
- [5] S. A. Endow, H. Higuchi, *Nature* (London) **406**, 913 (2000).
- [6] K. Homma, M. Yoshimura, J. Salto, R. Ikebe and M. Ikebe, *Nature* (London) **412**, 831 (2001).
- [7] J. Howard, A. J. Hudspeth, and R. D. Vale, *Nature* (London) **342**, 154 (1989).
- [8] K. Svoboda, C. Schmidt, B. Schnapp, and S. Block, *Nature* (London) **365**, 721 (1993).
- [9] K. Svoboda and S. Block, *Cell* **77**, 773 (1994).
- [10] M. J. Schnitzer and S. M. Block, *Nature* (London) **388**, 386 (1997).
- [11] W. Hua, E. C. Young, M. L. Fleming, and J. Gelles, *Nature* (London) **388**, 390 (1997).
- [12] W. O. Hancock and J. Howard, *J. Cell Biol.* **140**, 1395 (1998).
- [13] M. Thormählen, A. Marx, S. A. Mueller, Y.-H. Song, E.-M. Mandelkow, U. Aebi, and E. Mandelkow, *J. Mol. Biol.* **275**, 795 (1998).
- [14] S. Gilbert, M. Moyer, and K. Johnson, *Biochemistry* **37**, 792 (1998).
- [15] K. Visscher, M. J. Schnitzer, and S. M. Block, *Nature* (London) **400**, 184 (1999).
- [16] Y. Okada and N. Hirokawa, *Science* **283**, 1152 (1999).
- [17] A. D. Mehta, R. S. Rock, M. Rief, J. A. Spudich, M. S. Mooseker, and R. E. Cheney, *Nature* (London) **400**, 590 (1999).
- [18] M. Rief, R. S. Rock, A. D. Mehta, M. S. Mooseker, R. E. Cheney, and J. A. Spudich, *Proc. Nat. Acad. Sci. USA* **97**, 9482 (2000).
- [19] A. Mehta, *J. Cell Sci.* **114**, 1981 (2001).
- [20] C. Veigel, F. Wang, M. L. Bartoo, J. R. Sellers and J. E. Molloy, *Nature Cell Biol.* **4**, 59 (2002).
- [21] Z. Wang and M. P. Sheetz, *Biophys. J.* **78**, 1955 (2000).
- [22] S. King, *Biochimica Acta - Mol. Cell Res.* **1496**, 60 (2000).
- [23] E. Hirakawa, H. Higuchi, and Y. Y. Toyoshima, *Proc. Nat. Acad. Sci. USA* **97**, 2533 (2000).

- [24] R. Lipowsky, S. Klumpp, and Th. M. Nieuwenhuizen, *Phys. Rev. Lett.* **87**, 108101.1 (2001).
- [25] Th. M. Nieuwenhuizen, S. Klumpp, and R. Lipowsky, *Europhys. Lett.* **58**, 468 (2002).
- [26] Th. M. Nieuwenhuizen, S. Klumpp, and R. Lipowsky, in preparation.
- [27] S. Klumpp, *Movements of Molecular Motors: Diffusion and Directed Walks* (Dissertation, Potsdam, 2003).
- [28] R. D. Vale and R. A. Milligan, *Science* **288**, 88 (2000).
- [29] P. Reimann, *Brownian motors: noisy transport far from equilibrium*, *Phys. Rep.* **361**, 57 (2001).
- [30] T. R. Kelly, I. Tellitu, and J. P. Sestelo, *Angew. Chem. Int. Ed. Engl.* **36**, 1866 (1997).
- [31] K. L. Sebastian, *Phys. Rev. E* **61**, 937 (2000).
- [32] R. Feynman, *The Feynman lectures on physics* (Addison-Wesley, Reading, Massachusetts, 1963).
- [33] Several people have pointed out that Feynman's arrangement contains a misconception concerning reversibility, see e.g. Parrondo, Espanol, *Am. J. Phys.* **64** (9), September 1996 and Magnasco, Stolovitzky, *J. Stat. Phys.* **93**, Nos. 3/4, 1998.
- [34] A. F. Huxley, *Prog. Biophys. Mol. Biol.* **7**, 255 (1957).
- [35] J. Howard, A. J. Hudspeth, and R. D. Vale, *Nature* **342**, 154 (1989).
- [36] S. Leibler and D. A. Huse, *J. Cell Biol.* **121**, 1357 (1993).
- [37] J. Prost, J.-F. Chauwin, L. Peliti, and A. Ajdari, *Phys. Rev. Lett.* **72**, 2652 (1994).
- [38] T. Harms and R. Lipowsky, *Phys. Rev. Lett.* **79**, 2895 (1997).
- [39] F. Jülicher, A. Ajdari, and J. Prost, *Rev. Mod. Phys.* **69**, 1269 (1997).
- [40] R. Lipowsky and T. Harms, *Eur. Biophys. J.* **29**, 542 (2000).
- [41] R. Lipowsky, *Phys. Rev. Lett.* **85**, 4401 (2000).
- [42] L. Schimansky-Geier, M. Kschischo, and T. Fricke, *Phys. Rev. Lett.* **79**, 3335 (1997).
- [43] R. Lipowsky and N. Jaster, *J. of Stat. Phys.* **110**, 1141 (2003).
- [44] N. Jaster and R. Lipowsky, in preparation.
- [45] N. van Kampen, *Stochastic processes in physics and chemistry* (Elsevier, Amsterdam, 1992).
- [46] F. Schwabl, *Statistische Mechanik* (Springer, Berlin, 2000)
- [47] H. Risken, *The Fokker-Planck equation: methods of solution and applications* (Springer Verlag, Berlin, 1989).
- [48] R. Astumian and M. Bier, *Phys. Rev. Lett.* **72**, 1766 (1994).
- [49] A. Parmeggiani, F. Jülicher, A. Ajdari, and J. Prost, *Phys. Rev. E* **60**, 2127 (1999).
- [50] A. Kolomeisky and B. Widom, *J. of Stat. Phys.* **93**, 633 (1998).
- [51] M. E. Fisher and A. B. Kolomeisky, *Proc. Nat. Acad. Sci. USA* **98**, 7748 (2001).
- [52] G. Lattanzi and A. Maritan, *Biophys. J.* **82**, 2348 (2002).

- [53] W. D. Wallis, *A beginner's guide to graph theory* (Birkhäuser, Boston, 2000).
- [54] R. G. Busacker and T. L. Saaty, *Finite graphs and networks, an introduction with applications* (McGraw-Hill, 1965).
- [55] Mathematica and Maple.
- [56] W. H. Press and S. A. Teukolsky, *Numerical recipes in C: the art of scientific computing*, 2nd edition (Cambridge Univ. Press, 1992).
- [57] J. Stoer, R. Bulirsch, *Introduction to Numerical Analysis*, Second Edition (Springer-Verlag New York, Inc., 1993).
- [58] K. Meyberg and P. Vachenaue, *Höhere Mathematik*, 2. Auflage (Springer-Verlag Berlin, 1997).
- [59] A. J. Lichtenberg and M. A. Lieberman, *Regular and Chaotic Dynamics*, Second Edition (Springer-Verlag New York, Inc., 1992).
- [60] R. Diestel, *Graph Theory*, Second Edition (Springer-Verlag New York, Inc., 2000).
- [61] K. Kruse and F. Jülicher, *Phys. Rev. Lett.* **85**, 1778 (2000).
- [62] K. Kruse, S. Camalet and F. Jülicher, *Phys. Rev. Lett.* **87**, 138101 (2001).
- [63] A. T. Bharucha-Reid, *Elements of the Theory of Markov Processes and their Applications* (McGraw-Hill, 1960).
- [64] J. G. Kemeny and J. L. Snell, *Finite Markov Chains* (Springer-Verlag New York, Inc., 1976).
- [65] <http://mathstat.wu-wien.ac.at>.
- [66] S. C. Ammal, H. Yamataka, M. Aida, M. Dupuis, *Science* **299**, 1555 (2003).
- [67] N. K. Bose and P. Liang, *Neural network fundamentals with graphs, algorithms, and applications* (McGraw-Hill, 1996).
- [68] J. Falbe, M. Regnitz, *Römpp Lexikon Chemie*, 9. Auflage (Thieme Verlag Stuttgart 1989).
- [69] H. Bisswanger, *Enzymkinetik, Theorie und Methoden*, 2. Auflage (VCH Verlagsgesellschaft mbH Weinheim, 1994).
- [70] K. Burton, *J. Muscle Res. Cell Motil.* **13**, 590 (1992).
- [71] T. Yanagida, Y. Harada and A. Ishijima, *Trends Biochem. Sci.* **18**, 319 (1993).
- [72] K. J. Böhm, R. Stracke and E. Unger, *Cell Biol. Int.* **24**, No. 6, 335 (2000).
- [73] T. J. Harms, *Transporteigenschaften geordneter und ungeordneter Ratschen* (Dissertation, Potsdam, 1998).